

STUDY OF AIR INFILTRATION ENERGY CONSUMPTION

A Dissertation

By

MINGSHENG LIU

Submitted to the Office of Graduate Studies of
Texas A&M University
in partial fulfillment of the requirements for the degree of

DOCTOR OF PHILOSOPHY

August 1992

Major Subject: Mechanical Engineering

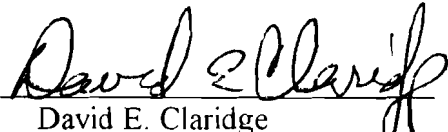
STUDY OF AIR INFILTRATION ENERGY CONSUMPTION

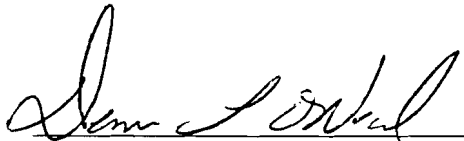
A Dissertation

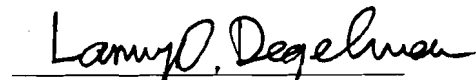
By

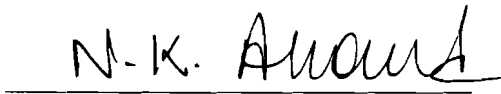
MINGSHENG LIU


Approved as to style and content by:


David E. Claridge
(Chair of Committee)


Dennis O'Neal
(Member)


Larry O. Degelman
(Member)


N. K. Anand
(Member)


for W. L. Bradley
(Head of Department)

August 1992

ABSTRACT

Study of Air Infiltration Energy Conservation. (August 1992)

Mingsheng Liu, B. S.; M. S., Harbin Architectural & Civil Engineering Institute

Chair of Advisory Committee: Dr. David E. Claridge

The influence of heat recovery on the energy impact of air infiltration, and the systematic error due to the steady-state method were studied both experimentally and theoretically. Two methodologies suitable for measurement of the overall heat loss factors in full-size houses have been developed and validated.

Dynamic measurements of Infiltration Heat Exchange Effectiveness (IHEE), which expresses the air infiltration heat recovery as a fraction of the classical value of air infiltration energy consumption, showed that results from earlier steady-state measurements can be approximately applied to dynamic conditions when solar radiation is not present. However, this study has shown for the first time that IHEE is strongly dependent on air flow direction due to the impacts of air flow on the recovery or rejection of solar radiation energy. IHEE values greater than one and less than zero have been measured. These values are impossible in the absence of solar radiation. The results highlight the necessity of considering the air infiltration heat recovery and improving the current design methods for calculating the heating and cooling loads in buildings.

The experimental and theoretical investigation show that steady-state methodology can:

- be used without systematic error in the case of constant air flow
- result in IHEE prediction error in a range of 1% to 8% when one-way dynamic air flow is present
- cause significantly larger error when balanced dynamic air flow is present.

The SSP (Single input and Single output data Pair) method can identify UA_0 of an enclosure using short term measurement data, typically a few hours long. It has overcome most of the typical problems in UA_0 identification, such as errors due to thermal storage, ground heat transfer, inter-correlated multi-inputs, and solar radiation. The STAM (Short Term Average Method) has also been developed which makes it possible for the first time to determine both the UA and the solar aperture precisely under outdoor conditions from a two-day or a three-day test. These methods were developed and used to measure heat loss factors needed to determine IHEE values in this study.

ACKNOWLEDGMENTS

I would like to express my deep gratitude to Professor David E. Claridge for his guidance and friendship. Thank you also Professor Dennis O'Neal, Professor Larry Degelman, Professor N. K. Anand and Professor Joseph Sonnenfeld who, as members of my dissertation committee, offered useful critiques of this work. Special thanks is given to Dr. Reddy who gave me much help in writing my dissertation, to Frank Scott, who helped me build the outdoor test cell, and to Ms. Daralyn G. Wallance, who helped me with editorial work. Also, thanks to you, my friends and office-mates here for your jokes. Jokes did help my work.

I am especially indebted to my wife Jinrong for her patience and love, and to my daughters Fei and Young, who are such nice children and always understand me. I would like to respectfully dedicate this dissertation to my beloved parents and brother Jinsheng who led me to college 15 years ago.

This research was sponsored by the Texas Higher Education Coordinating Board under Energy Research and Applications program (ERAP) project #227.

TABLE OF CONTENTS

	Page
CHAPTER I INTRODUCTION.....	1
CHAPTER II LITERATURE REVIEW.....	2
ENERGY IMPACT OF AIR FLOW	5
MEASUREMENT OF HOUSE THERMAL PERFORMANCE	16
LITERATURE SUMMARY	22
CHAPTER III EXPERIMENTAL FACILITY	23
INDOOR TEST CELL.....	23
OUTDOOR TEST CELL.....	27
CHAPTER IV EXPERIMENTAL METHODOLOGY FOR TEST CELL.....	37
METHODOLOGY FOR INDOOR TEST CELL.....	37
METHODOLOGY FOR OUTDOOR TEST CELL.....	40
CHAPTER V MEASUREMENT RESULTS	45
INDOOR CELL TESTS AND RESULTS.....	46
OUTDOOR CELL TESTS AND RESULTS.....	52
DISCUSSION.....	62
SUMMARY	68
CHAPTER VI UA0 MEASUREMENT IN HOUSES	71
FUNDAMENTAL THEORY.....	72
PROCEDURE.....	80
THE APPLICATION OF THE SSP METHOD.....	97
CHAPTER VII UA MEASUREMENT IN HOUSES	102
THE FUNDAMENTAL THEORY	102
STAM METHOD.....	113
EXPERIMENTAL VALIDATION OF STAM.....	115
SUMMARY	126

TABLE OF CONTENTS (continued)

	Page
CHAPTER VIII COMBINED SOLAR RADIATION, INFILTRATION, AND CONDUCTION MODELS.....	127
COMBINED MODELS	127
SIMULATION AND NUMERICAL RESULTS.....	141
APPLICATION	150
SUMMARY.....	157
CHAPTER IX SYSTEMATIC ERROR DUE TO THE STEADY-STATE METHODOLOGY	158
DIFFERENTIAL EQUATION	159
DISCRETIZATION OF THE DIFFERENTIAL EQUATION	161
EXTERNAL NODE EQUATIONS	164
DISCRETIZATION EQUATIONS.....	169
WEATHER DATA GENERATION	171
SIMULATION CALCULATION	174
SUMMARY.....	183
CHAPTER X CONCLUSIONS AND RECOMMENDATIONS.....	184
CONCLUSIONS	184
BENEFIT AND IMPACTS.....	187
RECOMMENDATIONS FOR FUTURE WORK	188
REFERENCES.....	189
APPENDIX A1	195
APPENDIX A2	200
APPENDIX A3	204
APPENDIX B1	212
APPENDIX B2	228

TABLE OF CONTENTS (continued)

	Page
APPENDIX B3	233
APPENDIX B4	236
APPENDIX B5	250
APPENDIX B6	254
VITA.....	266

LIST OF TABLES

Table	Page
3-1 Description of Data Acquisition Sensor Channels	35
3-2 Data Acquisition Channels for Period Integrated Signals	36
6-1 Summary of Cell Heat Loss Factor Results.....	101
8-1 Typical Energy Performance Data for the Wall.....	142
8-2 Typical Energy Performance Data for the Attic with Infiltration	144
8-3 Typical Energy Performance Data for the Attic with Cross Ventilation	146
8-4 Typical Energy Performance Data for the Combined Attic Model.....	148
8-5 Energy Saving Comparison of Three House Models.....	157

LIST OF FIGURES

Figure	Page
2-1 Schematic of Various Dynamic Insulations	9
2-2 Schematic of Optimum Ceiling	12
2-3 Schematic of Ventilated Curtain-Wall Component.....	13
3-1 Schematic of Hole Positions for Indoor Test Cell	25
3-2 Schematic of Thermocouple Positions for Indoor Test Cell	26
3-3 Schematic of the Outdoor Test Cell.....	28
3-4 Schematic of the North Wall	29
3-5 Schematic of Thermocouple Positions for Outdoor Test Cell.....	31
3-6 Schematic of Thermocouple Positions for Room Temperature Measurement	32
3-7 Schematic of Pressure Sensor Distribution.....	33
4-1 Schematic of Dynamic Test Profile for Indoor Test Cell	39
4-2 Simplified Block Diagram of "OUTCELL.FOR"	44
5-1 IHEE Comparison for Diffuse Leakage Configuration	47
5-2 Heat Loss Factor Comparison for Diffuse Leakage Configuration	48
5-3 IHEE Comparison for Different Leakage Configurations.....	50
5-4 Heat Loss Factor Comparison for Different Leakage Configurations	51
5-5 IHEE for Diffuse Leakage Configuration.....	53
5-6 Total Energy Saving Ratio for Diffuse Leakage Configuration	55
5-7 IHEE for Concentrated Leakage Configuration	56
5-8 Total Energy Saving Ratio for Concentrated Leakage Configuration.....	57

LIST OF FIGURES (continued)

Figure	Page
5-9 IHEE for Crack Leakage Configuration	59
5-10 Total Energy Saving Ratio for Crack Leakage Configuration.....	60
5-11 IHEE vs Equivalent Solar Radiation and Air Infiltration Rate for Quasi-Diffuse Leakage Exfiltration Configuration	61
6-1 An Artificial Heat Input and Room Temperature Response Data Pair.....	74
6-2 The Normalized Magnitude Spectrum of the Artificial Heat Input and Room Temperature Response Data Pair	75
6-3 Magnitude of Idealized and Designed Filter for the Artificial Heat Input and Room Temperature Response Data Pair	76
6-4 Heat Input (q_f) and Room Temperature Response (T_f) After the Filter for the Artificial Data Pairs	79
6-5 Measured Heat Input, Cell and Room Temperatures for the Indoor Cell Test.....	88
6-6 Magnitude Spectrum of Sampled Signals in Indoor Test Cell Test	89
6-7 Magnitude of the Filter for Indoor Cell Test Data.....	90
6-8 Comparison of Original and Filtered Signals	92
6-9 Response Factors vs the Time Index for Different "Order" Models.....	94
6-10 Magnitude Spectrum or Gain vs Frequency for Different "Order" Models.....	95
6-11 Response Factor and Magnitude of Transfer Function for Indoor Cell	97

LIST OF FIGURES (continued)

Figure	Page
6-12a Comparison of Measured and Predicted Cell Temperature by Transfer Function (6-32)	98
6-12b Comparison of Measured and Predicted Cell Temperature by Transfer Function (6-33)	99
6-12c Comparison of Measured and Predicted Cell Temperature by Transfer Function (6-34)	100
7-1 Schematic of a House Thermal System	104
7-2 An Example of Equivalent Solar Radiation for ASHRAE, SHACSEJ, and Horizontal Models	118
7-3 The Equivalent Solar Radiation on the Test Cell for SHRAE & SHACSEJ Models and Ratio vs Horizontal Solar Radiation	119
7-4 Comparison of IHEE Determined Using ASHRAE, SHACSEJ, and Horizontal Solar Models as a Function of Non-dimensional Air Flow Rate for Diffuse Infiltration and Diffuse Exfiltration.....	121
7-5 Comparison of IHEE Determined Using STAM and DAM Methods as a Function of Non-dimensional Air Flow Rate for Diffuse Infiltration and Diffuse Exfiltration.....	123
7-6 Start and End Time Distribution of the Periods for STAM.....	124
7-7 Time Period Deviation From 24 Hours or its Multiples for STAM.....	125
8-1 Schematic of Diffuse Wall Base System.....	129
8-2 Schematic of Combined Model for Walls.....	133
8-3 Schematic of Combined Model for Attic-I.....	136
8-4 Schematic of Combined Model for Attic-II.....	138
8-5 Schematic of Combined Model for Attic-III	140
8-6 IHEE of Combined Diffuse Wall Model	143

LIST OF FIGURES (continued)

Figure	Page
8-7 IHEE of Combined Model for Attic-I.....	145
8-8 Energy Savings of Attic-II	147
8-9 IHEE of Combined Model for Attic-III.....	149
8-10 Schematic of the Idealized House Model.....	152
8-11 Energy Saving Ratio of the Idealized to Normal House Models.....	154
8-12 Energy Saving Ratio of the Idealized to Designed House Models.....	155
8-13 Energy Saving Ratio of the Normal to Designed House Models.....	156
9-1 Schematic of Control Volume Element for Energy Balance	159
9-2 Schematic Diagram of Internal Nodes	162
9-3 Schematic Diagram of External Nodes	165
9-4 Schematic of Discretization of Wall and Ceiling	170
9-5 Solar Radiation Kernel Function Used in the Program "DANA".....	175
9-6 A Sample of Weather Data and Simulation Results.....	178
9-7 Energy Prediction Error Due to Steady-State Methodology	180
9-8 IHEE Prediction Error Due to Steady-State Methodology	182

NOMENCLATURE

A	summation of the response factors
C	specific heat of solid material (J/Kg °C)
C_p	specific heat of air (J/Kg °C)
E	east
f	frequency (Hz)
Δf	frequency resolution (Hz)
h	heat transfer coefficient (W/m ² °C)
H	transfer function
I	solar radiation (W/m ²)
k	heat conductance (W/m °C)
\dot{m}	air flow rate (Kg/m ² s)
\dot{M}	air flow rate (Kg/s)
M	magnitude
q	heat input (W)
Q	heat loss (W)
R	multiplier, resistance
T	temperature (°C)
ΔT	temperature difference (°C)
δT	temperature difference (°C)
UA	heat loss factor (W/°C)
W	west
α	no-dimensional air flow rate, response factor
β	energy saving ratio, resistance ratio
β_n	phase shift (rad)
θ	no-dimensional temperature

NOMENCLATURE (Continued)

ρ	specific density of solid material (Kg/m^3)
ρ_p	specific density of air (Kg/m^3)
τ	time (s)
$\Delta\tau$	time step (s)
ω	angular frequency (rad)
ψ	solar indicator ($\text{W/m}^2 \text{ } ^\circ\text{C}$)
ϵ	infiltration heat exchange effectiveness
δ	discrete number
ϵ_{ds}	systematic error of steady state model

SUBSCRIPTS

0	zero air flow
a	ambient, outside, apparent
bo	outside boundary
classical	conventional design method
cond	conduction
conv	convection
d	design, dynamic
r	room
s	scale, steady state
w	walk, wall

CHAPTER I*

INTRODUCTION

Air infiltration is defined by Liddament [1986] as "uncontrolled flow of air through penetrations in the building fabric caused by pressure differences generated across these openings by the action of wind and temperature." It has a profound influence on both the internal environment and the energy needs of buildings.

It is an intriguing task to estimate the air infiltration energy consumption of a house because of the uncontrolled nature of air infiltration and the complexity of interaction between heat transfer and air flow in building components. Consider a simplified example, in which cold air leaks from outside into a warm room through a porous insulation wall. As the air flows through the wall, it extracts heat energy from the insulation. Subsequently, its temperature goes up. When the air leaves the wall and enters the room, its temperature may be very close to the room temperature. Clearly, the room heater does not need to heat the air from the outside temperature to the room temperature because it has already captured part of the conduction heat flowing through the wall. To properly estimate house energy consumption or design the HVAC system, the air infiltration heat recovery must be accurately calculated.

It has been universally assumed when calculating the heating and cooling loads of buildings that the amount of energy required to heat (or cool) infiltration air is the same as that required to heat (or cool) outside air to the indoor conditions: this is the product of

*Journal model is ASME Journal of Solar Energy Engineering.

the specific enthalpy difference between indoor and outdoor conditions and the mass flow rate of the infiltrating air. Using this assumption, the house heat loss factor ($UA_{\text{classical}}$), defined as the energy consumption rate per unit temperature difference between room and outside is:

$$UA_{\text{classical}} = UA_o + \dot{M}C_p \quad (1-1)$$

where:

$UA_{\text{classical}}$ = heat loss factor of house when air infiltration is present ($W/^\circ C$)

UA_o = heat loss factor of house when air infiltration is not present
($W/^\circ C$)

\dot{M} = air infiltration rate (kg/s)

C_p = specific heat capacity of air ($J/kg^\circ C$).

The interaction between heat transfer and air flow is totally ignored in this equation, which is the methodology adopted in current design handbooks.

Recent theoretical studies and experimental tests [Anderlind 1985, Guo and Liu 1985, Claridge and Bhattachayya 1989, 1990, 1992] found the actual air infiltration energy consumption of windows and a test cell under laboratory conditions to be 20% to 80% of the values given by Equation (1-1). However, these studies did not investigate air infiltration energy performance under dynamic conditions, nor the effects of solar radiation on the air infiltration energy consumption.

The primary objectives of the current investigation are to experimentally investigate air infiltration energy performance under dynamic temperature conditions, and outdoor conditions. However, new methodology has to be developed in order to measure air

infiltration energy performance under outdoor conditions since current methods cannot provide the necessary accuracy. Moreover, the steady-state methodology has to be validated because actual heat transfer process is non-linear when air flow is present, consequently, it can result in systematic error. The methodology developed was used to measure air leakage heat recovery under dynamic conditions in an indoor test cell and an outdoor test cell, also suitable for making measurements of an leakage heat recovery in full-size houses. This investigation is part of a project begun at Texas A&M University in 1986 which is conducting a systematic study of air infiltration heat recovery in houses and house components.

This dissertation includes a review of the available and relevant literature, a description of the experimental facilities, discussion of the measurement results, theoretical development and experimental tests of the methodology for the dynamic full-sized houses, analytical and numerical modeling of air infiltration heat recovery in walls and attics, and concluding remarks. Chapter II summarizes the literature reviewed for this study. The review was undertaken to ascertain the current state of knowledge in the area of the air infiltration energy consumption and house thermal parameter identification. Chapter III provides the design and construction details of the experimental facilities. Chapter IV describes the methodology developed for measuring the air infiltration heat recovery in an indoor test cell under dynamic conditions as well as the outline of a methodology for an outdoor test cell under outdoor conditions. The measurement results are discussed in Chapter V for the dynamic tests performed in both the indoor test cell and the tests performed in the outdoor test cell.

Chapter VI describes an innovative method used for UA_0 identification, including the theory and an application example. The theoretical development and experimental test of the methodology for UA and solar aperture identification are given in Chapter VII. These

two chapters provide a methodology of infiltration energy performance measurement under outdoor conditions which was used to determine the results presented in Chapter V.

The outdoor experiment results suggested that air infiltration energy performance is not only dependent on the air flow rate and leakage configuration but also dependent on the solar radiation absorbed by the test cell or building. In order to confirm this discovery, the models which combine the influences of solar radiation, air infiltration, and conduction, are developed. The models, procedures, and results are discussed in Chapter VIII.

The validation of a "steady-state" methodology for use under dynamic temperature conditions was performed experimentally; however, the validation of a "steady-state" methodology suitable for use with dynamic air flow rates requires equipment that was not available for the project. Therefore, it was investigated numerically under certain idealized conditions. The theory, procedures, and results of this investigation are reported in Chapter IX. Finally, the concluding remarks are assembled in Chapter X.

CHAPTER II

LITERATURE REVIEW

Energy consumption in buildings has been extensively studied worldwide during the last two decades. Special attention has been paid to air infiltration since the Air Infiltration and Ventilation Center (AIVC) was established with the sponsorship of the International Energy Agency in 1974. Thirteen countries participate in the AIVC research. This worldwide effort has resulted in important advances in air infiltration modeling, measurement methods, air leakage reduction techniques [Charlesworth 1988, Liddament 1986, Jackman 1984, Harrje 1984, Uvslokk 1984, and Boman 1984], and measurement methods of building energy performance [Norlen 1990, Baudier 1991, and Subbarao 1988]. However, the impact of air infiltration on energy consumption in houses has received little attention.

The previous work relevant to this dissertation falls into two categories: methods for measuring the building heat loss factor (UA), and the energy impact of air flow (air infiltration heat recovery modeling and measurement).

ENERGY IMPACT OF AIR FLOW

This topic can be further subdivided into: (i) the energy impact of natural infiltration; (ii) the energy impact of ventilation; and (iii) general considerations and observations.

Energy Impact of Natural Infiltration

The energy impact of air infiltration on double frame windows, porous insulation, and wood frame walls was studied and reported by a number of researchers. Burse and Green

[1970] measured the overall heat loss factor of the double frame window with a hot box, where both infiltration and temperature difference were present. It was found that the overall heat loss factor U was 10% to 30% lower than the design calculation value. Unfortunately, due to the lack of a logical way to express this air infiltration heat recovery, it was concluded that it would be difficult to incorporate it into an industry standard. Guo and Liu [1985] did both theoretical analysis and experimental testing on double frame windows. Their work established the correction equations for U and air infiltration energy consumption, and good agreement was found between the test data and the theoretical prediction. But neither of these studies accounted for solar radiation.

Anderlind [1985] proposed concentrated-flow and diffuse-flow concepts, in which concentrated-flow (CF) was defined as a short pass flow, such as air flow through doors, windows, and large cracks or holes. Diffuse-flow (DF) was defined as the long pass flow, in which the air travels several feet before leaving the wall. Both of these definitions will be used through this thesis. Anderlind demonstrated that air infiltration heat recovery was influenced by the type of the leakage configuration. The combined heat transfer models for diffuse walls and roofs can be found in a number of different sources [Anderlind 1985, Liu 1987, Bailly 1987, Arquis 1986, and Golovkin 1960], and are almost identical. The models assume uniform infiltration, identical air and solid temperature at the same position, one-dimensional, and steady-state condition. The models were generally expressed by a simple explicit analytical formula which predicted that significant heat recovery existed in walls and roofs. Although different energy calculation methods were proposed by different authors, it seems that Anderlind gave the most logical expression:

$$Q_{inf} = R\dot{M}C_p (T_r - T_a) \quad (2-1)$$

where:

$$Q_{inf} = \text{air infiltration energy consumption (W)}$$

- R = a multiplier, which varies from 0 to 1 according to the structure of the wall with R approaching 1 for concentrated flow and zero for diffuse flow
- \dot{M} = air infiltration rate (Kg/s)
- C_p = specific heat capacity of air (J/Kg °C)
- T_r = room air temperature (°C)
- T_a = outside or ambient air temperature (°C).

Wolf [1966] developed a theoretical formula of heat conductance for fibrous insulations with air circulation, and predicted that the conductance of the insulation would increase significantly with the air circulation rate. This theory was applied to wood-frame walls [Wolf 1966], where it was found that the circulation could increase U values up to 100%. However, this study did not cover cross ventilation, or infiltration and exfiltration, which is common in real house walls.

The influence of air infiltration on the heat resistance of porous insulation materials was extensively studied [Powell 1989, Adderley 1990]. Unfortunately, these studies focused only on the relation of the insulation conductance to the air flow rate. The enthalpy change of the air flow was ignored, as was the air infiltration heat recovery.

Energy Impact of Ventilation

Ventilation has been used to reduce house energy consumption for many years. Ventilated attics, air flow windows, and dynamic walls have been studied most extensively. Attic or roof ventilation has been used as a means of reducing the solar load

of buildings for many years, but such studies ignored the influence of infiltration and the combined effects [Lamberts 1985].

Air flow windows, where either fresh or exhausted air is made to pass through the air space between panes of glass, originated in Scandinavia and have been successfully used in northern climates for almost three decades. These windows have proven useful in these cold regions by providing maximum space comfort and energy savings to building owners throughout northern and central Europe, and more recently in the northern states of the United States. Ripatti [1985] investigated the application of the air flow window in a hot climate, and found that the air flow window could provide comfortable thermal indoor conditions in both arid and tropical weathers, with lower cooling load and energy consumption.

A dynamic insulation system was proposed and studied [Timusk 1987, Mcleister 1990, Bailly 1987, Dubois 1983], where the interaction of heat and mass transfer was used to reduce the house heating energy consumption. Bailly [1987] subdivided dynamic insulation systems into three sub-systems parietodynamic, permeodynamic, and thermodynamic (Figure 2-1).

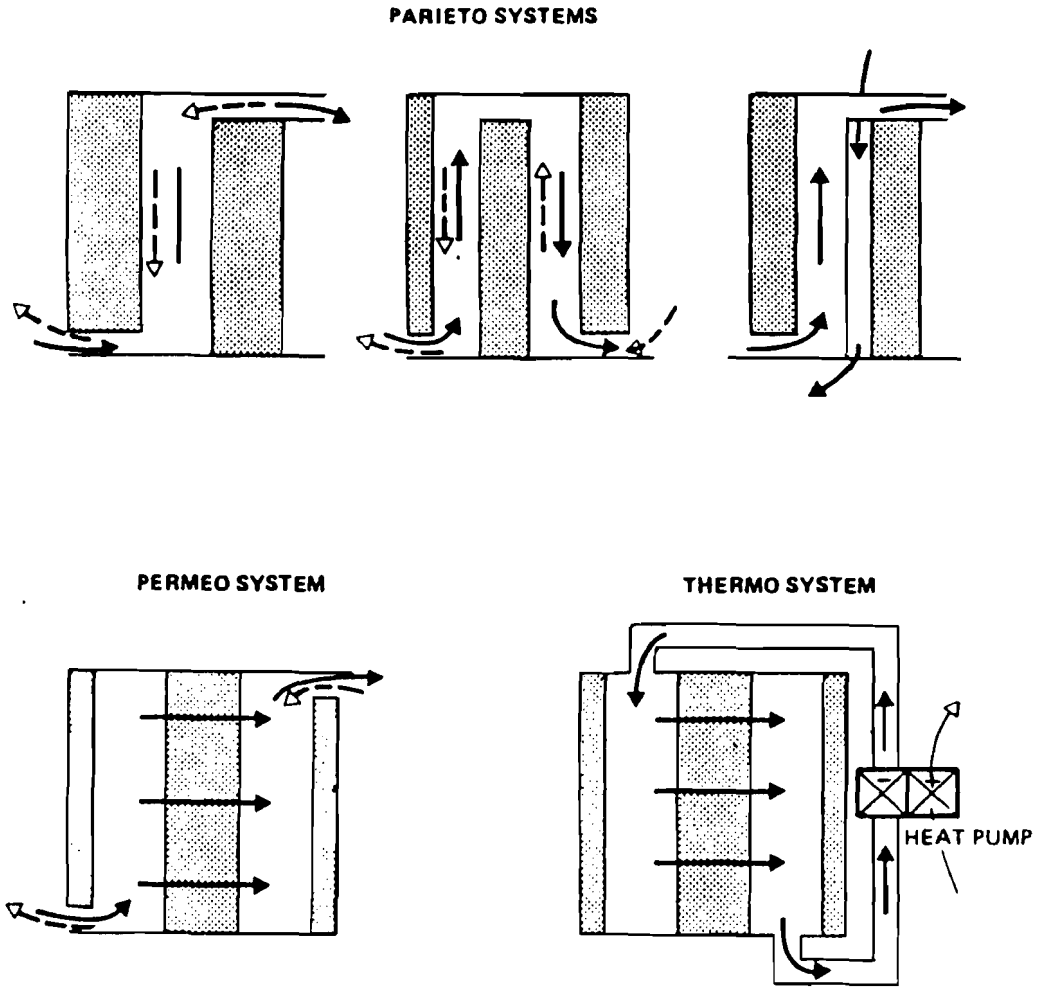


Figure 2-1: Schematic of Various Dynamic Insulations

The parietodynamic insulation system circulated the ventilation air along the wall, using either fresh or exhausted air. The fresh air was preheated before entering the room. The exhausted air increased the temperature of the solid component and reduced the conduction energy consumption. An air gap was essential for the parietodynamic insulation system.

The permeodynamic insulation system had a diffuse porous core with a cover on either side where the porous medium acted as a heat exchanger. Part of the conduction energy loss was captured by the incoming fresh air, or was blocked by the exhausted air as the air diffused through the medium.

The thermodynamic insulation system used a heat pump to capture heat energy from the air warmed by the permeodynamic insulation system and returned to the cold side of the porous medium after it passed over the heat pump evaporator. This configuration reduced air infiltration rate, but required the use of a heat pump.

Prototype dynamic insulation houses were built in France and Canada [Timusk 1987, and Bailly 1987]. Research showed 23% potential heating energy saving, but no detailed theoretical analysis was presented, and the importance of each of the weather and insulation parameters was not clear. This made it hard to apply the results to a house design.

The OPTIMA (Optimum) ceiling and floor, which evolved from the dynamic insulation concept, was tested by Andersson and Wadmark [1987] (Figure 2-2). Fresh air was taken into the house via the roof structure and infiltrated through the ceiling insulation and a control film to a collecting space in the bottom of the ceiling; from there it was let out to the living room and bedrooms by special air supply units. After using the air in these

rooms it was passed on to the bathroom, and lavatory through slots under the doors. From there, it was drawn to the main ventilator and distributed under the entire house in the upper part of the floor structure. Then it leaked through a polymer fabric to the lower part, where it was drawn upwards by an exhaust fan. The test showed that the OPTIMA ceiling and roof could recover most of the ceiling heat loss in a single family house.

Masoero and Aghemo [1985] analyzed a ventilated curtain-wall, which consisted of an internal concrete load-bearing slab, and an external concrete finish panel, separated by a ventilated air cavity that could be put in communication either with the outdoor or the indoor environment through a set of thermostatically controlled dampers (Figure 2-3). During the heating season, in the presence of sufficient solar radiation, natural circulation of indoor air takes place in the cavity. Alternatively, the component may be coupled to a mechanical ventilation system, acting as a preheater of incoming outdoor air. In the summer the air cavity is open to the outside, and the natural air circulation through the cavity removes part of the solar heat gain. The analysis showed significant energy savings, and improved comfort conditions in the unconditioned space (no heating, no cooling, no mechanical ventilation).

Homma and Guy [1979] investigated the effects of ventilation in the space between a main wall and exterior siding on the cooling load. The results showed that ventilation of this air space had the potential to reduce the radiative heat gain of both opaque walls and of triple glass windows.

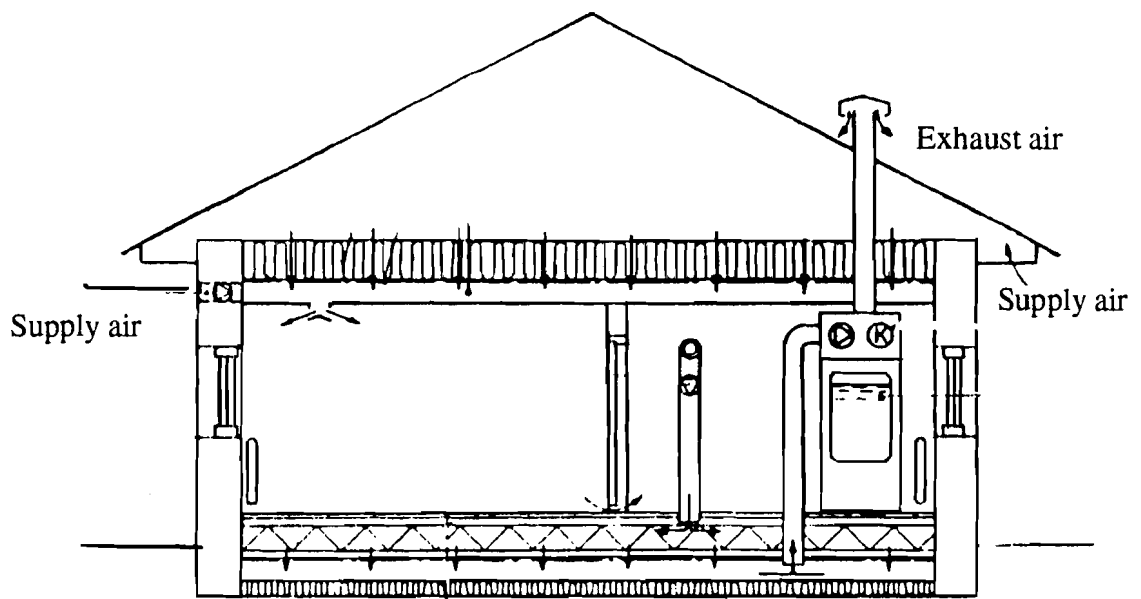


Figure 2-2: Schematic of Optimum Ceiling

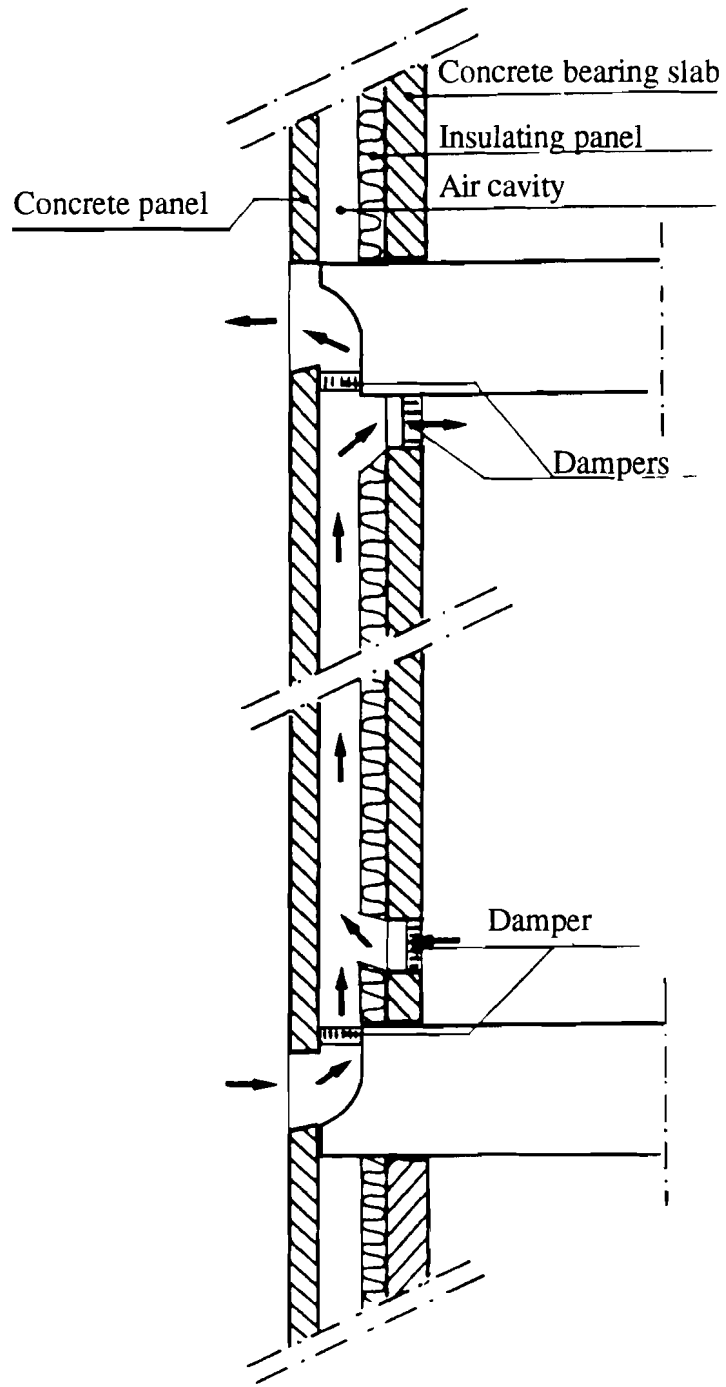


Figure 2-3: Schematic of Ventilating Curtain-Wall Component

General Consideration and Observation

Air infiltration heat recovery has been observed in numerous houses and reported to reduce loads. Beyea et al., and Harrje [1977, 1979] found that the temperature in attics was higher than that predicted by resistance models of attic insulation. Claridge et al. [1984] found that attic temperature in nine of 25 houses had less than half the temperature drop expected across attic insulation, resulting from the air bypassing the insulation. Claridge et al. [1985] also found that the predicted overall house loss factor was about 50% higher than that obtained by regressing the measured data, which could have implied that part of the infiltration energy was recovered.

Sonderegger, Condon, and Modera [1980] measured the air infiltration load with the electric co-heating method, where the air infiltration rate was given a jump up or down and the load response was monitored. It was found that the heat load responded to the infiltration rate change very slowly, with a delay of about two hours, moreover that both the peak load and total energy consumption during this dynamic period were less than the calculated values. This effect was explained as a regenerative heat exchanger. However, this was very likely caused by more solar energy gain due to the infiltrating air and air infiltration heat recovery due to interaction between conduction and air flow. Because of the relatively long time delay of the load response, it is obvious that the air infiltration was the concentrated flow (CF), so significant heat recovery should be expected for this kind of natural infiltration.

The effects of combined heat transfer on the overall building were also studied. Guo, Xu, and Li [1985] applied a double frame window model [Liu 1985] to a four story dormitory energy balance calculation, and found that the prediction and measured energy consumption agreed within 5%. The double window model was also used to optimize

window types, and leakage configurations in buildings by Liu [1986, 1987]. Kohonen, Tech, and Virtanen [1987] studied numerically and experimentally the overall energy recovery effect of air infiltration in a house. They suggested a correction factor of 0.8 for the opaque envelope conduction energy consumption for the heating season.

Recently, the combined heat transfer effects of air infiltration and conduction were studied carefully at Texas A&M for the wood frame wall both in a test cell [Claridge and Bhattacharyya 1989, 1990], and a hot box [Bhattacharyya and Claridge 1992]. The concept of Infiltration Heat Exchange Effectiveness (IHEE or ϵ) was proposed, and was defined as the fraction of the maximum infiltration energy consumption which was recovered. This is given by:

$$\epsilon = 1 - \frac{Q_{inf}}{\dot{M}C_p (T_r - T_a)} \quad (2-2)$$

where:

- ϵ = infiltration heat exchange effectiveness
- Q_{inf} = heat loss due to air infiltration (W)
- \dot{M} = air flow rate (Kg/s)
- C_p = specific heat of air (J/Kg $^{\circ}$ K)
- T_r = room temperature ($^{\circ}$ C)
- T_a = outside or ambient air temperature ($^{\circ}$ C).

The studies revealed that the IHEE was dependent on both the air flow rate and air leakage configuration with measured values from 0.05 to 0.9 for an indoor test cell and from 0.16 to 0.7 for a stud cavity wall. It was inferred that significant energy recovery existed in actual houses. IHEE will be used throughout this thesis as the quantitative measure of infiltration heat recovery.

This literature survey reveals that significant air infiltration heat recovery has been reported by a number of researchers from different subjects, such as windows, walls, simple test cells, and full-sized houses. However, the theoretical studies are limited to idealized components and steady-state conditions. The experimental studies were limited to either a steady state laboratory condition or a rough overall measurement, that gave a single saving number for a long period. Although it was recognized that the air infiltration energy consumption is a complicated non-linear process, the energy performance under weather or dynamic conditions was not investigated. Likewise, no measurements or analysis of the impact of solar radiation on the air flow infiltration energy consumption was reported.

MEASUREMENT OF HOUSE THERMAL PERFORMANCE

House thermal performance is generally characterized by its heat loss factor (steady-state parameter) defined as the heat loss rate under unit temperature difference between house and ambient, and its transfer function (dynamic parameters), which relates the house energy consumption to indoor temperature and weather parameters by a set of coefficients. The typical methods for building thermal performance measurement [Reddy 1989, Rabl 1988] include co-heating, equivalent thermal parameter, Auto-Regression Moving Average (ARMA) or Z-transfer function, and calibrated computer simulation method; some other methods are also available, such as the differential equation, and artificial neural networks methods.

Co-Heating Method

Co-heating is a well-known method [Sonderegger 1979, Fang 1985] for measuring house heat loss factors. It replaces the heating system with an electric heater and maintains the house temperature as constant as possible during the measurement. This method has short period and long period options. The short period option determines UA from average heat input and temperature difference during a night period when the outside temperature is relative stable. Thermal storage often causes severe problems for this option. The long period option determines UA using the average parameter values of house temperature, ambient temperature, solar radiation, and heat input of a period from few weeks to few months. Solar treatment is difficult and floor heat transfer presents problems for this approach.

Sonderegger, Condon, and Modera [1979, 1980] applied short term option of Co-Heating to measure the furnace efficiency, the heat loss factor, and the air infiltration load in a house. The measured UA values had 28% variation between different tests. Feuermann [1989] applied long term option of Co-Heating to a single unit in a multifamily building and concluded that this method was highly intrusive. It required use of the apartment for approximately one month, and the cooperation of the tenants of the neighboring apartments.

Subbarao [1990] proposed a method to improve the electric co-heating accuracy by introducing a computer-generated correction term to the energy balance equation, which was based on an audit of the house. However, no real house results are as yet available. Improvements are needed in terms of better treating effects such as thermal storage, solar radiation, and floor heat transfer problems, as well as reducing testing length.

Equivalent Thermal Parameter (ETP) Method

ETP is the most widely used method today. It represents the building by a basic physical equation of an electrical circuit. The coefficients of the basic equation are estimated by fitting the measured inputs and outputs, such as solar radiation, outside temperature, room temperature, and power, to the basic equation. Sonderegger [1978] and Nielsen [1985] used this method for houses, Penman [1990] used it on a working school, while Hammarsten, Hattem and Colombo [1988] applied this method to an outdoor test cell. Baudier and Marchio [1991] applied the state space technique to treat the equivalent circuit. Hammarsten [1985] used frequency domain analysis to identify a model for the energy performance of five houses. The researchers claimed that the time periods required for model identification were ten to fifteen days. Generally, no attempt was made to estimate the house heat loss factor.

Recently, Norlen [1990] pointed out that the ETP method could not describe both the steady-state and dynamic thermal characteristics, and that the models were very hard to explain physically because of the arbitrary choice of the model. In fact, the model choice depended mostly on experience or a rule of thumb if no experience is available. Generally, the identification was done by regressing the room temperature against outside temperature, horizontal solar-radiation/south vertical solar-radiation, and heat gain. Because of the correlation of solar radiation and air temperature, the improper parameter estimations could result from using this method. Also, solar radiation was improperly treated in this method, because the impact of solar radiation on a house depends not only on south or vertical solar radiation, but also on the window distribution, surface color, and etc., which vary from house to house.

ARMA or Transfer Function Method

The time series or Auto-regression Moving Average (ARMA) method is the most attractive because it can identify both steady-state and dynamic parameters. This method regards the system as a black box linear system. Subsequently, the input and output can be expressed by an ARMA model. The measured input and output data pairs are used to estimate the coefficients of the ARMA model. The order of the ARMA model is automatically determined by the optimum regression. Norlen [1990] used this method for test cell parameter identification. His test showed reasonable agreement of measured parameters with expected values, when three weeks were used for the model identification. However, this long time period could cause severe problems, such as non-constant parameter system (that is the air infiltration variation can cause a large variation in the heat loss factor). It should be noted that the regression used correlated inputs rather than independent inputs, which violates the basic regression assumption. Also, the determination of the order of the system often lacks a physical basis because the best fit sometimes gives non-physical parameter estimates. Therefore, this regression estimation process is likely to generate unreliable parameter estimates.

Barakat [1987] investigated the cooling-load Z-transfer function coefficients due to solar gain input as well as due to the room-air transfer function coefficient by using a special outdoor test house facility. This facility consisted of three one-story insulated wood-frame buildings with basements. For the solar transfer function experiments, the shade on the south window was totally or partially removed on a sunny day to allow solar gain through the window for 1 hour. This created a 1-hour solar input pulse on the room. The magnitude of the pulse (size of the opening) was chosen so that the room-air temperature would not exceed the set point temperature. All the parameters, including the electric heating power consumption for the room, were measured every five-minute. Mid-

hour values were used for analysis. For the room-air temperature function experiments, the window remained fully shaded and an additional electric heater, placed in the center of the unit, was started at the prescribed time during the night, and kept on for three or four hours, causing the room to overheat. The temperature rise above the reference value is the output response. The coefficients of the transfer function of the room temperature vs the weather were regressed first, then they were used to generate the response of the impulse power and the solar input by subtracting the weather response from the measured total room response. Finally, the coefficients of the transfer function were determined by multiple linear regression. The adequacy of these coefficients was checked by using them to predict the power consumption during an other period.

Improvements for this method are needed in order to overcome the effects of inter-correlated inputs, and the requirement of long stream data collection.

Calibrated Computer Simulation Method

Although it was impossible to get exact house information, the general information could be gotten by investigating the house or by checking the house design plan. These kinds of information can be served as program inputs, then the house thermal parameters can be estimated by a normal simulation calculation. Based on the simulation results, the overall thermal parameters can be deduced, such as the transfer functions between heat input and house temperature, between solar radiation and house temperature, between outside temperature and house temperature, and over all heat loss factor, and the house system may be also simplified to a network with few storage capacities and few resistances. The thermal parameters estimated by this method may not be accurate, but they can serve as valuable reference values in most cases, so the house parameters can be identified by using short term measurement data to modify the simulation results because

the numbers of the thermal parameters have greatly reduced. This is called the calibrated computer simulation method.

PSTAR [Subbarao 1988] is one of the calibrated computer simulation method, which requires an audit description first, then the audit description is renormalized by the measured data. This method has been simplified to measure the house heat loss factor [Subbarao 1990].

All the physical models currently used in simulation programs are classical, and no interaction between the air infiltration and conduction is considered. Therefore, use of these models to deal with air infiltration heat recovery measurement is likely to lead to errors unless all parameters are kept constant during the measurement.

Artificial Neural Network

The artificial neural network [Wang and Kreider 1990] is a new tool for building energy predictions. The neural network predicts future values by identifying operation model. This approach does not currently provide physical models. Therefore, it is not appropriate for building thermal parameter estimation.

Recently, Reddy [1989] evaluated the ETP, ARMA, and time derivative methods with data obtained in three test houses. He concluded that the time derivative approach had poor parameter identification capabilities. He also found that the ETP might not be suitable for the inverse model identification due to lack of a systematic procedure for identifying the most appropriate network, while ARMA had the potential to overcome these drawbacks. Rabl [1988] reviewed the measurement methods, such as ETP, model analysis, differential equation, ARMA model, Fourier series, and calibrated computer

simulations (such as PSTAR). He also concluded that the ARMA method was most suitable for numerical work, and that the differential equation approach was most powerful because it could be integrated analytically. He pointed out that a good fit could be obtained with incorrect parameters in a real building. The poor estimation may result from a poor solar aperture model, the correlation of solar radiation and temperature, and the lack of the understanding of the air infiltration model. Although Reddy and Rabel did not agree on the advantages of the differential equation method, both advocated the ARMA or transfer function method.

LITERATURE SUMMARY

Over a dozen studies which have directly and indirectly investigated infiltration heat recovery have been reviewed. These papers clearly show, based on analysis, steady-state measurements, and inferences from occupied building data, that infiltration heat recovery can be significant. However, no outdoor tests have been performed, nor were comparisons of dynamic and steady-state results reported. The theoretical models do not include solar radiation. Therefore this study was initiated as an attempt to fill in that void.

Six methods for determining building thermal parameters have been reviewed. None of these methods can be used directly to measure house thermal performance from two to three days without systematic error, due to thermal storage, floor heat transfer, and/or inter-correlated input problems. Furthermore, all of the methods were developed based on the linear system assumption; however, a building thermal envelope cannot be regarded as a linear system when interaction of air infiltration and conduction is considered. A new measurement method is needed.

CHAPTER III

EXPERIMENTAL FACILITY

A series of experiments was devised to 1) measure the IHEE (infiltration heat exchange effectiveness) under both dynamic and steady-state conditions, and compare the results; 2) measure the IHEE in an outdoor test cell; and 3) develop a measurement methodology for IHEE in full-size houses. To perform the above tasks, an indoor test cell built for steady-state measurement [Claridge and Bhattacharyya, 1989] was modified, and an outdoor test cell was built at the Texas A&M Riverside Campus. The design and construction details of each facility are described below:

INDOOR TEST CELL

The test cell was constructed using standard frame construction for the six walls, ceiling, and floor surfaces. This construction consisted of:

- 1 cm (3/8 inch) plywood sheathing
- 5x10 cm (2x4) studs on 40-cm (16-inch) centers
- R-11 fiberglass batt insulation between the studs
- 1 cm (3/8 inch) plywood sheathing

The external measurements of the test cell are 1.43 m (56.5 inches) wide by 1.2 m (48 inches) high by 2.4 m (96 inches) long. Each surface was constructed separately, and then all six surfaces were bolted together and caulked. One of the 1.43 m (56.5 inches) by 1.2 m (48 inches) end-walls contained a removable 0.6 m (24 inches) square window glazed with 1 cm (3/8 inches) Plexiglas and covered by polystyrene weather shield insulation.

The test cell has two holes for concentrated flow: hole "A", which is 5 cm (2 inches) in diameter, and hole "P", which is 1.3 cm (1/2 inch) in diameter. Moreover, each wall has a diffuse entry hole on the interior plywood panel, and one diffuse exit hole on the exterior plywood panel at diagonally opposite corners. The schematic of the hole position is given in Figure 3-1. The sheathing is fully caulked so most of the air flow must traverse the entire distance from the diffuse entry hole to the diffuse exit hole. These holes were used to simulate the following air leakage configurations in tests:

- (1) diffuse flow wall (DF): no holes open except "P" in the walls, air introduced to test cell through hole "P";
- (2) quasi-diffuse flow wall (QDF): diffuse holes open, air introduced to test cell through hole "P";
- (3) concentrated flow (CF): air exhausted through hole "A", air introduced through hole "P"; and
- (4) double flow (DDF): walls configured as in case 2, but air is introduced through the diffuse holes in two side walls, and leaked out through the others.

This test cell was initially built and used for the IHEE measurement under steady state conditions [Claridge and Bhattacharyya 1989, 1990]. It has been modified for use in the dynamic tests. The rota-meter was replaced by two calibrated orifices (1 cm and 1.5 cm in diameters respectively, 0.02 to 0.8 l/s and 0.8 to 2.75 l/s in air flow rate ranges respectively), to permit essentially continuous measurement of the air flow rate, and the internal heating system was modified to provide more uniform temperature distribution and permit a high accuracy measurement of heat input (Ohio Semielectric, GW5, accuracy ± 5 W). The room temperature was measured by ten type-T thermocouples surrounding the test cell to provide a better measurement of mean room temperature. The schematic

$$\frac{T - T_w}{T_r - T_w} = \frac{1 - e^{-m_c R}}{1 - e^{-m_c R_w}}$$

for T inside wall

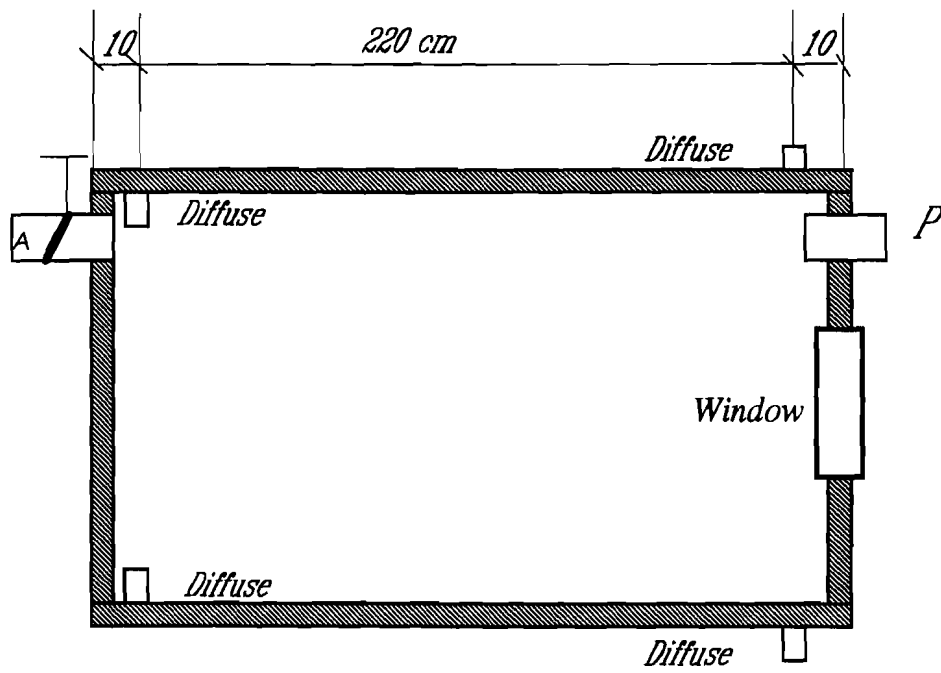


Figure 3-1: Schematic of Hole Positions for Indoor Test Cell

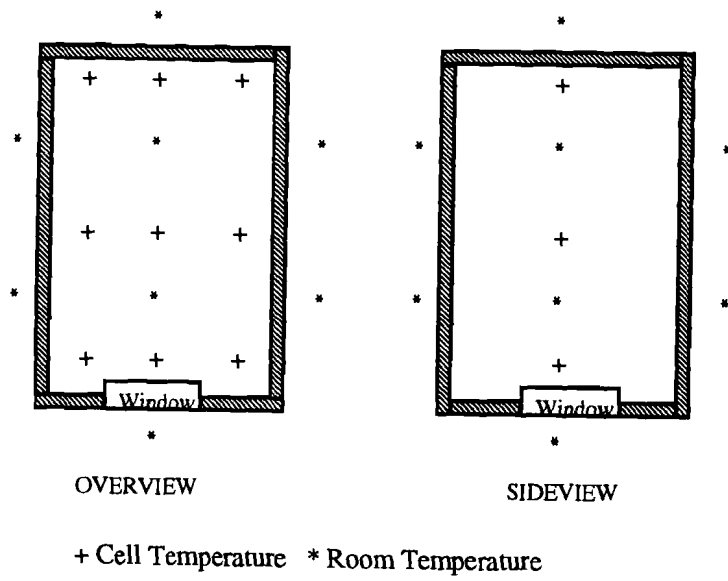


Figure 3-2: Schematic of Thermocouple Positions for Indoor Test Cell

of the thermocouple position is shown in Figure 3-2. Use of a computer data acquisition system (Acurex, Netpac) permitted high frequency data sampling with high accuracy.

OUTDOOR TEST CELL

The outdoor test cell, built especially for air infiltration heat recovery measurement in 1990, is located at the Texas A&M Riverside Campus. The cell is a 2.4 meter cube (8 feet) topped with a small attic. It is supported by 4 jacks, and painted white on both the interior and exterior. The walls are the standard 5x10 cm (2 x 4) frame construction (studs on 40 cm centers) with exterior plywood, R-11 insulation, and interior plywood. The ceiling and the roof are constructed of plywood, with R-19 insulation, attic air space, plywood, and asphalt roofing. The gable of the attic is made of a single 1.3 cm (1/2 inch) plywood sheet. The schematic of the test cell is shown in Figure 3-3.

Each wall has 16 pre-cut diffuse holes (1/2 inch in diameter). The north wall has two more holes. Hole "A" (10 cm or 4 inches in diameter) served as the air outlet/inlet. Hole "B" (5 cm or 2 inches in diameter) served as the concentrated flow path. Also, a quarter of the north wall was cut out and modified to as the access door. This door left a 1 cm wide straight crack surroundings, which was used to simulate the crack flow. The schematic of the north wall and the diffuse holes are shown in Figure 3-4.

These specific constructions of the test cell permit simulation of the four air leakage configurations:

- (1) concentrated flow (CFO) (air introduced/exhausted through hole "A", hole "B" open, diffuse holes blocked, and the cracks sealed);

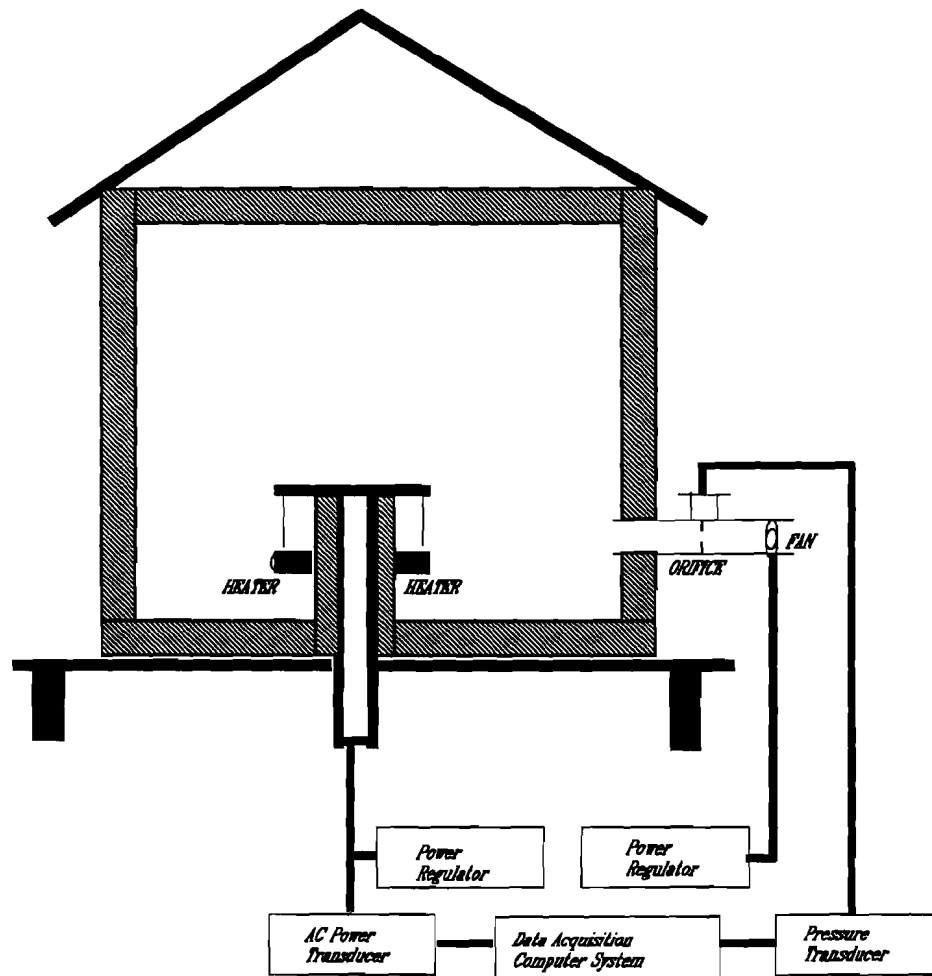


Figure 3-3: Schematic of the Outdoor Test Cell

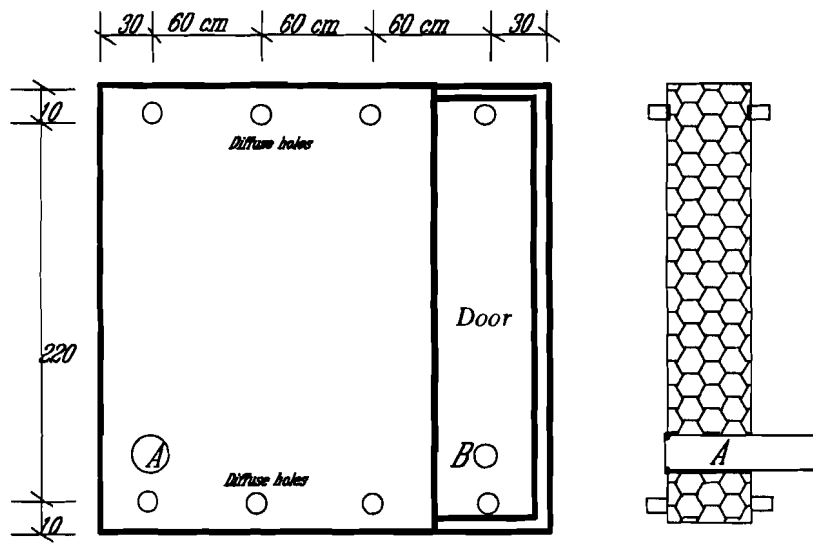


Figure 3-4: Schematic of the North Wall

- (2) diffuse flow (DFO) (air introduced/exhausted through hole "A", hole "B" closed, "diffuse" holes blocked, and "cracks" sealed);
- (3) quasi-diffuse flow (QDFO) (air introduced/exhausted through hole "A", hole "B" closed, "diffuse" holes open, and "cracks" sealed); and
- (4) large crack flow (LCFO) (air introduced/exhausted through hole "A", hole "B" closed, "diffuse" holes blocked, and "cracks" unsealed).

The cell mass temperatures were monitored by a total of 220 type T thermocouples (40 in each wall and floor, and 20 in the ceiling) stuck on the plywood surfaces inside the walls, roof, and floor. The average value measured by these sensors was used as the test cell mass temperature. The schematic of the thermocouples is shown in Figure 3-5.

The test cell air temperature was measured by 12 thermocouples, which were uniformly distributed inside the cell. The schematic of these thermocouples is shown in Figure 3-6.

Both the natural and mechanically induced pressures on the test cell envelope were monitored at 17 positions, shown in Figure 3-7. Each wall had four positions spaced equally on the out-surface of each facet. The average facet pressure was measured in experiments because the dominant factor was wind. One position was in the middle height of inside the test cell, and represented the pressure induced by the air flow. A total of five pressure transmitters (Modus, Model T20, Full scale -50 Pa to +50 Pa) were used to measure the pressure. The maximum natural pressure difference defined as the difference of the maximum and the minimum pressure on the four facets was used to check the validity of the test. If the maximum natural pressure was close to the

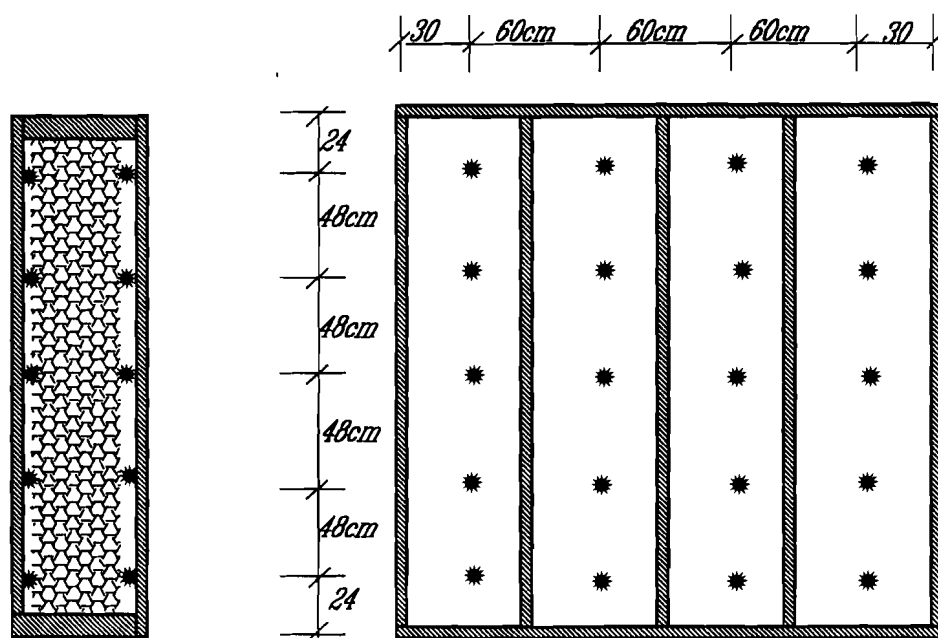


Figure 3-5: Schematic of Thermocouple Positions for Outdoor Test Cell

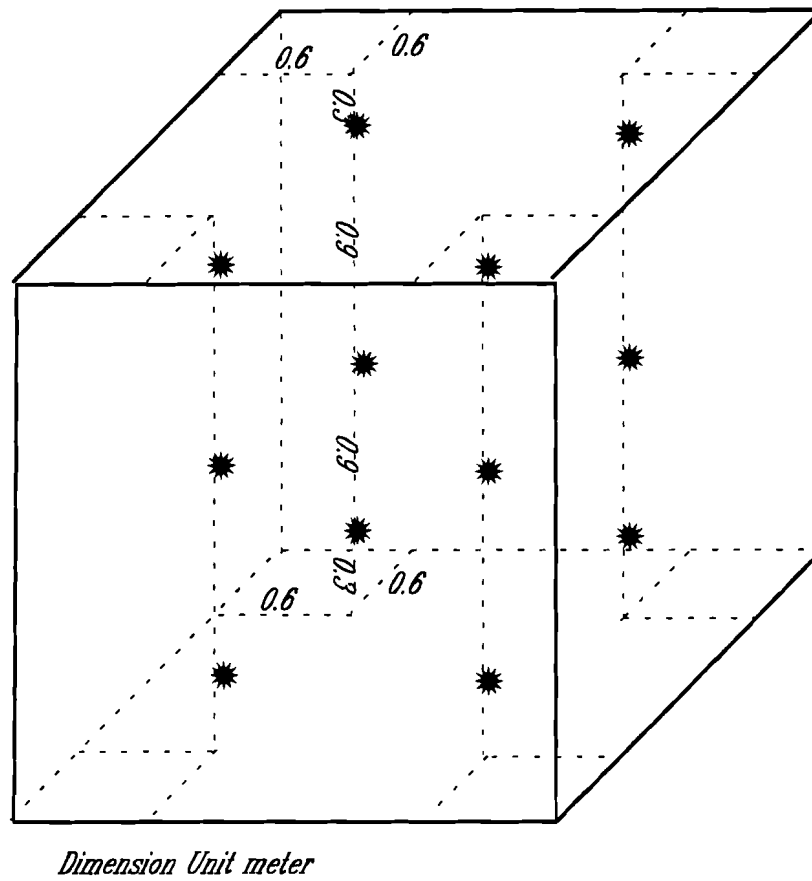


Figure 3-6: Schematic of Thermocouple Positions for Room Temperature Measurement

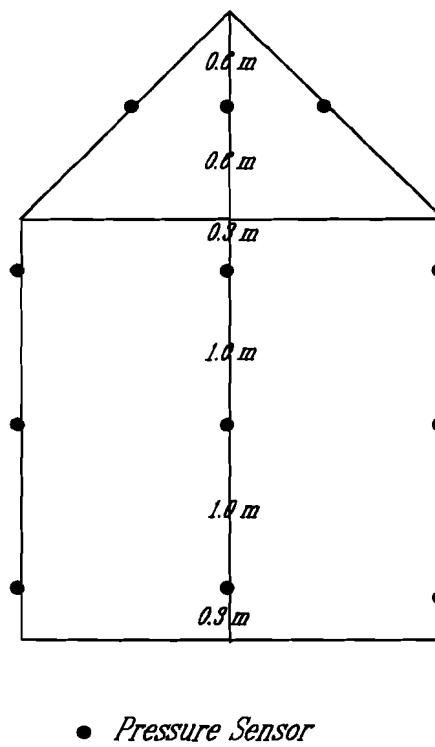


Figure 3-7: Schematic of Pressure Sensor Distribution

mechanical pressure, then the expected air flow model was deemed questionable, and the test needs to be rerun.

The outside temperature was measured by two well-shielded type T thermocouples located north of the cell. The horizontal solar radiation was measured by a Pyranometer on-site, and the air flow rate was controlled by a fan (ITT 34739-0031, Flow rate 0.07 m³/s) with the flow rate measured by an orifice (Calibrated in the Texas A&M University, Energy Systems Laboratory). The power was supplied by a heater with a 0 to 500 W adjustable range and was measured by a power transducer (Ohio Semielectric Model GW 5, Accuracy 1%).

A data acquisition system (Acurex Netpac, 100 Channels) was used to couple the sensors and a computer, where the signals were sampled, pre-calculated, and finally recorded in the computer. All the signals were sampled, converted to necessary engineering units every 10-second, and time average values over 10-minute interval were recorded on a hard disk in LOTUS format. The description of signal channels is given in Table 3-1 for instant sampling value and Table 3-2 for integrated value.

A special control room was built to serve the data acquisition system, the computer, the pressure sensors, and the power regulator. The control room was conditioned to provide a 18 °C to 25 °C temperature environment for the data acquisition system.

Table 3-1: Description of Data Acquisition Sensor Channels

#Ch	Signal	Unit
000	Cell Temperature at Top Position	°C
001	Cell Temperature at Middle Height	°C
002	Cell Temperature at Lower Position	°C
003	Attic Temperature	°C
004	Average Ceiling Temperature, Surface of the Plywood	°C
005	Average Floor Temperature, Outer Plywood Sheathing	°C
006	Average Floor Temperature, Inner Plywood Sheathing	°C
007	Average North Wall Temperature, Outer Plywood Sheathing	°C
008	Average North Wall Temperature, Inner Plywood Sheathing	°C
009	Average East Wall Temperature, Inner Plywood Sheathing	°C
010	Average East Wall Temperature, Outer Plywood Sheathing	°C
011	Average South Wall Temperature, Inner Plywood Sheathing	°C
012	Average South Wall Temperature, Outer Plywood Sheathing	°C
013	Average West Wall Temperature, Inner Plywood Sheathing	°C
014	Average West Wall Temperature, Outer Plywood Sheathing	°C
015	Air Flow Temperature by Orifice	°C
018	Control Room Temperature	°C
019	Outside Air Temperature	°C
020	Heating Power	W
021	Pressure Created by Air Flow	Pa
022	Pressure Difference Between North Wall & Control Room	DC V
023	Pressure Difference Between South Wall & Control Room	DC V
024	Pressure Difference Between East Wall & Control Room	DCV
025	Pressure Difference Between West Wall & Control Room	DCV
027	Solar Radiation Horizontal Surface	W/m ²
028	Solar Radiation South Vertical Wall Surface	W/m ²
029	Pressure Across Orifice	DCV
030	Pressure Difference Between North Wall & Control Room	Pa
031	Pressure Difference Between South Wall & Control Room	Pa
032	Pressure Difference Between East Wall & Control Room	Pa
033	Pressure Difference Between West Wall & Control Room	Pa
034	Pressure Difference Cross Orifice	Pa
035	Air Flow Rate Calculation	NA
036	Air Flow Rate	CFM
037	Average Room Temperature	°C

Table 3-2: Data Acquisition Channels for Period Integrated Signals

#Ch	Signal	Unit
039	Air Flow Temperature	°C
040	Heating Power	W
041	Air Flow Rate	CFM
042	Cell Temperature	°C
043	Outside Air Temperature	°C
044	Horizontal Surface Solar Radiation	W/m ²
045	Skip	
046	House Pressure Created by Air Flow	Pa
047	Pressure Difference Between North Wall & Control Room	Pa
048	Pressure Difference Between South Wall & Control Room	Pa
049	Pressure Difference Between East Wall & Control Room	Pa
050	Pressure Difference Between West Wall & Control Room	Pa
051	Attic Air Temperature	°C
052	Ceiling Temperature, Surface of the Plywood	Pa
053	Floor Temperature, Outer Plywood Sheathing	Pa
054	Floor Temperature, Inner Plywood Sheathing	Pa
055	North Wall Temperature, Outer Plywood Sheathing	Pa
056	North Wall Temperature, Inner Plywood Sheathing	Pa
057	East Wall Temperature, Inner Plywood Sheathing	Pa
058	East Wall Temperature, Outer Plywood Sheathing	Pa
059	South Wall Temperature, Inner Plywood Sheathing	Pa
060	South Wall Temperature, Out Plywood Sheathing	Pa
061	West Wall Temperature, Inner Plywood Sheathing	Pa
062	West Wall temperature, Out Plywood Sheathing	Pa
063	Control Room Temperature	°C

CHAPTER IV

EXPERIMENTAL METHODOLOGY FOR TEST CELLS

Two different test methods were developed for the indoor and outdoor test cells because of the distinctive test objectives and different ambient conditions. Each is described in this Chapter.

METHODOLOGY FOR INDOOR TEST CELL

A procedure for measuring IHEE under both dynamic and steady-state temperature conditions was developed to ensure determination of comparable results from both steady-state and dynamic conditions.

The system was calibrated before the dynamic tests were performed. The system calibration investigated the test cell temperature rise due to the radiation reception from room lighting. The cell and room temperatures were measured continuously for a week with the room illuminated by lights day and night. It was found that the average test cell temperature was 0.4 °C higher than average room temperature due to the light radiation absorbed by the test cell surfaces. This average temperature difference was defined as systematic error (δT_{se}).

The dynamic tests measured air infiltration heat recovery under both steady-state and dynamic conditions by following the standard test profile shown in Figure 4-1. This dynamic temperature profile consists of three periods:

- (1) a 24-hour period (SS-1) where 250 watts of heating is supplied continuously until the cell reaches a quasi-steady state;
- (2) a dynamic period where heat input is switched off and on at 3-hour intervals for a total of 15 hours; and
- (3) a second quasi-steady period (SS-2), where 250 watts heat input is supplied for 36 hours until the cell again reaches a quasi-steady state.

The total heat loss factor can be calculated according to the following formula for different periods:

$$UA = \frac{\sum_{i=1}^k Q(i) - UA_o \delta T_{se}}{\sum_{i=1}^k \Delta T(i)} \quad (4-1)$$

$$UA_{\text{classical}} = UA_o + \dot{M}C_p \quad (4-2)$$

where

- UA = total heat loss factor (conduction and infiltration) (W/°C)
- Q = heat input (W)
- UA_o = heat loss factor when air infiltration is not present (W/°C)
- δT_{se} = systematic error of the system (°C)
- ΔT = average temperature difference between cell and laboratory
- UA_{classical} = calculated heat loss factor based on the design method
- Ṁ = air leakage rate (Kg/s)
- C_p = specific heat capacity of air (J/Kg°C)
- i = time (hour).

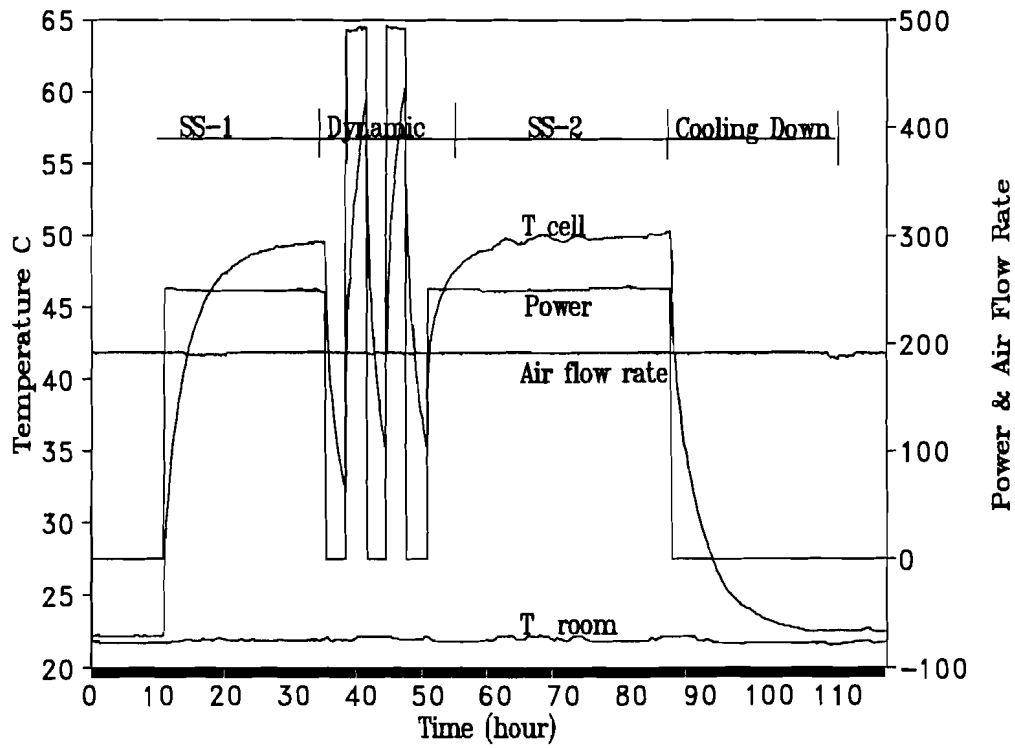


Figure 4-1: Schematic of Dynamic Test Profile for Indoor Test Cell

Using this equation, both UA and $UA_{\text{classical}}$ can be calculated from the first quasi-steady state period, dynamic period, and the second quasi-steady state period. The difference between UA and $UA_{\text{classical}}$ is called air infiltration heat recovery, which can be expressed as a portion of $\dot{M}C_p$ or a portion of $UA_{\text{classical}}$.

$$IHEE = \frac{UA_{\text{classical}} - UA}{\dot{M}C_p} \quad (4-3)$$

$$\beta_e = \frac{UA_{\text{classical}} - UA}{UA_{\text{classical}}} \quad (4-4)$$

IHEE is called infiltration heat exchange effectiveness since it quantitatively represents effects of interaction between air infiltration and conduction. β_e is called the energy saving ratio because it is the total energy recovery over the classical energy consumption.

The IHEE tests were carried out for the following four leakage configurations (defined in Chapter III.): DF, QDF, CF, and DDF. Tests were performed at non-dimensional air flow rates (defined as the ratio of $\dot{M}C_p$ to UA_0) from 0.05 to 0.2 for DF (diffuse leakage) configuration, but a single flow rate of 0.2 was used for the rest of the leakage configurations.

METHODOLOGY FOR OUTDOOR TEST CELL

The indoor steady-state tests [Claridge and Bhattacharyya 1989, 1992] proved that IHEE was affected by the air flow rate and leakage configurations. However, the solar radiation and air flow direction may also influence IHEE under outdoor conditions since the solar energy gain may be influenced by the air flow direction. The following procedure

was developed to measure IHEE in an outdoor test cell. The theoretical basis for this procedure, called the short term average method (STAM), is developed in Chapter VII.

The tests consisted of three phases: determination of the solar contribution; determination of the heat conductance; and air infiltration heat recovery tests. The solar contribution was defined as the cell temperature rise due to unit solar radiation on the cell when no air infiltration was present. It was determined from a seven-day test with no heat input and the cell tightly caulked using:

$$\delta T_{\text{sol}} = \frac{\sum_{i=1}^k T_r(i) - T_a(i)}{\sum_{i=1}^k I(i)} \quad (4-5)$$

where:

- δT_{sol} = solar contribution to the cell temperature ($^{\circ}\text{C}/\text{W}/\text{m}^2$)
- T_r = cell air temperature ($^{\circ}\text{C}$)
- T_a = outside temperature ($^{\circ}\text{C}$)
- I = equivalent solar radiation on the cell (W/m^2)
- i = time index of a 10-minute time period (1 beginning, k ending).

It should be noted here that the solar radiation used in the equations could be either the horizontal solar radiation or equivalent solar radiation defined as the ratio of total solar reception on the cell to the exterior area (See Chapter VII and Appendix A3).

The heat loss factor due to conduction (UA_0) was measured using data from a week long test with a constant heat input and the following formula:

$$UA_o = \frac{\sum_{i=1}^k q(i)}{\sum_{i=1}^k [T_r(i) - T_a(i) - I(i)\delta T_{sol}]} \quad (4-6)$$

where:

q = heat input (W)

UA_o = heat loss factor due to conduction only (W/°C)

Other symbols have been defined in Equation (4-5).

The constant heat input and air flow rate were given for each air infiltration heat recovery test. Then the heat loss factor of the test cell was calculated by using the following formula for a selected period:

$$UA = \frac{\sum_{i=1}^k [q(i) - UA_o I(i)\delta T_{sol}]}{\sum_{i=1}^k [T_r(i) - T_a(i)]} \quad (4-7)$$

where:

UA = heat loss factor (conduction plus infiltration) of the test cell (W/°C).

Then the infiltration heat exchange effectiveness (IHEE) and the energy saving ratio (β_e) can be calculated using Equations (4-3) and (4-4).

In order to eliminate the thermal storage effects, the time period must be chosen according to the following rules (See Chapter VII):

- (1) both the beginning and the end should be between 11:00 p.m. to 6:00 a.m.;
- (2) the test cell temperature difference between the start and the end should be less than 0.1 °C; and
- (3) The moving average ambient and test cell temperatures from 1 to k with window width of the period length should be constant. The theoretical basis for this selection is described in Chapter VII.

The tests were performed on four different leakage configurations (DFO, CFO, QDFO, and LCFO), defined in Chapter III with different air flow rates under both infiltration and exfiltration conditions.

Each test was performed with a constant heat input 250W. There was no control on the test cell temperature. Consequently, the variation of the test cell temperature was dependent on the ambient temperature and solar radiation. The average test cell temperature was about 8 to 12 °C higher than average ambient temperature.

The test data were analyzed by the program "OUTCELL.FOR" using the method developed in Chapter VII. The simplified block diagram is given in Figure 4-2, and the source code is listed in Appendix B1.

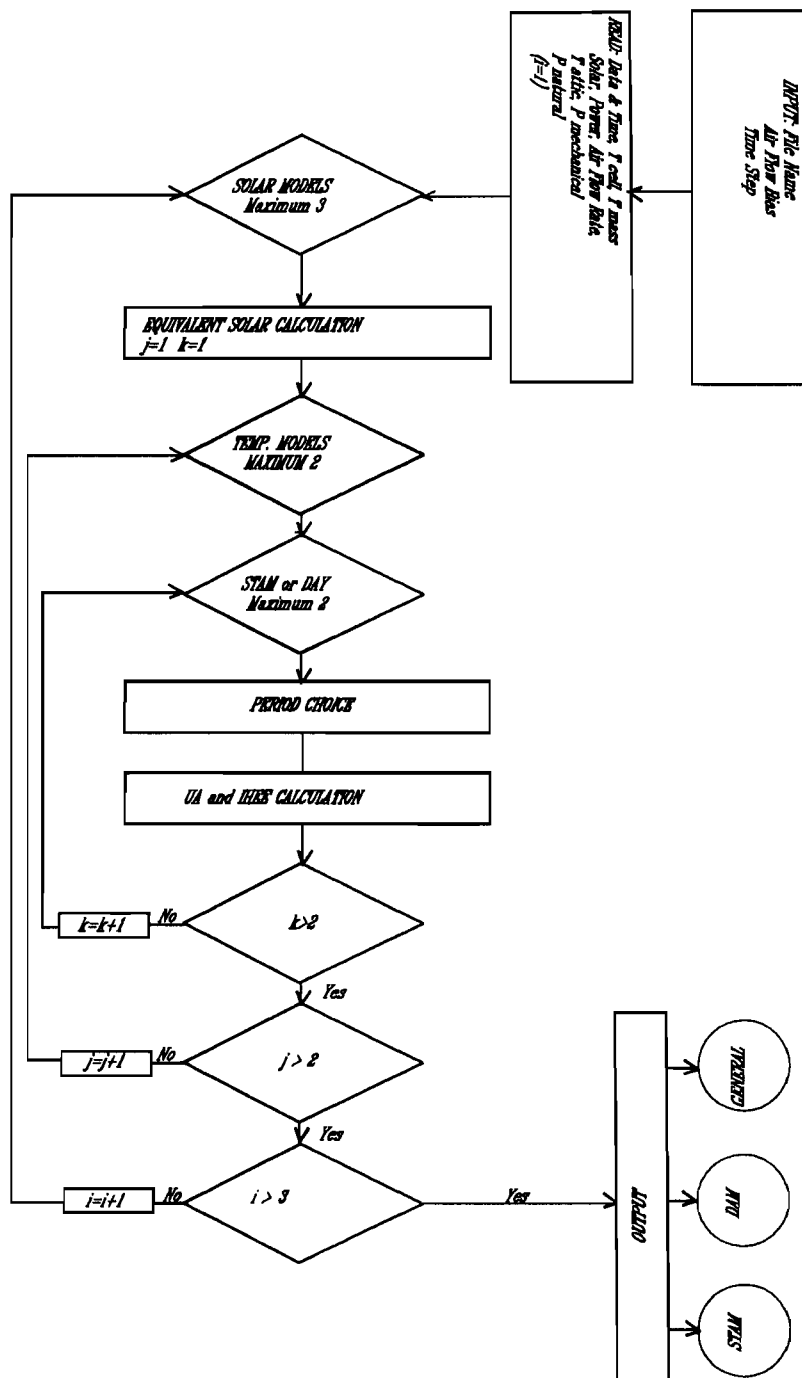


Figure 4-2: Simplified Block Diagram of "OUTCELL.FOR"

CHAPTER V

MEASUREMENT RESULTS

The air infiltration heat recovery was measured with four different air leakage configurations and different air flow rates under both the dynamic and steady-state conditions in the indoor test cell, and with four different air leakage configurations and different air flow rates from summer of 1990 to autumn of 1991 on the outdoor test cell. The results are reported in this chapter, including IHEE and energy saving ratio. The effects of dynamic temperature profile, leakage configuration, air flow rate, air flow direction, and solar radiation on the air infiltration heat recovery are discussed based on the measurement results.

The measured values of air infiltration heat recovery are generally shown as a function of a non-dimensional air flow rate which is a major influence factor to air infiltration heat recovery. The non-dimensional air flow rate [Anderlind 1985] is defined as the ratio of the product of air flow rate and heat specific of air to the heat loss factor due to conduction only.

$$\alpha = \frac{\dot{M}C_p}{UA_0} \quad (5-1)$$

\dot{M} is air flow rate, C_p is specific heat of air, and UA_0 is heat loss factor without air infiltration. For typical leakages in buildings, α will be less than unity. It will exceed unity only when classical air leakage gains/losses exceed conduction gains/losses. The IHEE values of the idealized diffuse wall (Chapter VIII) with zero solar radiation are also labeled as "**Model**" in the corresponding figures. Next two sections describe general results only. The fundamental explanation will be given in the discussion section.

INDOOR CELL TESTS AND RESULTS

A total of ten tests were performed on the indoor test cell. Each test took seven days and had similar test profile shown in Figure 4-1. The laboratory room temperature was controlled to have a average value of 21°C with $\pm 1^\circ\text{C}$ variation. The test cell temperature varied from 21°C to 60°C when the test cell was heated up. Data were analyzed using the methodology described in Chapter VI for the indoor cell test.

Figure 5-1 shows measured IHEE results of the diffuse leakage configuration for the indoor cell test, which was intended to investigate the effects of the dynamic temperature profile. The symbol "SS-1" represents the results from the first steady-state period, "Dynamic" from the dynamic period, and "SS-2" from the second steady-state period shown in Figure 4-1, and linear regression of the measured IHEE values gave the "Regression". The results show clearly that the IHEE decreased with increasing air flow rate, and there seems to be no systematic difference between IHEE values between dynamic and steady-state conditions for the same air flow rate.

Figure 5-2 shows both the heat loss factor and energy saving ratio of the diffuse leakage configuration for indoor cell test. The symbols used in this figure are the same as in Figure 5-1. The $UA_{\text{classical}}$ is the heat loss factor calculated as the sum of UA_0 and MC_p . The figure shows clearly that the actual heat loss factors are always smaller than the design values, and the energy saving ratio increased with increase in the air flow rate because infiltration energy consumption becomes more important with increasing air flow rate. The figure shows also that the UA from the "SS-1" has the maximum value and UA from "SS-2" has the minimum value for the same air flow rate. Because the chronological order of the periods was SS-1, Dynamic, and SS-2, it was concluded that the UA values decreased with time after the test was started.

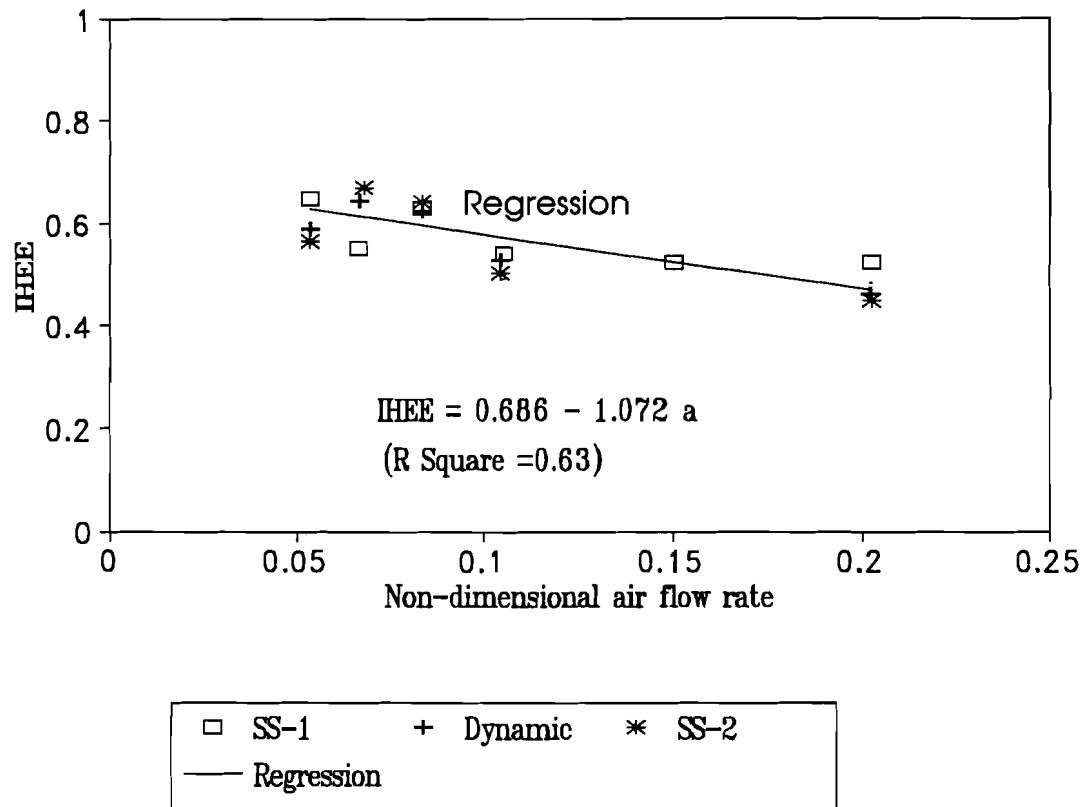


Figure 5-1: IHEE Comparison for Diffuse Leakage Configuration
 SS-1- First steady-state period; Dynamic - Dynamic period;
 SS-2 - Second steady-state period; Regression - Regression results;
 (Measurement Uncertainty Varies from $\pm 34\%$ to $\pm 15\%$ with Increasing Air Flow Rate)

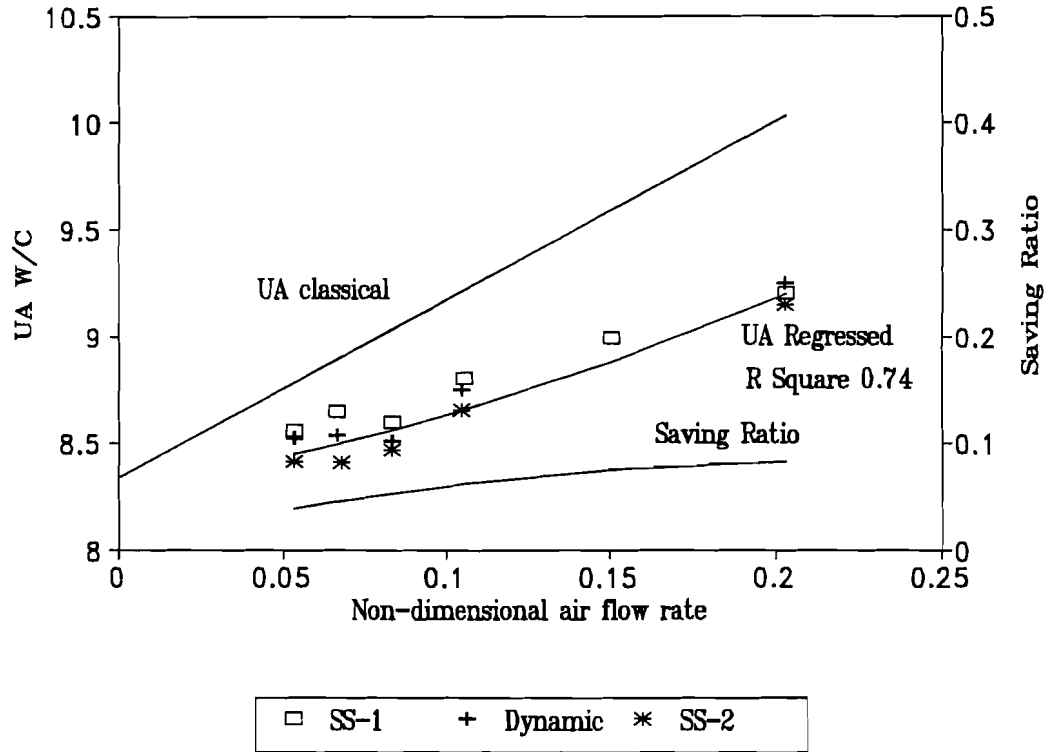


Figure 5-2: Heat Loss Factor Comparison for Diffuse Leakage Configuration (Measurement Uncertainty: $\pm 6\%$)

Figure 5-3 shows the measured IHEE values in indoor test cell for different air leakage configurations with a non-dimensional air flow rate of 0.2. Case 1 refers to the concentrated leakage configuration, case 2 to the diffuse leakage configuration, case 3 to the quasi-diffuse leakage configuration, and case 4 to the double flow leakage configuration. The legends used here are the same as in Figure 5-1, and "Limit" refers to the value calculated by a diffuse wall model. These leakage configurations were defined in Chapter 3. The results show that the concentrated leakage configuration had smallest IHEE value (0.25), double flow leakage configuration had largest IHEE value (0.84), while the diffuse and quasi-diffuse leakage configurations are essentially similar (0.46).

Figure 5-4 shows both measured UA values and energy saving ratio in the indoor test cell with a non-dimensional air flow rate of 0.2. The symbols used in this figure are the same as in Figure 5-3. The numerical results show that the actual heat loss factors are smaller than designed values for all the four leakage configurations. The energy saving ratio changes significantly with the leakage configuration. The concentrated leakage configuration had the smallest value of 0.05, double flow had the largest value of 0.14, and diffuse and quasi-diffuse leakage configuration had moderate value of 0.08.

It was very interesting that both the diffuse and quasi-diffuse leakage configurations showed similar heat recovery results although the quasi-diffuse leakage configuration had the diffuse holes open. Since the open status of the diffuse holes could only result in a possible corner to corner flow within the walls, the area affected by the air infiltration was essentially the same as that in the diffuse flow case. Therefore, it was generalized that the heat recovery is dependent on the ratio of the air flow rate to the area affected by the air infiltration.

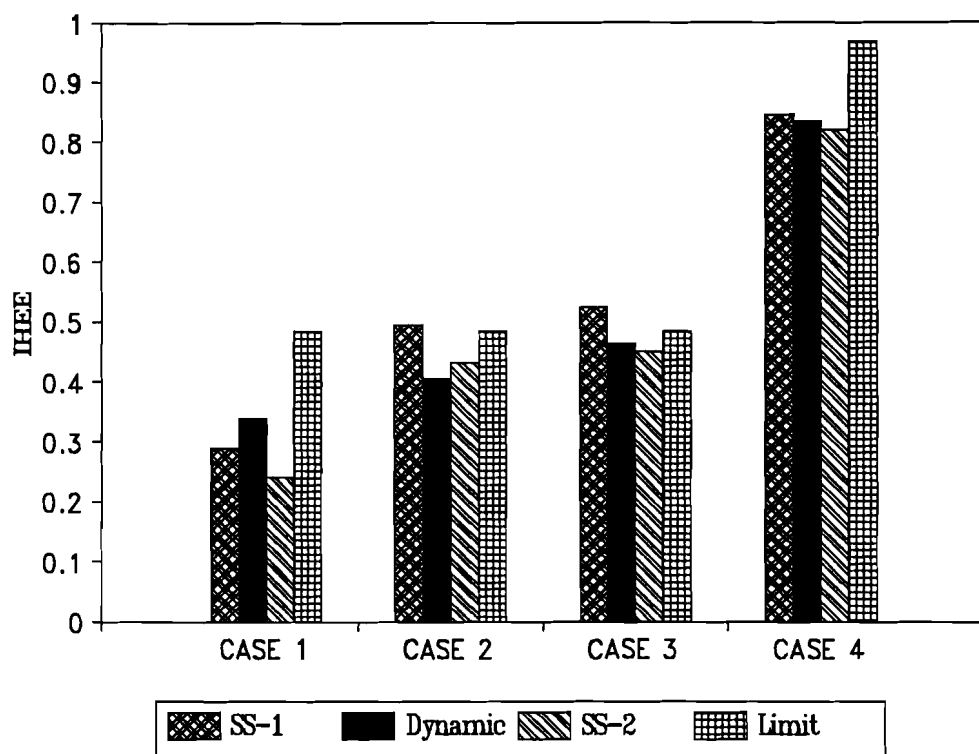


Figure 5-3: IHEE Comparison for Different Leakage Configurations
 Case 1 - Concentrated flow; Case 2 - Diffuse flow;
 Case 3 - Quasi-diffuse flow; Cases 4 - Double flow.
 (Measurement Uncertainty: $\pm 15\%$)

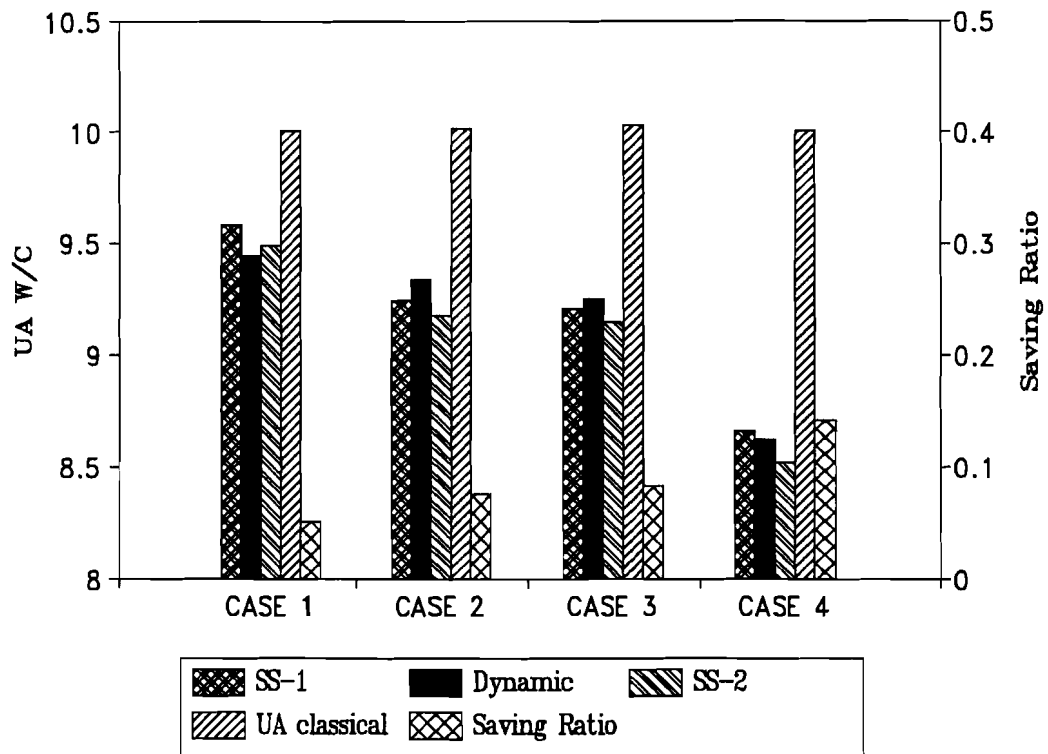


Figure 5-4: Heat Loss Factor Comparison for Different Leakage Configurations
 Case 1 - Concentrated flow; Case 2 - Diffuse flow;
 Case 3 - Quasi-diffuse flow; Case 4 - Double flow
 (Measurement Uncertainty: $\pm 6\%$)

OUTDOOR CELL TESTS AND RESULTS

Tests were performed from summer of 1990 to autumn of 1991. However, data used here are from the tests performed during 1991 because the tests performed in 1990 were used to validate the methodology (Chapter VII). Each test took a minimum of 2-day period to a maximum of 7-day period and had a constant air flow rate and heat input about 250W. The average temperature of the test cell was about 8 °C to 10 °C higher than average ambient temperature. Data were analyzed using Short Term Average Method (STAM) developed in Chapter VII.

Figure 5-5 shows IHEE results of the diffuse leakage configuration for the outdoor cell test. IHEE changed from 0.53 to 0.4 when the non-dimensional air flow rate varied from 0.4 to 1.4 for infiltration flow, and from 0.4 to 0.3 when the non-dimensional air flow rate changed from 0.6 to 1.1 for exfiltration flow. IHEE decreased with air flow rate for both the infiltration and exfiltration air flow, and the infiltration air flow had higher IHEE than the exfiltration air flow does. It also seemed that IHEE from the exfiltration air flow decreased with the air flow rate faster than those from the infiltration air flow. The differences of the IHEE value and the trend between the infiltration and exfiltration air flow might be caused by the different energy gain due to solar radiation because the infiltrating air could carry more solar energy into the test cell than could the exfiltrating air. The wide scatter of IHEE values might be due to measurement error and the different solar radiation levels during different measurement periods. IHEE is influenced by solar radiation and the figure shows only the dependence on flow rate; it does not account for the impact of the solar radiation. The idealized wall model simulation (Chapter VIII) shows that IHEE can have a change of 0.1 when solar radiation has variation of 25W/m^2 .

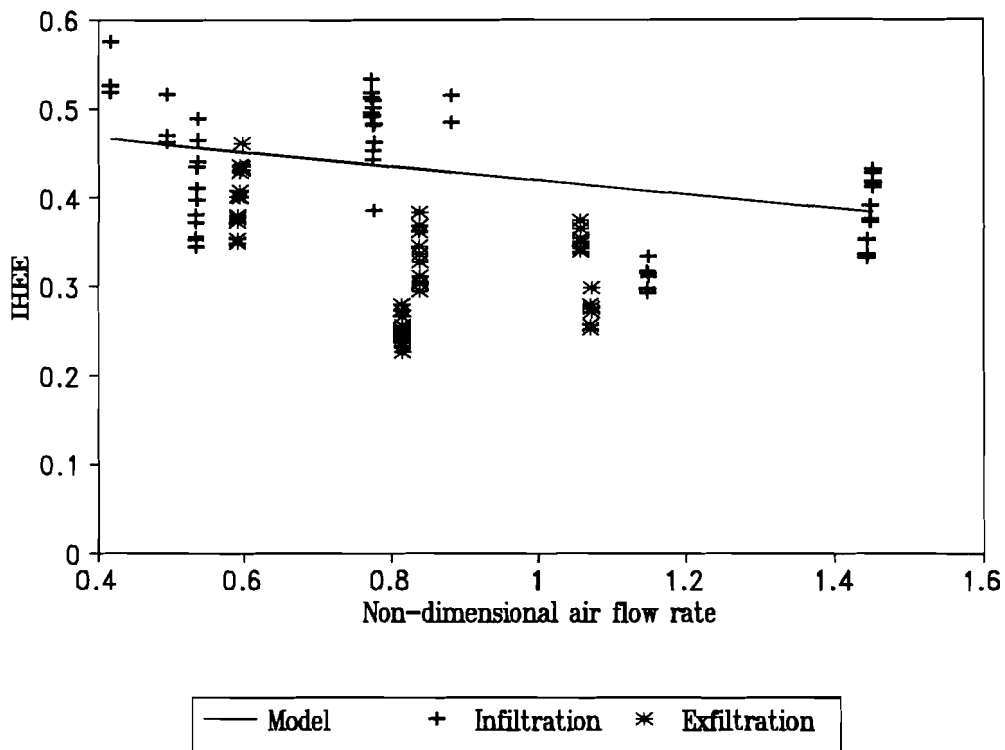


Figure 5-5: IHEE for Diffuse Leakage Configuration
 (Model - Steady-state diffuse wall model)
 (Measurement Uncertainty Varies from $\pm 26\%$ to $\pm 16\%$ with Increasing Air Flow Rate)

Figure 5-6 shows the energy saving ratio results of the diffuse leakage configuration for the outdoor cell test. The energy saving ratio changed from 0.17 to 0.25 for the infiltration flow when the non-dimensional air flow rate varied from 0.4 to 1.4, and from 0.15 to 0.16 for the exfiltration flow when the non-dimensional air flow rate varied from 0.6 to 1.1. The figure shows that the energy saving ratio increased with the air flow rate increase for the infiltration flow because air infiltration energy consumption becomes more important with increasing air flow rate, and more energy can be recovered by the air infiltration.

Figure 5-7 shows the IHEE results of the concentrated leakage configuration for the outdoor cell test. IHEE changed from 0.37 to 0.35 for the infiltration flow, and from 0.33 to -0.12 for the exfiltration flow when the non-dimensional air flow rate changed from 0.7 to 1.4. The negative IHEE value (-0.12) was very likely due to exfiltration air rejecting more solar radiation energy to the outside because the solar radiation was much stronger than in other two tests (equivalent solar radiation was 80 W/m^2 , while it was 40 W/m^2 for other two tests).

Figure 5-8 shows measured energy saving ratio results of the concentrated leakage configuration for the outdoor cell test. The results show 0.15 to 0.2 total energy savings for the infiltration flow and 0.14 to -0.08 energy savings for the exfiltration flow when the non-dimensional air flow rate varied from 0.7 to 1.4. In this case, the energy saving ratio increased with increasing air flow rate for the infiltration flow, and decreased with the increasing air flow for the exfiltration flow. This might reflect that the solar energy contribution is strongly dependent on the air flow direction.

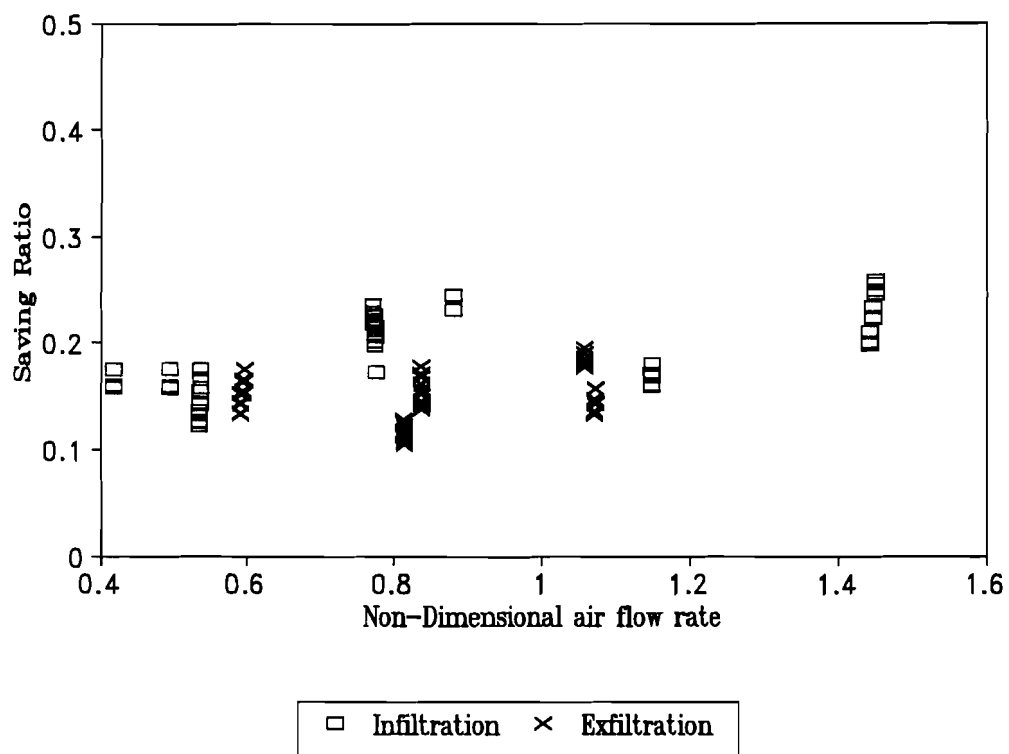


Figure 5-6: Total Energy Saving Ratio for Diffuse Leakage Configuration
(Measurement Uncertainty: $\pm 9\%$)

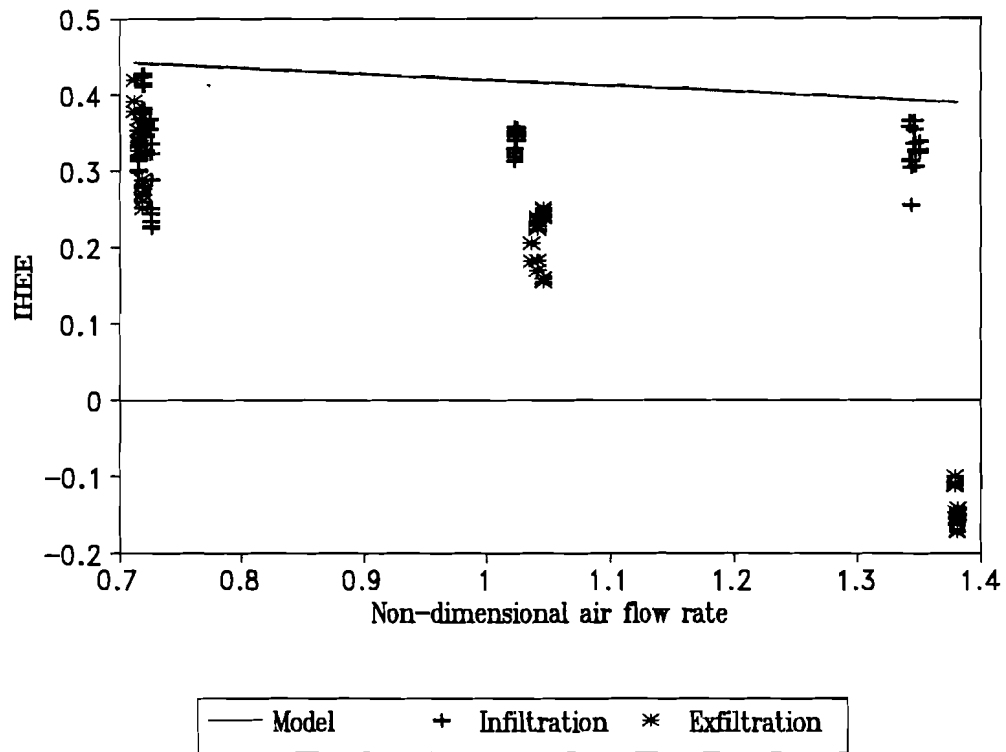


Figure 5-7: IHEE for Concentrated Leakage Configuration
(Model - Steady-state diffuse wall model)
(Measurement Uncertainty Varies from $\pm 20\%$ to $\pm 16\%$ with Increasing Air Flow Rate)

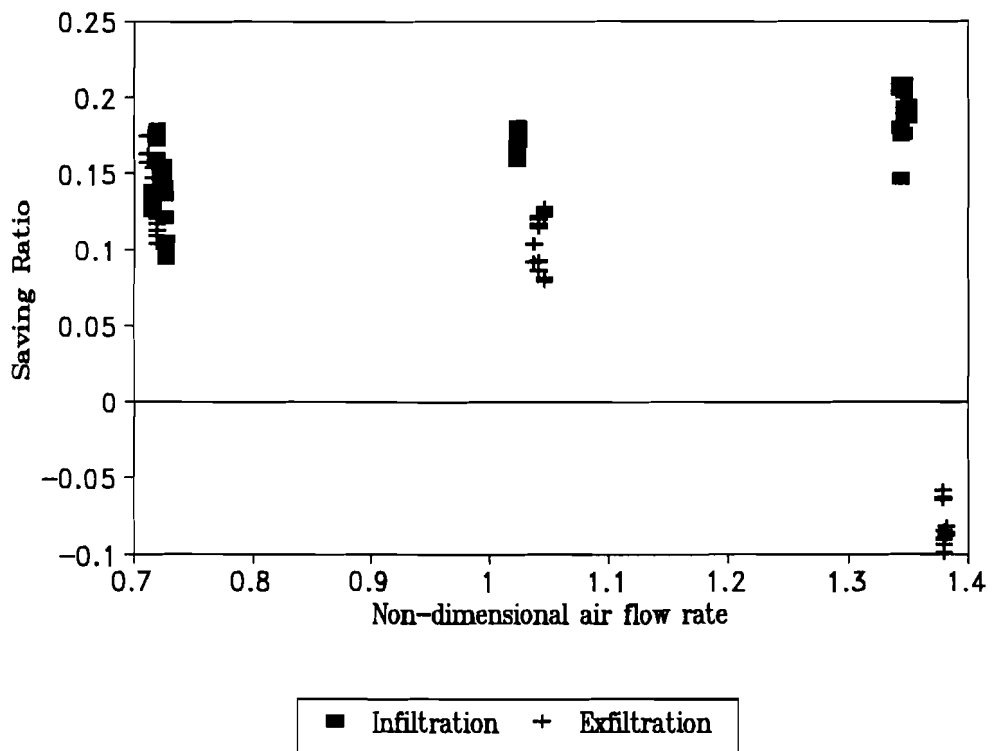


Figure 5-8: Total Energy Saving Ratio for Concentrated Leakage Configuration
(Measurement Uncertainty: $\pm 9\%$)

Figure 5-9 shows the measured IHEE of the crack leakage flow for the outdoor test cell. IHEE changed from 0.31 to 0.24 for the infiltration flow and from 0 to -0.07 for the exfiltration when the non-dimensional air flow rate varied from 0.4 to 1.3. This big difference in the IHEE values between infiltration and exfiltration flow might be due to that infiltration carried more solar energy into the test cell consequently it reduced heating load.

Figure 5-10 shows energy saving ratios from 0.05 to 0.15 for the infiltration flow and -0.05 to -0.012 for the exfiltration flow when the non-dimensional air flow rate is varied from 0.4 to 1.3. The energy saving ratio increased with increasing air flow rate for the infiltration flow and decreased with increasing air flow rate for the exfiltration flow. This is an important indicator of the heat recovery impact of solar radiation.

Figure 5-11 shows the measured IHEE results of the diffuse leakage configuration for the outdoor cell test. In this case, only the exfiltration flow is investigated. The IHEEs are shown as a function of both equivalent solar radiation and air flow rate in the figure. The IHEE corresponding to zero solar radiation was measured from a single night period. IHEE decreased dramatically with increasing solar radiation, and decreased slightly with increasing air flow rate. However, the effects of the air flow on the IHEE increased with increasing solar radiation. This figure was created by an interpolating procedure between measured data. The relationship of the solar radiation and the IHEE seems worth investigating further since this test showed promising benefit.

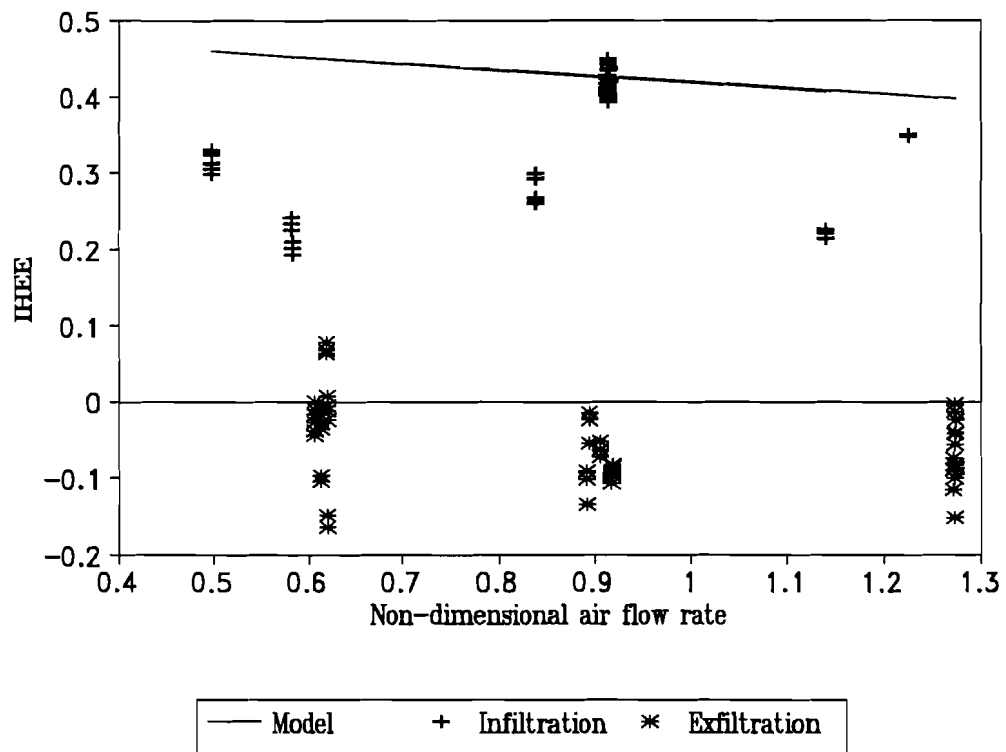


Figure 5-9: IHEE for Crack Leakage Configuration
 (Model - Steady-state diffuse wall model)
 (Measurement Uncertainty Varies from $\pm 26\%$ to $\pm 16\%$ with Increasing Air Flow Rate)

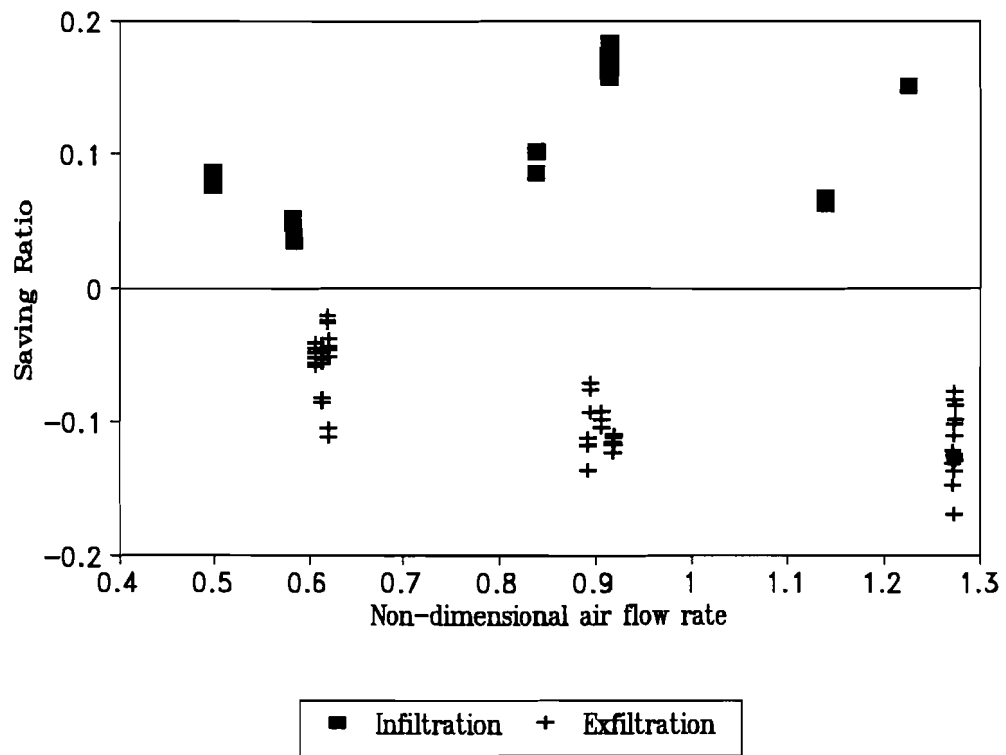


Figure 5-10: Total Energy Saving Ratio for Crack Leakage Configuration
(Measurement Uncertainty: $\pm 9\%$)

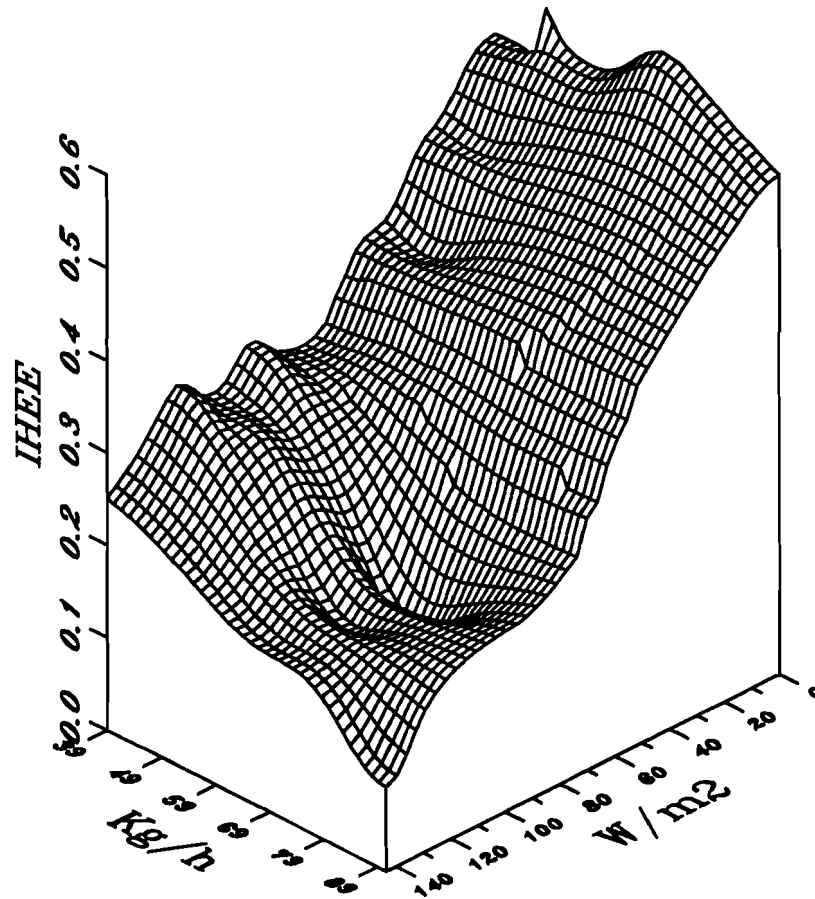


Figure 5-11: IHEE vs Equivalent Solar Radiation and Air Infiltration Rate for Quasi-Diffuse Leakage Exfiltration Configuration
(Test Cell Was Pressurized by Fan)
(Measurement Uncertainty Varies from $\pm 26\%$ to $\pm 16\%$ with Increasing Air Flow Rate)

The larger scatter of both IHEE and energy saving ratio values in Figures 5-5 to 5-10 might be mainly due to the variation of the solar radiation since these figures do not show the impact of solar radiation. This hypothesis was confirmed by idealized combined solar radiation, air infiltration, and conduction models (developed in Chapter VIII) for walls and attics, which show that IHEE can have a change of 0.1 if the solar radiation has a change of 25 W/m^2 .

The measurement results are also summarized in Appendix B5, where the test cell temperature, ambient temperature, equivalent solar radiation, air flow rate, heat input, IHEE, and energy saving ratio are given for each test.

DISCUSSION

The measurement results show that air infiltration heat recovery is dependent on a number of factors, which include air flow rate, air flow direction, solar radiation, and air leakage configuration. There is another concern about the dynamic performance of air infiltration heat recovery, namely the effect due to the variation of ambient temperature because the heat transfer process cannot be treated as linear due to the interaction between conduction heat transfer and air flow. All of these questions are further discussed below.

Effects of Dynamic Temperature Profile

In order to investigate the effects of a dynamic temperature profile on the air infiltration heat recovery, both the IHEE and total energy saving ratio were measured under different leakage configurations, air flow rates, and under both dynamic and steady state conditions. The results (Figures 5-1 to 5-4) show that the UA value from the first steady-state period was the maximum, that from the dynamic period was intermediate, and

the UA value from the second steady-state period was the minimum. Since the chronological order of the periods was the first steady-state, the dynamic, and the second steady-state periods, this difference of the UA values for the different periods could be explained by time varying properties of the test cell.

In fact, the moisture content of the test cell changed with time after the test was started because the temperature of the test cell varied significantly. If it is assumed that the test cell had a temperature of 20°C (293°K), and a moisture content ω g/m³ before the test, and 40°C (313°K) during the test then the moisture content of the test cell would be only 94% of ω because of the decrease in density of air inside. Because this moisture change could not be accomplished within the test cell materials in a short period, this may have resulted in a gradual change of the UA value over the course of a seven-day experiment.

The test results of different leakage configurations show no systematic difference between steady-state and dynamic conditions. The consistence of the dynamic and steady-state energy performance can be theoretically explained by the differential equation deduced in Chapter IX for an ideal diffuse wall.

$$\rho C \frac{\partial T}{\partial \tau} = k \frac{\partial^2 T}{\partial x^2} - \dot{m} C_p \frac{\partial T}{\partial x} \quad (5-2)$$

where:

- ρ = specific density of solid wall material (Kg/m³)
- C = specific heat capacity of solid wall material (J/Kg °C)
- T = temperature (°C)
- τ = time (s)
- k = heat conductance of solid wall material (W/m °C)

- x = dimensional of wall (m)
 \dot{m} = air infiltration rate ($\text{Kg/m}^2 \text{ s}$)
 C_p = specific heat capacity of air ($\text{J/Kg } ^\circ\text{C}$).

If air flow rate was constant, then Equation (5-2) is a linear second order partial differential equation. Consequently, the diffuse wall can be taken as a linear system so that no matter what the temperature profile, no systematic difference should exist between steady-state and dynamic conditions. Although the leakage configurations investigated in this study were not those of an ideal diffuse wall, it seemed that this conclusion did apply to them as well. Therefore, it was concluded that the house envelope can be treated as a linear system. Consequently the time average technique or steady-state method can be used for data processing without introducing systematic error as soon as the air flow rate is constant.

Effects of Leakage Configuration

Both the indoor and the outdoor test results demonstrated that the diffuse leakage configuration recovers more energy than the other leakage configurations do. The indoor test cell results show that the IHEE was about 0.84 for the double diffuse wall flow, 0.46 for the diffuse and quasi-diffuse flow, and 0.25 for the concentrated flow (see Figure 5-3). The corresponding energy saving ratios are 5% for the concentrated leakage configuration, 8% for the diffuse and quasi-diffuse leakage configuration, and 14% for the double flow leakage configuration (see Figure 5-4). If 0.84 (or 14%) was taken as the IHEE (or energy saving ratio) of a well built and maintained house, and 0.25 (or 5%) was taken as the IHEE (or energy saving ratio) of a poorly built and leak house, then the air infiltration energy consumption of the well-built house would be only 35% of that of leaky

house. The well-built house would consume 9% less energy than the leaky house, even if both have same amount of fresh air.

The outdoor test results show that the IHEE values (0.52 to 0.4 for the infiltration flow, and 0.4 to 0.3 for the exfiltration flow, see Figure 5-5) of the diffuse leakage configuration were much higher than those of both the concentrated and crack leakage configurations (IHEE values from 0.35 to -0.15, see Figure 5-7 and 5-8) since the uniform diffuse flow had higher energy exchange effectiveness if the wall was regarded as a heat exchanger. These numbers demonstrated that if a house was constructed to have such a tight structure that the air leaked in through half of the building envelope and diffused out through another half, the house was likely to have a IHEE from 0.92 to 0.7 under the weather conditions similar to those under which the tests were done. If a house was constructed such that crack leakage is dominant, it was assumed to have a IHEE from 0.1 to 0. Obviously, a leaky house could consume as much as 9 times more air infiltration energy as that of a tight house.

The outdoor test results showed that the total energy saving ratios were about 0.15 to 0.25 for the diffuse infiltration, 0.10 to 0.20 for the diffuse exfiltration, 0.10 for the crack infiltration, -0.10 for the crack exfiltration, 0.15 for the concentrated infiltration, and 0.10 for the concentrated exfiltration. From these results, it was inferred that if the test cell had diffuse infiltration over half of the envelope and diffuse exfiltration over the other half, then it was assumed that the energy saving ratio could be up to 35%. However, the test cell might have an energy saving ratio less than zero if the air leaked in through big cracks in the walls without incident solar radiation and leaked out through sunny walls. Obviously, houses could have very different energy consumption due to the air infiltration configurations even if the houses had the same geometrical profile, the same level of insulation, and the same weather.

Similar heat recovery effects (IHEE and energy saving ratio) were observed for the diffuse and the quasi-diffuse leakage configurations (see Figures 5-3, and 5-4). This result might suggest that the air infiltration heat recovery depends on the ratio of area affected by the air flow to the air flow rate. This ratio was the same for these two cases although the quasi-diffuse leakage configuration had diffuse holes open; therefore, a corner to corner flow might be present.

Effects of Air Flow Rate

The results of both the indoor and outdoor tests showed that the IHEE decreased with increasing air flow rate in all the leakage configurations. The results of the diffuse leakage configuration (Figure 5-1) showed that the IHEE changed from 0.65 to 0.5 when the non-dimensional air flow rate changed from 0.05 to 0.2 for the indoor cell test. The outdoor test results showed that the IHEE decreased with the air flow rate in all the leakage configurations, and the slope was very close to the slope of IHEE from an idealized diffuse wall steady-state model.

The indoor test results showed that the total energy saving ratio changed from 0.05 to 0.08 when the non-dimensional air flow rate varied from 0.05 to 0.2 (see Figure 5-2). This demonstrated that the energy saving ratio increased with increasing air flow rate. However, the outdoor test results showed that energy saving ratio increased with increasing air flow rate when the infiltration air flow was present, but decreased with increasing air flow rate when the exfiltration air flow was present (see Figures 5-6, 5-8, and 5-9) for all the three leakage configurations. These demonstrated that the energy gains due to solar radiation increased with increase in air flow rate when infiltration flow was present but decreased with increase in air flow rate when the exfiltration flow was present.

Effects of Air Flow Direction

The measurement results of the outdoor cell showed that the infiltration flow had higher IHEE than those of the exfiltration flow when the test cell was heated to temperature higher than outside. The diffuse leakage configuration had infiltrating IHEE from 0.52 to 0.4 and exfiltrating IHEE from 0.4 to 0.3; the concentrated leakage configuration had infiltrating IHEE from 0.35 to 0.32 and exfiltrating IHEE from 0.3 to -0.15; and the crack leakage configuration had infiltrating IHEE from 0.3 to 0.25 and exfiltrating IHEE from -0.05 to -0.15. This IHEE difference reflected the varying solar energy contribution under infiltration and exfiltration conditions. Under infiltration condition, the air could carry more solar energy captured by the wall surface into the cell, while under exfiltration conditions, the air could reject more solar energy to the outside. To generalize this discovery, it was inferred that exfiltration should result in higher IHEE for cooling since the exfiltration could reject more solar energy to outside and subsequently reduce the cooling energy consumption.

It must be pointed out here that all the measurements conducted under indoor conditions concluded that the air infiltration heat recovery is independent on the air flow direction because no solar radiation is present. Consequently, all the indoor studies concluded that air infiltration will result in energy saving in the range of IHEE from 0 to 1. However, the IHEE of a house may be larger than one or less than zero when solar radiation is present.

Effects of Solar Radiation on IHEE

The impact of solar radiation on the air infiltration heat recovery was noticeable in a number of different ways. Due to the solar radiation, the IHEE has no longer any

theoretical limits. The results of diffuse infiltration flow (Figure 5-5) show IHEE with a value of greater than its theoretical limit value of 0.5 because air infiltration carried more solar energy into the test cell. On the other hand, the results for the crack and concentrated exfiltration flow (Figures 5-7 and 5-9) show IHEE having a value smaller than the limit value of 0 because the exfiltration air rejected more solar energy to the outside. Due to the presence of solar radiation, the energy saving ratio could either increase or decrease with increasing air flow rate. The measurement results show that the energy saving ratio increases with air flow rate for the infiltration flow, and decreases with air flow rate for the exfiltration flow due to the dependence of the solar energy contribution on the air flow direction. However, this conclusion is only valid for the heating model of the house. For cooling model, the energy saving ratio will decrease with increase in air flow rate for the infiltration air flow, but increase with air flow rate for exfiltration air flow.

The general results of the quasi-diffuse leakage configuration (Figure 5-11) show that the IHEE decreased dramatically with increasing solar radiation, and that the IHEE decreased slightly with air flow rate. However, the effects of the air flow on the IHEE increased with the solar radiation. The relationship of solar radiation and IHEE was worth investigating further since this test showed promising benefit.

SUMMARY

The tests performed in the indoor test cell showed that the dynamic and steady-state energy performances were the same when a constant air flow rate was present. Therefore, a house envelope can be regarded as a linear system, and the steady-state methodology or time-averaging technique can be used to determine IHEE provided the air infiltration flow rate is a constant.

The tests performed on both the indoor and outdoor test cells demonstrated that the air infiltration energy performance (IHEE and energy saving ratio) was dependent on the air leakage configuration, air flow rate, and the ratio of the area affected by the air infiltration to the air flow rate. These results confirm the importance of heat recovery under dynamic conditions which was hypothesized from the steady-state results of Bhattacharyya and Claridge [1992]. Moreover, the outdoor tests led to the discovery that the energy performance was strongly dependent on the air flow directions and on the incidence of solar radiation. It was found that the diffuse leakage configuration had higher IHEE than either concentrated or crack leakage configuration, and that the IHEE decreased with the air flow rate. However, under heating conditions, the energy saving ratio increased with the air flow rate for the infiltration flow, and decreased with increase in the air flow rate for the exfiltration flow under heating conditions. The most significant discovery of the test was that the infiltration could result in higher IHEE value for heating and exfiltration for cooling since the solar energy contribution was substantially influenced by the direction of air infiltration.

The numerical results showed that a leaky house could consume as much as 9 times the air infiltration energy as that of a tight house, and that an infiltration air flow model could save about 15% to 40% in air infiltration energy consumption for heating as compared to a exfiltration air flow model. The results of the outdoor cell also demonstrated that up to 35% total energy savings could be achieved by constructing a cell with equal area of diffuse leakage infiltration and exfiltration.

The dependence of IHEE on solar radiation should be further investigated, and tests in a real house should be carried out eventually to confirm the energy savings detected in our test cell.

The error analyses of the measurement results are given in Appendix A1. The error analysis showed the uncertainty in IHEE increased with decreasing air flow rate, and varied from 15% to 34% with the air flow rate range used in the indoor tests, and from 16% to 26% for outdoor cell tests.

CHAPTER VI

UA₀ MEASUREMENT IN HOUSES

Estimating or measuring UA₀, defined as the heat loss rate of a house with unit temperature difference between inside and outside when air infiltration is not present, is of crucial importance for identifying air infiltration heat recovery in houses. However, this is not an easy task because of the presence of solar radiation, air infiltration, and ground heat transfer in houses. On the other hand, UA₀ of a test cell can be measured easily under laboratory conditions because both the ambient and the cell temperature can be accurately controlled under steady state conditions. Of more importance is the fact that the solar radiation, the ground heat transfer, and the air infiltration can be totally eliminated. The major function of the laboratory is to prevent the intrusion of the natural forces on our physical system.

A digital filter can serve the same function as the laboratory for measuring UA₀ in houses. It can pick up only the necessary frequency components of the controlled signals (heat input) and its responses (room temperature), and block all the natural forces such as solar radiation, air infiltration, and ground temperature. If it is designed properly based on the spectrum (distribution of signals with frequency) information of these signals, this filter can create a Single input and Single output data Pair (SSP) from measured signal samples such as room temperature, outside temperature, solar radiation, air infiltration etc. These samples can then be used to estimate the UA₀ of the house. This technique is called the SSP method.

This Chapter describes the fundamental theory, procedure, and prototype application of a digital filter to determine UA₀ in the indoor test cell.

FUNDAMENTAL THEORY

SSP is based on signal processing and linear system theory. The most important relevant concepts are briefly described below.

A signal, for example, ambient temperature, can always be expressed in both the time domain (a physical parameter varying with time) and the phase domain (a sum of a series of periodic functions with homonym frequencies, in which the ratio of frequencies is an integer for any two periodic function terms). These expressions are related by the Discrete Fourier Transform (DFT) [Strum et al. 1988] pair:

$$X(k\Delta f) = \sum_{n=0}^{N-1} x(nT)e^{-j(2\pi/N)nk} \quad (6-1)$$

$$x(nT) = \frac{1}{N} \sum_{k=0}^{N-1} X(k\Delta f)e^{j(2\pi/N)nk} \quad (6-2)$$

$$\Delta f = \frac{1}{NT} = \frac{1}{T_0} \quad (6-3)$$

where

$X(k\Delta f)$ = value of the samples at frequency $k\Delta f$

$x(nT)$ = value of the sample at time nT

T = sampling time interval (s)

Δf = frequency resolution of the DFT in Hz

T_0 = length of the sampled period (s)

k = 0, 1, ..., N-1

n = 0, 1, ..., N-1

N = number of the samples.

A signal is generally characterized by its magnitude spectrum, $M(k\Delta f)$, in the phase domain. It is calculated by the following formula:

$$M(k\Delta f) = |X(k\Delta f)| \quad (6-4)$$

The time domain shows variation of a signal with time, but the phase domain shows the energy distribution of a signal with frequency. Figure 6-1 shows an artificial heat input (q) and room temperature response (T) pair in the time domain. The normalized magnitude spectrum, defined as the magnitude range from 0 to 1, is shown in Figure 6-2 which indicates that both the heat input and room temperature signals have three important sinusoid components with frequencies of 0.05, 0.1, and 0.125 (1/hour) or period lengths 20, 10, and 8 hours. The sampling frequency is 1 (1/hour). Note that in Figure 6-2 the non-zero magnitudes are spread around the frequencies 0.05, 0.1, and 0.125 (1/hour), due to the finite signal length.

Example: Application of a Butterworth Filter

A *digital filter* can help identify the system parameters. Consider a filter designed to pick up the 0.05 (1/hour) frequency component in the sample data pair. Ideally, this filter will have unit gain in the frequency range (pass band) 0.0375 to 0.0625 (1/hour), and zero for any other frequency (see Figure 6-3). This means that the frequency components within the pass band will be multiplied by one. Consequently there is no change made in these components by the filter. However, the frequency components outside this range will be multiplied by zero, and so the filter blocks these frequencies. Both the order of the filter and the signal feature must be considered jointly to choose the pass-band.

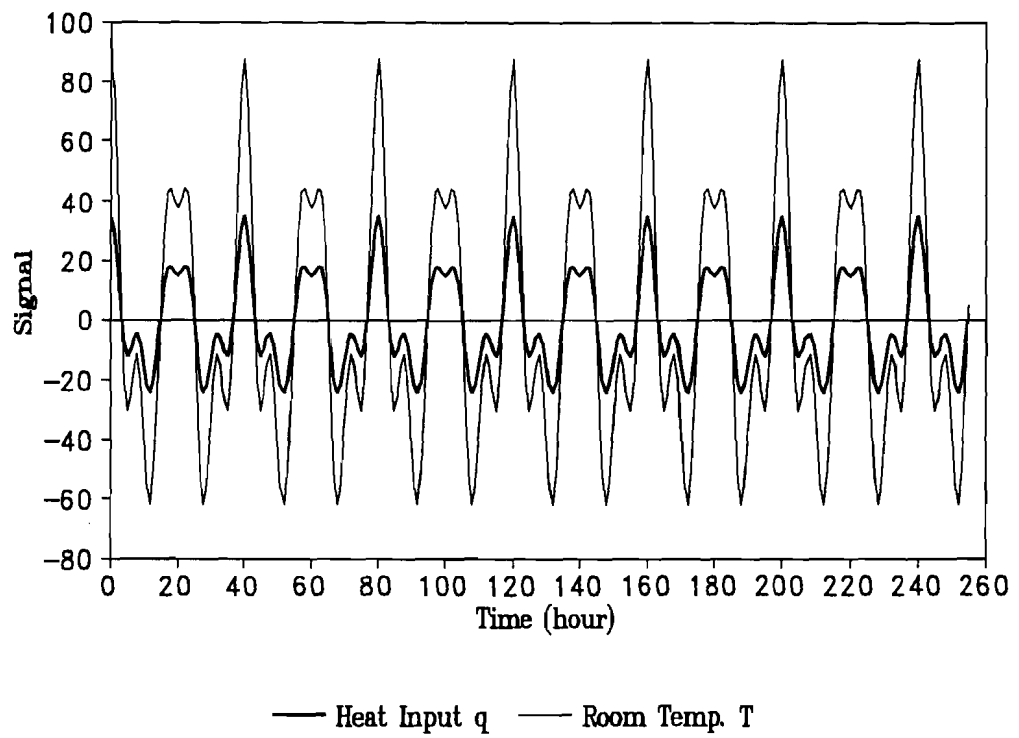


Figure 6-1: An Artificial Heat Input and Room Temperature Response Data Pair

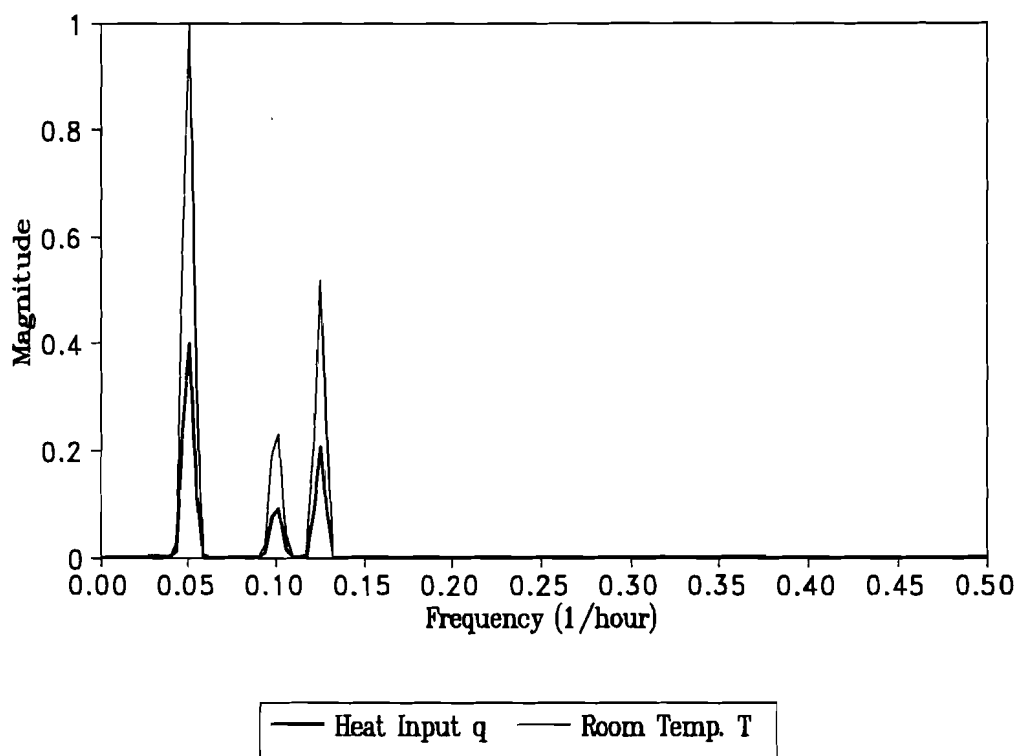


Figure 6-2: The Normalized Magnitude Spectrum of the Artificial Heat Input and Room Temperature Response Data Pair

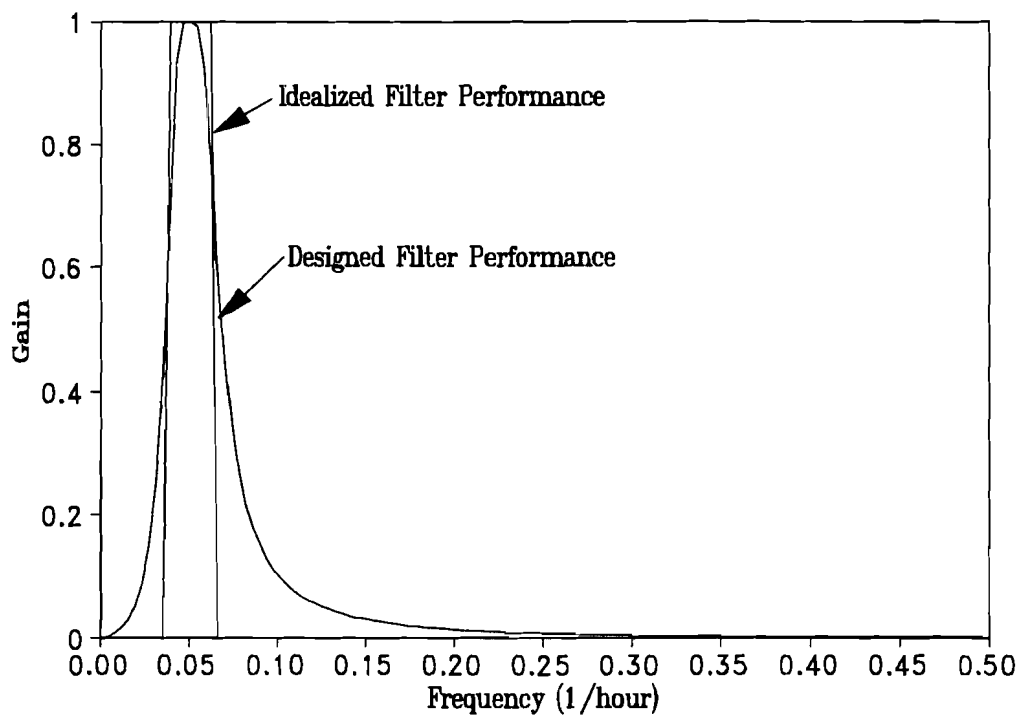


Figure 6-3: Magnitude of Idealized and Designed Filter for the Artificial Heat Input and Room Temperature Response Data Pair

The design of a digital filter involves a process of finding a transfer function that has the required performance. A Butterworth band-pass filter [Strum et al. 1988] with four poles, which approximates the idealized performance and has no attenuation at a frequency of 0.05 (1/hour) will be discussed as an example. The transfer function of this filter is given below:

$$H(Z) = \frac{0.06226 (1 - Z^{-2})}{1 - 1.847 Z^{-1} + 0.913 Z^{-2}} * \frac{0.0859 (1 - Z^{-2})}{1 - 1.75 Z^{-1} + 0.8804 Z^{-2}} \quad (6-5)$$

This transfer function indicates that this filter consists of two second order systems in series. From the magnitude spectrum (Figure 6-3), it is clear that this filter will pass frequency components 0.05 (1/hour) and attenuate others if it is applied to a signal.

To apply a filter to a signal involves a simple convolution calculation. For example, this filter can be applied to the artificial heat input {q} and room temperature response {T} by performing the following calculation:

$$y_q(i) = 1.847y_q(i-1) - 0.913y_q(i-2) + 0.06226(q(i) - q(i-2)) \quad (6-6a)$$

$$q_f(i) = 1.75q_f(i-1) - 0.8804q_f(i-2) + 0.0859(y_q(i) - y_q(i-2)) \quad (6-6b)$$

$$y_T(i) = 1.847y_T(i-1) - 0.913y_T(i-2) + 0.06226(T(i) - T(i-2)) \quad (6-7a)$$

$$T_f(i) = 1.75T_f(i-1) - 0.8804T_f(i-2) + 0.0859(y_T(i) - y_T(i-2)) \quad (6-7b)$$

where:

q = heat input samples

T = room temperature samples

y_T = intermediate output for room temperature

y_q = intermediate output for heat input

q_f = heat input signal after the filter

T_f = room temperature signal after the filter.

The output of the filter is shown in Figure 6-4. Clearly, the input $\{q_f(i)\}$ and output $\{T_f(i)\}$ are simply connected by a factor of 2.5. From this simple case, the system is identified as:

$$T = 2.5q \quad (6-8)$$

This simple example shows that the filter does help system identification by creating simpler input and output data pairs.

These fundamental theories can be used to construct a methodology for determining the UA_0 in houses. First, the magnitude spectrum of the natural signals, such as solar, ambient temperature, and ground temperature, can be obtained by measurement. This information will indicate the frequency ranges in which the natural forces place their energy. According to this information, a heat input signal can be designed and applied to the house, which places its major energy in a frequency range outside those of the natural signals. A filter can be designed with this frequency range as the pass-band. Finally, this filter can be applied to measured signals, such as ambient temperature, solar radiation, heat input, and room temperature. This filter should pass only heat input and room temperature signals because only heat input and room temperature have energy within the pass-band of the filter. Sequentially a single input (heat input) and single output (room temperature) data pair is created. The transfer function between heat input and room temperature can be identified by using these data pairs. The heat loss factor can then be identified from the coefficients of the transfer function.

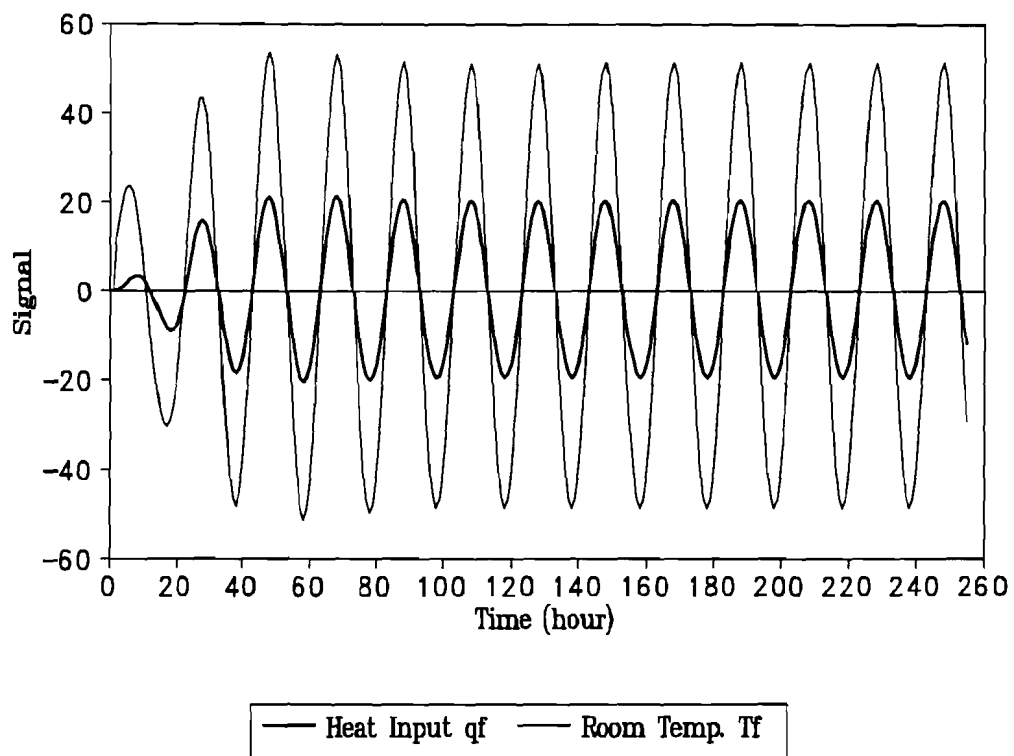


Figure 6-4: Heat Input (q_f) and Room Temperature Response (T_f) after the Filter for the Artificial Data Pairs

PROCEDURE

To apply the fundamental theory to UA_0 identification, the following steps are required:

- (1) conduct a signal frequency analysis and determine the sampling frequency;
- (2) design controllable input signal;
- (3) design the filter;
- (4) filter the signal and estimate the transfer function;
- (5) validate the transfer function;
- (6) calculate the heat loss factor.

Signal Frequency Analysis and Sampling

The sampling theorem states that the sampling frequency should be at least twice as fast as the highest frequency in the signals [Strum et al. 1988]. Generally, it is reasonable to assume that uncontrollable signals have the highest significant frequency of 0.33 (1/hour) because both outside temperature and solar radiation can be regressed well with one to four sinusoid function terms (e. g. 3, 6, 12, 24 hour periods), and controllable signals would have the highest significant frequency of 4 (1/hour) in houses. Consequently, the sampling frequency should be at least 8 (1/hour), and so a five-minute time step should be suitable.

Controllable Input Signal

The controllable input signal, defined as the auxiliary heat input to a house or cell, should have an unique magnitude spectrum different from that of the uncontrollable input

signals such as solar radiation, ambient temperature, and air infiltration. In other words, the controllable signal should place its energy in the frequencies where the uncontrollable signals do not. This feature allows a filter to pass the selected controllable signal components but to block others.

The controllable signal should place substantial energy within frequencies from 0.5 to 4 (1/hour), because uncontrollable signals place their major energy at frequencies below 0.3 (1/hour), and the damping ratio, defined as the modulus ratio of a sinusoid heat input to its room temperature response, is too large when the frequency is higher than 4 (1/hour) [Liu 1987]. A controllable signal with these characteristics can be created by a single rectangular impulse with a width of 1 hour.

Band-pass Filter Design

To design a band-pass filter, the pass band characterized by the center frequency (f_c) and the band width (δf) should be defined first. The band-width choice depends on tradeoffs among several factors, including filter linearity and length of the testing period [Strum and Kirk 1988]. Generally, the sampling frequency (f_s) is known.

The center frequency and width of the pass band are chosen by examining the magnitude spectra of both the controllable and uncontrollable signals. The magnitude spectrum of the samples is calculated by the following equations:

$$X(0) = \frac{2}{M} \sum_{k=1}^M x(k\Delta\tau) \quad (6-9)$$

$$X(n\Delta f) = \sqrt{a_n^2 + b_n^2} \quad (6-10)$$

$$a_n = \frac{2}{M} \sum_{k=1}^M x(k\Delta\tau) \cos\left(\frac{2\pi nk}{M}\right) \quad (6-11)$$

$$b_n = \frac{2}{M} \sum_{k=1}^M x(k\Delta\tau) \sin\left(\frac{2\pi n k}{M}\right) \quad (6-12)$$

where:

$x(k\Delta\tau)$ = signal in the time domain

$X(n\Delta f)$ = coefficient of frequency components ($n\Delta f$), whose modulus is the magnitude of the spectrum of the samples at frequency $n\Delta f$

k = time series number from 1 to M , where M is the number of samples in the time domain

$\Delta\tau$ = sampling time step

n = frequency index, which must be less than or equal to $\frac{M}{2}$

$\Delta f = \frac{2\pi}{M}$ = frequency resolution.

From the magnitude spectrum, a relatively high frequency can be picked as the center of a pass-band where the controlled input has an important component but other inputs do not. The band width of the filter is designed to be the range around the center frequency where uncontrolled signals are not important.

Many methods and software packages are available for filter design [e. g. Strum 1989, Phillips 1990, Mahmoud 1984]. A standard procedure adopted from Strum [1989] for designing a Butterworth band-pass filter is described below:

A low pass prototype filter with four poles is expressed as:

$$H(Z) = \frac{0.094(Z+1)^4}{Z^4 + 0.486Z^2 + 0.018} \quad (6-13)$$

To transform it to a band-pass filter, the following calculation should be carried out:

$$\theta_u = 2\pi \frac{f_c + \delta f / 2}{f_s} \quad (6-14)$$

$$\theta_1 = 2\pi \frac{f_c - \delta f / 2}{f_s} \quad (6-15)$$

$$\theta_c = 2\pi \frac{f_c}{f_s} \quad (6-16)$$

$$\alpha = \frac{\cos(\theta_u / 2 - \theta_1 / 2)}{\cos(\theta_u / 2 + \theta_1 / 2)} \quad (6-17)$$

$$k = \tan \frac{\theta_c}{2} \cot(\theta_u / 2 - \theta_1 / 2) \quad (6-18)$$

$$\Gamma = - \frac{Z^2 - \frac{2\alpha k}{k+1} Z + \frac{k-1}{k+1}}{1 - \frac{2\alpha k}{k+1} Z + \frac{k-1}{k+1} Z^2} \quad (6-19)$$

To obtain the band-pass filter, replace Z in Equation (6-13) with Γ .

It is conventional to factor Equation (6-13) into the following format:

$$H(Z) = \frac{c_0 + c_1 Z^{-1} + c_2 Z^{-2}}{1 + d_1 Z^{-1} + d_2 Z^{-2}} * \frac{e_0 + e_1 Z^{-1} + e_2 Z^{-2}}{1 + f_1 Z^{-1} + f_2 Z^{-2}} \quad (6-20)$$

where:

c, d, e, f = coefficients of the filter transfer function.

Filtering and Parameter Estimation

Filtering data is a relatively simple convolution calculation. The output of the filter $\{z(i)\}$ is related with input $\{x(i)\}$ through an intermediate output $y(i)$ by the following formula:

$$y(i) = d_1y(i-1) + d_2y(i-2) + c_0x(i) + c_1x(i-1) + c_2x(i-2) \quad (6-21)$$

$$z(i) = f_1z(i-1) + f_2z(i-2) + e_0y(i) + e_1y(i-1) + e_2y(i-2) \quad (6-22)$$

where

$x(i)$ = value of the sample at time step i

$y(i)$ = intermediate output

$z(i)$ = output of the filter.

If the filter is properly designed, it will block all the uncontrollable input signals or block them for a particular time period. The filtered heat input $\{q_f(i)\}$ and filtered temperature response $\{T_f(i)\}$ data pairs can be used to determine the coefficients of the ARMA model by regression:

$$T_f(i) = h_1T_f(i-1) + h_2T_f(i-2) + \dots + h_nT_f(i-n) \\ + g_0q_f(i) + g_1q_f(i-1) + g_2q_f(i-2) + \dots + g_nq_f(i-n) \quad (6-23)$$

where

T_f = filtered temperature response

q_f = filtered heat input

h, g = regression coefficients.

The order of the ARMA model is generally 2 but may be as high as 5, depending on the mass of the house. A first order model is suggested to try first, then it may be increased sequentially until it meets criteria defined in the next section.

The data sets used for regression should be chosen carefully. It is preferable to have zero values for both initial and final values of the filtered input q_f . The suggested time period is one to two cycles.

Validation of the Parameter Estimates

The ARMA model can be expressed in the system transfer function format:

$$H(Z) = \frac{g_0 + g_1 Z^{-1} + g_2 Z^{-2} + \dots + g_n Z^{-n}}{1 + h_1 Z^{-1} + h_2 Z^{-2} + \dots + h_n Z^{-n}} \quad (6-24)$$

The damping ratio of the house to a sinusoidal input signal should increase with frequency; this ratio is essentially the same as the reciprocal of the magnitude of the transfer function at the same frequency. In other words, the magnitude spectrum of the transfer function should decrease with the frequency. The response factors, $\{h(i)\}$, should change smoothly with index i . The magnitude spectrum and the response factors can be used to validate the ARMA model or the transfer function. If a wrong order is used, the regressed transfer function will give abnormal values for one or both of the response factors and of the damping ratio.

The response factors can be obtained from the transfer function by long division, and the magnitude spectrum can be derived by introducing the Z operator into the transfer function equation:

$$Z = \exp(j\omega) \quad (6-25)$$

$$H(\omega) = \frac{g_0 + g_1 e^{-j\omega} + g_2 e^{-j2\omega} + \dots + g_n e^{-jn\omega}}{1 + h_1 e^{-j\omega} + h_2 e^{-j2\omega} + \dots + h_n e^{-jn\omega}} \quad (6-26)$$

where:

ω = angular frequency (rad).

If the response factor and magnitude obey the above rules, then both the order and coefficients are properly estimated.

Heating Load Factor Calculation

The heat loss factor can be easily calculated from the transfer function coefficient. The room temperature can be expressed according to the transfer function in the time domain as follows:

$$T(i) = -e_1 T(i-1) - e_2 T(i-2) + d_0 Q(i) + d_1 Q(i-1) + d_2 Q(i-2) \quad (6-27)$$

If constant heat input is present for a long time, one expects a constant room temperature, so the heat loss factor (UA) can be deduced from the above equation as:

$$UA = \frac{Q(i)}{T(i)} = \frac{1 + e_1 + e_2}{d_0 + d_1 + d_2} \quad (6-28)$$

If the house has light components, such as doors, windows, and concentrated infiltration, then the heat loss factor for concentrated infiltration and light parts (UA_i) can be calculated by the formula (Appendix A2):

$$UA_i = \frac{2}{1 \pm \sqrt{1 - 4d_0}} \quad (6-28a)$$

THE APPLICATION OF THE SSP METHOD

SSP was applied to identify the heat loss factor of the indoor cell. It serves as an example and demonstration of the method, moreover to validate the method. The measured test cell temperature, heat input, and room temperature are shown in Figure 6-5. There was no infiltration present in this test, and the sampling step was 5 minutes.

Filter Design

The sample spectrum of the measured data is shown in Figure 6-6, which contains spectrum distributions of both input (heat input, room temperature), and output (cell temperature). Similarity of the spectrum for both the input and output is clearly seen, which demonstrates that the system behaves linearly since a frequency component f in the input signal will create the same frequency component in the output [Phillips and Nagle 1990].

Two major frequency components can be easily identified as 0 and 0.125 (1/hour). The periodic peaks after 0.125 are multiple of 0.125 and cannot be counted as major frequencies (Newton 1988). Therefore, the specifications of the filter include a pass-band center frequency of 0.125 (1/hour), and pass-band width of 0.18 (1/hour) based on the width of the spectral peak observed in Figure 6-6.

The filter was designed by DSPLAY (a software package for control system design). The spectrum of the designed filter is shown in Figure 6-7. The transfer function is given below:

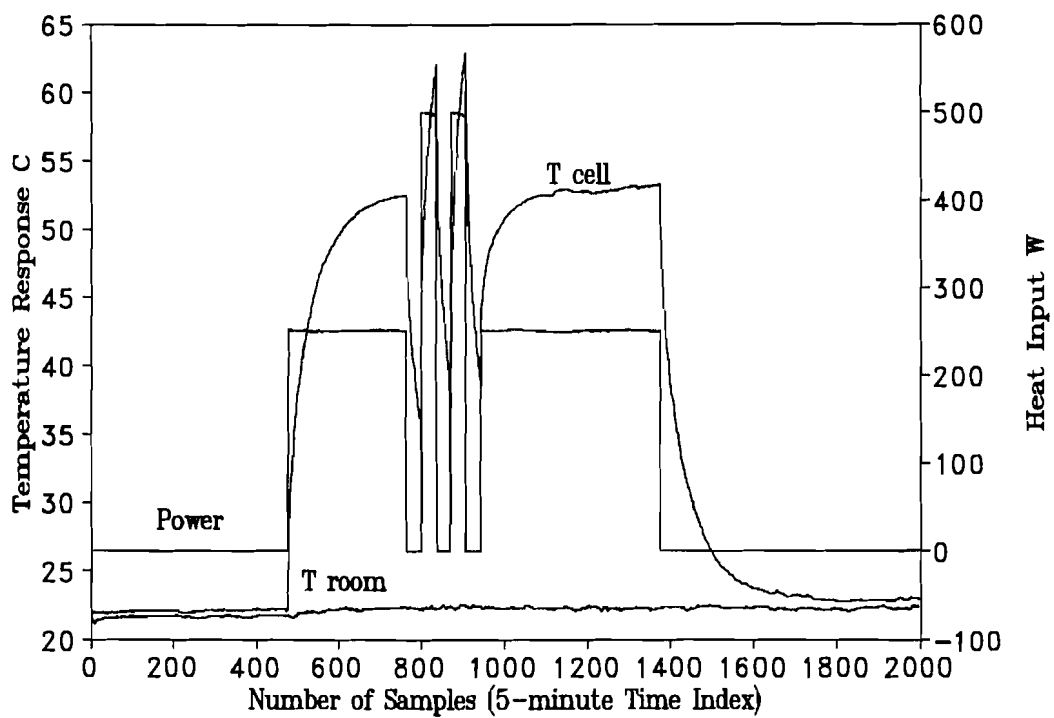


Figure 6-5: Measured Heat Input, Cell and Room Temperatures for the Indoor Cell Test

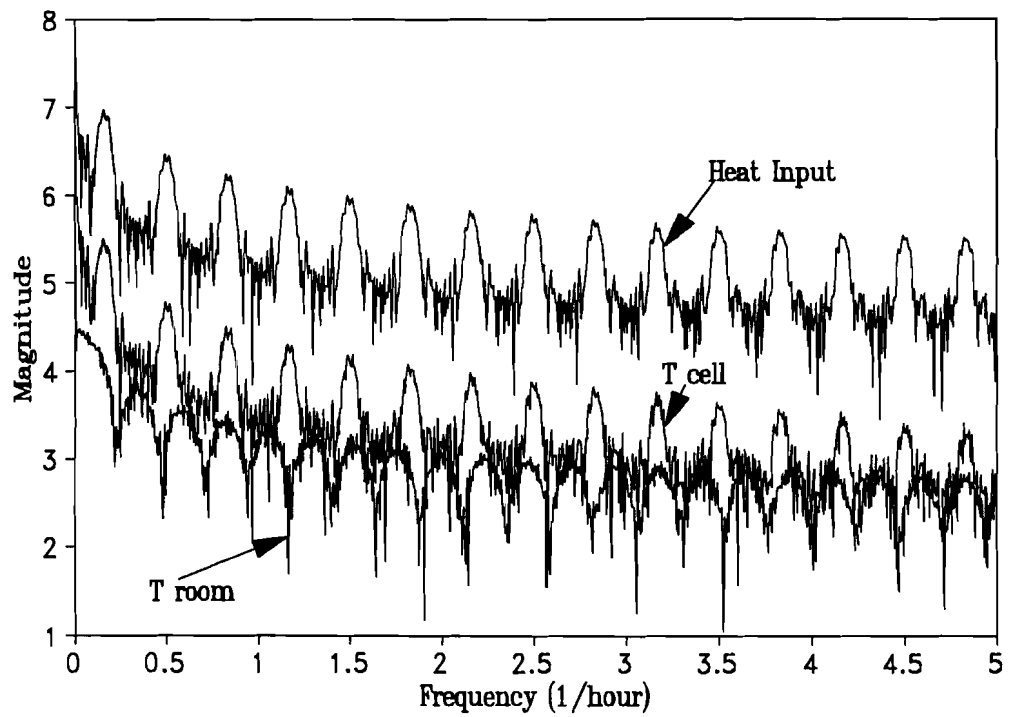


Figure 6-6: Magnitude Spectrum of Sampled Signals in Indoor Test Cell Test

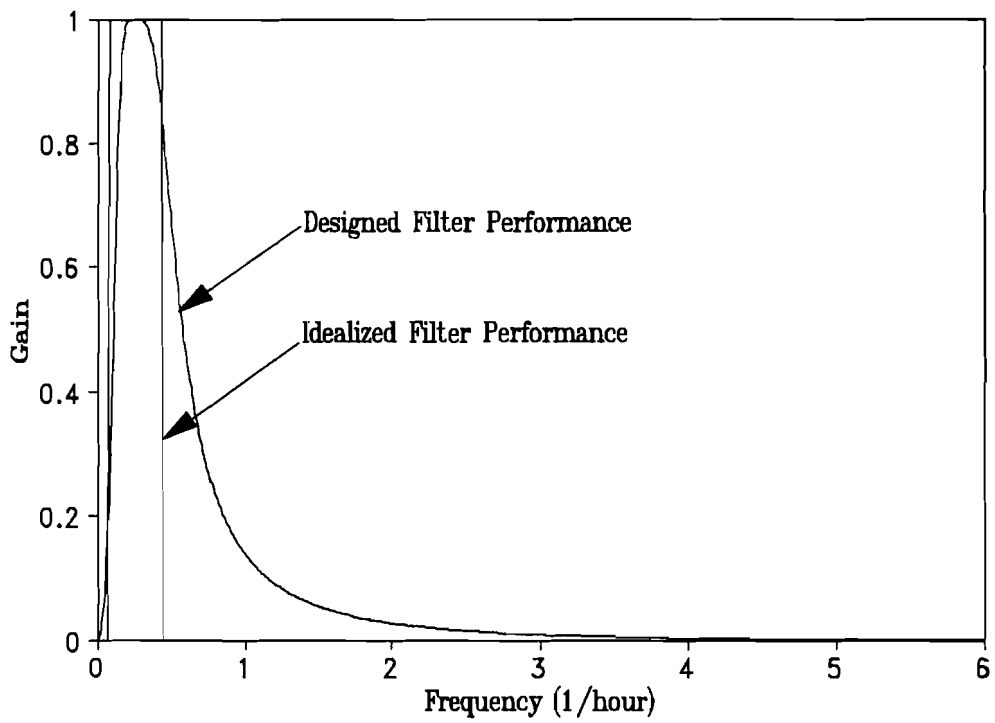


Figure 6-7: Magnitude of the Filter for Indoor Cell Test Data

$$H(Z) = \frac{0.05335866(1 - Z^{-2})}{1 - 1.92845Z^{-1} + 0.93423Z^{-2}} * \frac{0.14523(1 - Z^{-2})}{1 - 1.775Z^{-1} + 0.82099Z^{-2}} \quad (6-29)$$

Filtering and Parameter Estimation

Filtering the samples involves a relatively simple convolution calculation. If $\{x(i)\}$ is the signal sample to be filtered, the output $\{z(i)\}$ of the filter can be calculated by the following formulas:

$$y(i) = 1.928451y(i-1) - 0.93423y(i-2) + 0.05335866[x(i) - x(i-2)] \quad (6-30)$$

$$z(i) = 1.775000z(i-1) - 0.82099z(i-2) + 0.14523[y(i) - y(i-2)] \quad (6-31)$$

The room temperature, cell temperature, and the heat input data were filtered using the above equations. The outputs of the filter are shown in Figure 6-8, which shows a zero signal for the room temperature after the convolution calculation stabilized. Three periods (time index 478-586, 764-850, and 1377-1484) were chosen to identify the system parameters where the filtered room temperature was zero. In these cases, the filtered cell temperature can be regarded as the response from the filtered heat input only since the filter blocked all the temperature response due to room temperature. The regressions were carried out for the orders from 1 to 20 by using first period data sets. The second order was used for the other two periods.

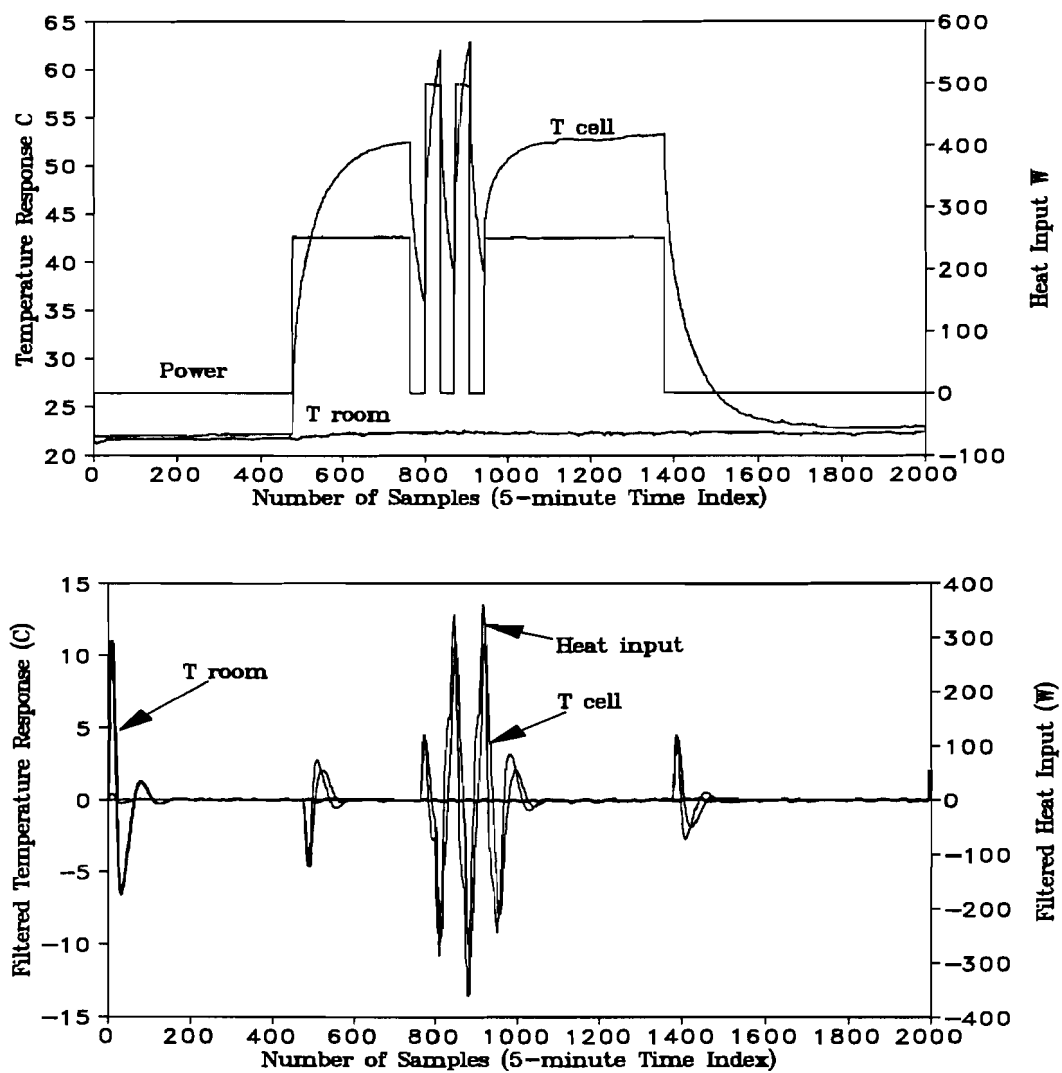


Figure 6-8: Comparison of Original and Filtered Signals

Validation of the Estimates

The "response factors" and the "magnitude" were calculated by using the regressed coefficients of the ARMA models. Figure 6-9 shows the "response factors" for first, second and third order models. The "response factors" of the first order model change suddenly at time step 2, while the response factors of the second order showed smooth change with the time index. The "response factors" of the third order model and all higher order models oscillated, and showed $h(3)$ was less than zero. This means the response factor predicted heat input will decrease the room temperature after three time steps which is physically impossible.

Figure 6-10 shows the magnitude spectrum for three different order models (1st, 2nd, and 9th). The "transfer function magnitude" of the 9th order model oscillated and jumped to extremely high values at the high frequencies. This demonstrates that this "transfer function" will greatly amplify the high frequency components in the input signal. If the input signal contains a high frequency component, then the output of the "transfer function" will be abnormal since the "transfer function" enlarges high frequency components of the input signal instead of eliminating them. If the input signal does not contain high frequency components, the output of this "transfer function" will be normal since the spectra of the 9th and second order models are very close in the lower frequency range. This shows that agreement between the model and measured data for a single case does not prove whether the model is good or bad. The higher order ARMA models provide a better fit to the filtered data, but give unphysical predictions; hence the best regression fit does not necessarily imply the best model.

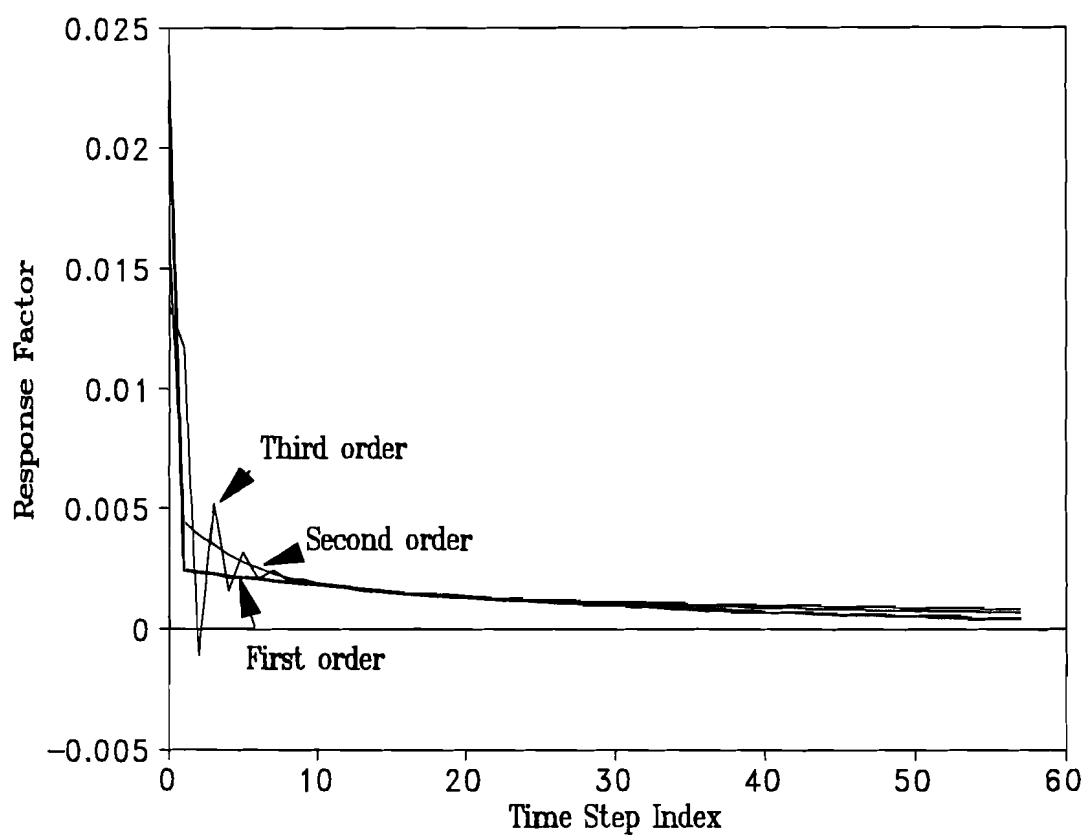


Figure 6-9: Response Factors vs the Time Index for Different "Order" Models

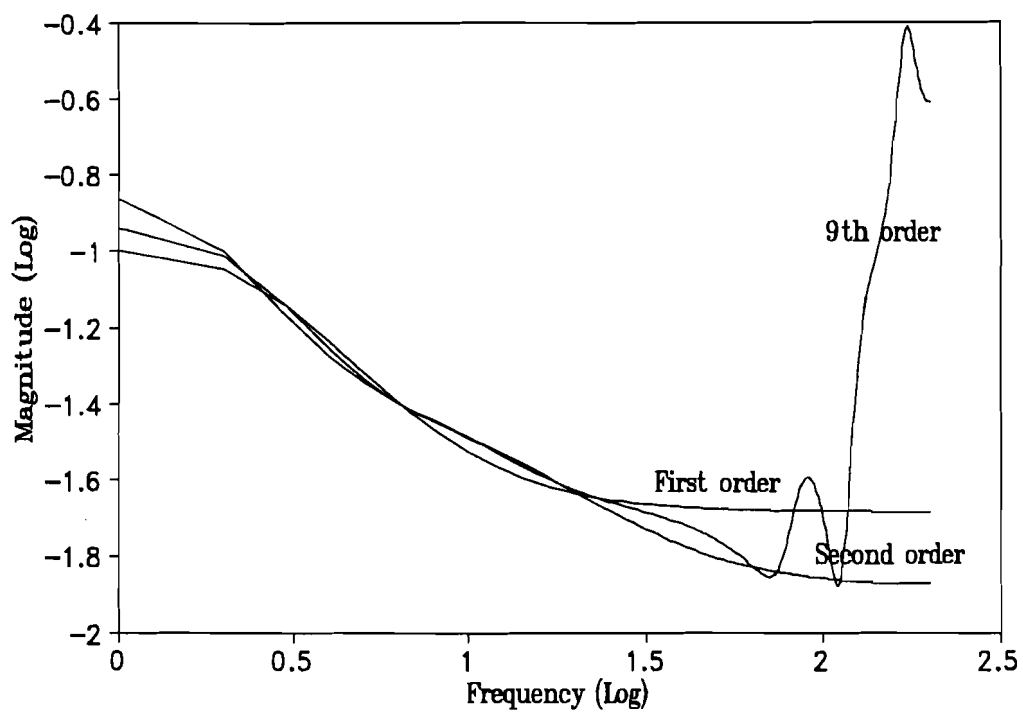


Figure 6-10: Magnitude Spectrum or Gain vs Frequency for Different "Order" Models

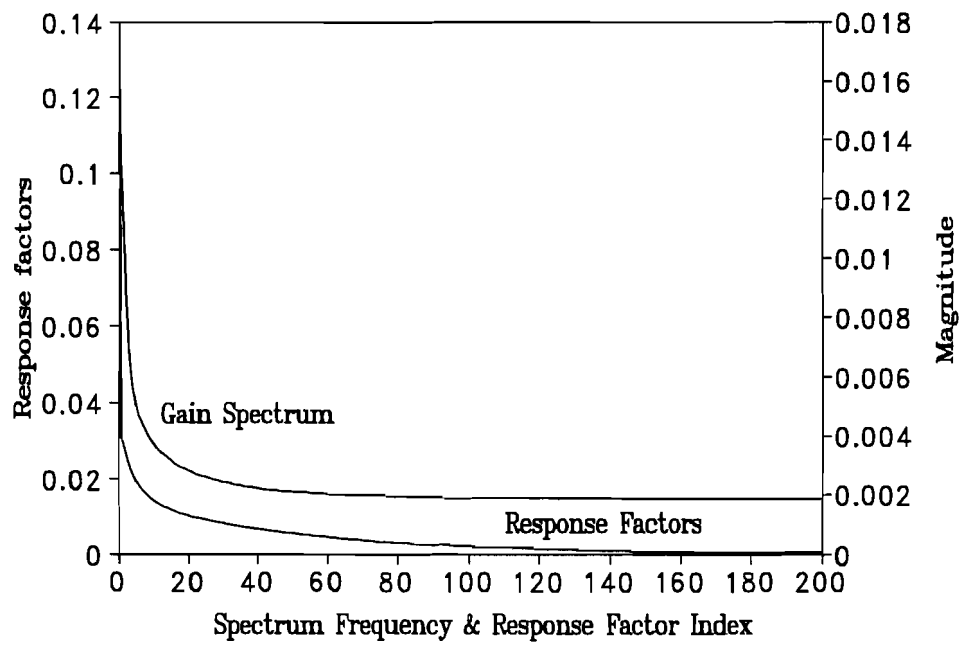


Figure 6-11: Response Factor and Magnitude of Transfer Function for Indoor Cell

The "transfer function magnitude" of the first order model also showed relatively high gain for high frequency component. The transfer function magnitude of the second order showed a smooth decrease with frequency. According to the magnitude and response factor rules, this test cell is a second order system.

Three transfer functions were obtained from the three different periods and are given below.

$$H_1(Z) = \frac{0.01697 - 0.02448Z^{-1} + 0.008184Z^{-2}}{1 - 1.7146Z^{-1} + 0.7059Z^{-2}} \quad (6-32)$$

$$H_2(Z) = \frac{0.01372 - 0.02092Z^{-1} + 0.007533Z^{-2}}{1 - 1.7977Z^{-1} + 0.8004Z^{-2}} \quad (6-33)$$

$$H_3(Z) = \frac{0.01630 - 0.02659Z^{-1} + 0.01061Z^{-2}}{1 - 1.8343Z^{-1} + 0.8370Z^{-2}} \quad (6-34)$$

Although some differences in the transfer function coefficients can be observed from Equations (6-32), (6-33), and (6-34), it was found that their response factors and magnitude spectra are essentially identical and cannot be distinguished (Figure 6-11). The predictions using these three transfer functions are very close to each other and are consistent with the measured cell temperature (see Figures 6-12a, 6-12b, and 6-12c). The standard errors of the temperature prediction are 1.2 °C for transfer function (6-32), and 0.7 °C for transfer functions (6-33) and (6-34). The relatively larger prediction errors were caused by the time variant property of the system. These demonstrated that all the three equations can be used to approximate the system transfer function.

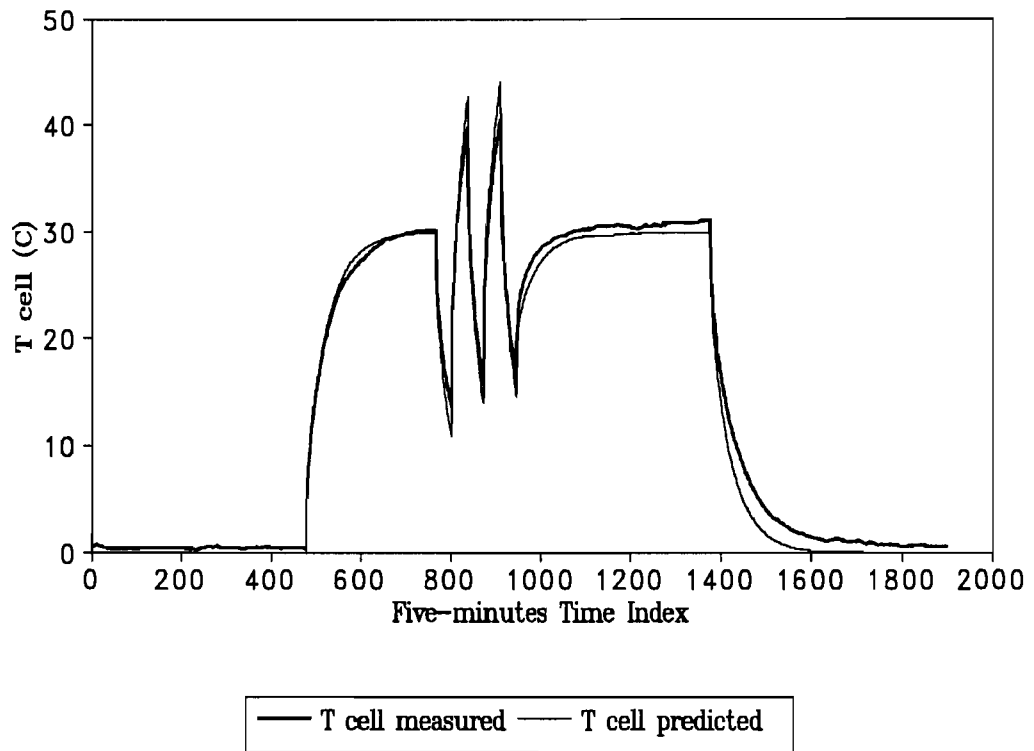


Figure 6-12a: Comparison of Measured and Predicted Cell Temperature by Transfer Function (6-32)

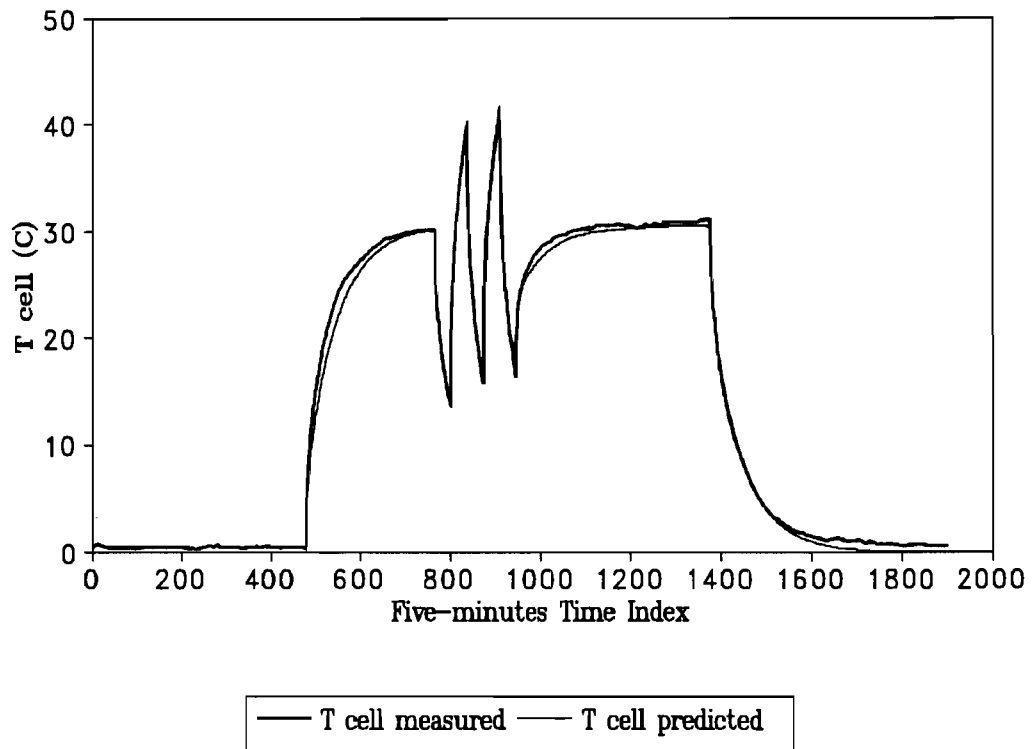


Figure 6-12b: Comparison of Measured and Predicted Cell Temperature by Transfer Function (6-33)

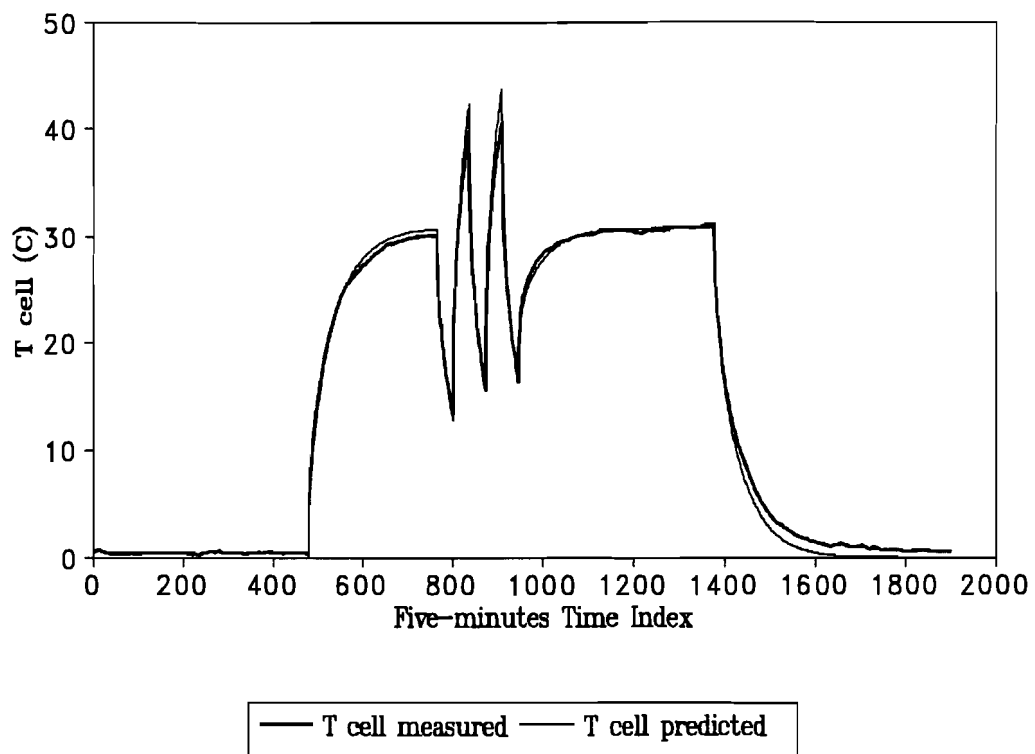


Figure 6-12c: Comparison of Measured and Predicted Cell Temperature by Transfer Function (6-34)

Heating Load Factor Calculation

The UA values calculated from the transfer function coefficients according to Equation (6-28) and from the conventional steady state measurement method are given in Table 6-1.

Table 6-1: Summary of Cell Heat Loss Factor Results

	SS-1	Dynamic	SS-2
Conventional	8.46	8.34	8.22
SSP	8.40	8.24	8.15
Relative Difference	0.7%	1.2%	0.9%

The results show consistency (relative difference 1%) between the conventional measurement method and the SSP method. The UA values varied from period to period, and as discussed in Chapter V, may do so because of time dependent moisture content.

SSP was developed based on signal processing and linear system theory, and has been used successfully to estimate UA_0 of an indoor test cell. The results show excellent agreement (relative difference 1%) between the conventional steady state and the SSP methods. To compare with calorimetric method, this method has the following advantages: use shorter time; use simpler test equipment; do not intrude normal operation conditions. Consequently, it can be used to identify UA of damp enclosures, and enclosures under weather or noise conditions, where the calorimetric methods are incapable to do so.

CHAPTER VII

UA MEASUREMENT IN HOUSES

The heat loss factor UA must be measured in order to determine air infiltration heat exchange effectiveness (IHEE). The SSP method has been developed especially to measure the heat loss factor UA_0 due to conduction only. Neither the SSP method nor other methods available for use can accurately measure UA of a building subjected to outdoor conditions using only two or three days' data.

A Short Term Average Method (STAM) was developed to measure the heat loss factor of a building under outdoor conditions with changing temperature, solar radiation, and wind velocity. The fundamental theory, test procedure, and validation tests conducted are described below.

THE FUNDAMENTAL THEORY

STAM can be defined as a method that uses the average weather, air flow, and heat input parameters for a short period, such as two or three days, in order to estimate the house heat loss factor. If the average room temperature during the period is purely due to the weather, air flow, and heat input parameters within the period, the UA values can be accurately estimated by using the average values of these parameters provided the house can be treated as a linear system. However, the room temperature variation is generally due to these parameters both during the period and outside the period; these parameters during the period contribute to the room temperature not only during the period but also outside the period because of heat storage effect. For example, if a period was chosen from 2 am to 10 pm, then the room temperature at 3 am is not only influenced by the ambient temperature at 3 am but also by the temperature at 2 am, 1 am and so on; the

ambient temperature at 9 pm will influence the room temperature not only at 9 pm but also at 10 pm, 11 pm, and so on. These thermal storage effects must be properly treated if a short period is used to estimate UA.

Although it is impossible to define a period in which the parameters (such as solar, ambient temperature etc) affect room temperatures only during the same period, it is possible to define a period in which the energy contribution from the parameters outside the period is the same as the effects of the parameters within the period on the outside of the period. This is called *the equivalent rule*. For example, the ambient temperature outside (before) the period may contribute to the room 100 KJ heat energy, and the ambient temperature within the period may also contribute to the room 100 KJ heat energy outside (after) of the period. The UA of the house can be estimated by using the average parameters of this period. The rules for choosing this period are developed in this section.

A house subjected to solar radiation, ambient temperature, room air temperature, ground temperature, and heating or cooling is idealized as an enclosure shown in Figure 7-1. Using the inner surface of the house as the control surface, the energy balance equation at time i can be expressed as:

$$q_{\text{ground}}(i) + q_{\text{power}}(i) + q_{\text{house}}(i) + q_i(i) + q_{\text{solar}}(i) + q_{\text{air}}(i) = q_{\text{stor}}(i) \quad (7-1)$$

where :

$q_{\text{ground}}(i)$ = heat flux at control surface due to ground temperature

$q_a(i)$ = heat flux at control surface due to ambient temperature

$q_{\text{house}}(i)$ = heat flux due to room temperature

$q_{\text{solar}}(i)$ = heat flux due to solar radiation

$q_{\text{power}}(i)$ = heat input to the house

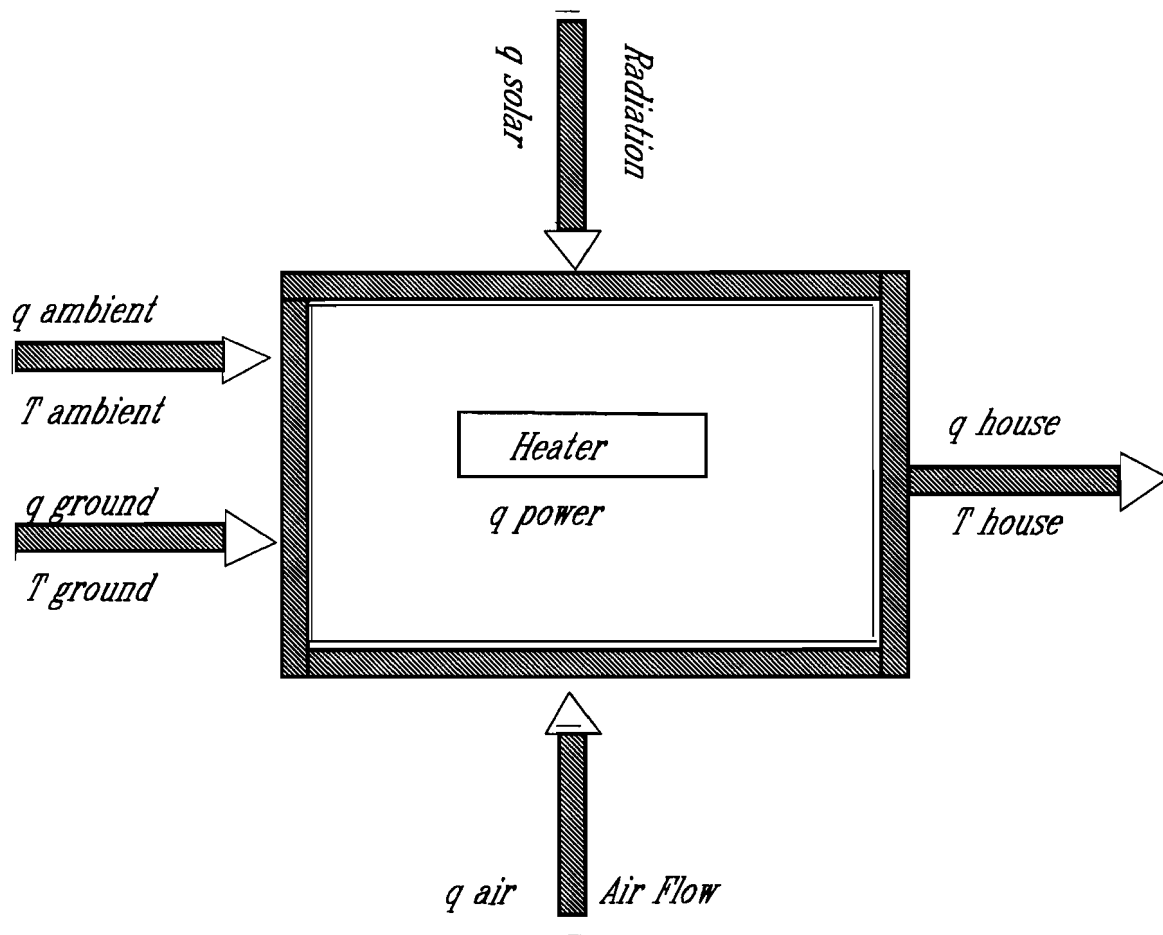


Figure 7-1: Schematic of a House Thermal System

- $q_{\text{air}}(i)$ = heat flux due to air infiltration
 $q_{\text{stor}}(i)$ = heat gain of thermal mass inside of the house.

The convention adopted is that heat flux is defined as positive for gains, negative for losses. If the heat transfer process is linear, then the heat fluxes can be calculated separately by using individual variables. Stephenson and Mitalas [1967] demonstrated that the current heat flux, for example $q_a(i)$, is the result of current and previous ambient temperatures, e.g. $T_a(i)$, $T_a(i-1)$, ..., $T_a(i-n)$, and that $q_a(i)$ can be expressed as a summation of the products of the previous input values and a set of coefficients that are called response factors. According to the response factor concept, these heat fluxes can be expressed as follows:

$$q_{\text{ground}}(i) = \sum_{j=0}^K T_{\text{ground}}(i-j) \alpha_{\text{ground}}(j) \quad (7-2)$$

$$q_a(i) = \sum_{j=0}^K T_a(i-j) \alpha_a(j) \quad (7-3)$$

$$q_{\text{house}}(i) = \sum_{j=0}^K T_{\text{house}}(i-j) \alpha_{\text{house}}(j) \quad (7-4)$$

$$q_{\text{solar}}(i) = \sum_{j=0}^K I(i) \alpha_{\text{solar}}(j) \quad (7-5)$$

$$q_{\text{air}}(i) = \sum_{j=0}^K \dot{m}(i) \alpha_{\text{air}}(j) \quad (7-6)$$

$$q_{\text{stor}}(i) = MC_{\text{mass}}(T_{\text{mass}}(i) - T_{\text{mass}}(i-1)) \quad (7-7)$$

where:

α = heat flux response factors due to parameters indexed as the
 subscript

\dot{m} = air flow rate (Kg/s)

- K = the maximum number of the response factor terms
 I = solar radiation (W/m^2)
 MC_{mass} = heat capacity of the house (W/K)
 T_{mass} = thermal mass temperature of the house ($^{\circ}\text{C}$).

Introducing these expressions in the basic energy balance Equation (7-1), it then follows:

$$\begin{aligned}
 & \sum_{j=0}^K T_{\text{ground}}(i-j)\alpha_{\text{ground}}(j) + \sum_{j=0}^K T_a(i-j)\alpha_a(j) + \sum_{j=0}^K T_{\text{house}}(i-j)\alpha_{\text{house}}(j) \\
 & + q_{\text{power}}(i) + \sum_{j=0}^K \dot{m}(i-j)\alpha_{\text{air}}(j) = MC_{\text{mass}}(T_{\text{mass}}(i) - T_{\text{mass}}(i-1)) \quad (7-8)
 \end{aligned}$$

It is assumed that UA will be estimated using a period data indexed with time step 1 to N. Summing the energy balance equation over the period results in:

$$\begin{aligned}
 & \sum_{i=1}^N \sum_{j=0}^K T_{\text{ground}}(i-j)\alpha_{\text{ground}}(j) + \sum_{i=1}^N \sum_{j=0}^K T_a(i-j)\alpha_a(j) + \\
 & \sum_{i=1}^N \sum_{j=0}^K T_{\text{house}}(i-j)\alpha_{\text{house}}(j) + \sum_{i=1}^N \sum_{j=0}^K I(i-j)\alpha_{\text{solar}}(j) + \sum_{i=1}^N q_{\text{power}}(i) + \\
 & \sum_{i=1}^N \sum_{j=0}^K \dot{m}(i-j)\alpha_{\text{air}}(j) = MC_{\text{mass}}(T_{\text{mass}}(N) - T_{\text{mass}}(1)) \quad (7-9)
 \end{aligned}$$

Clearly, $T_{\text{mass}}(N)$ should be equal to $T_{\text{mass}}(1)$ in order to cancel the influence of the thermal storage. This is the first rule. Introducing this rule and exchanging the summation sign in the equation, we get:

$$\begin{aligned}
 & \sum_{j=0}^K \alpha_{\text{ground}}(j) \sum_{i=1}^N T_{\text{ground}}(i-j) + \sum_{j=0}^K \alpha_a(j) \sum_{i=1}^N T_a(i-j) + \\
 & \sum_{j=0}^K \alpha_{\text{house}}(j) \sum_{i=1}^N T_{\text{house}}(i-j) + \sum_{j=0}^K \alpha_{\text{solar}}(j) \sum_{i=1}^N I(i-j) +
 \end{aligned}$$

$$\sum_{i=1}^N \dot{q}_{\text{power}}(i) + \sum_{j=0}^K \alpha_{\text{air}}(j) \sum_{i=1}^N \dot{m}(i-j) = 0 \quad (7-10)$$

In order to warrant the linear system assumption, a constant air flow rate is required for tests. Introducing this condition to Equation (7-11), it then becomes:

$$\begin{aligned} & \sum_{j=0}^K \alpha_{\text{ground}}(j) \sum_{i=1}^N T_{\text{ground}}(i-j) + \sum_{j=0}^K \alpha_a(j) \sum_{i=1}^N T_a(i-j) + \\ & \sum_{j=0}^K \alpha_{\text{house}}(j) \sum_{i=1}^N T_{\text{house}}(i-j) + \sum_{j=0}^K \alpha_{\text{solar}}(j) \sum_{i=1}^N I(i-j) + \\ & \bar{q}_{\text{power}} + \dot{m}N \sum_{j=0}^K \alpha_{\text{air}}(j) = 0 \end{aligned} \quad (7-11)$$

In order to simplify Equation (7-11), it is assumed that: the *moving summations or averages of ambient, ground, and room temperatures are constants*.

$$\frac{1}{N} \sum_{i=1}^N T_{\text{ground}}(i-j) = \bar{T}_{\text{ground}} = \text{constant} \quad (\text{for } j=1,2,\dots,K) \quad (7-12)$$

$$\frac{1}{N} \sum_{i=1}^N T_a(i-j) = \bar{T}_a = \text{constant} \quad (\text{for } j=1,2,\dots,K) \quad (7-13)$$

$$\frac{1}{N} \sum_{i=1}^N T_{\text{house}}(i-j) = \bar{T}_{\text{house}} = \text{constant} \quad (\text{for } j=1,2,\dots,K) \quad (7-14)$$

This is called option 1 of the second rule. This rule assumes that the temperature profiles from time step -K to 0, such as ground, house, and ambient temperatures, should be exactly similar as those from step N-K to N. This is one special case satisfying the equivalent rule. This rule can be approximately satisfied under normal or little turbulence weather by adjusting both the start and end times of the period. However, the equivalent rule for temperatures can be generalized if the response factors can be calculated from audit data of houses.

$$\sum_{j=0}^K T_{\text{ground}}(-j) \sum_{i=j}^K \alpha_{\text{ground}}(i) = \sum_{j=0}^K T_{\text{ground}}(N-j) \sum_{i=j}^K \alpha_{\text{ground}}(i) \quad (7-15)$$

$$\sum_{j=0}^K T_a(-j) \sum_{i=j}^K \alpha_a(i) = \sum_{j=0}^K T_a(N-j) \sum_{i=j}^K \alpha_a(i) \quad (7-16)$$

$$\sum_{j=0}^K T_{\text{house}}(-j) \sum_{i=j}^K \alpha_{\text{house}}(i) = \sum_{j=0}^K T_{\text{house}}(N-j) \sum_{i=j}^K \alpha_{\text{house}}(i) \quad (7-17)$$

The left side of Equations (7-15), (7-16), and (7-17) represents the heat gains due to the temperatures during the period from $-K$ to 0 , the right side represents the heat contributions outside the period due to the temperature during the period. Therefore these equations reflect the equivalent rule precisely. In order to simplify these equations, the concept of summation of response factors is introduced below:

$$A(j) = \sum_{i=j}^K \alpha(i) \quad (7-18)$$

Introducing this concept into Equations (7-15), (7-16), and (7-17), these equations become:

$$\sum_{j=0}^K T_{\text{ground}}(-j) A_{\text{ground}}(j) = \sum_{j=0}^K T_{\text{ground}}(N-j) A_{\text{ground}}(j) \quad (7-19)$$

$$\sum_{j=0}^K T_a(-j) A_a(j) = \sum_{j=0}^K T_a(N-j) A_a(j) \quad (7-20)$$

$$\sum_{j=0}^K T_{\text{house}}(-j) A_{\text{house}}(j) = \sum_{j=0}^K T_{\text{house}}(N-j) A_{\text{house}}(j) \quad (7-21)$$

Equations (7-19), (7-20), and (7-21) are called option 2 of the second rule. Obviously, the period which satisfies second option is easier to use. However, the response factors have to be calculated based on the audit data of the building in this case. Therefore, the reliability of the audit data will influence the accuracy of measurement results.

Introducing the second rule to the energy balance Equation (7-11), it then reduced to:

$$A_{\text{ground}} \bar{T}_{\text{ground}} + A_a \bar{T}_a + A_{\text{house}} \bar{T}_{\text{house}} + \bar{q}_{\text{power}} + \dot{m} A_{\text{air}} + \frac{1}{N} \sum_{j=0}^K \alpha_{\text{solar}}(j) \sum_{i=1}^N I(i-j) = 0 \quad (7-22)$$

where

A = summation of the response factors with $j=0$.

To apply the equivalent rule to solar radiation, the third rule then requires that the solar radiation must be zero from time $-K$ to 0 , and from $N-K$ to N . Introducing the third rule into Equation (7-22), the last term can then be expressed as the product of the average solar radiation and the solar conductance (A_{solar}).

$$A_{\text{ground}} \bar{T}_{\text{ground}} + A_a \bar{T}_a + A_{\text{house}} \bar{T}_{\text{house}} + \bar{q}_{\text{power}} + \dot{m} A_{\text{air}} + A_{\text{solar}} \bar{I}_{\text{solar}} = 0 \quad (7-23)$$

T_{ground} has been defined as the parameter that in combination with house temperature dominates the floor heat transfer in Equation (7-2). According to this definition, the ground temperature is closely related to the previous outside air temperature although the relationship is strongly dependent on the structure of the floor which is coupling to ground, the period of time, and the season. To simplify the analysis, we introduce the ratio of ground temperature to ambient temperature β_t :

$$\beta_t = \frac{\bar{T}_{\text{ground}}}{\bar{T}_a} \quad (7-24)$$

Introducing β_t into Equation (7-23), it then follows:

$$(A_{\text{ground}} \beta_t + A_a) \bar{T}_a + A_{\text{house}} \bar{T}_{\text{house}} + \bar{q}_{\text{power}} + A_{\text{air}} \dot{m} + A_{\text{solar}} \bar{I}_{\text{solar}} = 0 \quad (7-25)$$

The physical meaning of a summation of response factors can be defined by examining a few special cases using Equation (7-25).

Assume that neither solar nor air infiltration is present. Then the Equation (7-25) becomes:

$$(A_{\text{ground}} \beta_t + A_a) \bar{T}_a + A_{\text{house}} \bar{T}_{\text{house}} + \bar{q}_{\text{power}} = 0 \quad (7-26)$$

It is assumed that the heat input can be expressed as:

$$q_{\text{power}} = UA_0 (\bar{T}_{\text{house}} - \bar{T}_a) \quad (7-27)$$

Comparing Equations (7-26) and (7-27), one finds:

$$A_{\text{ground}}\beta_t + A_a = -A_{\text{house}} = UA_0 \quad (7-28)$$

UA_0 is a constant. However, it is expressed with a temperature ratio β_t in Equation (7-28). This means that the test can only produce correct results when β_t is a constant. Fortunately, if the house has an unconditioned basement or a craw space that are well ventilated, T_{ground} , in fact, can be well approximated by the ambient air temperature. The outdoor test cell is one such example. If the house has a slab-on-grade floor, then the heat flux through floor is dominated by both the ambient and ground soil temperatures. If the soil temperature is assumed constant (at its annual average ambient temperature), then β_t may be simplified as a function of the ratio of the width and length of the floor. This issue needs to be studied carefully.

Assume that there is no solar radiation. Then Equation (7-25) can be expressed as:

$$UA_0 (\bar{T}_a - \bar{T}_{\text{house}}) + q_{\text{power}} + A_{\text{air}}\dot{m} = 0 \quad (7-29)$$

Under this special condition, the heat input can be expressed as:

$$q_{\text{power}} = UA_0 (\bar{T}_{\text{house}} - \bar{T}_a) + \dot{m}C_p (1 - \text{IHEE})(\bar{T}_{\text{house}} - \bar{T}_a) \quad (7-30)$$

Comparing Equations (7-29) and (7-30), A_{air} becomes:

$$A_{\text{air}} = - (1 - \text{IHEE})(\bar{T}_{\text{house}} - \bar{T}_a) C_p \quad (7-31)$$

Finally the energy balance equation is:

$$(UA_0 + (1 - \text{IHEE})C_p\dot{m})(\bar{T}_{\text{house}} - \bar{T}_a) - \bar{q}_{\text{power}} - A_{\text{solar}}\bar{I}_{\text{solar}} = 0 \quad (7-32)$$

The actual heat loss factor (UA) of the house under both air infiltration and conduction can be defined by the following formula:

$$UA = UA_0 + (1 - \text{IHEE}) C_p\dot{m} \quad (7-33)$$

Introducing it into the energy balance equation, we get:

$$UA(\bar{T}_{\text{house}} - \bar{T}_a) - \bar{q}_{\text{power}} - A_{\text{solar}}\bar{I}_{\text{solar}} = 0 \quad (7-34)$$

Equation (7-34) holds for periods, which obey the following rules: (1) the internal thermal mass has the same capacity at both the beginning and ending of the period; (2) the moving average temperatures of ground, enclosure, and ambient temperatures with window width as the period length during $-K$ to 0 of the time period are constant; or the Equations (7-19), (7-20), and (7-21) hold; and (3) the period begins K time steps after sunset, and ends before sunrise. In addition, a constant air flow is required for tests, if a non-constant air flow rate is present, this method cannot guarantee the accurate results because of non-linearity of heat transfer processes. Nevertheless good results may be actually achieved in practice.

According to Equation (7-34), there are two options to determine UA and the solar aperture (A_{solar}).

Option 1

Since there are only two unknown parameters in Equation (7-34), both UA and solar aperture can be determined if two periods are chosen. It must be pointed out that these two periods must have the same air flow rate and leakage configurations. Assume that the superscript 1 represents the first period, 2 represents the second period, then the UA and solar aperture can be calculated from the measured parameters by the following formula:

$$UA = \frac{\bar{q}_{\text{power}}(\bar{I}_{\text{solar}}^1 + \bar{I}_{\text{solar}}^2)}{\bar{I}_{\text{solar}}^2(\bar{T}_{\text{house}}^1 - \bar{T}_a^1) + \bar{I}_{\text{solar}}^1(\bar{T}_{\text{house}}^2 - \bar{T}_a^2)} \quad (7-35)$$

$$A_{\text{solar}} = \frac{\bar{q}_{\text{power}}(\bar{T}_{\text{house}}^2 + \bar{T}_a^2)}{\bar{I}_{\text{solar}}^2(\bar{T}_{\text{house}}^1 - \bar{T}_a^1) + \bar{I}_{\text{solar}}^1(\bar{T}_{\text{house}}^2 - \bar{T}_a^2)} \quad (7-36)$$

The solar aperture is dependent on air flow rates and air flow directions because infiltration air flow carries more solar energy into houses than exfiltration air flow does. Therefore, this option is suitable for separately investigating energy impact of air

infiltration on heat conduction and solar radiation, and for estimating the actual solar aperture and UA values under different conditions.

Option 2

The second option measures the solar aperture when there is no air infiltration present. This solar aperture is then used in other tests where air infiltration is present. This option consists of three steps.

First, the solar aperture, A_{solar} , can be determined from a test conducted with no air flow and no power input. The energy balance equation is then:

$$UA_0 (\bar{T}_{\text{house}} - \bar{T}_a) - A_{\text{solar}} \bar{I}_{\text{solar}} = 0 \quad (7-37)$$

So the summation of the solar response factor is:

$$A_{\text{solar}} = UA_0 \frac{\bar{T}_{\text{house}}^* - \bar{T}_{\text{am}}^*}{\bar{I}_{\text{solar}}^*} = UA_0 f_s \quad (7-38)$$

where \bar{T}_{house}^* and \bar{T}_{am}^* represent the house and ambient temperatures ($^{\circ}\text{C}$) from a test without air flow and power input, and f_s is defined as a solar factor ($^{\circ}\text{C m}^2/\text{W}$).

Introducing f_s into the energy balance equation yields:

$$UA(\bar{T}_{\text{house}} - \bar{T}_a) - \bar{q}_{\text{power}} - UA_0 f_s \bar{I}_{\text{solar}} = 0 \quad (7-39)$$

Determining UA_0 by running a test with power input but without air flow, the energy equation under this condition is:

$$UA_0 (\bar{T}_{\text{house}} - \bar{T}_a) - \bar{q}_{\text{power}} - UA_0 f_s \bar{I}_{\text{solar}} = 0 \quad (7-40)$$

The UA_0 can be determined:

$$UA_0 = \frac{\bar{q}_{\text{power}}}{\bar{T}_{\text{house}} - \bar{T}_a - f_s \bar{I}_{\text{solar}}} \quad (7-41)$$

Finally, the tests can be carried out with both air flow and power input, and the UA and IHEE can be calculated by using the following formula:

$$UA = \frac{\bar{q}_{\text{power}} + UA_0 f_s \bar{I}_{\text{solar}}}{\bar{T}_{\text{house}} - \bar{T}_a} \quad (7-42)$$

$$\text{IHEE} = 1 - \frac{UA - UA_0}{\dot{m} C_p} \quad (7-43)$$

This option is suitable for investigating the overall energy impact of air infiltration on both heat conduction and solar radiation. However, it takes longer than does option 1. Therefore, this option is most suitable for the systematic investigation of air infiltration heat recovery where air infiltration can be accurately controlled.

STAM METHOD

According to the fundamental theory, STAM requires that tests be performed with constant air flow rates. However, no special limit is placed on either heat input or house temperature. Therefore, tests can be performed with either constant heat input or constant house temperature according to the actual test facilities and house conditions.

The constant heat input option is suitable for single cell buildings that have no internal thermal mass because under this conditions the thermal mass temperature is the same as that of the building air. Also the heating system can be greatly simplified because lower sampling frequency is then possible and no control is needed.

The constant temperature option is suitable for buildings with internal thermal masses, such as partition wall and furniture. It is expected that the thermal mass has the same heat capacity during the test when direct solar gain on the internal mass is minimized. Consequently, the first rule is automatically satisfied with this test option, and there is no need to characterize or measure the thermal mass temperature.

Time periods can be chosen using the following procedure: 1) implement the third rule to choose the basic periods; 2) implement the first rule in the basic periods and between two basic periods to choose candidate periods; and 3) implement the second rule to check the candidate periods and to decide whether each candidate period should be rejected or used to determine IHEE.

The third rule requires that no solar radiation be present K time steps before the beginning and ending of the period. The physical meaning is that the solar radiation used for the calculation should be totally consumed in the period. K time steps are the time period during which the solar impulse influences the house. Generally, it is about 4 to 6 hours for low mass houses. Therefore, the basic period should start 4 to 6 hours after sun set and end before sun rise. For example, if sun-set is at 7 PM, and sun-rise is at 6 AM, then the basic period is from 11 PM to 6 AM.

Candidate periods are chosen from the basic period and between any two basic periods, where the temperature difference between the beginning and the ending of the period is less than $0.1\text{ }^{\circ}\text{C}$, which is dependent on the length of the time step. Generally, there are several candidate periods for each basic period, or between two basic periods.

The final time periods are chosen from the candidate periods according to the second rule. The second rule requires a constant moving average temperature that can be checked by one of the following methods: (1) calculate the variance of the sequence of the moving average temperatures; if the variance is larger than a pre-assumed limit, then reject the period; (2) check the maximum difference of the sequence of the moving average temperature, if it is larger than a pre-assumed limit then reject the period; OR (3) use a white noise check.

The white noise check can be implemented as follows. Assume $\{T(i)\}$ is the moving average temperature sequence. If the moving average temperature is a constant, then the sequence of differences between the moving average temperature and its non-bias estimates (average value) $\{T(i) - \sum_{j=1}^N T(j)/N\}$ should be a random sample or white noise. The hypothesis can be checked out by a standard method [Newton 1988].

The final period can also be verified by using Equations (7-19), (7-20), and (7-21).

If only one candidate period is chosen from each basic period or from any two basic periods, the maximum periods (M) can be determined from the basic period (N) by using the combination rule:

$$M = N + \frac{1}{2} C_N^2 \quad (7-44)$$

where C_N^2 is number of combinations of N distinct basic periods taken two at a time.

Although a test that covers two nights and one day period can generate three periods, it is suggested that a test covers at least two-night and two-day time because the period, which does not cover day time, can result in unreliable UA estimation due to under-estimation of solar radiation energy gain. Generally, it is possible to identify both UA and solar aperture under a specific air flow rate and known flow directions using a two days test. However, if the weather is extremely abnormal, longer test time may be necessary.

EXPERIMENTAL VALIDATION OF STAM

STAM was tested during the summer of 1990 (July 21 to September 20) in the outdoor test cell under both infiltration and exfiltration conditions with non-dimensional air flow rates from 0.35 to 1.2. A total of 13 tests were carried out; the first 6 tests used

exfiltrating air flow, where the fan supplied air directly to the test cell and air was forced to leak out through the envelope, and the other tests used infiltrating flow, where the fan exhausted air to outside and air was forced to leak in through the envelope. Each test took at least two days. The basic period was from 11 pm to 7 am. The candidate periods had a cell temperature difference of less than 0.1 °C between the starting and ending. The final periods had a variance of the moving average temperature less than 0.02 °C. Constant heat input option (Option 2) was used because the major purpose of the experiment was to systematically investigate air infiltration heat recovery. The constant heat input option was used with 250 W heat input being used during each test.

In order to investigate the solar radiation influence, the following solar models were used: horizontal solar radiation, it is assumed that the solar radiation intercepted by the test cell was the same as the horizontal solar radiation; ASHRAE model, the direct and diffuse solar radiations were calculated from measured horizontal solar radiation according to the ASHRAE model, then the equivalent solar radiation of the test cell was calculated as the ratio of the sum of solar radiation on the whole test cell to the envelope area; SHACSEJ (Society of Heating and Air-Conditioning and Sanitary Engineers of Japan) model, the direct solar and diffuse solar radiation were broken down from horizontal solar radiation according to the SHACSEJ model, then the equivalent solar radiation of the test cell was calculated as the ratio of the sum of solar radiation on all the surfaces of the test cell to the envelope area of the cell (see Appendix A3).

In order to demonstrate the advantage of the STAM method, the UA and IHEE were also calculated with the daily average method, with the period chosen as 24 hours (from 0:00 clock to 24:00 clock) or its multiples. The comparisons of the solar models, STAM and DAM are discussed below.

Comparison of Solar Models

One example of the equivalent solar radiation and its ratio with horizontal solar radiation is shown in Figure 7-2. The x-axis is time, the first y-axis is the ratio of equivalent solar and horizontal solar radiation, and the second y-axis is the horizontal and equivalent solar radiation. Distinct features can be seen for the ratios of the ASHRAE and the SHACSEJ models. The ASHRAE model showed that the ratio was dependent on time only, and so the equivalent solar radiation was similar to horizontal solar radiation in shape. The SHACSEJ model showed that the ratio was dependent on both time and horizontal solar radiation. The common feature of both models was a high ratio during sunset and sunrise time because the vertical surfaces of the cell intercepted more solar radiation than a horizontal surface.

The ratio and equivalent solar radiation are shown in Figure 7-3 vs horizontal solar radiation. The distinct similarity for high radiation can be seen, but a totally different feature appears for low solar radiation. The ratio dropped to zero quickly when the horizontal solar radiation was lower than 200 W/m^2 for the SHACSEJ model, but the ratio remained constant for the ASHRAE model. A very wide band seems to be present in both of the models when the solar radiation was low. These phenomena reflected sunset and sunrise, and cloudy weather. It was surprising that the ASHRAE model gave a 0.2 ratio for a sunny day at noon, while the SHACSEJ model gave a value of 0.4.

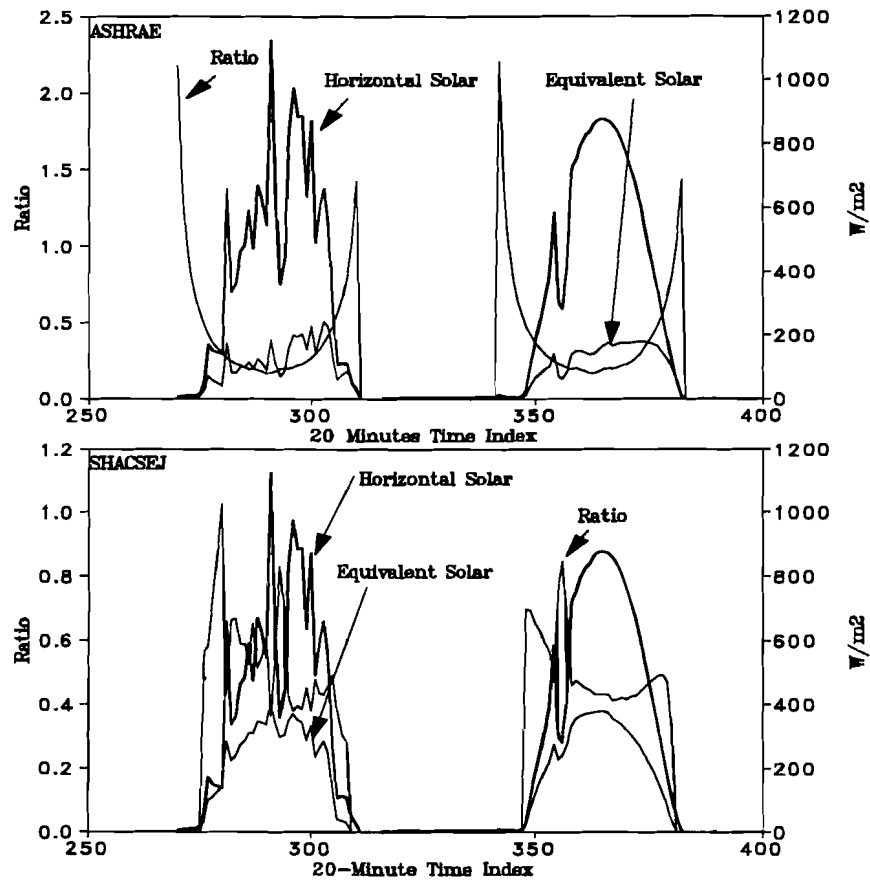


Figure 7-2: An Example of Equivalent Solar Radiation for ASHRAE, SHACSEJ, and Horizontal Models (Time Series Format)

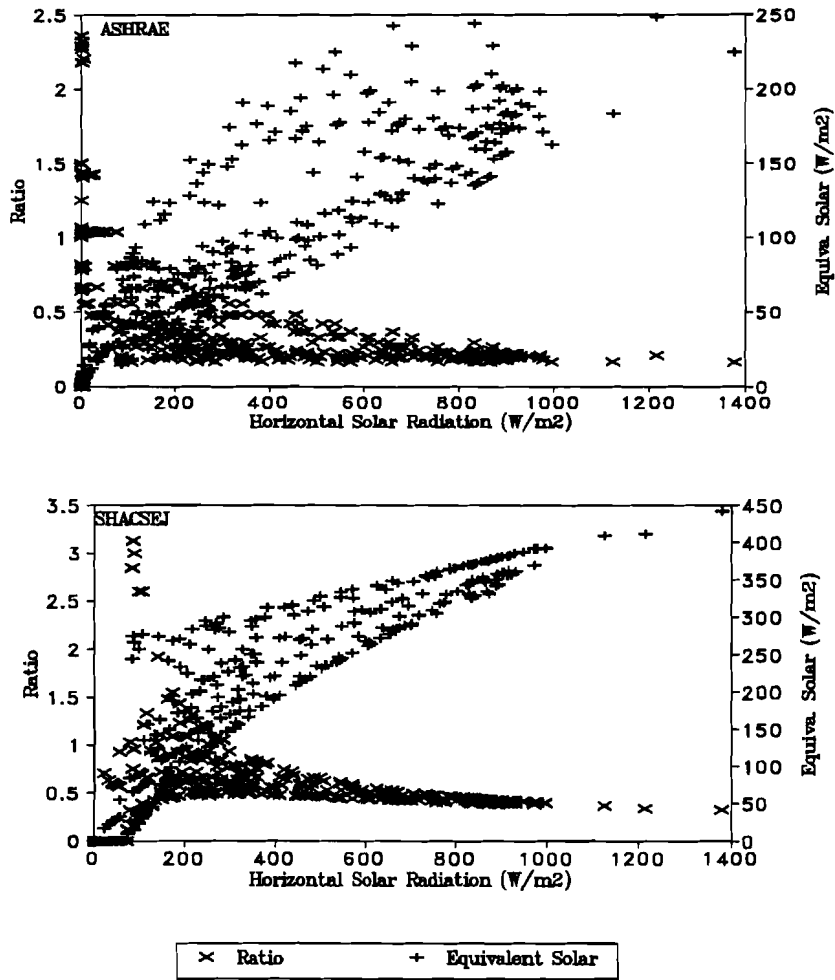


Figure 7-3: The Equivalent Solar Radiation on the Test Cell for ASHRAE & SHACSEJ Models and Ratio vs Horizontal Solar Radiation

The IHEEs calculated using the three solar models for STAM are shown in Figure 7-4. An excellent agreement between the models was observed. A factor akin to the root mean square, called the equivalent scatter factor, is introduced here to compare the average random error due to these models:

$$\Delta\epsilon = \sqrt{\frac{\sum_{i=1}^n [IHEE(\dot{m}) - \overline{IHEE}(\dot{m})]^2}{n}} \quad (7-45)$$

where $\overline{IHEE}(\dot{m})$ is the average IHEE for air flow rate \dot{m} .

The equivalent IHEE scatter factors were calculated: 0.055 (13%) for ASHRAE solar model, 0.050 (12%) for SHACSEJ solar model, 0.056 (13%) for Horizontal solar model under diffuse infiltration condition, and 0.0383 (10%) for ASHRAE solar model, 0.0314 (8%) for SHACSEJ solar model, and 0.0387 (10%) for horizontal solar model under diffuse exfiltration conditions. Although the solar models were quite different, the IHEEs were consistent. Therefore, it was concluded that any of the three solar models could be used with satisfactory accuracy.

Comparison of STAM and DAM

The results of the ASHRAE solar model were used to compare STAM and DAM methods because ASHRAE solar model was stable during sunrise and sunset periods, and gave good accuracy of IHEE results as compared to other models.

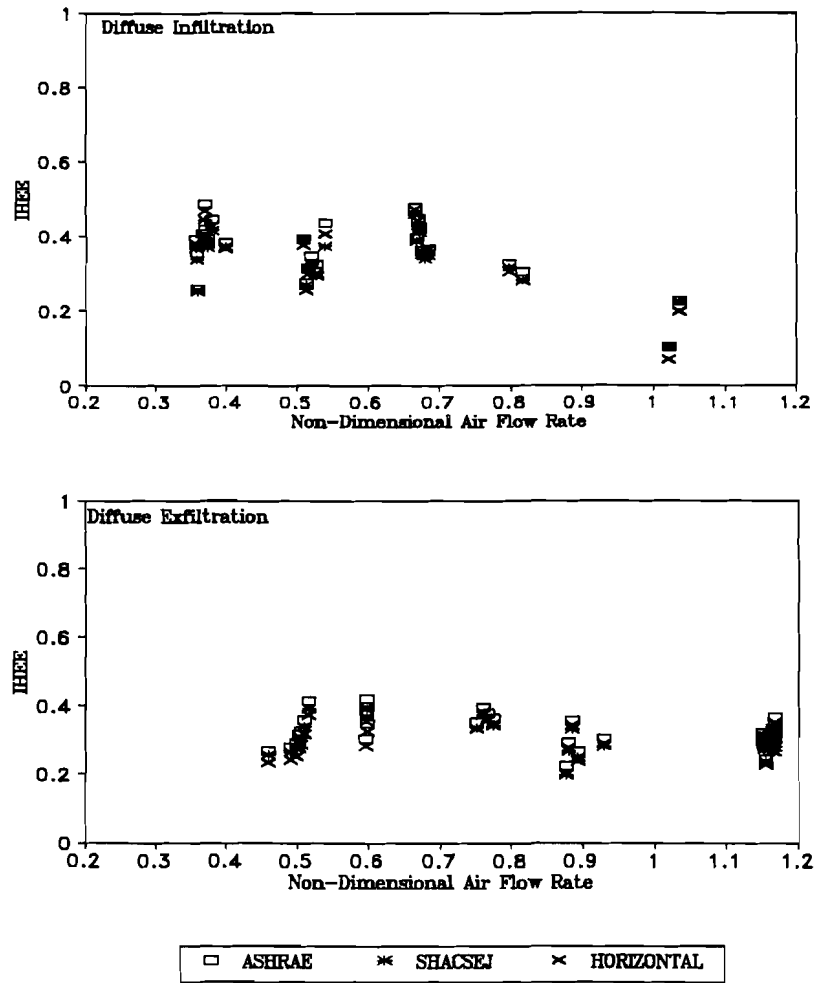


Figure 7-4: Comparison of IHEE Determined Using ASHRAE, SHACSEJ, and Horizontal Solar Models as a Function of Non-dimensional Air Flow Rate for Diffuse Infiltration and Diffuse Exfiltration

The results of IHEE are shown in Figure 7-5 for both STAM (69 values) and DAM (90 values). The IHEEs of DAM were more scattered than those of STAM. The equivalent scatter factor calculations showed 0.050 (12%) for STAM diffuse infiltration, 0.143 (36%) for DAM diffuse infiltration, 0.0384 (10%) for STAM diffuse exfiltration, and 0.0713 (18%) for DAM diffuse exfiltration. The results generated by DAM had 2 to 3 times more scatter than those of STAM.

The distribution of starting and ending times of the STAM final periods are shown in Figure 7-6. The x-axis shows the time, and the y-axis the probability of a starting and ending during the interval 23:00 -7:00. This probability generally decreased gradually with time from 0.19 to 0. This trend might be caused by the searching procedure, which began at 23:00 and marched sequentially. Obviously, both start and end times were weather dependent.

The thermal storage influence was investigated by examining the probability distribution of the deviation of period lengths from 24 hours or its multiples, calculated by the formula:

$$\delta T = (T - 24 * \text{int}(T / 24)) - 24 \quad (7-46)$$

The results are shown in Figure 7-7. Only 6% of the time periods had a length of 24 hour or its multiples with most periods 1 to 3 hours from 24 hours or its multiples. This demonstrates that the period lengths needed to be adjusted from 24-hour multiples to compensate for thermal storage effects due to abnormal weather variation.

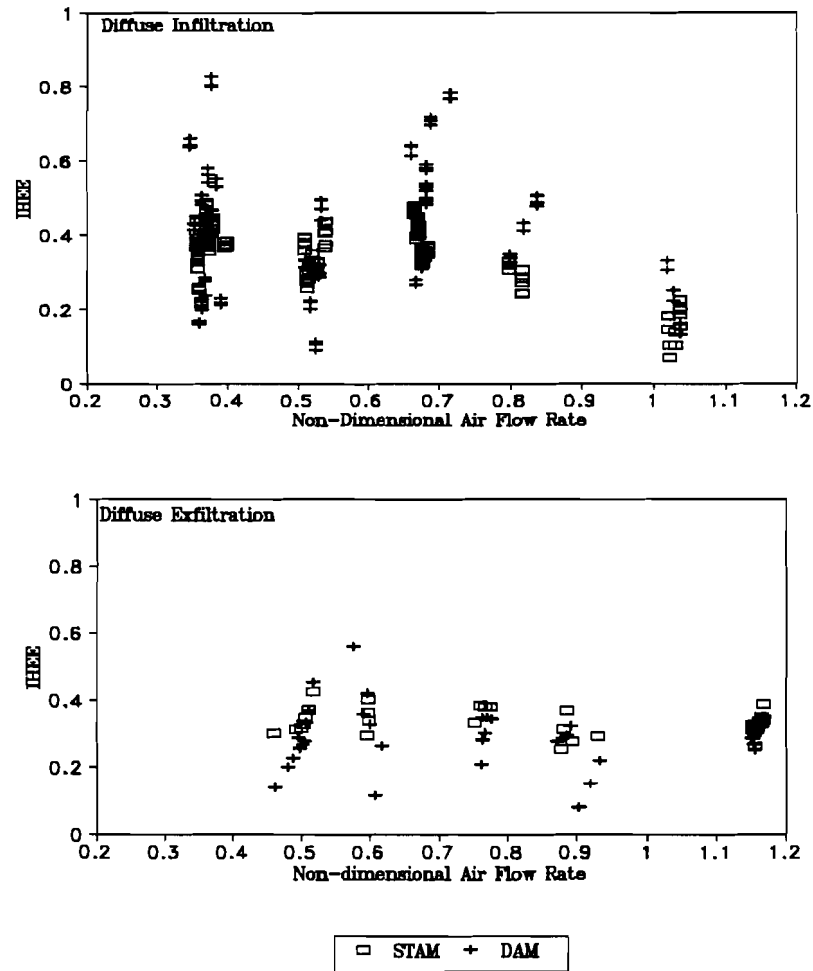


Figure 7-5: Comparison of IHEE Determined Using the STAM and DAM Methods as a Function of Non-dimensional Air Flow Rate for Diffuse Infiltration and Diffuse Exfiltration

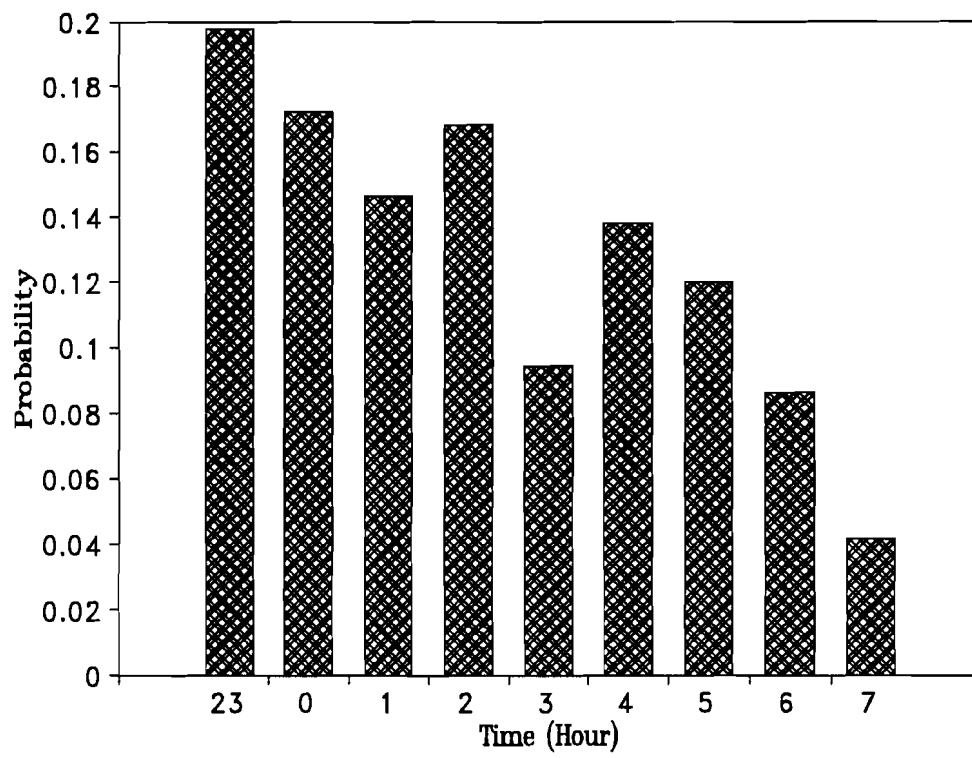


Figure 7-6: Start and End Time Distribution of the Periods for STAM

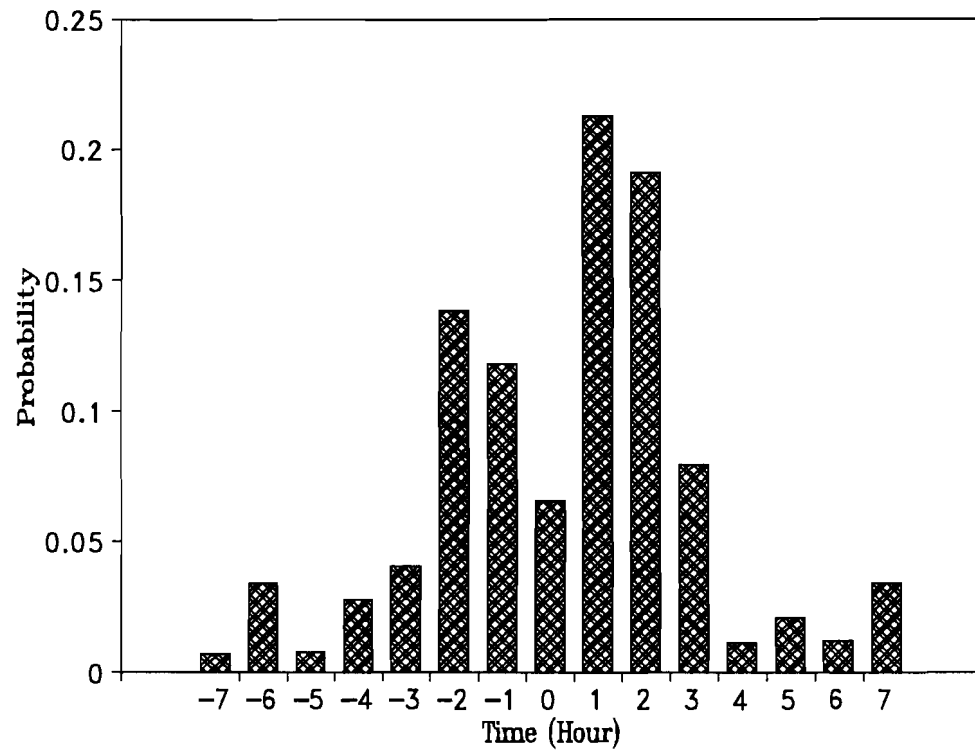


Figure 7-7: Time Period Deviation From 24 Hours or Its Multiples for STAM

STAM rejected 21 out of 90 possible periods by using option 1 of the second rule (moving average temperature), and had 94% of the time periods differ from multiple of 24-hour. STAM automatically rejected tests that cannot be used to determine IHEE.

SUMMARY

STAM was developed based on transfer function theory. This method can measure UA and solar aperture with a minimum two days test. It takes account of the external wall thermal storage problem due to abnormal weather condition by adjusting the time period automatically. The internal thermal storage problem can be avoided by using the constant room temperature option; consequently, there is no need to characterize the thermal mass temperature. Moreover, STAM greatly improved measurement accuracy comparing to the DAM method.

The measurement results of STAM validation are summarized in Appendix B6, where both IHEE and energy saving ratio are given with the test period, test cell temperature, ambient temperature, solar radiation, air flow rate, and heat input.

The tests have also found that UA calculated from a few hours' data at night has a lower value than that calculated from over 20 hours. It seems that solar radiation still influences cell temperature at night, so it is possible to under-estimate the UA value by 10% to 30% using a few hours' data at midnight, depending on the type of the house and the solar radiation of the previous day.

CHAPTER VIII

COMBINED SOLAR RADIATION, INFILTRATION, AND CONDUCTION MODELS

The outdoor tests showed that IHEE was not only dependent on the air flow rate and air leakage configuration, but also on the solar radiation. However, the existing models [Anderlind 1985, Liu 1987, Bailly 1987] do not include the influence of solar radiation.

This chapter describes the development of the combined solar radiation, air infiltration, and conduction models for ideal diffuse attics and walls, gives the numerical results of the models, and presents an application which shows the potential energy savings due to optimized air infiltration in a model house.

COMBINED MODELS

The ideal diffuse wall and attics are defined such that air flows through the wall and the ceiling are uniform with both the solid material and air having the same temperature at any location. In order to make the analysis simpler, a wall or attic is separated into two subsystems: an "outside" system (physically from the outside air to the outside surface of the wall or to the attic air) and a base system (physically from the outside surface of the wall or attic air to the room air). It is assumed that the outside surface temperature is known when the base system is investigated. The outside surface temperature can be obtained by combining an outside and a base system.

Base System

A base part of an ideal diffuse wall or attic is shown in Figure 8-1. It sustains an air infiltration rate \dot{m} ($\text{Kg/m}^2 \text{ s}$) (defined as positive for infiltration, negative for exfiltration). The outside surface temperature and room temperature are represented by T_w and T_r respectively. The heat resistance of the wall from the outside surface to room air is R_w . The conductive and air infiltration heat flux within the base system are generally expressed as:

$$Q_c = -k \frac{dT}{dx} = - \frac{dT}{dR} \quad (8-1)$$

$$Q_a = \dot{m} C_p (T - T_r) \quad (8-2)$$

where

C_p = specific heat of air (J/Kg K)

\dot{m} = air flow rate ($\text{Kg/m}^2 \text{ s}$)

T = temperature of the wall section at R ($^{\circ}\text{C}$)

R = heat resistance of the wall from outside to the position (K m/W)

T_r = room temperature ($^{\circ}\text{C}$).

The differential equation (8-3) was established by balancing the energy fluxes of a finite element under steady state conditions.

$$\frac{d^2T}{dR^2} - \dot{m} C_p \frac{dT}{dR} = 0 \quad (8-3)$$

with boundary conditions:

$$T(R = 0) = T_w \quad (8-4)$$

$$T(R = R_w) = T_r \quad (8-5)$$

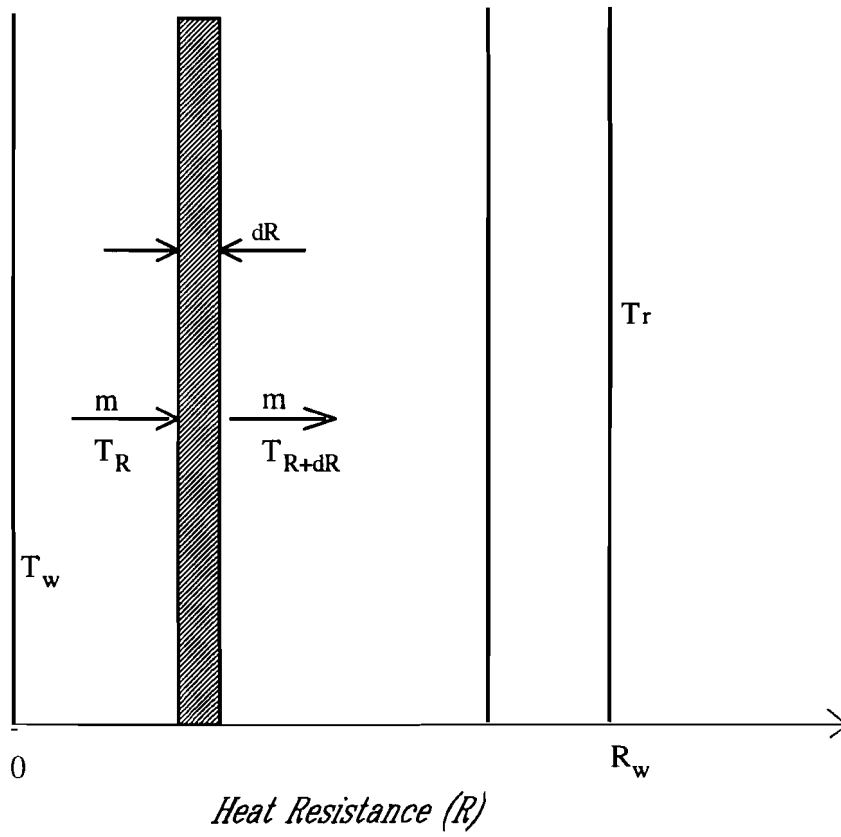


Figure 8-1: Schematic of Diffuse Wall Base System

The solution of this equation is:

$$\frac{T - T_w}{T_r - T_w} = \frac{1 - \exp(\dot{m}C_p R)}{1 - \exp(\dot{m}C_p R_w)} \quad (8-6)$$

$\dot{m}C_p R_w$ is the ratio of maximum heat loss factors ($\dot{m}C_p$, and $1/R_w$) due to infiltration and conduction respectively. It is called the non-dimensional air flow rate and expressed by α_w since the heat loss factor due to conduction is considered as a constant for a wall. Similarly, $\dot{m}C_p R$ is expressed as α . Introducing this convention into equation (8-6), it then follows:

$$\frac{T - T_w}{T_r - T_w} = \frac{1 - \exp(\alpha)}{1 - \exp(\alpha_w)} \quad (8-7)$$

The conduction heat flux is obtained by introducing Equation (8-7) into Equation (8-1):

$$Q_c = - \frac{dT}{dR} = (T_r - T_w) \frac{\dot{m}C_p \exp(\alpha)}{1 - \exp(\alpha_w)} \quad (8-8)$$

The total heat loss is calculated simply by letting $\alpha = \alpha_w$ in Equation (8-8), since the air infiltration heat flux is zero when $R = R_w$.

$$Q = (T_r - T_w) \frac{\dot{m}C_p \exp(\alpha_w)}{1 - \exp(\alpha_w)} \quad (8-9)$$

The overall/apparent heat transfer coefficient is then calculated by:

$$U_A = \frac{-Q}{T_r - T_a} = (1 - \theta) \frac{\dot{m}C_p \exp(\alpha_w)}{1 - \exp(\alpha_w)} = (1 - \theta) \frac{\phi}{R_w} \quad (8-10)$$

where:

$$\theta = \frac{T_w - T_a}{T_r - T_a} \quad (8-11)$$

$$\phi = \frac{\alpha_w \exp(\alpha_w)}{1 - \exp(\alpha_w)} \quad (8-12)$$

$$U = \frac{\Phi}{T_r - T_a} = (1 - \theta) \frac{\Phi}{R_w} \quad \text{E-10}$$

$$\theta = \frac{T_{co} - T_a}{T_r - T_a}$$

$$\frac{T_a - T_w}{R_{bo}} + I - \Phi + \dot{m} c_p (T_a - T_w) = 0$$

$$-\dot{m} c_p + \frac{T_a - T_w}{R_{bo}(T_r - T_a)} + \frac{I - \Phi}{T_r - T_a} = 0$$

SF

$$-\dot{m} c_p + \frac{\theta}{R_{bo}} + \text{SF} - (1 - \theta) \frac{\Phi}{R_w} = 0$$

$$\theta \left(\frac{\Phi}{R_w} - \frac{1}{R_{bo}} \right) + \text{SF} - \dot{m} c_p - \frac{\Phi}{R_w} = 0$$

$$\theta = \frac{\frac{\Phi}{R_w} + \dot{m} c_p - \text{SF}}{\frac{\Phi}{R_w} - \frac{1}{R_{bo}}} = \frac{-\Phi + \dot{m} c_p R_w - \text{SF} R_w}{-\Phi - \frac{R_w}{R_{bo}}}$$

The heat loss under the same conditions using the classical design calculation with the influence of solar radiation included is:

$$Q_{\text{classical}} = \begin{cases} \left(\frac{1}{R_t} + mCp \right) (T_r - T_a) - I \frac{R_{b0}}{R_t} & \text{Infiltration} \\ \frac{1}{R_t} (T_r - T_a) - I \frac{R_{b0}}{R_t} & \text{Exfiltration} \end{cases} \quad (8-13)$$

where:

R_t = resistance from outside air (wall) or attic air to room air

T_a = outside air temperature

$Q_{\text{classical}}$ = heat flux calculated according to the design method

I = solar radiation absorbed by the wall (W/m^2)

R_{b0} = heat resistance of outside convective boundary layer.

The apparent heat transfer coefficient for the design method, then, is:

$$UA_{\text{classical}} = \begin{cases} \frac{1}{R_t} + mCp - \frac{R_{b0}}{R_t} \beta \psi & \text{Infiltration} \\ \frac{1}{R_t} - \beta \psi & \text{Exfiltration} \end{cases} \quad (8-14)$$

where:

$$\psi = \frac{I}{T_r - T_a} \quad (8-15)$$

$$\beta = \frac{R_w}{R_{b0}} \quad (8-16)$$

ψ is called the solar indicator, the ratio of solar radiation absorbed by the wall surface to the temperature difference between room and outside. It has a positive value in winter and a negative value in summer. β is the ratio of wall resistance to outside boundary layer resistance.

Thus IHEE, and the energy saving ratio (β_e) are calculated by:

$$\varepsilon = \frac{Q_{\text{classical}} - Q}{\dot{m}C_p(T_r - T_a)} = \frac{UA_{\text{classical}} - UA}{|\dot{m}C_p|} \quad (8-17a)$$

$$\beta_e = \frac{Q_{\text{classical}} - Q}{Q_{\text{classical}}} = \frac{UA_{\text{classical}} - UA}{UA_{\text{classical}}} \quad (8-17b)$$

These equations hold for both walls and attics because it is presumed that outside surface temperature is known. Subsequently, the model combines the "outside" system with the base system to find the outside surface non-dimensional temperature (θ).

Combined Model for Walls

The schematic of the heat transfer process of the ideal diffuse wall is shown in Figure 8-2. The outside surface boundary layer is treated as a separate layer because the solar radiation penetrates without resistance. The wall absorbs a constant solar radiation I (W/m^2), with air flow rate \dot{m} ($\text{Kg}/\text{m}^2 \text{ s}$) and the temperature difference $T_r - T_a$. The control surface of the system is shown in the figure with a dashed line. The energy balance on the control volume led to the following equation:

$$\frac{T_a - T_w}{R_{b0}} + I - Q + \dot{m}C_p T_a - \dot{m}C_p T_r = 0 \quad (8-18)$$

Dividing both sides of the Equation (8-18) by $T_r - T_a$, and introducing Equation (8-10) into Equation (8-18), it follows:

$$-\theta \frac{1}{R_{b0}} + \psi - (1 - \theta) \frac{\phi}{R_w} - \dot{m}C_p = 0 \quad (8-19)$$

Rearranging Equation (8-19), the non-dimensional temperature is then expressed as:

$$\theta = \frac{\alpha_w + \phi - \psi R_w}{\phi - \beta} \quad (8-20)$$

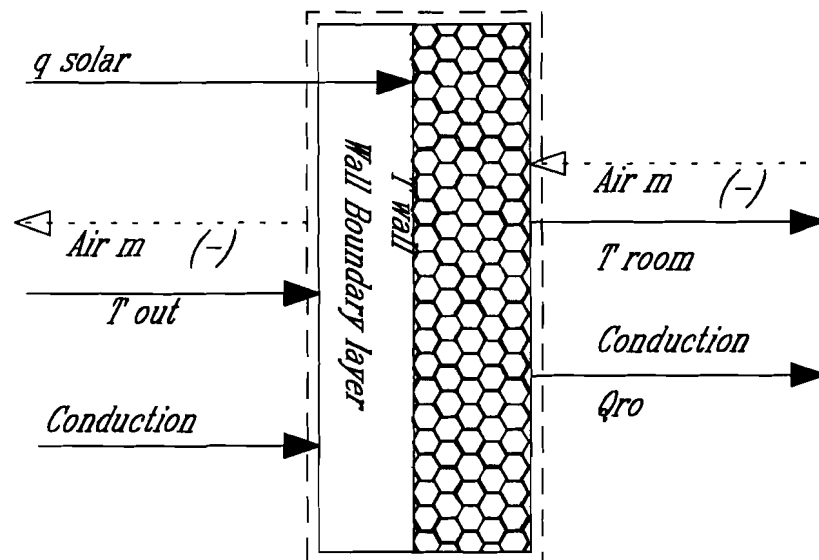


Figure 8-2: Schematic of Combined Model for Walls

Combined Model of Attic I

Attic I, defined as an attic without cross ventilation, is idealized as a two-layer system, shown in Figure 8-3. It is assumed that the air bypasses the roof shingle without the heat exchange effect; in other words, the air is at ambient temperature when infiltration leaks through the shingles, and at the attic temperature when it exfiltrates. These characteristics require different models for infiltration and exfiltration.

Taking the control system as the dashed line shown in Figure 8-3 (infiltration), the energy balance equation for the infiltration case is:

$$\dot{m}C_p T_a + I \frac{R_{b0}}{R_1} + (T_a - T_{attic}) \frac{1}{R_1} = \dot{m}C_p T_r + Q \quad (8-21)$$

where

\dot{m} = infiltration rate through the ceiling (Kg/m²s)

R_1 = heat resistance of the outer-layer (shingle) (W/m²K)

T_{attic} = attic temperature (°C).

Combining Equations (8-9) and (8-21), the non-dimensional temperature then follows as:

$$\theta = \frac{\phi - \psi\beta R_{b0} + \alpha_w}{\phi - \beta} \quad (8-22)$$

where:

$$\beta = \frac{R_w}{R_1} \quad (8-23)$$

$$\theta = \frac{T_{\text{attic}} - T_a}{T_r - T_a} \quad (8-24)$$

where:

R_w = heat resistance from attic air to room air.

The only difference between infiltration and exfiltration for attic I is that the air leakage temperature at the outside surface of the roof system is T_{attic} rather than T_a (see Figure 8-3 exfiltration). Thus the energy balance equation is:

$$\dot{m}C_p T_{\text{attic}} + I \frac{R_{b0}}{R_1} + (T_a - T_{\text{attic}}) \frac{1}{R_1} = \dot{m}C_p T_r + Q \quad (9-25)$$

The non-dimensional temperature can be deduced by a procedure similar to that used for infiltration:

$$\theta = \frac{\phi + \alpha_w - \psi\beta R_{b0}}{\phi + \alpha_w - \beta} \quad (8-26)$$

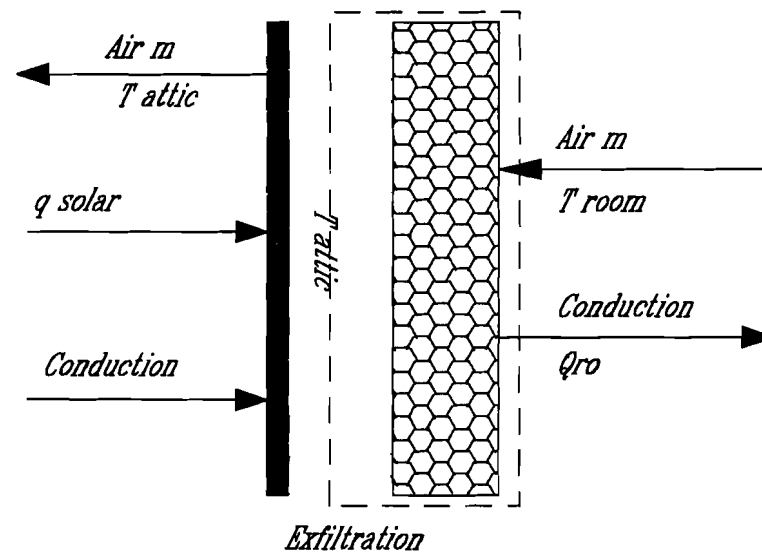
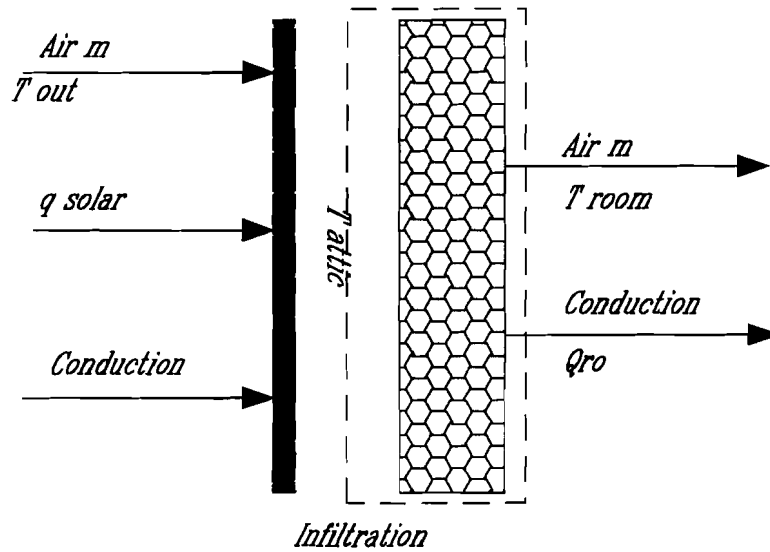


Figure 8-3: Schematic of Combined Model for Attic-I (without cross ventilation)

Combined Model of Attic II

The schematic of Attic II, defined as a roof system sustaining a cross ventilation (\dot{m}_c) only, is shown in Figure 8-4. The energy balance equation on the control volume is expressed as:

$$(T_a - T_{attic}) \frac{1}{R_1} + (T_r - T_{attic}) \frac{1}{R_w} + I \frac{R_{b0}}{R_1} + \dot{m}_c C_p T_a - \dot{m}_c C_p T_{exit} = 0 \quad (8-27)$$

where

T_{exit} = air temperature when the air leaves the attic

\dot{m}_c = cross ventilation rate ($\text{Kg}/\text{m}^2\text{s}$).

The attic temperature is defined as:

$$T_{attic} = \frac{1}{2} (T_{exit} + T_a) \quad (8-28)$$

The non-dimensional attic temperature is obtained by combining Equations (8-9), (8-27), and (8-28):

$$\theta = \frac{1 + \psi \beta R_{b0}}{1 + \beta + 2\alpha_c} \quad (8-29)$$

where:

$$\alpha_c = \dot{m}_c C_p R_w \quad (8-30)$$

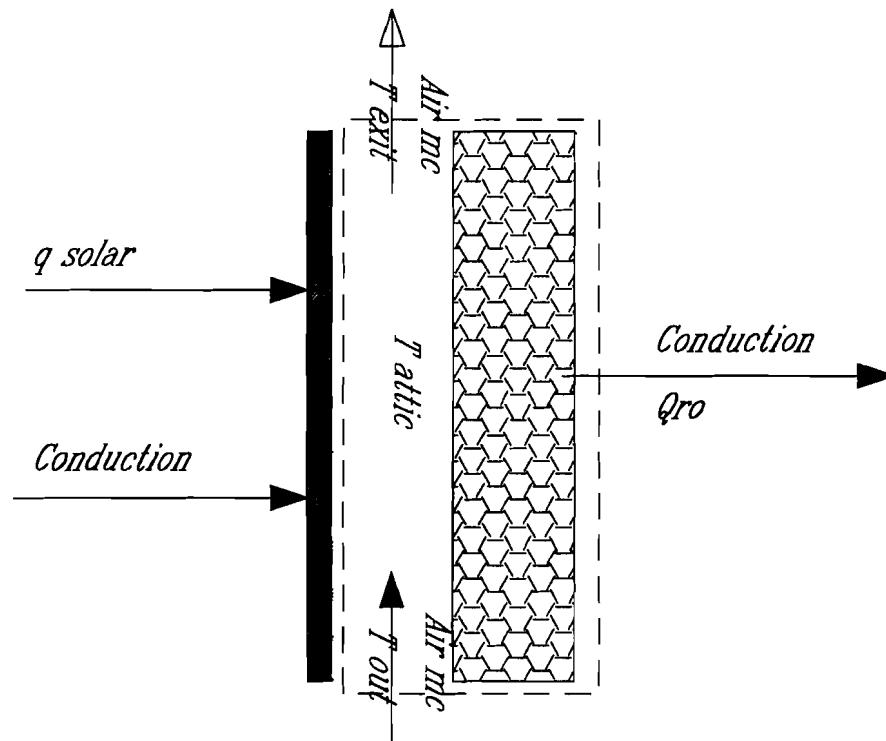


Figure 8-4: Schematic of Combined Model for Attic-II (with cross ventilation only)

Combined Model of Attic III

The schematic of Attic III, defined with both the infiltration and cross ventilation present, is shown in Figure 8-5. The energy balance equation is established according to the schematic figure:

$$(T_a - T_{attic}) \frac{1}{R_1} + \dot{m}_c C_p T_a + I \frac{R_{b0}}{R_1} - \dot{m} C_p T_r - Q - (\dot{m}_c - \dot{m}) C_p T_{exit} = 0 \quad (8-31)$$

where:

T_{exit} = air temperature when the air leaves the attic

$$T_{attic} = \frac{1}{2} (T_a + T_{exit}) \quad (8-32)$$

The non-dimensional attic temperature is deduced from Equation (8-9), (8-31), and (8-32) as:

$$\theta = \frac{\phi + \alpha_w - \psi \beta R_{b0}}{\phi + 2\alpha_w - \beta - \alpha_c} \quad (8-33)$$

where:

$$\alpha_c = \dot{m}_c C_p R_w \quad (8-34)$$

The analysis above shows that the combined energy consumption can be expressed by the solar indicator (ψ), the non-dimensional air flow rate (α), the resistance ratio (β), and the boundary layer resistance (R_c). These ratio parameters make it possible to obtain general idealized results with limited simulation calculations.

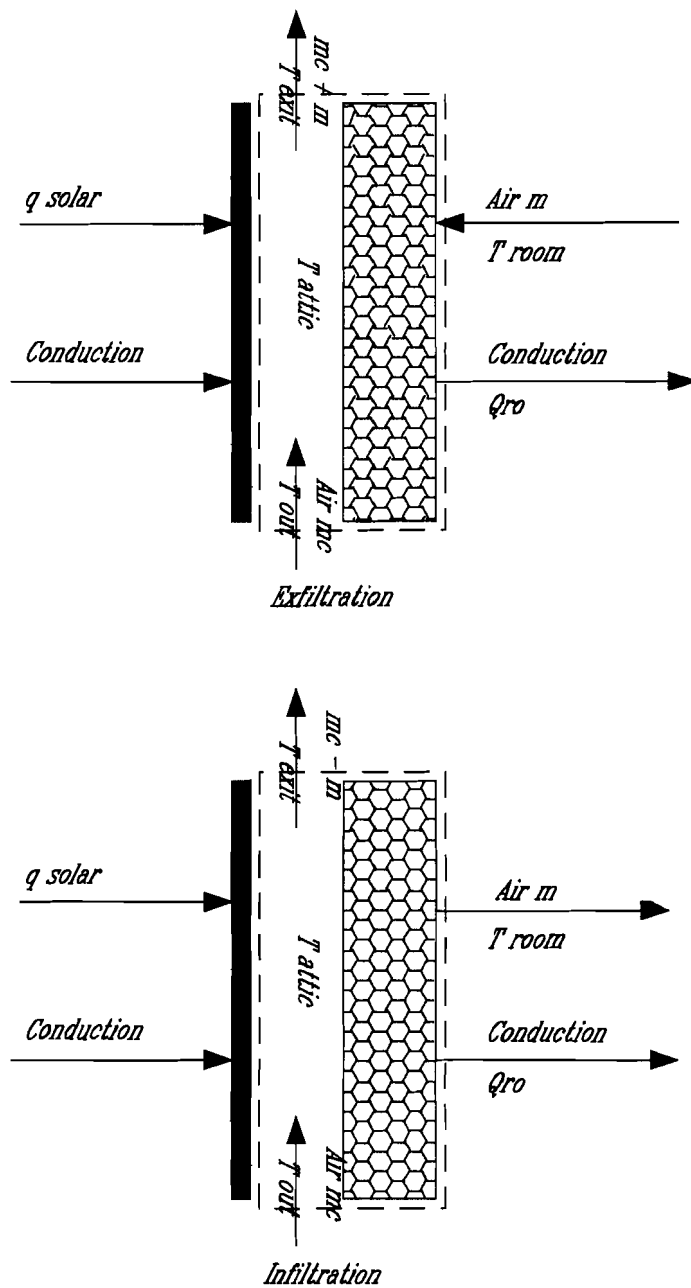


Figure 8-5: Schematic of Combined Model for Attic-III

radiation under the infiltration model but decreases under the exfiltration model because infiltration carries more solar radiation into rooms and reduces heat loss. In the cooling season, IHEE increases with solar radiation under the exfiltration model but decreases under the infiltration model because the exfiltration rejected more solar radiation energy to the outside and reduces the cooling load. Under the ranges of the solar radiation and air flow rates simulated, the IHEE varied from -2.3 to 2.8. These values show that the IHEE does not have minimum (0) and maximum (0.5) limits as soon as solar radiation is considered. Therefore, the combined effects of air infiltration, solar radiation, and conduction do not always lead to lower energy consumption in house components as compared to that given by the classical model.

The heat loss, energy savings, energy saving ratio, and IHEE are given in Table 8-1 for an air flow rate of 0.6 and solar indicator of 20 W/m²K for winter heating conditions, and an air flow rate of 0.6 and solar indicator -40 W/m²K for summer cooling conditions. These conditions corresponded to seasonal average weather conditions for the Houston area.

Table 8-1. Typical Energy Performance Data for the Wall

Code	U (W/m ² K)	U _d (W/m ² K)	Saving (W/m ² K)	Saving ratio	IHEE
Heating Infiltration	0.01	0.30	0.29	0.97	0.97
Heating Exfiltration	0.29	0.30	0.01	0.02	0.02
Cooling Infiltration	1.94	1.76	-0.18	-0.10	-0.59
Cooling Exfiltration	1.37	1.76	0.39	0.22	1.31

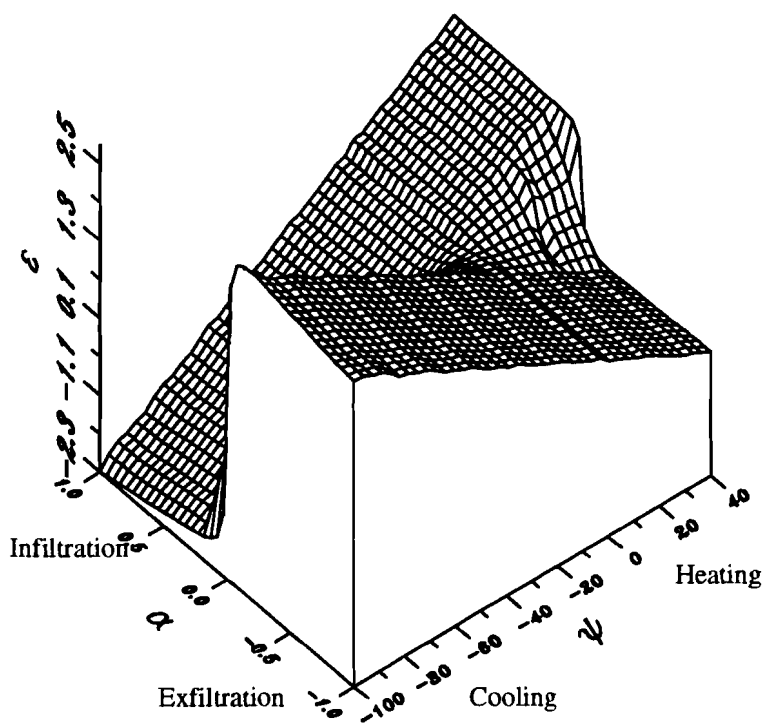


Figure 8-6: IHEE of Combined Diffuse Wall Model
 ϵ - IHEE, ψ - solar indicator ($\text{W}/\text{m}^2\text{C}$), α - non-dimensional air flow rate

It was observed that a substantial amount of energy could be saved if infiltration is present in winter and exfiltration in summer. However, if infiltration is present in summer and exfiltration in winter, the energy saving ratio changed from 97% to 2% for heating, and from 23% to -10% for cooling, the IHEE from 0.97 to 0.02 for heating, and from 1.31 to -0.59 for cooling.

The IHEEs of attic I shown in Figure 8-7 are generally similar to those of Figure 8-6, though there is some difference in the values. The energy performance values under seasonal average weather conditions are given in Table 8-2.

Table 8-2: Typical Energy Performance Data for the Attic with Infiltration

Code	U (W/m ² K)	U _d (W/m ² K)	Saving (W/m ² K)	Saving Ratio	IHEE
Heating Infiltration	0.01	0.17	0.16	0.95	0.95
Heating Exfiltration	0.17	0.17	0.00	0.00	0.00
Cooling Infiltration	1.09	0.99	-0.10	-0.10	-0.55
Cooling Exfiltration	0.76	0.99	0.23	0.23	1.34

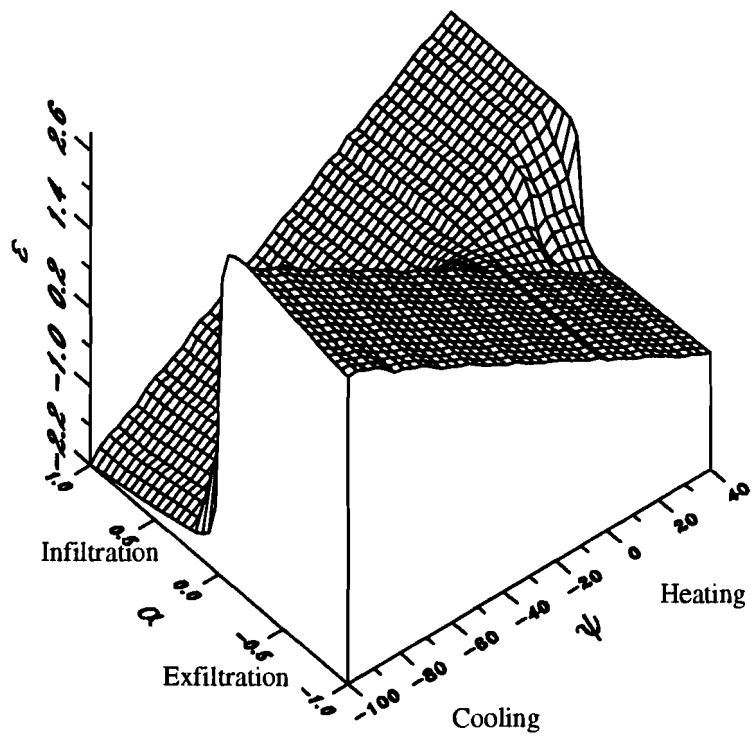


Figure 8-7: IHEE of Combined Model for Attic-I
 e - IHEE, y - solar indicator ($W/m^2\text{°C}$), a - non-dimensional air flow rate
 (Diffuse Infiltration/Exfiltration Only)

Table 8-2 showed that the heating energy consumption of Attic I could be reduced by 95% in the heating season by using infiltration rather than exfiltration. The cooling energy consumption could be reduced about 22% by using exfiltration and a 6% extra cooling energy consumption would be caused by using infiltration. The air infiltration energy recovery could be as high as 95% of the maximum air infiltration energy consumption for the heating season, and up to 134% for the cooling season. It is worth mentioning that the infiltration model could cause about 55% extra air infiltration energy consumption or 6% higher than the design method cooling energy consumption.

Attic II is a special case because there was no infiltration present. The energy saving ratios are given in Figure 8-8. The results show that energy savings decrease with the cross ventilation rate and solar radiation for heating, but increase with both the cross ventilation rate and solar radiation. The thermal performance values under the average seasonal weather conditions are given in Table 8-3, where the cross ventilation rate was 5.

Table 8-3. Typical Energy Performance Data for Attic with Cross Ventilation

Code	U (W/m ² K)	U _d (W/m ² K)	Saving (W/m ² K)	Saving Ratio
Heating	0.08	0.00	-0.08	0.00
Cooling	0.67	0.82	0.16	0.19

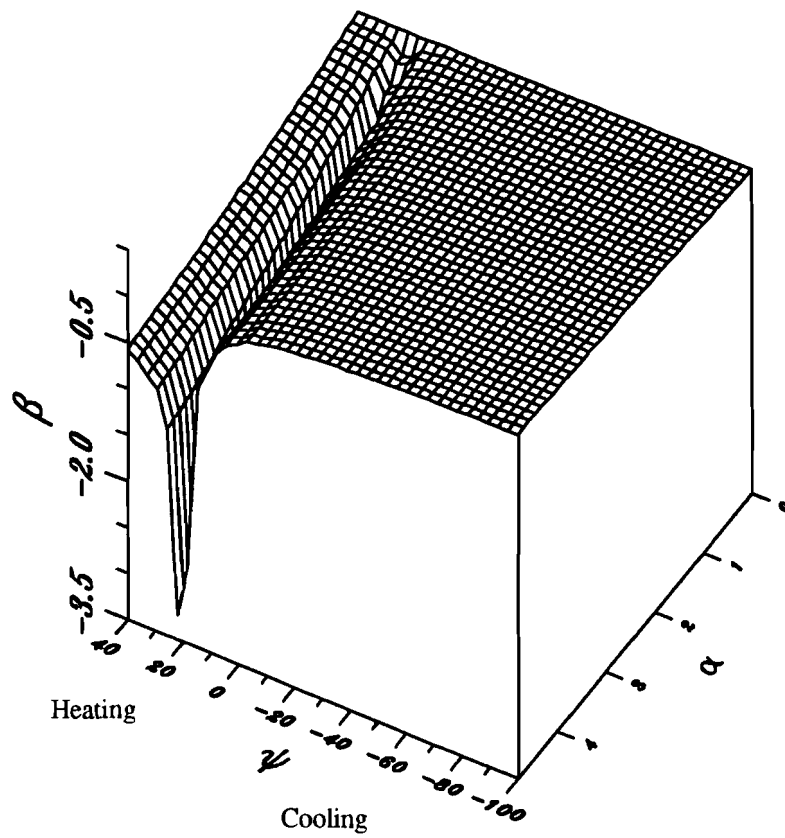


Figure 8-8: Energy Savings of Attic-II
 β - energy saving ratio, ψ - solar indicator ($\text{W}/\text{m}^2\text{C}$),
 α - non-dimensional air flow rate
(Cross Ventilation Only)

Table 8-3 showed that extra attic heating energy was consumed, and the cooling energy could be reduced by about 19% by cross ventilation under the seasonal average weather conditions. Obviously, attic cross ventilation should be avoided in winter to save energy.

The IHEEs of attic III are given in Figure 8-9 which shows an IHEE profile very different from those of walls and attic I. The IHEE increases sharply with solar radiation in the summer when the air flow rate was small, but decreases sharply with solar radiation in the winter for a small air flow rate. These results show that the cross ventilation was the dominant factor when the air infiltration was low. The thermal energy performance values under seasonal average weather conditions are given in Table 8-4.

Table 8-4. Typical Energy Performance Data for the Combined Attic Model

Code	U (W/m ² K)	U _d (W/m ² K)	Saving (W/m ² K)	Saving Ratio	IHEE
Heating Infiltration	0.06	0.17	0.11	0.66	0.66
Heating Exfiltration	0.21	0.17	-0.04	-0.23	-0.23
Cooling Infiltration	0.99	0.99	0.00	0.00	0.00
Cooling Exfiltration	0.69	0.99	0.30	0.30	1.76

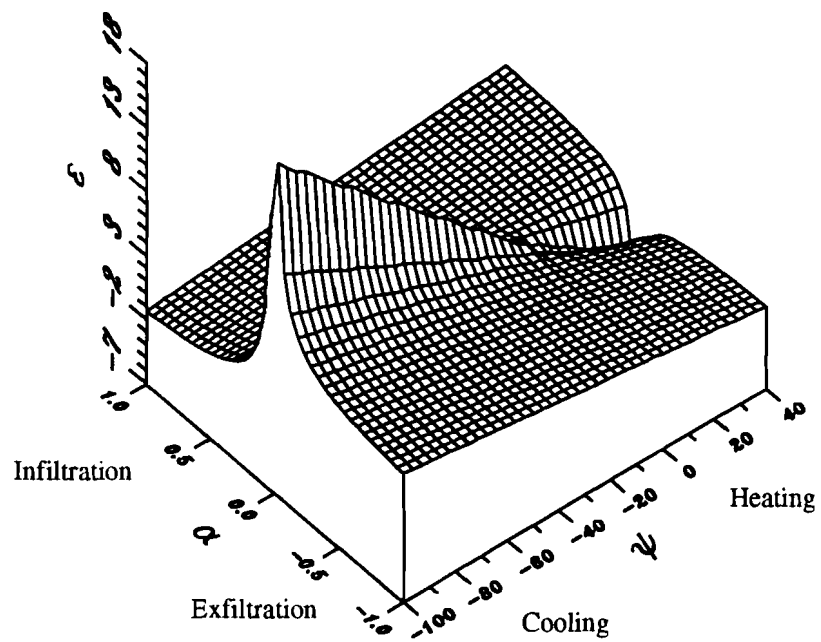


Figure 8-9: IHEE of Combined Model for Attic III
 ϵ - IHEE, ψ - solar indicator ($\text{W/m}^2\text{°C}$), α - non-dimensional air flow rate
 (Both Diffuse Infiltration/Exfiltration and Cross Ventilation Present)

Comparing Table 8-2 and Table 8-4, it is clear that attic III consumed 30% more heating energy and 7% less cooling energy than attic I under the seasonal average weather conditions. Obviously attic cross ventilation should be avoided in winter.

APPLICATION

The model analysis showed that infiltration can result in much lower energy loss than exfiltration in winter, and exfiltration can result in much lower energy consumption than infiltration in summer for walls and attics. This led to the hypotheses that depressurizing a house in winter and pressurizing it in summer by a fan might result in lower house energy consumption since this fan would permit an infiltration flow through the house envelope in winter and exfiltration flow in summer. Subsequently, a simplified house model was chosen to verify this assumption. The construction of the house, the definition of the house model, and simulation results are reported below:

The house was assumed to have external dimensions of 12 x 15 x 2.4 meters. The walls were assumed to be a standard wood frame structure with resistance of $2 \text{ m}^2\text{K/W}$. The ceiling was assumed to have R-19 insulation, with resistance from attic air to room air of $3.5 \text{ m}^2\text{K/W}$, and outside to attic air of $0.15 \text{ m}^2\text{K/W}$. The outside boundary layer resistance was $0.05 \text{ m}^2\text{K/W}$. The ceiling area was 180 m^2 , and wall area was 129.6 m^2 . It was assumed that 80% of the envelope was opaque component, so the opaque wall area was about 103.7 m^2 .

The idealized house model was defined as a house which was depressurized in winter and pressurized in summer by a fan, and had uniform infiltration (Figure 8-10). The "uniform infiltration" meant that both the opaque wall and the ceiling had identical non-

dimensional air flow rates. It was further assumed that the total air flow through the ceiling was the same as that through the windows. No heat recovery was considered for the windows.

The normal house model was defined such that air leaked in through half of the wall area and out through another half diffusely, and the ceiling had infiltration in summer and exfiltration in winter because of the thermal stack effect. Again, both the opaque wall and the ceiling had the same non-dimensional air flow rate. No combined effect was considered for the windows and doors.

The designed house model calculated the total energy consumption as the sum of the conduction and the air infiltration energy consumption where no interaction was considered. This model essentially represent a "leaky" house where no air infiltration heat recovery occurs.

The simulation assumed that the attic had no cross ventilation, and the solar radiation on the wall was $2/3$ of the radiation on the roof. The simulation covered non-dimensional air flow rates ranging from 0 to 1 with steps of 0.05, and the roof solar indicator ranged from -100 to 40 with steps of 2. The output of the simulation included the energy consumption under unit temperature difference for three house models, energy saving ratios of the idealized house to the normal house (I/N), the idealized house to the designed house(I/D), and the normal house to the designed house(N/D). It should be mentioned that the simulation did not include the window conduction and radiation, and the floor energy consumption.

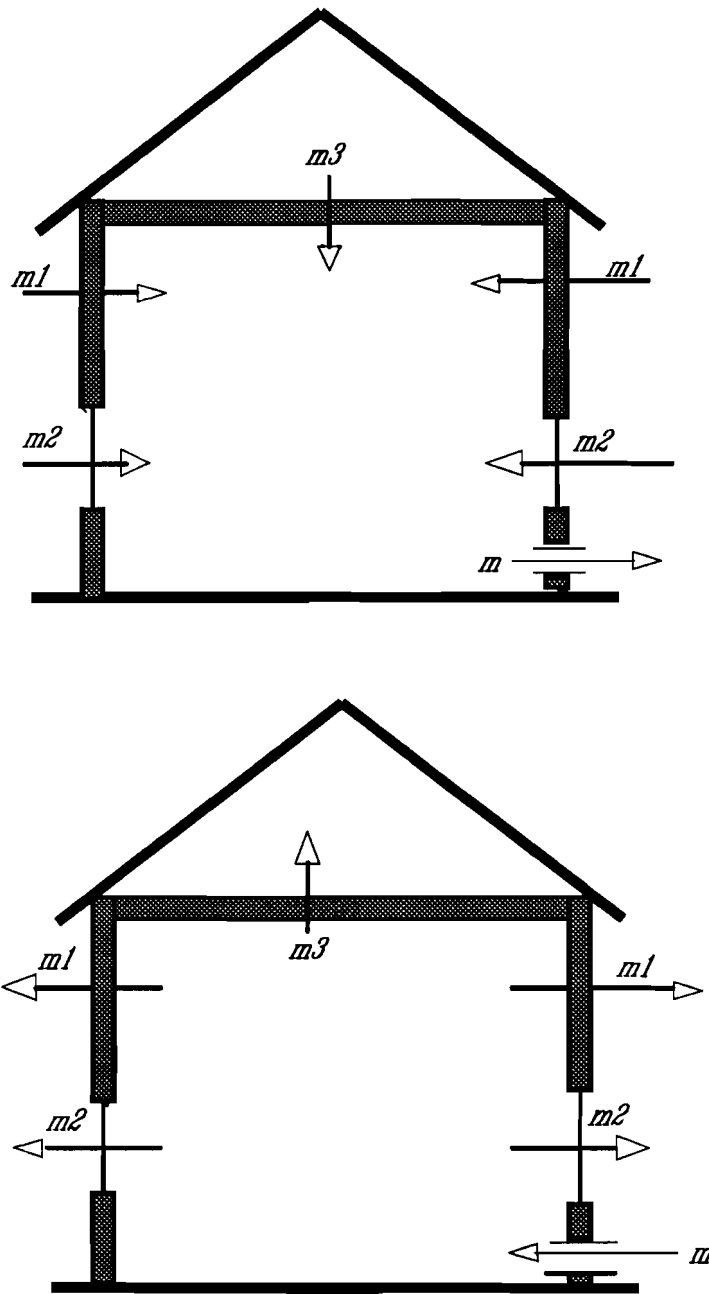


Figure 8-10: Schematic of the Idealized House Model

The comparison of the energy consumption of the idealized and normal house models is given in Figure 8-11. The results show that the energy savings of the idealized house increase with the solar radiation and air flow rates, and can be up to 100% for heating and 50% for cooling. These results demonstrated that substantial energy savings could be achieved by idealizing the house air flow directions by means of a fan. A slight negative savings is also observed when solar radiation approaches zero since the normal house model had double flow model which resulted in higher energy recovery when no solar radiation was present.

The comparison of energy consumption of the idealized and designed house models is given in Figure 8-12. The results showed that the savings ratio increases with solar radiation and air flow rate for cooling, except for the very low air flow rate. The savings ratio also increases with solar radiation and air flow rate for heating. The savings might be up to 100% in winter and 27% in summer. Therefore, the current design method could substantially overestimate the heating and cooling energy consumption of the idealized house.

The comparison of the normal and designed house models is given in Figure 8-13. The negative savings ratios (up to -40%) were observed for the high flow rates and high solar radiation in summer. Therefore, the current design method could underestimate the cooling energy consumption under these conditions. However, the positive savings covered most conditions for cooling and all for heating. Subsequently, the chances of overestimating with the current method decreased with solar radiation for cooling, but increased for heating. The energy saving values are given in Table 8-5 for seasonal average weather conditions.

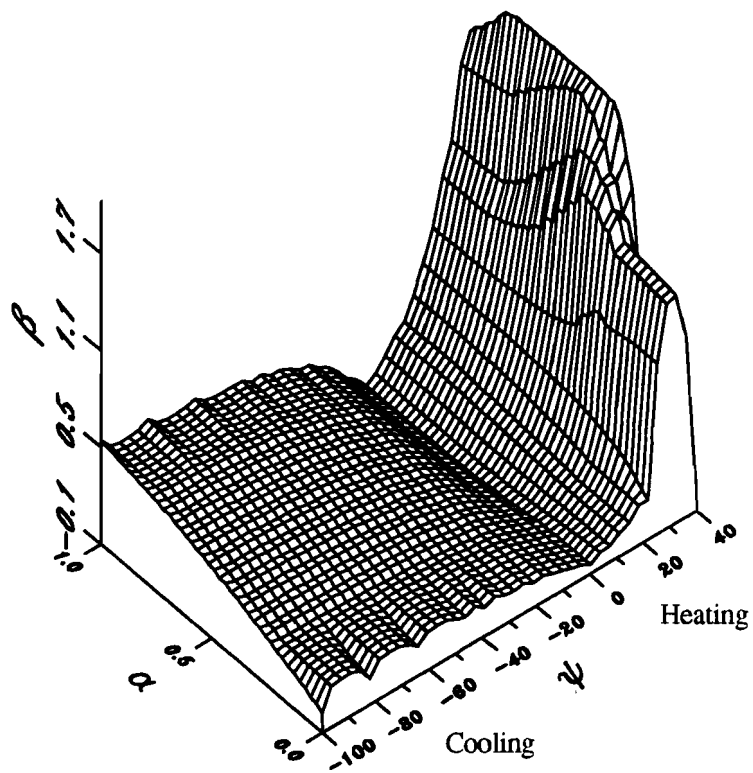


Figure 8-11: Energy Saving Ratio of the Idealized to Normal House Models
 β - energy saving ratio, ψ - solar indicator ($\text{W}/\text{m}^2\text{C}$),
 α - non-dimensional air flow rate

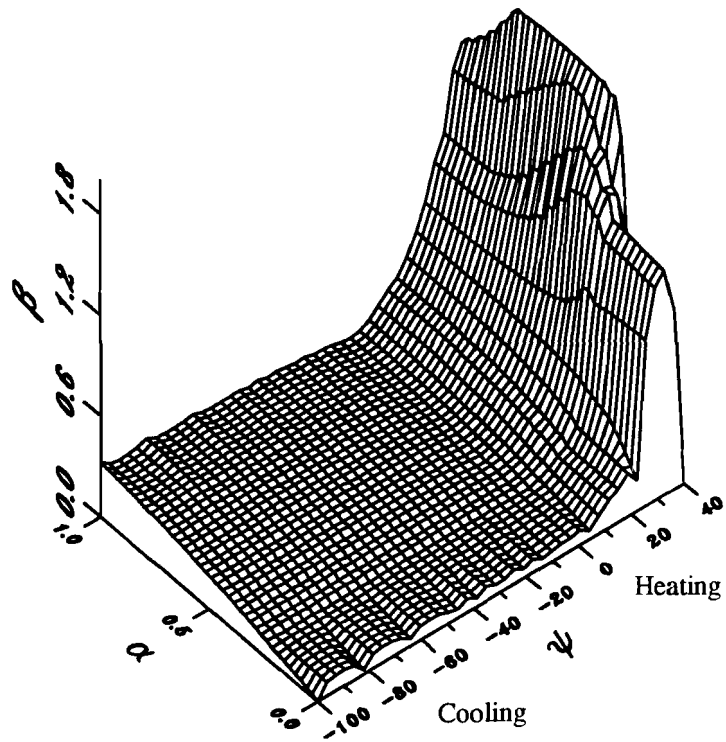


Figure 8-12: Energy Saving Ratio of the Idealized to Designed House Models
 β - energy saving ratio, ψ - solar indicator ($\text{W}/\text{m}^2\text{°C}$),
 α - non-dimensional air flow rate

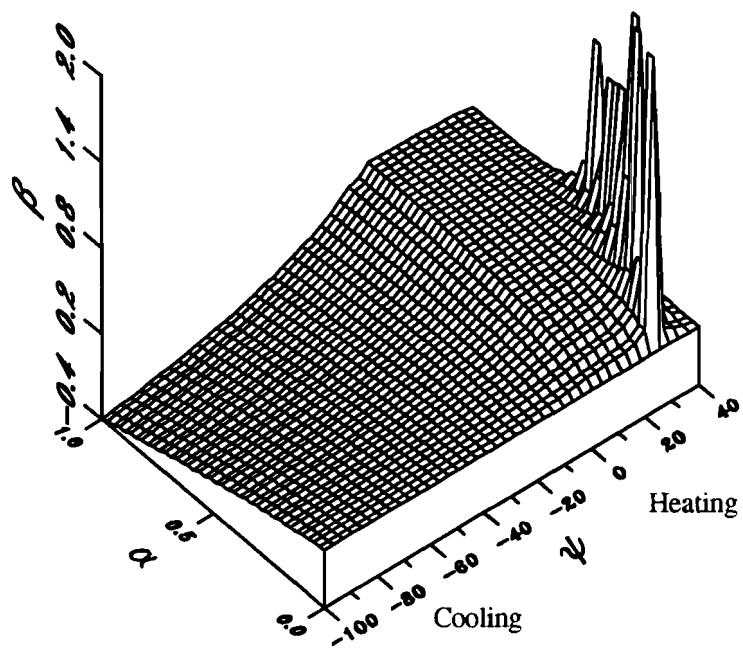


Figure 8-13: Energy Saving Ratio of the Normal to Designed House Models
 β - energy saving ratio, ψ - solar indicator ($\text{W}/\text{m}^2\text{C}$),
 α - non-dimensional air flow rate

Table 8-5. Energy Saving Comparison of Three House Models

Code	Solar	Air	I & N	I & D	N &D
Heating	10	0.6	0.02	0.27	0.26
Heating	20	0.6	0.32	0.49	0.26
Cooling	-40	0.6	0.25	0.20	-0.07
Cooling	-60	0.6	0.31	0.22	-0.14

Table 8-5 shows that the idealized house model has the potential to save heating energy by 2% to 30%, and cooling energy by 25% to 31% under the seasonal average conditions. If the current design method was used for the idealized house model calculation, it might overestimate heating energy by 29% to 49% and cooling energy by 20% to 22%. The current design might overestimate heating energy by 26% and underestimate cooling energy by 6% to 14% for a "normal" house.

SUMMARY

The combined solar-radiation, air-infiltration, and conduction model study discovered that the total energy consumption of the idealized wall and attics is not always less than the designed value as is currently assumed, and that infiltration air flow consumes less energy than exfiltration in winter but more in summer.

The idealized house model analysis showed that depressurizing a house in winter and pressurizing a house in summer by a fan could reduce the house energy substantially, since this permitted infiltration in winter and exfiltration in summer over the house envelope.

CHAPTER IX

SYSTEMATIC ERROR DUE TO THE STEADY-STATE METHODOLOGY

The differential equation of the diffuse wall was established in Chapter VIII under steady-state conditions. The simulation results showed that the actual energy consumption of the idealized wall and attics under outdoor conditions could be significantly different from the design values. The idealized house model results revealed that the house energy performance could be improved significantly by assuming proper air flow direction. However, the steady-state methodology can have a systematic prediction error because the heat transfer is a non-linear process under outdoor conditions where air flow rate, temperature, and solar radiation change with time. Therefore, both the steady-state methodology and the results of Chapter VIII must be validated.

A differential equation is developed for an idealized diffuse wall under dynamic conditions. Both the dynamic and steady-state behaviors of the idealized wall are simulated under different outdoor conditions generated by superimposing a modified Random-walk factor to the basic outdoor parameter profiles. The possible systematic error of the steady-state method is investigated by comparing the numerical results of both the steady-state and dynamic simulations. This chapter describes the development of the differential equation, discretization of the differential equation, generation of the weather data, and the results of the numerical simulation.

DIFFERENTIAL EQUATION

The idealized diffuse wall assumed that an infiltrative air flow \dot{m} is present, and that both the air and the solid material had identical temperature at any position. The energy gain of a control volume within the diffuse wall component (see Figure 9-1) should be equal to the difference of the energy fluxes of flow in and flow out:

$$Q_x - Q_{x+dx} + Q_{a,x} - Q_{a,x+dx} = \delta Q \quad (9-1)$$

where:

- Q_x = heat flux entering the control volume due to conduction
- Q_{x+dx} = heat flux leaving from the control volume due to conduction
- $Q_{a,x}$ = energy carried in by the air flow
- $Q_{a,x+dx}$ = energy carried out by the air flow
- δQ = heat storage rate of the control volume.

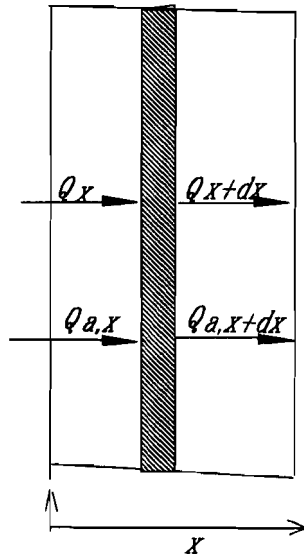


Figure 9-1: Schematic of Control Volume Element for Energy Balance

These terms are expressed as:

$$Q_x = -k \frac{\partial T}{\partial x} \delta\tau \quad (9-2)$$

$$Q_{x+dx} = -k \frac{\partial T}{\partial x} \delta\tau - k \frac{\partial^2 T}{\partial^2 x} \delta x \delta\tau \quad (9-3)$$

$$Q_{a,x} = \dot{m} C_p T \delta\tau \quad (9-4)$$

$$Q_{a,x+dx} = \dot{m} C_p T \delta\tau + \dot{m} C_p \frac{\partial T}{\partial x} \delta x \delta\tau + C_p T \frac{\partial \dot{m}}{\partial x} \delta x \delta\tau \quad (9-5)$$

$$\delta Q = \frac{\partial T}{\partial \tau} (\rho C + \gamma \rho_a C_p) \delta x \delta\tau \quad (9-6)$$

where

\dot{m} = air infiltration rate (Kg/m²s) which is positive for infiltration and negative for exfiltration

C_p = specific heat of air (J/Kg K)

C = specific heat of solid material (J/Kg K)

ρ = density of solid materials (Kg/m³)

ρ_a = density of air (Kg/m³)

γ = porosity of wall (%)

k = conductance of the solid material (W/m K)

T = temperature (°C).

The heat capacity of air ($\gamma \rho_a C_p$) is very small compared to the solid part (ρC) for most of the insulation materials so the second term in Equation (9-6) is neglected. The air flow might change with the flow path, but it is usually small. So, neglecting the third term in Equation (9-5) would not introduce a noticeable error. Finally, the differential equation is written as:

$$\rho C \frac{\partial T}{\partial \tau} = k \frac{\partial^2 T}{\partial x^2} - \dot{m} C_p \frac{\partial T}{\partial x} \quad (9-7)$$

This is a one-dimensional second-order non-linear dynamic equation because the air infiltration (\dot{m}) might change with both time and position. It is impossible to get an explicit analytical solution under outdoor conditions because of its non-linearity. Therefore, a discrete numerical method is used to investigate this phenomenon.

DISCRETIZATION OF THE DIFFERENTIAL EQUATION

A typical node schematic diagram is shown in Figure 9-2. P is the center node on which the discrete equation is established. The neighbor nodes are W and E. The control volume is taken from w to e. Time and space integration on the Equation (9-7) are applied for the control volume, yielding:

$$\int_{\tau}^{\tau+\Delta\tau} \int_x^{x+\Delta x} \rho C \frac{\partial T}{\partial \tau} dx d\tau = \int_{\tau}^{\tau+\Delta\tau} \int_x^{x+\Delta x} k \frac{\partial^2 T}{\partial x^2} dx d\tau - \int_{\tau}^{\tau+\Delta\tau} \int_x^{x+\Delta x} \dot{m} C_p \frac{\partial T}{\partial x} dx d\tau \quad (9-8)$$

It is assumed that $\frac{\partial T}{\partial \tau}$, ρ , C , \dot{m} , and C_p are constants within the control volume (Δx).

This assumption is reasonable if the control volume is small enough. It is also assumed that k is constant in the east and west neighbors (δx_e , and δx_w). The integration in the second term is the difference of heat fluxes at the east and west control surfaces.

Integrating along control volume Δx , the equation becomes:

$$\int_{\tau}^{\tau+\Delta\tau} \rho C \frac{\partial T}{\partial \tau} \Delta x d\tau = \int_{\tau}^{\tau+\Delta\tau} \left(\left(k \frac{\partial T}{\partial x} \right)_e - \left(k \frac{\partial T}{\partial x} \right)_w \right) d\tau - \int_{\tau}^{\tau+\Delta\tau} \dot{m} C_p (T_e - T_w) d\tau \quad (9-9)$$

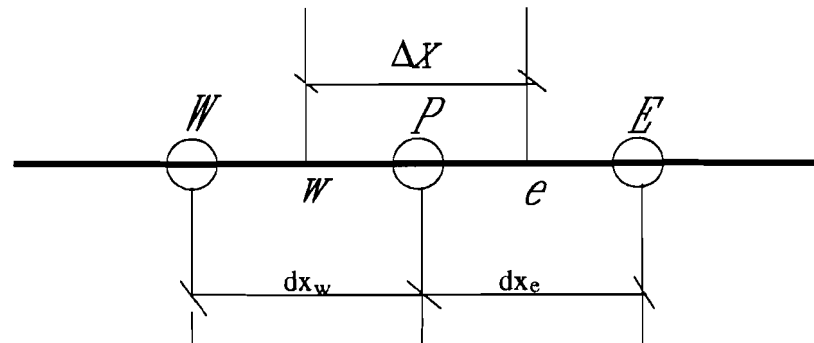


Figure 9-2: Schematic Diagram of Internal Nodes

Introducing an approximate expression for the first differential terms [Patanker 1980] into Equation (9-9), it then follows that:

$$\int_{\tau}^{\tau+\Delta\tau} \rho C \frac{\partial T}{\partial \tau} \Delta x d\tau = \int_{\tau}^{\tau+\Delta\tau} \left[\left(\frac{k}{dx} \right)_e (T_E - T_P) - \left(\frac{k}{dx} \right)_w (T_P - T_w) \right] dt - \int_{\tau}^{\tau+\Delta\tau} \dot{m} C_p (T_e - T_w) dt \quad (9-10)$$

Integrating Equation (9-10) over time step $\Delta\tau$ by the fully explicit method, we then obtain:.

$$\rho C \Delta x (T_P - T_P^0) = \left(\frac{k}{\delta x} \right)_e (T_E - T_P) \Delta\tau - \left(\frac{k}{\delta x} \right)_w (T_P - T_W) \Delta\tau - \dot{m} C_p (T_E - T_W) \Delta\tau \quad (9-11)$$

where:

T_P^0 = temperature of center node P at previous time

T_P = temperature of center node P at current time

T_E = temperature of east node at current time

T_w = temperature of west node at current time.

Rearranging Equation (9-11), it then becomes:

$$\begin{aligned} T_p \left[\frac{\rho C \Delta x}{\Delta \tau} + \left(\frac{k}{\delta x} \right)_e + \left(\frac{k}{\delta x} \right)_w \right] + T_w \left[- \left(\frac{k}{\delta x} \right)_w - \dot{m} C_p \right] + T_E \left[- \left(\frac{k}{\delta x} \right)_e + \dot{m} C_p \right] \\ = \frac{\rho C \Delta x}{\Delta \tau} T_p^0 \end{aligned} \quad (9-12)$$

The following coefficients are defined in order to get a general form of the discrete equation:

$$a_w = - \left(\frac{k}{\delta x} \right)_w - \dot{m} C_p \quad (9-13)$$

$$a_e = - \left(\frac{k}{\delta x} \right)_e + \dot{m} C_p \quad (9-14)$$

$$a_p^0 = \frac{\rho C \Delta x}{\Delta \tau} \quad (9-15)$$

$$a_p = a_p^0 - a_w - a_e \quad (9-16)$$

Introducing the coefficients into Equation (9-12), the discrete equation is finally written as:

$$a_w T_w + a_p T_p + a_e T_E = a_p^0 T_p^0 \quad (9-17)$$

The differential Equation (9-9) holds for homogeneous materials only, but the discrete expression (9-17) holds as soon as the control volume is organized such that the material is homogeneous within the control volume, and the conductivity is homogeneous between the neighbor nodes. It is possible that the material within the control volume is homogeneous. However, the conductivity often changes between neighbor nodes for multi-layer walls. In order to solve this problem, the conductivity is calculated by the following formula [Patanker 1980]:

$$k_w = \frac{2}{\left(\frac{\Delta x_w}{\delta x_w k_w} + \frac{\Delta x_p}{\delta x_p k_p} \right)} \quad (9-18)$$

$$k_e = \frac{2}{\left(\frac{\Delta x_p}{\delta x_p k_p} + \frac{\Delta x_E}{\delta x_w k_E} \right)} \quad (9-19)$$

Equation (9-17) is a general internal node equation, which can be used for single layer or multi-layer constructions when the conductivity is calculated by Equations (9-18) and (9-19). The external node equations are needed to incorporate the boundary conditions.

EXTERNAL NODE EQUATIONS

The external nodes include the outside surface of the wall, the inner surface of the wall, the attic air, and the outside surface of the ceiling. The external node equations are based on the energy balance principle.

Outside Surface of the Wall

The outside surface of the wall is subjected to solar radiation, ambient air temperature, and air infiltration. The surface node is taken as half of the normal control volume (Figure 9-3a). The energy balance equation on this control volume is:

$$T_P \dot{m} C_p - \frac{1}{2} (T_P - T_E) \dot{m} C_p + I + h_o (T_a - T_P) + \left(\frac{k}{\delta x} \right)_e (T_E - T_P) = \frac{(\rho C \Delta x)_e}{2 \Delta \tau} (T_P - T_P^0) \quad (9-20)$$

where:

T_P = temperature of outside surface of wall ($^{\circ}\text{C}$)

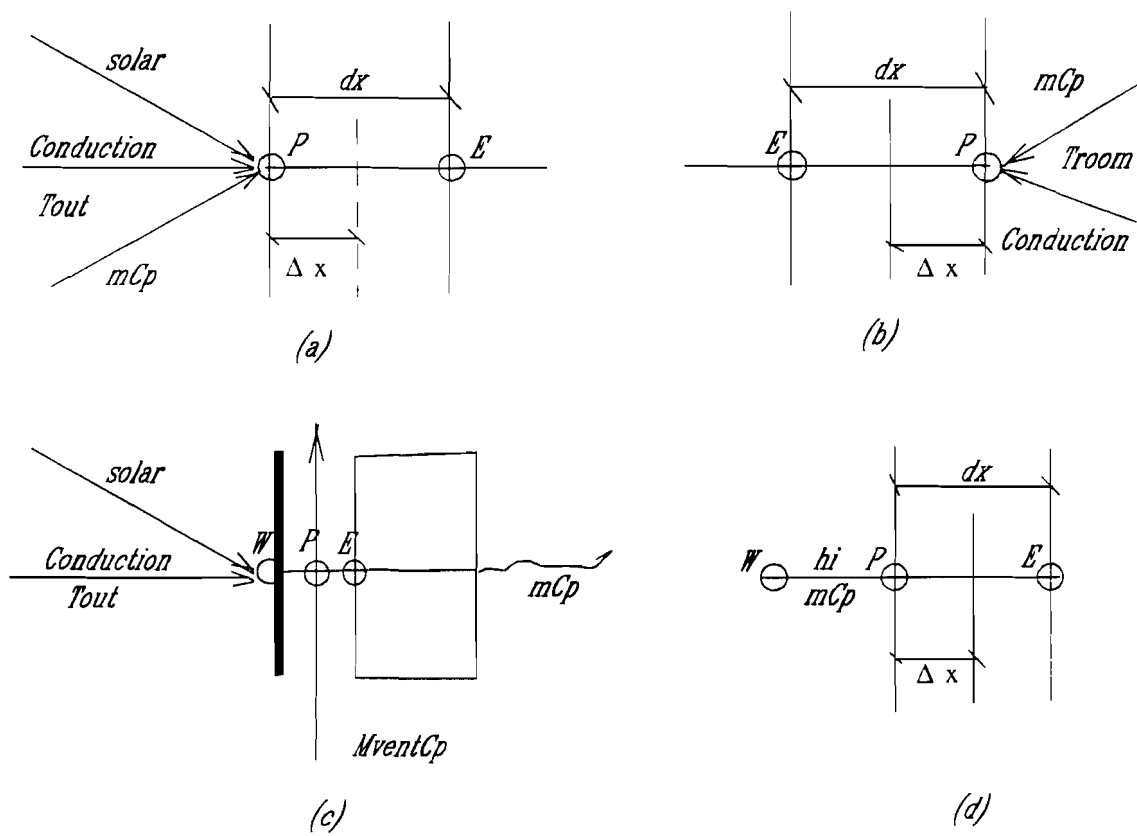


Figure 9-3: Schematic Diagram of External Nodes
 (a) outside surface of wall, (b) inside surface of wall, (c) attic air, and (d) top surface of ceiling

- T_E = temperature of east neighbor node ($^{\circ}\text{C}$)
 I = solar radiation absorbed by wall (W/m^2)
 h_o = heat transfer coefficient of outside boundary layer of wall ($\text{W}/\text{m}^2\text{^{\circ}\text{C}}$)
 T_a = ambient air temperature ($^{\circ}\text{C}$)
 $\Delta\tau$ = time step (s).

Rearranging Equation (9-20), it reduces to:

$$a_p T_p + a_e T_E = a_p^0 T_p^0 + S \quad (9-21)$$

$$a_e = -\left(\frac{k}{\delta x}\right)_e + \frac{1}{2} \dot{m} C_p \quad (9-22)$$

$$a_p^0 = \frac{\rho C \Delta x}{2 \Delta \tau} \quad (9-23)$$

$$a_p = a_p^0 - a_e + h_o \quad (9-24)$$

$$S = I + h_o T_a \quad (9-25)$$

Inside Surface of the Wall

The inside surface temperature of the wall is influenced by its west neighbor node temperature and the room air temperature. This surface node is shown in Figure 9-3b. The control volume is half of the normal node. The energy balance equation of this control volume is:

$$\left(\frac{k}{\delta x}\right)_w (T_w - T_p) + \frac{1}{2} (T_w + T_p) \dot{m} C_p - (T_p - T_r) h_i - \dot{m} C_p T_p = \frac{\rho C \Delta x}{2 \Delta \tau} T_p^0 \quad (9-26)$$

Rearranging Equation (9-26), it then follows:

$$a_p T_p + a_w T_w = a_p^0 T_p^0 + S \quad (9-27)$$

$$a_w = -\left(\frac{k}{\delta x}\right)_w - \frac{1}{2} \dot{m} C_p \quad (9-28)$$

$$a_p^0 = \frac{\rho C \Delta x}{2 \Delta \tau} \quad (9-29)$$

$$a_p = a_p^0 - a_w + h_i \quad (9-30)$$

$$S = h_i T_r \quad (9-31)$$

Attic Air Temperature

The attic air temperature is influenced by solar radiation, ambient air temperature, cross-ventilation, roof surface temperature, and the top surface temperature of the ceiling. The thermal storage capacity of shingles is neglected in this model because it is very small. The heat transfer process is shown in Figure 9-3c, and the energy balance equation is given as:

$$I - (T_1 - T_a) h_o - (T_1 - T_p) h_1 = 0 \quad (9-32)$$

$$(T_1 - T_p) h_1 + \dot{m}_c C_p T_a - \dot{m}_c C_p T_{\text{exit}} - (T_p - T_E) h_i - \dot{m} C_p T_E = 0 \quad (9-33)$$

where

T_1 = outside surface temperature of shingle ($^{\circ}\text{C}$)

T_p = attic air temperature ($^{\circ}\text{C}$)

h_1 = heat transfer coefficient from outside surface of shingle to attic air
($\text{W}/\text{m}^2 \text{K}$).

h_i = heat transfer coefficient of top boundary layer of ceiling ($\text{W}/\text{m}^2\text{C}$)

\dot{m}_c = cross ventilation rate ($\text{Kg}/\text{m}^2 \text{s}$)

T_{exit} = air temperature at exit of attic, which is expressed as:

$$T_p = \frac{1}{2} (T_{\text{exit}} + T_a) \quad (9-34)$$

Combining Equations (9-32), (9-33), and (9-34), it then reduces to:

$$a_p T_p + a_e T_E = S \quad (9-35)$$

$$a_p = \frac{h_i h_1}{h_i + h_1} + 2 \dot{m}_c C_p + h_i \quad (9-36)$$

$$a_e = \dot{m}C - h_i \quad (9-37)$$

$$S = I \frac{h_1}{h_i + h_1} + \left(\frac{h_i h_1}{h_i + h_1} + 2 \dot{m}_c C_p \right) T_a \quad (9-38)$$

Top Surface of the Ceiling

The top surface temperature of the ceiling is influenced by the attic air temperature and its east node temperature. The heat transfer process of the top surface of the ceiling is shown in Figure 9-3d, and the energy balance equation is given as:

$$\dot{m}C_p T_p - \frac{1}{2} (T_p - T_E) \dot{m}C_p + h_i (T_w - T_p) + \left(\frac{k}{\delta x} \right)_e (T_E - T_p) = \frac{(\rho C \Delta x)_e}{2 \Delta \tau} (T_p - T_p^0) \quad (9-39)$$

Rearranging Equation (9-39), it then follows:

$$a_w T_w + a_p T_p + a_e T_E = a_p^0 T_p^0 \quad (9-40)$$

$$a_w = - h_i \quad (9-41)$$

$$a_e = \frac{1}{2} \dot{m}C_p - \left(\frac{k}{\delta x} \right)_e \quad (9-42)$$

$$a_p^0 = \frac{(\rho C \Delta x)_e}{2 \Delta \tau} \quad (9-43)$$

$$a_p = a_p^0 - a_w - a_e \quad (9-44)$$

DISCRETIZATION EQUATIONS

If a wall is divided into $n-1$ layers, this creates n nodes (see Figure 9-4a), where the outside surface node is indexed with 1, and the inside surface node is indexed with n . If a ceiling is divided into $n-2$ layers, then n nodes would be created (see Figure 9-4b), where the attic air node is indexed 1, the top surface of ceiling is indexed 2, and the inside surface of ceiling is index n .

Each node equation can be written explicitly according to the equations described in the last two sections. However, the equations must be solved together because each node equation contains the temperature of its neighboring nodes. The general form of the discretization equation set is given as:

$$\begin{pmatrix} a_p^1 & a_e^1 & 0 & 0 & - & 0 & 0 \\ a_w^2 & a_p^2 & a_e^2 & 0 & - & 0 & 0 \\ - & - & - & - & - & - & - \\ - & - & - & - & - & a_w^n & a_p^n \end{pmatrix} \begin{pmatrix} T_1^1 \\ T_2^1 \\ - \\ T_n^1 \end{pmatrix} = \begin{pmatrix} a_p^0(1)T_1^0 \\ a_p^0(2)T_2^0 \\ - \\ a_p^0(n)T_n^0 \end{pmatrix} \quad (9-45)$$

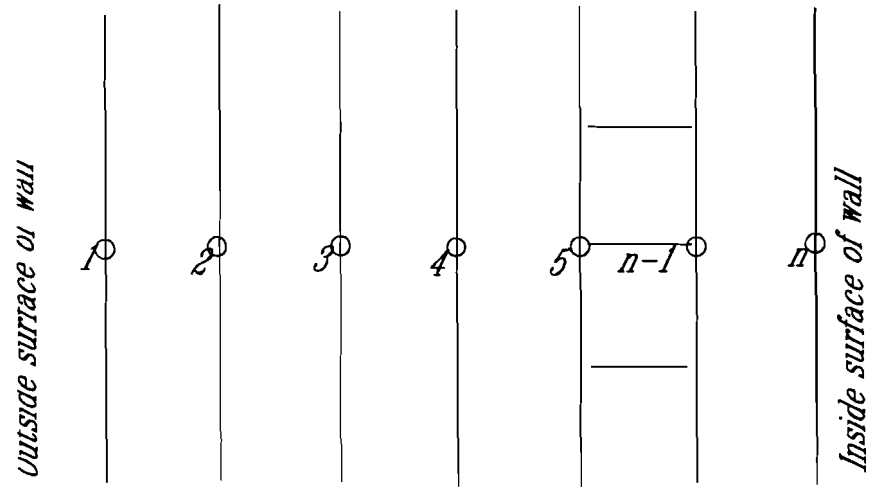
where:

T^1 = node temperature ($^{\circ}\text{C}$)

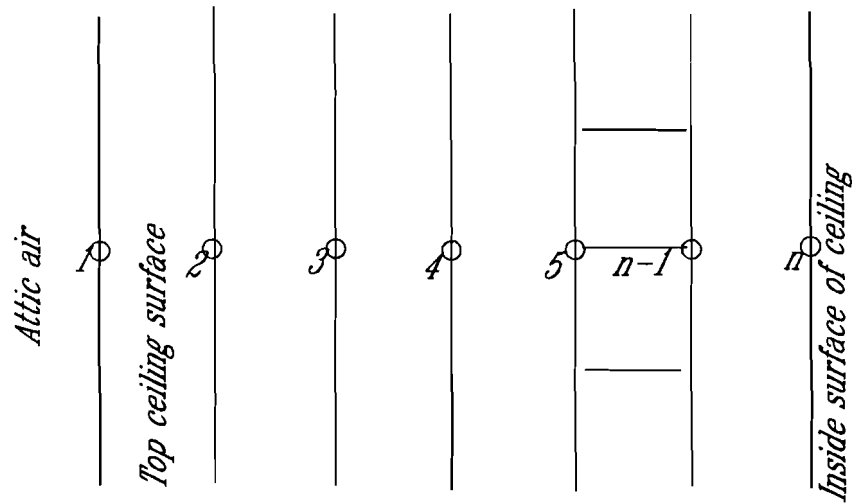
T^0 = temperature of previous time ($^{\circ}\text{C}$).

The standard Gauss method is used to solve the equations, and a zero initial temperature is taken to start the iterative calculation.

The direct calculation result is the node temperatures from Equation (9-45). The heat flux or energy consumption is calculated by the following formula:



(a)



(b)

Figure 9-4: Schematic of Discretization of Wall and Ceiling

$$q_a(i) = \begin{cases} (h_i + \dot{m}C_p)(T_r(i) - T_n(i)) & \text{Infiltration} \\ h_i(T_r(i) - T_n(i)) - \dot{m}C_p(T_n(i) - T_a(i)) & \text{Exfiltration} \end{cases} \quad (9-46)$$

where:

h_i = heat transfer coefficient of inside boundary layer of wall ($\text{W/m}^2\text{°C}$)

\dot{m} = air flow rate ($\text{Kg/m}^2\text{s}$)

C_p = specific heat capacity of air ($\text{J/Kg}^\circ\text{C}$)

T_r = room temperature ($^\circ\text{C}$)

T_n = inside surface temperature of wall ($^\circ\text{C}$)

T_a = ambient air temperature ($^\circ\text{C}$).

WEATHER DATA GENERATION

A series of independent weather data files are needed in order to numerically check the validity of the steady-state methodology. In order to reflect the daily profile and random features of the weather parameters, a weather data schedule is generated by superimposing a modified random-walk variant on a weather kernel function. The kernel function is a normalized daily variation profile of corresponding weather parameters. The modified random-walk function is used to represent unpredicted outdoor conditions, such as overcast days, cold spells, etc.

The solar radiation kernel function is a set of hourly solar radiation data on walls and horizontal surfaces from the ASHRAE handbook (ASHRAE, 1981). The actual solar radiation is constructed by using the following formula:

$$I(i) = I^k(i)(1 - \epsilon_w(i)\beta_i) \quad (9-47)$$

where:

$I(i)$ = solar radiation at time i (W/m^2)

- $I^k(i)$ = solar radiation calculated from the kernel function at time i (W/m^2)
 β_i = random scale factor for solar radiation (0 to 1)
 $\epsilon_w(i)$ = modified random walk function which is defined by

$$\epsilon_w(i) = \begin{cases} \epsilon_w(i-1) + (1 - \epsilon(i)) & |\epsilon_w(i)| < 1 \\ 0 & |\epsilon_w(i)| > 1 \end{cases} \quad (9-48)$$

where: ϵ is a standard random function which took the value from 0 to 1.

The ambient air temperature kernel function is constructed using the following formula:

$$T_a^k(i) = T_{wp} + 0.5 \Delta T \cos(15i - 225) \quad (9-49)$$

where:

- $T_a^k(i)$ = kernel ambient air temperature at time i ($^{\circ}C$)
 T_{wp} = daily average temperature ($^{\circ}C$)
 ΔT = daily temperature variation, i. e. the difference of the daily highest and lowest temperature ($^{\circ}C$).

The weather schedule of the ambient air temperature is created by the following formula:

$$T_a(i) = T_a^k(i)(1 + \epsilon_w(i)\beta_t) \quad (9-50)$$

where:

- β_t = random scale factor for ambient air temperature (0 to 1)
 $T_a(i)$ = outside temperature at time i ($^{\circ}C$).

The room temperature varies around the constant value. It is constructed by the following formula:

$$T_r(i) = T_r + \epsilon_w(i)\Delta T_r\beta_{tr} \quad (9-51)$$

where:

- $T_r(i)$ = room temperature at time i ($^{\circ}\text{C}$)
 T_r = reference room temperature or thermal state setting ($^{\circ}\text{C}$)
 ΔT_r = maximum variation of room temperature or thermal state band setting ($^{\circ}\text{C}$)
 β_{tr} = random scale factor for room temperature.

The air infiltration depends on the difference of the room and ambient air temperatures, the wind speed and direction, and the operation of the HVAC system, but it is neither convenient nor necessary to connect these parameters directly with the air flow rate for the current purpose. The air flow rate is simply generated by the temperature difference according to the formula:

$$\alpha(i) = \Gamma \frac{|T_r(i) - T_a(i)|}{\left|T_r - T_{wp} + \frac{\Delta T}{2}\right|} (\delta + \epsilon_w(i)\beta_m) \quad (9-52)$$

where:

- $\alpha = \frac{\dot{m}(i)C_p}{UA_0}$, non-dimensional air infiltration rate
 Γ = air infiltration constant which gave the limit of the maximum air flow rate, the infiltration is simulated by assigning a positive value, and exfiltration by a negative value
 β_m = random scale factor for air flow (0 to 1)
 δ = discrete number, either 0 or 1 which is called the mode code. The 0 corresponds to balanced infiltration. In this mode, both infiltration and exfiltration are possible and the theoretical average air flow rate is

zero. 1 corresponds to one-way air flow, either infiltration or exfiltration, depending on the values of Γ .

SIMULATION CALCULATION

As a prototype investigation, the heat flux and IHEE are simulated on a typical insulated frame wall under different air flow and outdoor conditions. The wall structure, air flow and outdoor conditions, and the simulation results are described in this section.

It is assumed that the wall has the following structure:

- 12 centimeter brick surface ($k = 1.100 \text{ W/m}^\circ\text{C}$; $\rho = 1900 \text{ Kg/m}^3$; $C_p = 1050 \text{ J/Kg}^\circ\text{C}$)
- 5 centimeter insulation ($k = 0.064 \text{ W/m}^\circ\text{C}$; $\rho = 150 \text{ Kg/m}^3$; $C_p = 1218 \text{ J/Kg}^\circ\text{C}$)
- 2 centimeter gypsum board ($k = 0.330 \text{ W/m}^\circ\text{C}$; $\rho = 1050 \text{ Kg/m}^3$; $C_p = 1050 \text{ J/Kg}^\circ\text{C}$).

The heat resistance of the wall is $1.12 \text{ m}^2\text{K/W}$. A total of 24 nodes are used for the wall discretization, 10 for the brick layer, 10 for the insulation, 2 for the gypsum board, and 2 for the surfaces. The boundary layer heat transfer coefficients are taken as 8, and $25 \text{ W/m}^2\text{K}$ for the inside and outside surfaces respectively.

The solar kernel function is shown in the Figure 9-5 for four vertical walls (N, E, W, S) and roof (Horizontal) of houses under typical January weather conditions in central Texas. The solar radiation random scale is taken as 0.5.

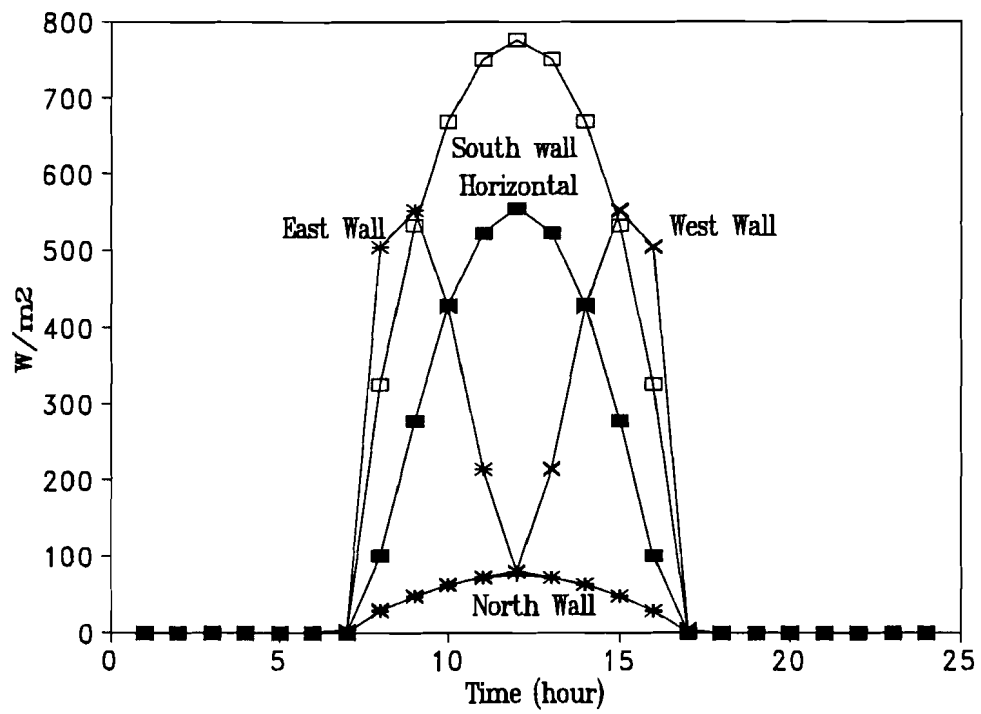


Figure 9-5: Solar Radiation Kernel Function Used in the Program "DYNA"

The average ambient air temperature is 4°C, and the difference between the highest and lowest ambient temperature is 10°C. The ambient air temperature random scale is 0.5. The average room temperature is assumed to be 20°C, and the thermal state band is 2°C. The room temperature random scale factor is 0.5.

The simulations covered four different air flow models:

- 1) no air ($\Gamma = 0$). This simulation demonstrates the possible numerical error due to the calculation. Perfect agreement between steady-state and dynamic simulation results is expected if there is no numerical calculation error;
- 2) infiltration ($\Gamma = 1$, $\beta_m = 0.5$, and $\delta = 1$). These conditions create an average non-dimensional air flow rate of 0.55;
- 3) exfiltration ($\Gamma = -1$, $\beta_m = 0.5$, and $\delta = 1$). These conditions create an average non-dimensional air flow rate of -0.55;
- 4) balance air leakage ($\Gamma = 1$, $\beta_m = 0.5$, and $\delta = 0$). These conditions create a non-dimensional air leakage rate varying from -0.6 to 0.6, with a zero average.

Each case covers four facets of houses and roof which is assumed to have the same structure as the walls, and each facet or roof is simulated under four different outdoor conditions. A total of 20 simulations are carried out for each case.

The outdoor condition is defined as a seven-day period in which the solar radiation, the air infiltration, and the temperature are generated according to the theory mentioned in the weather data generation section. The ambient air temperature is assumed to be constant and equal to the value of the daily average ambient temperature, the room temperature to be 20°C, and the air leakage rate to be 0 for the first and the last day of the

period, resulting in the same thermal conditions at the ends of both the first day and the last day. Subsequently, a six-day period is chosen to make comparison without the error of thermal storage. The simulation time step is 5 minutes in order to simulate the high frequency of air flow. The simulation calculations are carried out by a program named "dyna.for", listed in Appendix B4.

One of the outdoor conditions and simulation results are shown in Figure 9-6. The weather parameters include ambient air temperature, room temperature, solar radiation, and air infiltration. The output includes inside surface temperature of the walls, average wall temperature, and heat flux across the inside surface of the walls or energy consumption. It is observed that the wall had identical average temperature at the end of the first day (at time 24 hour) and the end of the seventh day (at 168 hour). Subsequently, there is no thermal storage error if the steady-state calculation is carried out during this time period. Both the solar radiation and ambient air temperature showed basic daily variation profiles. However, they are not the same for any two days. It appears that both the ambient temperature and solar radiation generated by the method simulate actual outdoor conditions. The inside surface temperature of the wall showed both daily variation due to the solar radiation and ambient temperature, and random variation due to the room temperature variation.

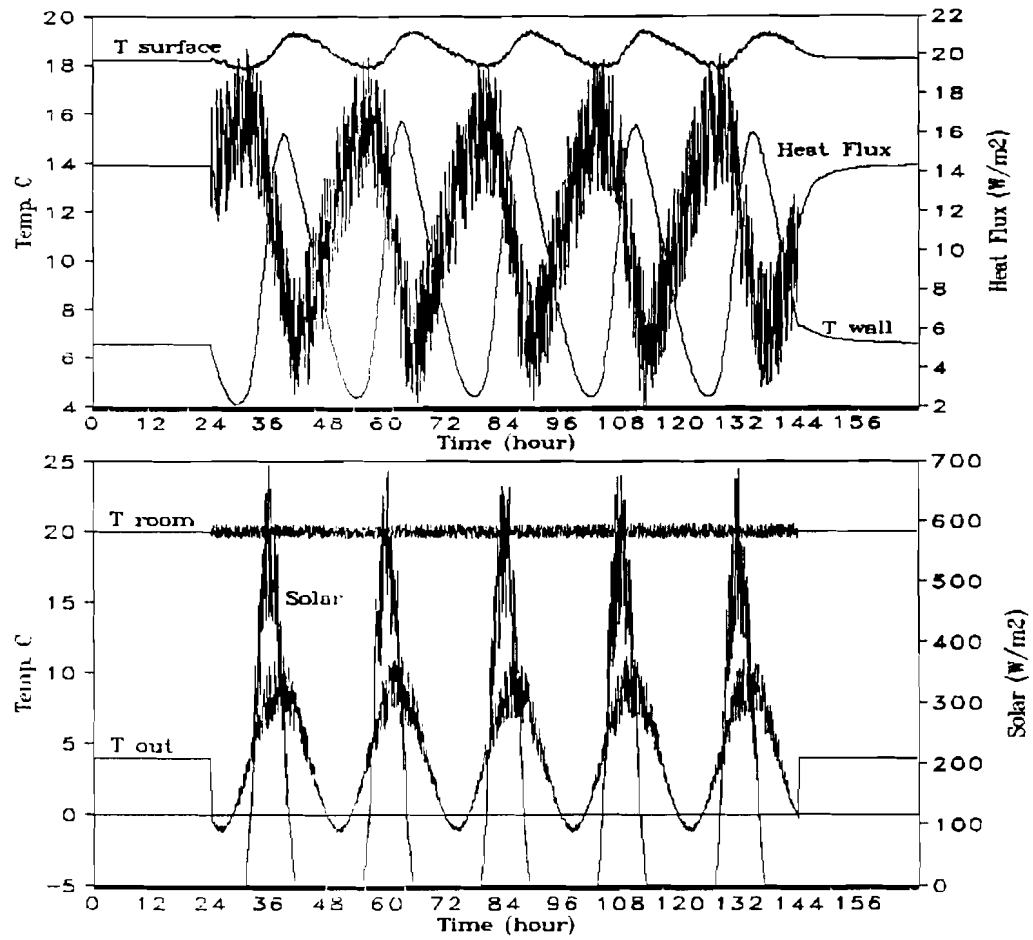


Figure 9-6: A Sample of Weather Data and Simulation Results

The systematic error of the steady-state methodology is expressed by the heat flux and IHEE prediction errors, which are defined by the following formulas:

$$\varepsilon_q = \frac{\bar{q}_d - \bar{q}_s}{\bar{q}_d} 100 \quad (9-53)$$

$$\varepsilon_i = \frac{\overline{\text{IHEE}}_d - \overline{\text{IHEE}}_s}{\overline{\text{IHEE}}_d} 100 \quad (9-54)$$

where:

ε_q = heat flux prediction error of steady-state methodology (%)

ε_i = IHEE prediction error of steady-state methodology (%)

q_d = average heat flux predicted by dynamic simulation (W/m^2)

q_s = heat flux predicted by steady-state simulation (W/m^2)

$\overline{\text{IHEE}}_d$ = average IHEE predicted by dynamic simulation

$\overline{\text{IHEE}}_s$ = IHEE predicted by steady-state simulation.

The heat flux prediction error due to steady-state methodology is given in Figure 9-7, where the simulation number serves as the horizontal axis in (a), and the solar radiation serves as the horizontal axis in (b).

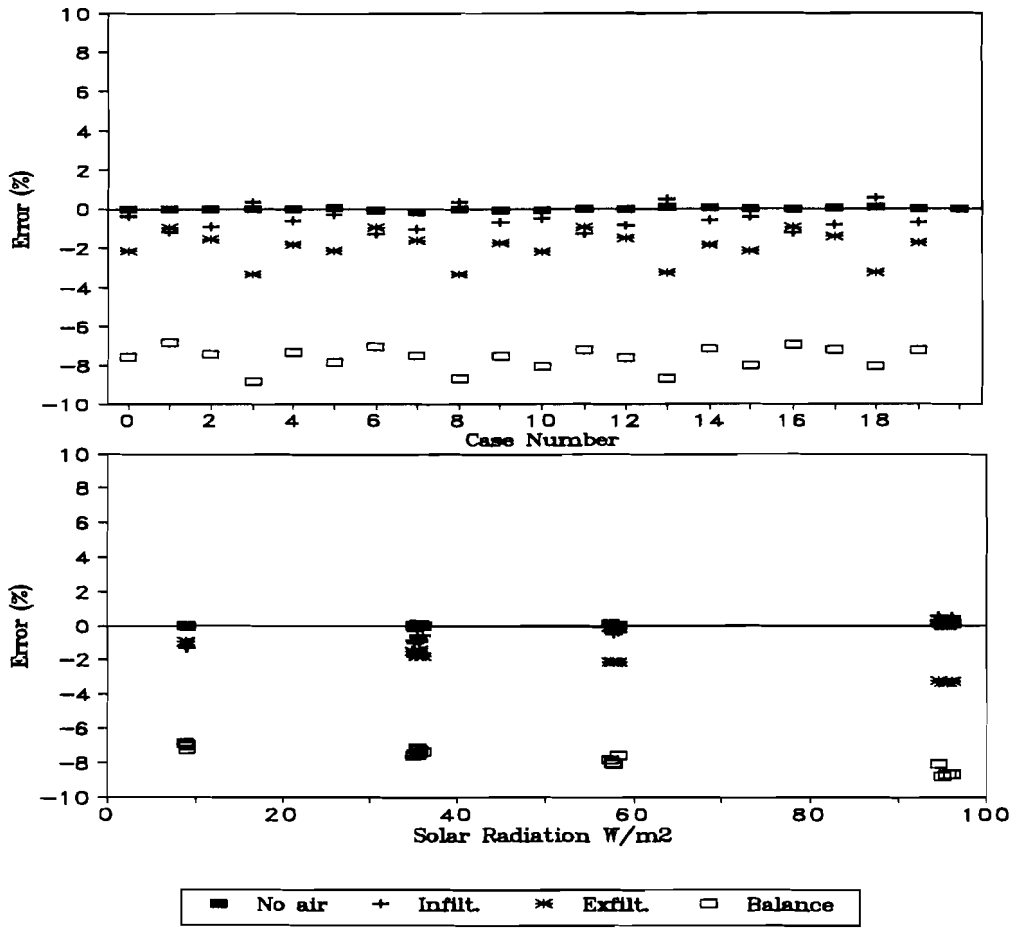


Figure 9-7: Energy Prediction Error Due to Steady-State Methodology

A zero error was observed for the no air flow case. This showed that the numerical calculation error was negligible in the simulations. The balanced air leakage case had a heat flux error of 7% to 9%. The infiltration and exfiltration cases had a heat flux error of 0.5% to 3.5%. A similar periodic variation of the error was observed in Figure 9-7a. This reflected the dependence of the error on solar radiation (Figure 9-7b). The error increased with solar radiation for the exfiltration and the balanced air flow models, but decreased for the infiltration model. These numbers showed that the steady-state method slightly underestimated the energy consumption when one-way air flow is present. However, this could cause a severe error when a balanced air flow is present.

The IHEE prediction error due to steady-state methodology is given in Figure 9-8. It is observed that the steady-state method tended to overestimate IHEE by about 5% to 8% for the exfiltration case. It might also overestimate or underestimate IHEE for the infiltration case under simulated conditions because the IHEE varied in the range of 1% to -3%. It is also observed that the IHEE errors of infiltration and exfiltration cases are symmetric about 4%. This might suggest that errors due to the air flow variation and the solar radiation are additive, but this needs further study because of the complexity of the non-linearity.

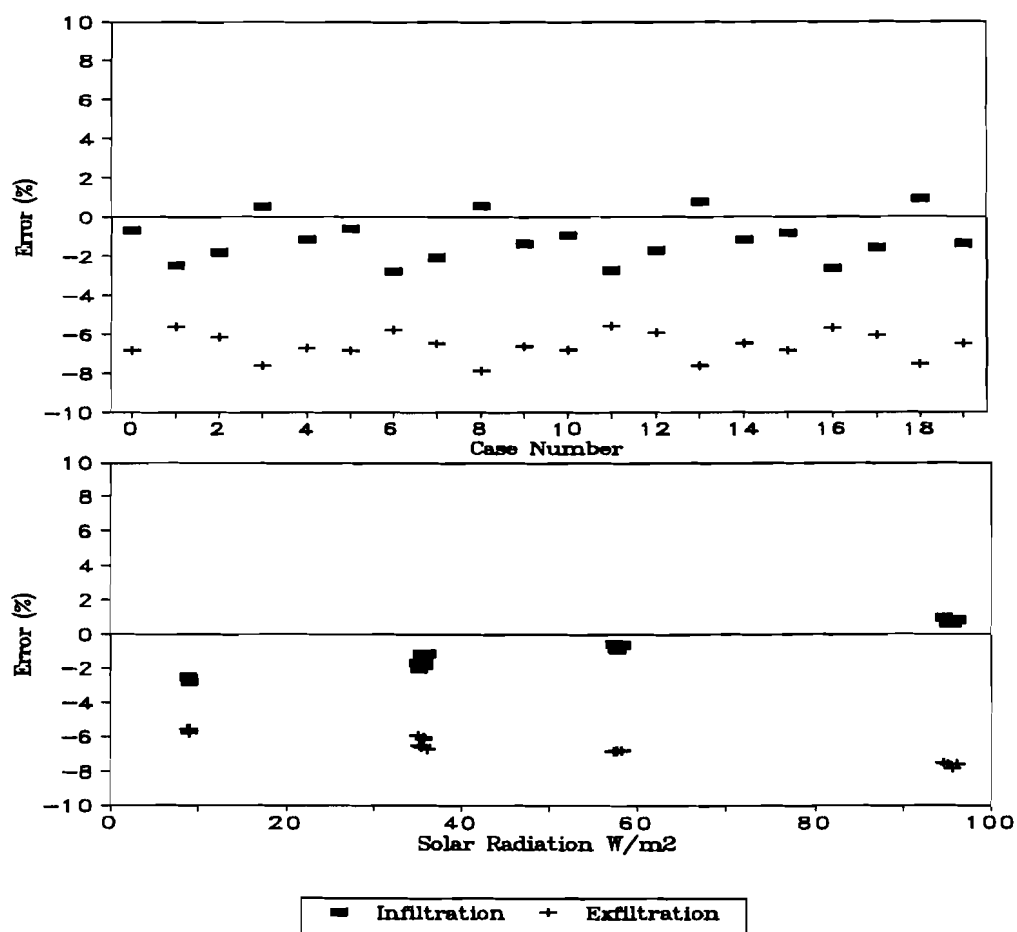


Figure 9-8: IHEE Prediction Error Due to Steady-State Methodology

SUMMARY

The systematic error of the steady-state methodology is investigated by comparing the energy consumption and IHEE from both steady-state and dynamic simulations under different outdoor conditions. This error depended on the air flow model and solar radiation under the simulated conditions. The simulation results showed that the steady-state method could result in upto 8% energy prediction error when balanced infiltration was present. This error fell to within 5% when one-way air flow was present. The results showed +1% to -8% prediction error of IHEE when the average non-dimensional air flow rate is about 0.55. Because of this relative small order of the systematic error, it is concluded that the results of Chapter VIII are reliable, and the results of Chapter V have no bias because the tests were performed under constant air flow rates. These systematic error numbers can also serve as a general error reference for the steady-state methodology under normal conditions because both the wall structures and the outdoor conditions used in the simulation are typical.

CHAPTER X

CONCLUSIONS AND RECOMMENDATIONS

The influence of heat recovery on the energy impact of air infiltration was investigated experimentally in an indoor test cell and an outdoor test cell under both dynamic and steady-state conditions. It was also theoretically studied by means of a combined solar radiation, air infiltration, and conduction model which was developed based on idealized diffuse wall and ceiling components under steady-state conditions. The systematic error of the steady-state methodology was investigated both experimentally and theoretically. Two new methodologies were developed for measuring air infiltration energy consumption in a full-size house, and were validated in the test cells. The conclusions drawn from the investigation are presented and discussed in this Chapter. The benefits and limitations of the study as well as recommendations for future work are also presented below.

CONCLUSIONS

Air Infiltration Heat Recovery

The measurements conducted on the indoor test cell and the outdoor test cell under conditions of dynamic temperature, power and solar radiation inputs show convincingly that IHEE:

- decreases with air flow rate increases
- has a higher value for a tight structure
- has a lower value for a leaky structure
- is always greater than zero when solar radiation is not present.

These results are consistent with those of Bhattachayya and Claridge [1992] from steady-state measurements in the absence of solar radiation. Moreover, the outdoor measurement discovered that when the cell is heated (not cooled), I_{HEE} :

- has higher values for infiltration flows (up to 0.50 for diffuse flow) than for exfiltration
- can be either positive or negative

These results differ markedly from the earlier steady-state experiments [Bhattachayya and Claridge, 1992] and theory [Anderlind, 1985] which showed $0 \leq I_{HEE} \leq 1$. These earlier studies ignored the influence of solar energy absorbed on the test cell or building surfaces.

The idealized house model, which was proposed to account for these factors of the outdoor cell measurements, showed that:

- infiltration air flow is preferable to exfiltration flow under heating conditions; the average heating load due to opaque envelopes may be reduced by up to 50% by properly controlled infiltration flow for the condition examined.
- exfiltration air flow is preferable to infiltration under cooling conditions; the average cooling load due to opaque envelopes may be reduced by up to 22% by exfiltration flow for the conditions examined.
- the current design method can either over-estimate or under-estimate space heating or cooling loads due to its failure to consider interactions between conduction, air leakage and solar radiation.

Systematic Error due to the Steady-State Methodology

When air flow is constant, the building thermal envelope is a linear system, and then the steady-state methodology is valid.

When air flow rate changes with time, the building thermal envelope is akin to a non-linear system, and then the steady-state methodology can result in systematic error. The steady-state method can be used to investigate thermal performance of the building envelope with UA errors of less than 5% under normal outdoor situations where the air flow rate changes slowly with time. The systematic error of the steady-state methodology depends on the solar radiation and air flow model. The simulation results show an IHEE error of -1% to 8% for a one-way air flow model. However, the steady-state method can cause UA errors of 8% for balanced air flow model due to steady-state methodology failure to account for the air flow.

Measurement Methods

The SSP (Single input and Single output data Pair) method can identify the heat loss factor without air infiltration (UA_0) of an enclosure using short term measurement data, typically a few hours long. It was developed based on signal processing theory, and uses a specially designed heat input waveform to the enclosure. Then, a digital band-pass filter is used to create a Single input and Single output data pair from the measured data sets by only picking up part of this input and its temperature response. The UA_0 is then identified using this data pair. This method has the following advantages, as compared to calorimetric and current model fitting methods. It (1) uses less time; (2) uses simpler equipment; (3) does not involve substantial intrusion into normal house operation; and (4) has the same level of accuracy. Most of the typical problems for UA_0 identification, such

as errors due to thermal storage, ground heat transfer, inter-correlated multi-inputs, and solar radiation also seem to have been overcome.

The STAM (Short Term Average Method) method makes it possible for the first time to determine both the UA and the solar aperture precisely without systematic error under outdoor conditions from a three-day test. Moreover, this methodology only requires a constant air flow, and measurement of the heat input, solar radiation, air flow rate, ambient temperature, and building air temperature. STAM takes account of the thermal storage problems due to abnormal weather variation by adjusting the time period; and automatically rejecting the test, in case it is incapable of identifying the UA value.

BENEFIT AND IMPACTS

The benefits and impacts of the outcome of the present investigation are expected to be quite significant in building science, in thermal system parameter identification, in room air pollution control, and in the HVAC area. They include:

- more accurate prediction of heating and cooling loads of a building system
- more accurate HVAC system sizing
- more insight into the fundamental understanding of attic and wall thermal behavior
- effective application of solar energy in residential houses
- effective control of ventilation in residential houses
- efficient and accurate estimation of thermal system parameters
- new methodology for thermal parameters determination
- improvement of indoor air quality issues.

RECOMMENDATIONS FOR FUTURE WORK

The SSP method was only tested in an indoor test cell. Although only a few hours were needed for UA_0 estimation and excellent estimates were achieved, additional factors, such as partition walls, may result in added complexity when applied to actual houses.

The STAM method was successfully tested in the outdoor test cell experiments. However, the outdoor test cell did not have ground heat transfer present. Although it appears reasonable on a theoretical basis that ground heat transfer may not cause serious problems for this method, it is wise to pay special attention to the house when STAM is used in houses.

Both steady-state and dynamic models have been investigated for idealized walls and attics, and no attempts were made to compare measured and model values. If the models can be improved or modified to be consistent with the measured results, the model will prove more powerful for predicting energy use.

The dynamic simulation of infiltration heat energy exchange effectiveness was limited to a single wall construction. More simulations and experiments are necessary to investigate the influence of the air flow rate, wall structure, etc. in real houses.

Finally, tests in a full-size house will be essential to confirm the findings, and to validate the methodology developed in this dissertation. It will be important for future studies to include the optimization of leakage distribution, optimization of solar energy utilization, and hybrid natural infiltration and ventilation system design.

REFERENCES

- Adderley, A. E., Probert S. D. and O'Callaghan, P. W. 1990, "Materials and Retro-fit Method for Reducing Rates of Heat Loss Through Walls," Applied Energy, Vol. 35, pp. 1-12.
- Anderlind, G. 1985, "Energy Consumption Due to Air Infiltration," Proceedings of the 3rd ASHRAE/DOE/BTECC Conference on Thermal Performance of the Exterior Envelopes of Buildings, Clearwater Beach, FL, pp. 201-208.
- Andersson K. A. and Wadmark, T. 1987, "Use of Ventilation and Insulation in Single Family Houses for Thermal Comfort, Energy Conservation and Protection Against Moisture, Dust and Radon, the OPTIMA Concept," Proceedings of the 3rd International Congress on Building Energy Management ICBEM'87, Vol. 3, Lausanne, Switzerland.
- Arquis, E. and Langlais, C. 1986, "What Scope for Dynamic Insulation?," Batiment International Building Research and Practice, Vol. 19, pp.84-93.
- ASHRAE, 1981, "ASHRAE Handbook: 1981 Fundamentals," American Society of Heating, Refrigerating and Air-Conditioning Engineers, Atlanta, GA.
- Bailly, N. R. 1987, "Dynamic Insulation Systems and Energy Conservation in Buildings," ASHRAE Transactions, Vol. 93, part 1, pp. 447-466.
- Barakat, S. A. 1987, "Experimental Determination of the Z-Transfer Function Coefficients for Houses," ASHRAE Transactions, Vol. 93, part 1, pp.146-161.
- Baudier, M. and Marchio, D. 1991, "Dynamic Model Identification Applied to the Measuring of Thermal Static Characteristics of Buildings," Energy and Building, Vol. 17, pp.21-24.
- Beyea, J., Dutt, G. and Wotecki, T. 1977, "Critical Significance of Attics and Basements in the Energy Balance of Twin Rivers Townhouses," Energy and Buildings, Vol. 1, pp. 261-269.
- Bhattacharyya, S. and Claridge D. E. 1992, "The Energy Impact of Air Leakage Through Insulated Wall," Proceedings of 1992 ASME Solar Energy Division Conference, Miami.
- Boman C. A. and Lyberg, M. D. 1984, "Measured and Building Code Values of Air Change Rate in Residential Building," Proceedings of 5th AIC Conference on The Implementation and Effectiveness of Air Infiltration Standards in Buildings, Reno, Nevada.

Burse, T. and Green, G. H. 1970, "Combined Thermal and Air Leakage Performance of Double Windows," ASHRAE Transactions, Vol 73, pp. 215-226.

Charlesworth, P. S. 1988, "Air Exchange Rate and Airtightness Measurement Techniques -----An Application Guide," Air Infiltration and Ventilation Centre, Coventry, Great Britain.

Claridge, D. E., Jeon H., and Bida, M. 1984, "Performance Analysis of the Colorado 50/50 Retrofit Program," Vol. 1, Submitted to the Solar Energy Research Institute by the University of Colorado, Dept. of Civil Engineering and Architecture Engineering.

Claridge, D. E., Jeon H., and Bida, M. 1985, "A Comparison of Traditional Degree-Day and Variable-Base Degree-Day Predication with Measured Consumption of 20 Houses in the Denver Area," ASHRAE Transactions, Vol. 91, part 2, pp865-874.

Claridge, D. E. and Bhattacharyya, S. 1989, "The Measured Energy Impact of "Infiltration" in a Test Cell," Proceedings of the Eleventh Annual ASME Solar Energy Conference, San Diego, CA.

Claridge, D. E. and Bhattacharyya, S. 1990, "The Measured Energy Impact of "Infiltration" in a Test Cell," Journal of Solar Energy Engineering, Vol. 112, pp. 132-139.

Dubois, P. 1983, "Energy Efficient Building Walls," Proceedings of the First E. C. Conference on Solar Collectors in Architecture, Venice, Italy, pp. 144-158.

Duffie J. A. and Beckman, W. A. 1980, Solar Engineering of Thermal Processes, Wiley Interscience Publication, New York.

Fang, J. B., Grot, R. A., and Park, H. S. 1985, "The Assessment of Accuracy of in-site Methods for Measuring Building Envelope Thermal Resistance," Proceedings of Thermal Performance of the Exterior Envelopes of Buildings, 3rd ASHRAE/DOE/BTECC Conference, Clearwater Beach, FL.

Feuermann, D. 1989, "Measurement of Envelope Thermal Transmittances in Multifamily Buildings," Energy and Buildings Vol. 13, pp. 139-148.

Golovkin N. A. 1960, "New Cold Store Insulation System," Bulletin de l'IIF, Annexe 1960-3 commission V, Conference de Marseille.

Guo, J. and Liu, M. 1985, "The Energy Saving Effect of Double Frame Windows," Proceedings of the CLIMA 2000 World Congress in Heating , Ventilating and Air-Conditioning, Copenhagen, Denmark, Vol. 2.

Guo J., Xu, J. and Li X. 1985, "Heat Balance Tests and Energy Conservation Studies for Buildings in Harbin," Proceedings of the CLIMA 2000 World Congress in Heating , Ventilating and Air-Conditioning, Copenhagen, Denmark, Vol. 2.

Guo J. and Liu, M. 1987, "The Effective & Ineffective Heat Loss By Infiltration---Field Measurement in a Dormitory," Proceedings of the 3rd International Congress on Building Energy Management ICBEM'87, Vol. 2, Lausanne, Switzerland.

Hammarsten, S. 1985, "Frequency Domain Analysis of Energy Balance of Houses," Proceedings of the CLIMA 2000 World Congress in Heating , Ventilating and Air-Conditioning, Copenhagen, Denmark, Vol. 2, pp. 459-464.

Hammarsten, S., Hattem, D. V., Bloem, H., and Colombo, R. 1988, "Passive Solar Component Testing With Identification Methods," Solar Energy, Vol. 41, No. 1, pp. 5-13.

Harrje, D. T. and Janssen, J. E. 1984, "A Standard for Minimum Ventilation," Proceedings of 5th AIC Conference on The Implementation and Effectiveness of Air Infiltration Standards in Buildings, Reno, Nevada.

Harrje, J., Dutt, G., and Beyea, J. 1979, "Locating and Elimating Obscure but Major Energy Losses in Residential Housing," ASHRAE Transactions, Vol. 85, part 2, pp. 521-59.

Homma, H., and Guy, R. W. 1979, "Ventilation of Back Space of Building Enclosure Siding for Solar Heat Gain Reduction," Proceedings of Thermal Performance of the Exterior Envelopes of Buildings, ASHRAE/DOE-ORNL Conference, Kissimmee, Florida.

Jackman, P. J. 1984, "Review of Building Airtightness and Ventilation Standards," Proceedings of 5th AIC Conference on The Implementation and Effectiveness of Air Infiltration Standards in Buildings, Reno, Nevada, pp. 1.1-1.24.

Janssen, J. E. and Rasmussen R. W. 1985, "An Instrument for Measuring Building Envelope Thermal Performance," Proceedings of Thermal Performance of the Exterior Envelopes of Buildings, 3rd ASHRAE/DOE/BTECC Conference, Clearwater Beach, FL.

Kimura, K. 1979, "Scientific Basis of Air Conditioning," Applied Science Publishers LTD, London.

Kohonen, R., Tech, D. and Wirtanen, M. 1987, "Thermal Coupling of Leakage Flows and Heating Load of Buildings," ASHRAE Transactions, Vol. 93, Part 2, pp2303-2318.

Lamberts, R., Fitzgerald, D., and Houghton-Evans, W. 1985, "The Importance of Attic Ventilation," Proceedings of the CLIMA 2000 World Congress in Heating , Ventilating and Air-Conditioning, Copenhagen, Denmark, Vol. 2, pp. 33-37.

Liddament, M. W. 1986, "Air Infiltration Calculation Techniques ----An Applications Guide," Air infiltration and Ventilation Centre, Berkshire, Great Britain.

Liu, M. 1987, "Thermal Techniques in Buildings," Harbin Architectural and Civil Engineering Institute Press, Harbin, China, pp. 3.85 - 3.90.

Liu, M. 1986, "Economy Analysis of Double Windows in the Middle of China," Proceedings of the fifth International PLEA Conference, Vol.1 C-13, Pecs, Hungary.

Liu, M. and Claridge, D. E. 1992(a), "The Measured Energy Impact of Infiltration under Dynamic Conditions," Proceedings of Symposium on Improving Building Systems in Hot and Humid Climates, Dallas, TX.

Liu, M. and Claridge, D. E. 1992(b), "The Measured Energy Impact of Infiltration in an Outdoor Test Cell," Proceedings of Symposium on Improving Building Systems in Hot and Humid Climates, Dallas, TX.

Liu, M. and Claridge, D. E. 1992(c), "The Energy Impact of Combined Solar-Radiation/Infiltration/Conduction Effects in Walls and Attics," Proceedings of Thermal Performance of the Exterior Envelopes of Buildings, 5th ASHRAE/DOE/BTECC Conference, Clearwater Beach, FL.

Mahmoud, M. S., and Singh, M. G. 1984, Discrete System Analysis, Control, and Optimization, Springer-Verlag, New York.

Masoero, M. and Aghemo, C., "Performance of an Innovative Ventilated Curtain-Wall Component," Proceedings of Thermal Performance of the Exterior Envelopes of Buildings III, Conference of ASHRAE/DOE/BTECC, pp. 1004-1018, Clearwater Beach, Florida.

Neter, J., Wasserman, W., & Kutner, M. J. 1989, Applied Linear Regression Models, IRWIN, New York.

Newton, H. J. 1988, Timeslab: A Time Series Analysis Laboratory, Wadsworth & Brooks/Cole Publishing Company, Pacific Grove, California.

Nielsen, A. A. 1985, "A Dynamic Test Method for the Energy Consumption of Small Houses, Model Set-up, Test Design, Measurement, Parameter Estimation and Simulation," Proceedings of the CLIMA 2000 World Congress in Heating, Ventilating and Air-Conditioning, Copenhagen, Denmark, Vol. 2, pp533-541.

Norlen, U. 1990, "Estimating Thermal Parameters of Outdoor Test Cells," Building and Environment, Vol. 25, No. 1, pp.17-24.

Patanker V. S. 1980, Nemurical Heat Transfer and Fluid Flow, Hemisphere Publishing Corporation, New York.

Penman, J. M. 1990, "Second Order System Identification in the Thermal Response of a Working School," Building and Environment, vol. 25, No. 2, pp. 105-110.

Powell, F. 1989, "Air Movement Influence on the Effective Thermal Resistance of Porous Insulations: A Literature Survey," Journal of Thermal Insulation, Vol. 12, pp.239-251.

Rabl, A. 1988, "Parameter Estimation in Buildings: Method for Dynamic Analysis of Measured Energy Use," Transactions of the ASME, Vol.110.

Reddy, T. A. 1989, "Application of Dynamic Building Inverse Models to Three Occupied Residences Monitored Non-Intrusively," Proceedings of Thermal Performance of the Exterior Envelopes of Buildings, Fourth ASHRAE/DOE/BTECC Conference, Orlando, Florida.

Ripatti, H. 1985, "Air Flow Windows in Hot Climates," Proceedings of the CLIMA 2000 World Congress in Heating, Ventilating and Air-Conditioning, Copenhagen, Denmark, Vol. 2, pp. 45-50.

Selby, S. M. 1967, Standard Mathematical Tables, The Chemical Rubber Co. Cleveland, Ohio.

Sharma, M. R., and Pal, R. S. 1965, "Interrelationships Between Total, Direct, and Diffuse Solar Radiation in the Tropics," The Journal of Solar Energy Science and Engineering, vol. 9, No. 4, pp.183-192.

Siala, F. M. F., Rosen, M. A., and Hooper, F. C. 1990, "Models for the Directional Distribution of the Diffuse Sky Radiance," Transactions of ASME, Vol. 112, pp. 102-109.

Sonderegger, R. C. 1978, "Diagnostic Tests Determining the Thermal Response of a House," ASHRAE Transactions, Vol. 84, part 1, pp.691-702.

Sonderegger, R. C. 1979, "Electric Co-Heating: A Method for Evaluating Seasonal Heating Efficiencies and Heat Loss Rates in Dwellings," Report 8949, Lawrence Berkeley Laboratory, Berkeley, CA.

Sondergger, R. C., Condon, P. E., and Modera, M. P. 1980, "In-situ Measurements of Residential Energy performance Using Electric Co-heating," ASHRAE Transactions, Vol. 86, part 1, pp.394-407.

Stephenson D. G. and Mitalas G. P. 1967, "Cooling Load Calculations by Thermal Response Method," ASHRAE Transaction Vol. 73, part 2.

Strum, R. D., and Kirk, D. E. 1988, First Principles of Discrete Systems and Digital Signal Processing, Addison-Wesley Publishing Company, New York.

Subbarao, K. 1988, "PSTAR--Primary and Secondary Terms Analysis and Renormalization," SERI/TR-254-3175, Solar Energy Research Institute, Golden, Colorado.

Subbarao, K, and Burch J. D. 1988, "Short Term Energy Monitoring (STEM): Application of the PSTAR Method to a Residence in Fredericksburg, Virginia," SERI/TR-24-3356, Solar Energy Research Institute, Golden, Colorado.

Subbarao, K., and Burch, C. E. Hancock, 1990, "How to Accurately Measure the Building Load Coefficient," SERI Draft Report, Solar Energy Research Institute.

Subbarao, K., and Kennedy, M. 1990, "Improving the Accuracy of the Coheat Method of Measuring the Building Load Coefficient," SERI/TP-254-4097 (Draft), Solar Energy Research Institute Golden, Colorado.

Timusk, J., Seskus, A. L., and Lio, M. 1987, "Performance Evaluation of the Dynamic Wall House," Project Report Prepared by Center for Building Science, University of Toronto, Toronto, Canada.

Uvslokk, S. and Vik, B. 1984, "A Consequence Analysis of New Norwegian Building Regulation On Air Infiltration," Proceedings of 5th AIC Conference on The Implementation and Effectiveness of Air Infiltration Standards in Buildings, Reno, Nevada.

Wang Xing An and Kreider, J. F. 1990, "Demonstration of Automated Generation of Energy Predicators for Commercial Buildings Using Artificial Neural Networks," Joint Center for Energy Management, University of Colorado, Boulder.

Wolf, S. 1966, "A Theory for the Effects of Convective Air Flow through Fibrous Thermal Insulation," ASHRAE Transactions, Vol. 72, part 2, pp. III2.1 - III3.8.

Wolf, S., Solvason and Wilson, A. G. 1966, "Convective Air Flow Effects with Mineral Wool Insulation in Wood-Frame Walls," ASHRAE Transactions, Vol. 72, part 2, pp. III. 3.1 - III. 3.8.

APPENDIX A1

ERROR ANALYSIS

The procedures for estimating uncertainty of both the indoor and outdoor cell measurement results are described in this appendix. The dependent variable was the IHEE, and independent variables were temperature, heat input, air flow rate, and solar radiation. The error limit of these independent variables are chosen based on data acquisition system error corresponding each signal, and are shown in Table A1-1. It was assumed all the temperature parameters had same relative error limit because they had limited variation in the tests. The relationship of error and air flow rate was developed because the air flow rate had significant influence on the error of the measurement results. The absolute error refers to the error in signal unit, and the relative error refers to the ratio of the absolute error to the signal.

Table A1-1: The Error Limits of the Basic Independent Variables

Term	Unit	Absolute Error	Relative Error
Temperature	°C	0.5	2%
Heat Input	W	5	2%
Solar Radiation	W/m ²		2%
Air Flow Rate (Full Scale)	Kg/s		10%

INDOOR CELL TEST

The IHEE was calculated by using the following formula for indoor cell test.

$$UA_0 = \frac{\sum_{i=1}^k Q(i)}{\sum_{i=1}^k \Delta T(i) - \delta T_{se}} \quad (A1-1)$$

$$UA = \frac{\sum_{i=1}^k Q(i) - UA_0 \delta T_{se}}{\sum_{i=1}^k \Delta T(i)} \quad (A1-2)$$

$$IHEE = 1 - \frac{UA - UA_0}{\dot{M}C_p} \quad (A1-3)$$

Although the average parameters, such as temperature, heat input, and air flow rate, were used in these formulas, the basic error limits (see Table A1-1) were used for the error analysis because it was impossible to separate system error and random errors.

According to formula (A1-1), the relative error of UA_0 can be written as:

$$\frac{\delta UA_0}{UA_0} = \left[\left(\frac{\delta Q}{Q} \right)^2 + 2 \left(\frac{\delta T_{cell}}{T_{cell}} \right)^2 + 2 \left(\frac{\delta T_{room}}{T_{room}} \right)^2 \right]^{1/2} \quad (A1-4)$$

Introduce the basic error limit from table (A1-1) to get:

$$\frac{\delta UA_0}{UA_0} = \left[(0.02)^2 + 2(0.02)^2 + 2(0.02)^2 \right]^{1/2} = 0.0447$$

According to equation(A1-2), the relative error of UA can be written as:

$$\frac{\delta UA}{UA} = \left[\left(\frac{\delta Q}{Q} \right)^2 + 2 \left(\frac{\delta T_{cell}}{T_{cell}} \right)^2 + 2 \left(\frac{\delta T_{room}}{T_{room}} \right)^2 + \left(\frac{\delta UA_0}{UA_0} \right)^2 \right]^{1/2} \quad (A1-5)$$

Introduce the basic error limits and relative error of UA_0 to equation (A1-5) to get:

$$\frac{\delta UA}{UA} = [(0.02)^2 + 2(0.02)^2 + 2(0.02)^2 + (0.0447)^2]^{1/2} = 0.0632$$

According to equation (A1-3), the relative error of IHEE can be written as:

$$\frac{\delta IHEE}{IHEE} = \left[\left(\frac{\delta UA_0}{UA_0} \right)^2 + \left(\frac{\delta UA}{UA} \right)^2 + \left(\frac{\delta \dot{M}}{\dot{M}} \right)^2 \right]^{1/2} \quad (A1-6)$$

Introduce the relative error limit of UA and UA_0 into equation (A1-6) to get:

$$\frac{\delta IHEE}{IHEE} = [0.005996 + \left(\frac{\delta \dot{M}}{\dot{M}} \right)^2]^{1/2} \quad (A1-7)$$

The full scale relative error of air flow is 0.10, however, the air flow range used in the test were 0.3 to 0.8 full scale. The measurement error limit of IHEE varies from 15% to 34% with air flow rate for indoor cell test.

OUTDOOR CELL TEST

The IHEE was calculated by using the following formula in outdoor cell test:

$$\delta T_{sol} = \frac{\sum_{i=1}^k T_r(i) - T_a(i)}{\sum_{i=1}^k I(i)} \quad (A1-8)$$

where:

δT_{sol} = solar contribution to the cell temperature ($^{\circ}C/W/m^2$)

T_r = cell air temperature ($^{\circ}C$)

T_a = outside temperature ($^{\circ}C$)

I = equivalent solar radiation on the cell (W/m^2)

i = time index of a 10-minutes time period (1 beginning, k ending).

$$UA_o = \frac{\sum_{i=1}^k q(i) + UA_o \sum_{i=1}^k I(i) \delta T}{\sum_{i=1}^k [T_r(i) - T_a(i)]} \quad (A1-9)$$

where:

q = heat input (W)

UA_o = heat loss factor due to conduction only (W/°C)

Other symbols have been defined in Equation (A1-8).

$$UA = \frac{\sum_{i=1}^k q(i)}{\sum_{i=1}^k [T_r(i) - T_a(i) - I(i) \delta T]} \quad (A1-10)$$

$$IHEE = 1 - \frac{UA - UA_o}{\dot{M}C_p} \quad (A1-11)$$

where:

\dot{M} = air infiltration/exfiltration rate (Kg/s)

C_p = specific heat of air (J/Kg °C).

According to equation (A1-8), the relative error limit of solar contribution δT_{sol} can be written as:

$$\frac{\delta(\delta T_{sol})}{\delta T_{sol}} = [2\left(\frac{\delta T}{T}\right)^2 + \left(\frac{\delta I}{I}\right)^2]^{1/2} \quad (A1-12)$$

Introduce the basic error limit from table A1-1 to equation (A1-12) to get:

$$\frac{\delta(\delta T_{sol})}{\delta T_{sol}} = [2(0.02)^2 + (0.02)^2]^{1/2} = 0.035$$

According to equation (A1-9), the relative error limit of UA_o can be written as:

$$\frac{\delta UA_0}{UA_0} = \left[\left(\frac{\delta q}{q} \right)^2 + \left(\frac{\delta(\delta T_{sol})}{\delta T_{sol}} \right)^2 + 2 \left(\frac{\delta T}{T} \right)^2 + 2 \left(\frac{\delta I}{I} \right)^2 \right]^{1/2} \quad (A1-13)$$

Introduce the basic error limits and relative error limit of δT_{sol} into equation (A1-13)

to get:

$$\frac{\delta UA_0}{UA_0} = [(0.02)^2 + (0.035)^2 + 2(0.02)^2 + (0.2)^2]^{1/2} = 0.0530$$

The equation (A1-10) shows UA has same relative error limit of UA_0 . Finally,

according to the equation (A1-11), the relative error limit of IHEE can be written as:

$$\frac{\delta IHEE}{IHEE} = \left[\left(\frac{\delta UA_0}{UA_0} \right)^2 + \left(\frac{\delta UA}{UA} \right)^2 + \left(\frac{\delta \dot{M}}{\dot{M}} \right)^2 \right]^{1/2} \quad (A1-14)$$

Introduce relative error limits of UA and UA_0 into equation (A1-14) to get:

$$\frac{\delta IHEE}{IHEE} = [(0.053)^2 + (0.053)^2 + \left(\frac{\delta \dot{M}}{\dot{M}} \right)^2]^{1/2} \quad (A1-15)$$

The error limit for full scale air flow rate is 10%, however, the air flow range used in the test was 40% to 70% of the full scale. The error limit of IHEE varies from 16% to 26% with air flow rate for outdoor test cell.

APPENDIX A2

FUNDAMENTAL THEORY OF UA CALCULATION

Generally speaking, a building envelope is a composite system because opaque walls, windows, and doors behave quite differently. The relationship of transfer functions for the composite building and its subsystems is described below. The method is also developed for decomposing the subsystem transfer function from the composite system transfer function. Finally, the heat loss factor calculation method is given.

Let us assume that the house system consists of a second order and zero order subsystems, which are parallel connected, see Figure A2-1.

$$H_1(Z) = \frac{T(Z)}{Q_1(Z)} = \frac{b_0 + b_1Z^{-1} + b_2Z^{-2}}{1 + a_1Z^{-1} + a_2Z^{-2}} \quad (\text{A2-1})$$

$$H_2(Z) = \frac{T(Z)}{Q_2(Z)} = c \quad (\text{A2-2})$$

where:

H_1 = transfer function for the second order subsystem, which represents opaque walls, floors, and roofs,

H_2 = transfer function for the zero order, which represents windows, doors, and concentrated air infiltration,

$T(Z)$ = Z transform of the room temperature,

$Q_1(Z), Q_2(Z)$ = Z transform of heat loss for the opaque part and the other part of the envelope, respectively,

b, a, c = coefficient.

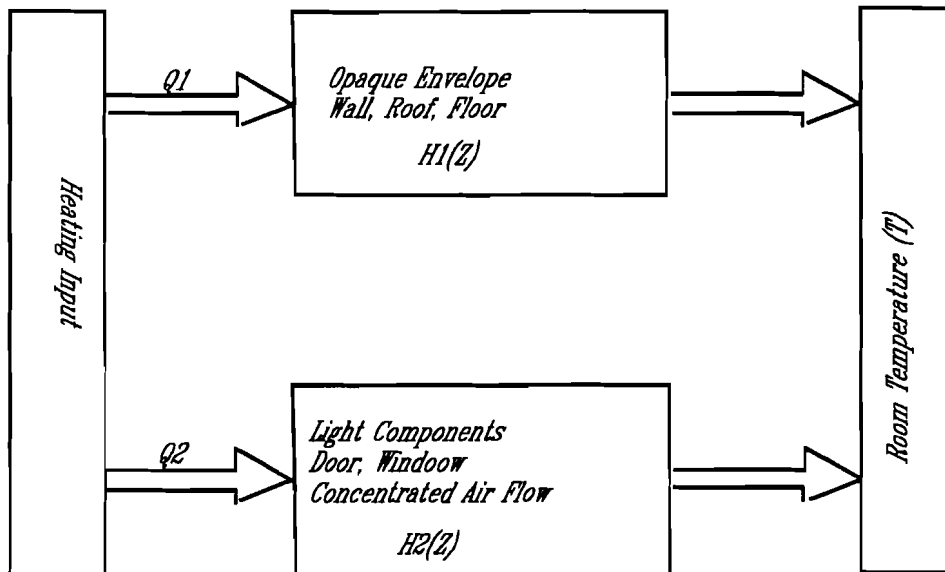


Figure A2-1: Thermal System Block Diagram for House Envelope

The transfer function of the composite or house system can be expressed as:

$$\begin{aligned} H(Z) &= \frac{1}{\frac{1}{H_1(Z)} + \frac{1}{H_2(Z)}} \\ &= \frac{b_0c + b_1cZ^{-1} + b_2cZ^{-2}}{(b_0 + c) + (b_1 + a_1c)Z^{-1} + (b_2 + a_2c)Z^{-2}} \end{aligned} \quad (A2-3)$$

This shows that the composite system has the order of the highest subsystem. It can be inferred that the composite house system can be expressed by a single transfer function. The transfer function of the house can be estimated by the test data, and can be expressed as:

$$H(Z) = \frac{T(Z)}{Q(Z)} = \frac{d_0 + d_1Z^{-1} + d_2Z^{-2}}{1 + e_1Z^{-1} + e_2Z^{-2}} \quad (A2-4)$$

where d and e are estimated transfer function coefficients. To compare the two equations above, the following calculation procedure can be used for the subsystem calculation.

$$c = \frac{1 + \sqrt{1 - 4d_0}}{2} \quad (A2-5)$$

$$b_i = \frac{d_i}{c} \quad i = 1, 2, \dots, n \quad (A2-6)$$

$$a_i = \frac{e_i - b_i}{c} \quad i = 1, 2, \dots, n \quad (A2-7)$$

It should be noted that the calculation may give two different numbers for c; the positive one should be chosen if the other is negative. If both of the c values are positive, further investigation should be carried out.

The heating load factor can be easily calculated from the transfer function coefficient. The room temperature can be expressed by the transfer function in the time domain as:

$$T(i) = -e_1T(i-1) - e_2T(i-2) + d_0Q(i) + d_1Q(i-1) + d_2Q(i-2) \quad (\text{A2-8})$$

If constant power is input for a very long time, one can expect that constant room temperature should result, so the heat loss factor can be deduced from the above equation as:

$$UA = \frac{Q(i)}{T(i)} = \frac{1 + e_1 + e_2}{d_0 + d_1 + d_2} \quad (\text{A2-9})$$

where UA is the total heat loss factor (W/K). One can use transfer function coefficient to calculate the heat loss factor for special part by the same method, however, the heat loss factor can be obtained by subtracting $1/c$ from the UA because $1/c$ is the heat loss factor for the door, window, and possible concentrated air infiltration.

APPENDIX A3

EQUIVALENT SOLAR RADIATION MODEL FOR OUTDOOR CELL

The equivalent solar radiation, defined as the resistance and area weighted average solar radiation on the cell, is calculated according to the measured horizontal solar radiation, time, the test cell geometric parameters, and the basic laws which describe the sun's movement. The basic procedures include calculation of solar time and position, breaking down global radiation, calculation of solar radiation on the wall, and calculation of the equivalent solar radiation for the test cell.

SOLAR RADIATION AND SOLAR POSITION

The solar position is determined by the solar altitude (β) and the solar azimuth angle (α) (degree). These can be expressed by the following formula [Liu 1986, Duffie 1980].

$$\sin(\beta) = \sin(\psi) \sin(\delta) + \cos(\psi) \cos(\delta) \cos(t) \quad (\text{A3-1})$$

$$\cos\alpha = \frac{\sin\psi \sin\beta - \sin\delta}{\cos\psi \cos\beta} \quad (\text{A3-2})$$

where:

β = solar altitude

α = solar azimuth angle

ψ = latitude of locality ($30^{\circ} 4'$ for College Station, Texas)

δ = declination angle

t = hour angle.

These quantities can be expressed by following equations:

$$\delta = 23.45 \sin(280.1 + 0.9863M) \quad (\text{A3-3})$$

$$t = 15 \left(t_s - \frac{L - L_s}{15} + \frac{e}{60} - 12 \right) \quad (\text{A3-4})$$

where

t_s = hour expressed in local standard time (h)

L = longitude of the locality (College Station, Texas, 96)

L_s = longitude of the standard location of solar time (90, according to the American Standard Meridians for continental U. S. time zones)

M = the day of the year

e = equation of time in minutes.

$$e = 9.87 \sin(2B) - 7.53 \cos(B) - 1.5 \sin(B) \quad (\text{A3-5})$$

$$B = \frac{360(M - 81)}{364} \quad (\text{A3-6})$$

The solar time is:

$$\tau = \frac{t}{15} + 12 \quad (\text{A3-7})$$

BREAKING DOWN OF GLOBAL SOLAR RADIATION

It is presumed that the measured horizontal solar radiation consisted of direct and sky diffuse radiation.

$$I_{TH} = I_{DH} + I_{SH} \quad (\text{A3-8})$$

where,

I_{TH} = measured horizontal surface radiation (W/m^2)

I_{DH} = direct solar radiation on horizontal surface (W/m^2)

I_{SH} = diffuse solar radiation on horizontal surface (W/m^2).

IDH and IDN are closely related to each other through the solar altitude angle, but the relationship of ISH and IDN depends on the altitude angle, the weather conditions, and the ground reflection conditions. Two simple models have been used in ASHRAE and SHACSEJ (Society of Heating and Air Conditioning and Sanitary Engineers of Japan) to break down the horizontal solar radiation to direct and diffuse components:

$$IDH = IDN \sin(\beta) \quad (A3-9)$$

$$ISH = C IDN \quad (\text{ASHRAE}) \quad (A3-10)$$

$$ISH = \frac{1}{2} I_0 \sin(\beta) \quad (\text{SHACSEJ}) \quad (A3-11)$$

where:

C = a constant which varies with time, the average monthly data are given in table A3-1.

I_0 = solar constant which can be calculated according to the day number of year.

$$I_0(M) = 1353 \left[1 + 0.033 \cos \frac{360 - M}{370} \right] \quad (A3-12)$$

The ASHRAE model is good only for clear day, but the SHACSEJ model is good for all weather conditions. Introduce equation (A3-9), (A3-10), and (A3-11) to equation (A3-9) to get:

$$IDN = \frac{ITH}{\sin\beta + C} \quad (\text{ASHRAE}) \quad (A3-13)$$

$$IDN = \frac{ITH}{\sin\beta} - \frac{I_0}{2} \quad (\text{SHACSEJ}) \quad (A3-14)$$

Table A3-1.Coefficient C

Month	January	Feb.	March	April	May	June
C	0.058	0.060	0.071	0.097	0.121	0.134
Month	July	August	Sep.	Oct.	Nov.	Dec.
C	0.136	0.122	0.092	0.073	0.063	0.057

Now, the direct and diffuse solar radiations can be determined based on the measured total solar radiation, time, and the number of regression formulas which describe the sun's movement.

SOLAR RADIATION ON THE WALLS

The solar radiation on the wall consists of direct, diffuse, and ground reflection radiation. Both direct and diffuse solar calculation formula have been given in the above section. The ground reflection radiation can be calculated by:

$$I_{dg} = \rho_g I_{TH} \quad (A3-15)$$

where:

ρ_g = reflection coefficients of the ground.

The test cell is placed on the top of a concrete floor, which is about 7 x 14 meters (20 x 40 feet) in size, beyond that is lawn, so the reflective coefficients are chosen as the average values of these two conditions. The ground reflective coefficients are given in table A3-2.

Table A3-2. Ground Reflection Coefficients

b	20	30	40	50	60	70
Lawn	0.21	0.22	0.23	0.25	0.28	0.38
Con.	0.22	0.22	0.22	0.23	0.23	0.25
USED	0.215	0.22	0.225	0.24	0.255	0.315

It must be pointed out here that the solar radiation is directional, although the diffuse term is used often. The wall radiation formulae are introduced below.

Direct solar radiation on a horizontal surface, a vertical surface, and a tilted surface can be calculated by the following formula.

$$IDH = IDN \sin\beta \quad (A3-16)$$

$$IDV = IDN \cos\beta \cos\gamma \quad (A3-17)$$

$$IDy = IDN(\sin\beta\cos\psi + \cos\beta\cos\gamma\sin\psi) \quad (A3-18)$$

$$\gamma = \alpha - \varepsilon \quad (A3-19)$$

where:

α = solar azimuth

ε = wall orientation, (0 for south, 90 for west, 180 for north, 270 for east)

γ = wall solar azimuth angle

ψ = tilted angle of the surface.

It should be pointed out that when this formula is used, different rules are introduced by different users. Here our rules are: (1) ψ is always positive; (2) if absolute value of γ is less than 90 degree then the absolute value is used; (sunny facade) (3) if the absolute value of γ is greater than 90 but solar altitude is greater than the tilted angle, the absolute value is used; and (4) under other situations, the solar radiation is taken as zero.

The diffuse sky radiation on a tilted and vertical surface is calculated based on horizontal intensity.

$$IS_{\psi} = \cos \frac{\psi}{2} \cos \frac{\psi}{2} IS_H \quad (A3-20)$$

The ground reflection radiation of the different surfaces is calculated by;

$$IR_{\psi} = (1 - \cos \frac{\psi}{2} \cos \frac{\psi}{2}) \rho_g ITH \quad (A3-21)$$

EQUIVALENT SOLAR RADIATION

Equivalent solar radiation was defined as the weighted average solar radiation intensity on all the walls of the house. Both dynamic effects (time delay and peak reduce term) and steady-state effects (amount of transfer) must be considered. For example, if solar radiation is incident on windows, it behaves much differently than that incident on walls, so it is impossible to get a single equivalent solar radiation intensity in a house without special treatment. Fortunately, the test cell had no window, and every component had almost the same dynamic performance (all four walls are the same, the floor and the ceiling have almost the same weight as the wall), although the steady-state R-values are different. So here only steady-state performance is considered when introducing equivalent solar radiation. The basic ideas are summarized as follows:

- (1) The ceiling and walls have almost the same dynamic performance, e.g. the response factor curve has the same shape but not necessarily the same magnitude.
- (2) The ratio of the heat gain contribution of the unit ceiling solar contribution and the unit wall solar contribution is equal to the ratio of the heat conductance of

these two parts. ($w=1:2$). It is defined as the weighting factor of the equivalent solar radiation.

(3) The weighting factor for the wall is defined as 1, 0.5 for the ceiling.

(4) The total solar radiation on the different surfaces is calculated by

$$Q(i) = F(i)(ID\psi(i) + IS\psi(i) + IR\psi(i)) \quad (A3-22)$$

where:

i = wall number

$Q(i)$ = total radiation incident on i th wall

$F(i)$ = surface area of the i th wall.

(5) The equivalent total solar radiation on i th wall is defined as the production of the total incident and its weighting factor.

$$Q_e(i) = \omega(i)Q(i) \quad (A3-23)$$

(6) The equivalent solar radiation of the test cell is defined as the total equivalent solar radiation on all the walls divided by the total surface area of the walls, floor, and ceiling.

$$Q_e = \frac{\sum Q_e(i)}{\sum F(i)} \quad (A3-24)$$

where:

Q_e = equivalent solar radiation intensity on the house

$Q_e(i)$ = equivalent solar radiation on i th surface

$F(i)$ = surface area for i th surface.

This solar model is used in the OUTCELL program for the data processing.

APPENDIX B1

SOURCE CODE OF "OUTCELL.FOR"

This program was used to the data processing in the outdoor cell tests.

```

program outcell
character dat(1000)*10,tim(1000)*8,fil*10,cha1*3
character cha2*21,com*40
real tcell(1000),tattic(1000),tout(1000)
real power(1000),air(1000),thouse(1000),SOLP(1000)
REAL Sol(1000),phouse(1000),xa(20),xb(20)
double precision azimuth,altitude
integer hour,minutes,month,day,year,kd(20)
real IDN,IDH,IDG,ISH,w1(2),w2(2)
INTEGER p1(20),p3(40),p(40),p2(40)
real tc(20),to(20),so(20),ai(20),po(20),dt(20),ds(20)
real ua(20),ep(20),covx(20),covy(20),CC(2,3),UA0
integer nx(40),ny(40)
integer kx(40),ky(40),kb,ke,km
adeal(a)=(exp(a)-1-a)/a/(exp(a)-1)
data xb/20*2000/
data w1,w2/0.49891,0.49,85.249,87.8/
data eps/10/
data ua0,cc/19.6,2*0.01011,2*0.0070,2*0.03733/
data tc,to,so,ai,po,dt,ds,ua,ep,covx,covy/220*0/

```

C normal, horizontal surface direct, ground reflection, and horizontal

C sky diffuse radiation

C Open data file

```

print*, '*****'
print*, 'This program was updated on August 12 1991'
print*, 'This program was updated on October 10 1991'
print*, 'This program was updated on November 14 1991'
print*, 'This program was updated on January 20 1991'
print*, 'The new UA calculatio formula'
print*, 'It is for the outdoor cell steady state method only.'
print*, 'The solar decomposition should consult the old program'
print*, '1: transfer date character string into number sub1'
print*, '2: solar time, azimuth, altitude          sub2'
print*, '5: radiation dicomposition              sub3'
print*, '7: eqvlent solar radiation              sub4'
print*, '8: UA, IHEE calculation based on three rules'
print*, '*****'

```

C The original input file is data file from data logger

```

print*, 'Input original data file name =>'
read (*,*)fil
COM=FIL
open(10,file=fil,status='old')
print*, 'Input time step in minutes '

```

```

read(*,*)ts
ko1=60/ts
ko2=ko1*24
fil=fil(1:4)//'1.PRN'
open(13,file=fil,status='unknown')
fil=fil(1:4)//'2.dat'
open(12,file=fil,status='unknown')
fil=fil(1:4)//'0.PRN'
open(14,file=fil,status='unknown')
print*, 'input bias of the air flow = '
read(*,*)bias
print*, 'Input fan code ex-1, in-2 '
read(*,*)kfan
909  format(a40)
      i=1
C Read contants from data file
      I=1
1    read(10,*,end=199)cha1,cha2,(xa(j),j=1,20)
      read(10,*,end=199)cha1,cha2,(xb(j),j=1,5)
      tcell(i)=xa(4)
      tim(i)=cha2(1:8)
      dat(i)=cha2(10:19)
      tattic(i)=xa(13)
      tout(i)=xa(5)
      power(i)=xa(2)
      phouse(i)=xa(7)
      thouse(i)=0
      do 632 lx=14,20
      thouse(i)=thouse(i)+xa(lx)
632  continue
      do 633 lx=1,4
      thouse(i)=thouse(i)+xb(lx)
633  continue
      thouse(i)=thouse(i)/11
      if(xa(3).lt.12)then
      air(i)=0
      else
      a1=xa(3)/w2(kfan)
      a2=a1**(1/w1(kfan))
      b1=bias/w2(kfan)
      b2=b1**(1/w1(kfan))
      a2=a2-b2
      xa(3)=w2(kfan)*a2**w1(kfan)
      air(i)=xa(3)*7.87*6*0.00001
      air(i)=air(i)*1.164*293/(xa(1)+273)
      endif
      sol(i)=xa(6)
      solp(i)=abs(xa(9)-xa(10))
      i=i+1
      if(i.gt.950) goto 199
      GOTO 1
199  L=L-1
C create raw data file tim dat tcell tout thouse tattic air power
C solar phouse

```

```

        write(14,929)
929  format(x,'dat   tim   tcell tout thouse tattic air power solar
      & phouse/')
      do 1333 i=1,l
        write(14,919)dat(i),tim(i),tcell(i),tout(i),thouse(i),tattic(i),
          &air(i)*3600,power(i),sol(i),phouse(i),solp(i)
1333  continue
C    PRINT*,'END OF READING DATA FILE'
C    PRINT*,'INPUT SOLAR TIME ALLOWANCE 10 '
C    READ(*,*)INSO
C    PRINT*,'INPUT SOLAR ALLOWANCE 0-10 '
C    READ(*,*)EPS
C    print*,'Input the fan code 1 or 2 =>'
C    read(*,*)kfan
      INSO=5
      EPS=5
C Chose solar model
c    print*,'Chose model 1.ASHRAE, 2.JAPAN, 3.HORIZONTAL==>'
c    read(*,*)km
c    km=2
C input solar resistance ratio
      sr=0.5
C Data file information
      CALL TTIM(5,MIN,TIM(1))
      CALL TTIM(2,MHO,TIM(1))
      k1=ko2-ko1*mho-min/ts
      k2=ko2
c    K1=144-6*MHO-MIN/10
c    K2=144
C defined legal period of the begin and end(23:00 to 7:00)
      KB=23
      KE=7
      write(12,1004)com,inso,eps,k1,k2
1004  format(2x,a40/2X,'time, solar, k1, k2',
      & i4,f5.1,2i4/x,'*****')
      write(12,1000)
1000  format(x,'Tcell|Tattic|Tout|Air(M^3/s)|Power|Solar|Phouse
      &DT Thouse UA IHEE'/x,'*****')
      &*****')
      write(13,2002)com,kfan,inso,eps,kb,ke
2002  format(2x,a40/2X,'fan code, time, solar, kb, ke',
      &2i4,f5.1,2i4/2x,'*****')
      write(13,3000)
3000  format(2x,' No.   Tcell Tout Solar Power   Air IHEEi T DT
      & power UA IHEE ')

      km=1
C EQUIVALENT SOLAR CALCULATION
911   M1=0
      DO 11 I=1,L
C tranfer date, time into hour,minutes, month, day, year
      call ttm(2,month,dat(i))
      call ttm(10,year,dat(i))
      call ttm(5,day,dat(i))

```

```

call sub1(hour,day,month,year,m)
IF(KM.EQ.3)THEN
CALL RISE(M,HOUR,MINUTES)
CALL TTIM(5,MIN,TIM(I))
CALL TTIM(2,MHU,TIM(I))
T1=HOUR+MINUTES/60.
T2=MHU+MIN/60.
IF(ABS(12-T2).LE.(12-T1))THEN
SOLP(I)=SOL(I)
ELSE
SOLP(I)=0
ENDIF
GOTO 11
ENDIF

```

```
lxm=0
```

C The time was dependent on computer clock

```

if(sol(i).gt.eps)then
lxm=1
call ttim(5,minutes,tim(i))
call ttim(2,hour,tim(i))
M1=M
ELSE
call ttim(5,minutes,tim(i))
call ttim(2,hour,tim(i))
M1=M
endif
if(km.eq.3) goto 11
if(lxm.eq.1)then
CALL sub2(m,hour,minutes,azimuth,altitude)
call sub3(km,month,altitude,sol(i),Idn,idh,ish,idg)
CALL sub4(2,sr,azimuth,altitude,idn,ish,idg,
& solP(i))
else
solP(i)=0
endif

```

11 CONTINUE

c Smoothing equivalent solar radiation

```

sol1=solP(1)
do 112 i=2,1-1
solP(i-1)=(solP(i-1)+solP(i)+solP(I+1))/3.

```

112 continue

```

do 113 i=1-1,2,-1
solP(i)=solP(i-1)

```

113 continue

```

solP(1)=sol1
k3=1
k4=(k3-k1)/k2
kd(1)=k1
do 232 i=1,k4
kd(i+1)=kd(i)+k2

```

232 continue

```

kd(k4+2)=k3
call average(tcell,kd,k4,k3,p,p2,ksize)

```

```

call average(tattic,kd,k4,k3,p,p2,ksize)
call average(tout,kd,k4,k3,p,p2,ksize)
call average(air,kd,k4,k3,p,p2,ksize)
call average(power,kd,k4,k3,p,p2,ksize)
call average(solP,kd,k4,k3,p,p2,ksize)
call average(phouse,kd,k4,k3,p,p2,ksize)
call average(thouse,kd,k4,k3,p,p2,ksize)

919  format(x,a8,x,a10,4f6.1,3f8.1,2f8.3)
do 333 i=1,KSIZE
k3=k3+1
ua1=(power(k3)+ua0*solp(k3)*cc(1,km))/(tcell(k3)-tout(k3))
if(air(k3).ne.0)then
hee=1-(ua1-ua0)/air(k3)/1013
else
hee=0
endif
call modc(kfan,air(k3),solp(k3),tcell(k3),tout(k3),eps0)
write(12,2001)tcell(k3),tattic(k3),tout(k3),
&air(k3)*3600/1.2,power(k3),solP(k3),phouse(k3),tcell(k3)-tout(k3),
&thouse(k3),ua1,hee,eps0
2001  format(x,3f6.2,x,f8.3,f7.1,f7.1,f6.1,f8.2,2f8.2,2f6.3)
333  continue
IF(KM.EQ.1)THEN
COM='  ASHRAE SOLAR MODEL '
ELSEIF(KM.EQ.2)THEN
COM='  SHACSEJ SOLAR MODEL '
ELSE
COM='  HORIZONTAL SOLAR RADIATION '
ENDIF
WRITE(12,8001)COM
8001  FORMAT(/X,A40/X,'*****'/)
write(12,8000)
8000  format(/)
if(km.eq.3) then
do 334 i=1,ksize
L=P(I)
L1=P2(I)
write(12,2000)L,L1,tim(L),dat(L),
& tim(L1),dat(L1)
334  continue
endif
2000  format(x,2i5,2x,'Begin at: ', a8,x,a10,2x,'End at: 'a8,x,a10)

k=kd(k4+2)
call combin(k,tcell,tout,air,power,thouse,solP
&,p1,p3,tc,to,so,ai,po,dt,
& ds,ua,ep,covx,covy,cc,ua0,
&kb,ke,km,kx,ky,nx,ny,KP,tim,1,ko1,ko2)

do 1230 i=1,kp/2
i1=i*2-1
lp1=p3(i1)
lp2=p3(i1+1)

```

```

if(abs(ai(i)).lt.0.0001)then
o0=0.5
else
o0=adeal(ai(i)*1013/ua0)
endif
o1=ai(i)*3600
call modc(kfan,ai(i),so(i),tc(i),to(i),eps0)
write(13,20001)lp1,lp2,tc(i),to(i),so(i),po(i),
& o1,o0,ua(i),ep(i),eps0
1230 continue
5000 format(/)
IF(KM.EQ.1)THEN
COM=' T HOUSE, ASHRAE SOLAR MODEL'
ELSEIF(KM.EQ.2)THEN
COM=' T HOUSE, SHACSEJ SOLAR MODEL'
ELSE
COM=' T HOUSE, HORIZONTAL SOLAR RADIATION'
ENDIF
WRITE(13,8001)COM
WRITE(13,5000)
WRITE(13,10091)
10091 format(x,' No1 No2 Time Date Time Date Nx Ny CovX
&CovY')
do 1220 i=1,kp/2
i1=i*2-1
lp1=p3(i1)
lp2=p3(i1+1)
write(13,10001)lp1,lp2,tim(lp1),dat(lp1),tim(lp2),dat(lp2),
&nx(i),ny(i),covx(i),covy(i)
1220 continue
10001 format(x,2i4,x,a8,x,a10,x,a8,x,a10,2i4,2f7.3)

20001 format(2x,2i4,3f8.2,f8.1,f8.2,f8.4,f7.2,f7.3,2f7.4)
print*,'combin 2'
call combin(k,tcell,tout,air,power,tcell,solP,
&p1,p3,tc,to,so,ai,po,dt,
& ds,ua,ep,covx,covy,cc,ua0,
&kb,ke,km,kx,ky,nx,ny,KP,tim,2,ko1,ko2)

do 1231 i=1,kp/2
i1=i*2-1
lp1=p3(i1)
lp2=p3(i1+1)
if(abs(ai(i)).lt.0.0001)then
o0=0.5
else
o0=adeal(ai(i)*1013/ua0)
endif
o1=ai(i)*3600
call modc(kfan,ai(i),so(i),tc(i),to(i),eps0)
write(13,20001)lp1,lp2,tc(i),to(i),so(i),po(i),
& o1,o0,ua(i),ep(i),eps0
1231 continue
IF(KM.EQ.1)THEN

```

```

COM=' T CELL, ASHRAE SOLAR MODEL'
ELSEIF(KM.EQ.2)THEN
COM=' T CELL, SHACSEJ SOLAR MODEL'
ELSE
COM=' T CELL, HORIZONTAL SOLAR RADIATION'
ENDIF
WRITE(13,8001)COM

write(13,5000)
write(13,10091)
1009  format(x,' No1  No2  Time  Date  Time Date      Nx Ny CovX
&CovY')
do 1221 i=1,kp/2
i1=i*2-1
lp1=p3(i1)
lp2=p3(i1+1)
write(13,10001)lp1,lp2,tim(lp1),dat(lp1),tim(lp2),dat(lp2),
&nx(i),ny(i),covx(i),covy(i)
1221  continue
km=km+1
if(km.le.3) goto 911
stop
end

subroutine modc(kfan,air,solar,troom,tout,eps)
C*****
C This subroutine calculates the IHEE according to the combined
C solar, air, and conduction model for the wall
C It is assumed that  $R_w$  equals  $R_w + R_{b0}$ 
C*****
data rb0,rw,bt/0.04,1.78,44.5/
data area,acp/35.67,1013/
air=air/area
if(kfan.eq.1)air=-air
alf=air*acp*rw
fi=solar/(troom-tout)
if(abs(alf).lt.0.0001)then
pc=-1
else
pc=alf*exp(alf)/(1-exp(alf))
endif
ct=(alf+pc-fi*rw)/(pc-bt)
uai=-(1-ct)*pc/rw
uad=(1/(rb0+rw)+abs(air)*acp)-fi*rb0/(rb0+rw)
if(kfan.eq.1) uai=uai+abs(air)*acp
if(abs(alf).lt.0.00001)then
eps=0.5
else
eps=(uad-uai)/air/acp
endif
air=abs(air*area)
return
end
subroutine ttim(k,m,cha)

```



```

C*****
C This subroutine transfer character into time and date
C*****
    character cha*10
    read(cha(k-1:k-1),*)k1
    read(cha(k:k),*)k2
    m=k1*10+k2
    if(k.eq.10)then
    m=19*100+m
    endif
    return
    end

    subroutine rise(m,hour,minutes)
C*****
C This sub calculate the sun rise time for day sequency number m
C*****
    integer m,hour,minutes
    data alat/30.0667/
    pi=3.1415926/180.
    dec=23.45*sin((280.1+0.9863*m)*pi)
    dec=dec*pi
    h=-tan(dec)*tan(alat*pi)
    h=acos(h)
C transfer to time
    h=h/pi/15.
    h=12-h
    hour=int(h/1)
    minutes=(h-int(h/1))*60
    return
    end

    subroutine average(x,kd,k4,k3,p,p2,ksize)
C*****
C This subroutine make k4+1 period average of X
C*****
    real x(1000)
    integer kd(20),p(40),P2(40)
    KSIZE=1
    do 10 k=1,k4
    DO 20 K1=K+1,K4+1
    x(k3+kSIZE)=0
    do 30 i=kd(k),KD(K1)-1
    x(k3+kSIZE)=x(k3+kSIZE)+x(i)
30    continue
    x(k3+kSIZE)=x(k3+kSIZE)/(kd(K1)-KD(K))
    P(KSIZE)=KD(K)
    P2(KSIZE)=KD(K1)-1
    KSIZE=KSIZE+1

20    CONTINUE
10    continue
    KSIZE=KSIZE-1
    return

```

end

subroutine sub1(hour,day,month,year,m)

```
C*****
C   This subroutine calculate sequence number of day in the year
C   Transfer summer time to normal time
C*****
  integer hour,day,month,year,m,d0(12),d1(12)
  data n1,n2/121,270/
  data d0,d1/30,58,89,119,149,180,210,240,270,300,331,365,
& 31,59,89,119,150,179,210,241,271,302,332,363/
C   Calculate M
  goto(10,20)year-1989
  print*,'Out of the range, Error may caused!'
10  m=d0(month-1)+day
  goto 30
20  m=d0(month-1)+day
30  continue
C   transfer summer time to real time
  if(m.ge.n1.and.m.le.n2)then
    hour=hour-1
  endif
  if(hour.eq.-1)then
    hour=23
    m=m-1
  endif
  return
end
```

subroutine sub2(m,hour,minutes,azimuth,altitude)

```
C*****
C   THIS SUBROUTINE CALCULATE AZIMUTH, ALTITUDE
C*****
  INTEGER M,HOUR,MINUTES
  double precision b,et,tsolar,h,at,al,az,azimuth,altitude
  DATA SLONG,ALONG/90,96.033/
  DATA aLAT/30.06667/
  pi=3.1415926/180.
c slong-LOCAL TIME BASED LATITUDE
c along-STATION LATITUDE
  dec=23.45*sin((280.1+0.9863*M)*PI)
  dec=dec*pi
  tstar=hour+minutes/60.+(slong-along)/15.-12
  b=360*(m-81)/364*pi
  et=9.87*sin(2*b)-7.53*cos(b)-1.5*sin(b)
  tsolar=tstar+et/60
  h=tsolar*15*pi
  at=alat*pi
  al=sin(at)*sin(dec)+cos(at)*cos(dec)*cos(h)
  altitude=asin(al)
  az=(sin(at)*sin(altitude)-sin(dec))/cos(at)/cos(altitude)
  IF(ABS(AZ).GT.1)THEN
    AZ=AZ/ABS(AZ)
```

```

    ENDIF
    azimuth=acos(az)
10    if(h.lt.0)then
        azimuth=2*3.14-azimuth
    endif
    return
    end
    subroutine sub3(km,month,altitude,ith,idn,idh,ish,idg)
C*****
C This subroutine breaking down total horizontal surface radiation
C Input
C   month
C   soalr altitude
C   Ith=total soalr radiation on horizontal surface
C Output
C   idn=normal radiation intensity
c   idh=direct solar radiation on horizontal surface
C   ish=horizontal surface sky diffuse radfiation
C   idg=ground reflection radiation
C*****
    real ith,idn,idh,ish,idg,i0
    double precision altitude
    real c(12),R(6)
    data i0/1353/
    data c/0.058,0.06,0.071,0.097,0.121,0.134,0.136,0.122,
& 0.092,0.073,0.063,0.057/
    DATA R/0.215,0.22,0.225,0.24,0.255,0.315/
    if(altitude.le.0)goto 199
    if(km.eq.2)then
c   if(altitude.le.0.0034) then
c   IDN=ITH/(SIN(ALTITUDE)+C(MONTH))
c   ISH=C(MONTH)*IDN
c   goto 1
c   endif
    IDN=ITH/SIN(ALTITUDE)-I0/2.
    ISH=I0/2*SIN(ALTITUDE)
    ENDIF
    IF(km.eq.1)THEN
    IDN=ITH/(SIN(ALTITUDE)+C(MONTH))
    ISH=C(MONTH)*IDN
    ENDIF

1   IDH=IDN*SIN(ALTITUDE)
    I=ALTITUDE*180/3.14/10-1
    IF(I.LT.1) THEN
        I=1
    ENDIF
    IF(I.GT.6) THEN
        I=6
    ENDIF
    IDG=ITH*R(I)
    RETURN
199  IDN=0
    IDH=0

```

```

ISH=0
IDG=0
RETURN
END

```

```

SUBROUTINE sub4(mk1,sr,azimuth,altitude,idn,ish,idg,Is)

```

```

C*****
C THIS SUBROUTINE CALCULATE EQAVELENT SOLAR RADIATION INTENSITY.
C   INPUT
C   AZIMUTH, ALTITUDE, ITH, IDN, IDH, ISH, IDG
C   OUTPUT
C   IS=EQAVELENT SOALR RADIATION INTENSITY
C   LOCAL VARIABLES
C   ORI=ORINATION OF THE WALLS(EIGHT PIECES SORTH-WEST-NORTH
C   -EAST, WALL AND CEILING)
C   ANG=TILTED ANGLES
C   RAT=HEAT RESISTANCE RATIO OF COMPONENT TO THE WALL
C   F=AREA OF THE COMPONENT M^2
C*****
REAL ORI(8),ANG(8),IDN,ISH,IDG,IS,SO(3,8)
REAL RAT(8),F(8),ref(8)
double precision azimuth,altitude
DATA ORI/0,90,180,270,0,90,180,270/
DATA ANG/90,90,90,90,45,90,45,90/
data ref/4*0.6,0.86,0.6,0.86,0.6/
DATA F/4*7.525,4.199,1.486,4.199,1.486/
do 1 i=1,4
  rat(i)=1
  rat(i+4)=sr
1  continue
  if(mk1.eq.1)then
    nn=4
  else
    nn=8
  endif
  IF(ALTITUDE.LT.0)GOTO 199
  PI=3.14/180.
C   DIRECT SOLAR RADIATION CALCULATION
  DO 10 I=1,nn
    AZI=AZIMUTH-ORI(I)*PI
    IF(ANG(I).gt.89)THEN
      IF(ABS(AZI).LE.90*PI.OR.ABS(AZI-6.28).LE.90*PI)THEN
        SO(1,I)=IDN*COS(ALTITUDE)*COS(AZI)*F(I)*RAT(I)*ref(i)
      ELSE
        SO(1,I)=0
      ENDIF
    ELSE
      a1=SIN(ALTITUDE)*COS(ANG(I)*PI)
      a2=COS(ALTITUDE)*COS(AZI)*SIN(ANG(I)*PI)
      if(ABS(AZI).LT.90*PI.or.abs(azi-6.28).le.90*pi.
      & or.altitude.gt.ang(i)*pi )THEN
        SO(1,i)=(a1+a2)*rat(i)*f(i)*ref(i)
      else
        so(1,i)=0

```

```

endif
ENDIF
10 CONTINUE
C SKY DIFFUSE RADIATION CALCULATION
DO 20 I=1,nn
SO(2,I)=COS(ANG(I)/2*PI)**2*ISH*F(I)*RAT(I)*ref(i)
20 CONTINUE
C CALCULATE REFLECTION RADIATION
DO 30 I=1,nn
SO(3,I)=(1-COS(ANG(I)*PI/2)**2)*IDG*F(I)*RAT(I)*ref(i)
30 CONTINUE
IS=0
DO 40 J=1,3
DO 50 I=1,nn
IS=IS+SO(J,I)
50 CONTINUE
40 CONTINUE
IS=IS/4./F(1)
if(is.lt.0)then
is=0
endif
RETURN
199 IS=0
RETURN
END
subroutine sub5(ndim,n1,n2,a,b,c,d)
C*****
C This subrouitne calculates the average values,maximum, minimum
C b-average
C c-maximum
C d-minimum
C*****
real a(ndim)
double precision x
b=0
c=-20000
d=20000
x=0
do 10 i=n1,n2
x=x+a(i)
if(c.lt.a(i))then
c=a(i)
endif
if(d.gt.a(i))then
d=a(i)
endif
10 continue
b=x/(n2-n1+1)
return
end
subroutine combin(k,tcell,tout,air,power,thouse,solar,
&p1,p3,tc,to,so,ai,po,dt,
& ds,ua,ep,covx,covy,c,ua0,
&kb,ke,km,kx,ky,nx,ny,KP,tim,FLAG,ko1,ko2)

```

```

C*****
C definition
C   M--Length of response factors of tout to heat flux
C   N--Length of response factors of tin to heat flux
C   M1--Length of response factors of solar to t cell
C   K--Number of the data set
C   K1--Number of non-solar periods
C   P--Index of the non-solar periods
C   P1--Index of the periods, which satisfy solar rule
C   P2--Index of the period, which satisfy house temperature rule
C   P3--Index of the periods which satisfy the moving average rule
C   eps--temperature allowance
C   eps1--air flow error allowance
C   eps2--power error allowance
C   eps3--solar error allowance
C*****
      real tcell(1000),tout(1000),air(1000),power(1000),thouse(1000)
      &,solar(1000)
      INTEGER P1(20),P3(40)
      real x(200),y(200)
      real tc(20),to(20),so(20),ai(20),po(20),dt(20),ds(20)
      real ua(20),ep(20),covx(20),covy(20),ua0,C(2,3)
      integer kx(40),ky(40),kb,ke,km,hour,FLAG,nx(40),ny(40)
      character tim(1000)*8
      data eps,eps1,eps2,eps3,eps4/0.2,0.0001,0.1,0.1,0.02/
      data m,n,m1/3*24/
C To find the number of no solar periods and its index
      if(ko1.lt.6)then
        eps=0.2
        eps4=0.1
        endif
        do 801 i=m+1,k
          call ttim(2,hour,tim(i))
          IF(HOUR.LT.KE) GOTO 805
          if(hour.eq.kb)goto 802
801  continue
802  continue
          p1(1)=i
          p1(2)=p1(1)+ko1*ke
          j=2
          GOTO 804
805  P1(1)=I
          P1(2)=I+(KE-HOUR-24+KB)*ko1
          P1(4)=P1(2)+ko2
          P1(3)=P1(4)-ko1*KE
          J=4
804  if((p1(j)+ko2).lt.k)then
          p1(j+1)=p1(j-1)+ko2
          p1(j+2)=p1(j)+ko2
          else
          goto 803
          endif
          j=j+2

```

```

      goto 804
803  continue

      k1=j
      kp=1
      kk=k1/2
C To find periods which satisfy house temperature rule
1    do 40 j=1,2*kk-1,2
      do 50 i=p1(1),p1(2)
      if(j.eq.1)then
      llx=i+5
      else
      llx=p1(j)
      endif
      do 60 i1=llx,p1(j+1)
      if(abs(thouse(i)-thouse(i1)).lt.eps)then
C to find periods which satisfy the constant average temperature rule
      mp=I1-I+1
      do 90 jL=1,m
      x(jL)=0
      y(jL)=0
      do 100 i2=I,I1
      x(jL)=x(jL)+tcell(i2-jL)/mp
      y(jL)=y(jL)+tout(i2-jL)/mp
100  continue
90   continue
      call wntest(x,m,kx(KP/2+1),nx(KP/2+1),covx(KP/2+1))
      call wntest(y,m,ky(KP/2+1),ny(KP/2+1),covy(KP/2+1))
      if(COVX(KP/2+1).LT.eps4.AND.COVY(KP/2+1).LT.eps4)then
      p3(KP)=I
      p3(KP+1)=I1
      KP=KP+2
      GOTO 40
      endif
      ENDIF
60   continue
50   continue
40   continue
C To shift second period to first period
      if(kk.ge.2)then
      kk=kk-1
      do 70 i=1,2*kk
      p1(i)=p1(i+2)
70   continue
      goto 1
      endif
C Thermal performance calculation
      do 110 i=1,kp/2
C calculate average parameters in the time period
      tc(i)=0
      to(i)=0
      so(i)=0
      po(i)=0
      ai(i)=0

```

```

    i1=i*2-1
    mp=p3(i1+1)-p3(i1)+1
    do 120 j=p3(i1),p3(i1+1)
    tc(i)=tc(i)+tcell(j)/mp
    to(i)=to(i)+tout(j)/mp
    so(i)=so(i)+solar(j)/mp
    po(i)=po(i)+power(j)/mp
    ai(i)=ai(i)+air(j)/mp
120  continue
C Temperature difference
    dt(i)=tc(i)-to(i)
C solar resistance calculation
    if(ai(i).lt.eps1.and.po(i).lt.eps2)then
    if(abs(so(i)).gt.0.01)then
    ds(i)=dt(i)/so(i)
    else
    ds(i)=0
    endif
    goto 110
    endif
C UA calculation
    ua(i)=(po(i)+so(i)*c(FLAG,km)*ua0)/dt(i)
C IHEE calculation
    if(ai(i).ne.0)then
    ep(i)=1-(ua(i)-ua0)/ai(i)/1013.
    else
    ep(i)=0
    endif
C write output to a data file
110  continue
    return
    end

    subroutine wntest(x,m,key,n,cov)
C*****
C This a subroutine for the white noise test
C The confidence is 95%
C*****
    real x(200),y(500)
C Removing the average value of the samples
    av=0
    do 10 i=1,m
    av=av+x(i)/m
10  continue
    do 20 i=1,m
    x(i)=x(i)-av
20  continue
C Find covariance of the samples
    cov=0
    do 30 i=1,m
    cov=cov+x(i)**2
30  continue
C Find autocovariance

```



```
do 40 j=1,m/2
  y(j)=0
  do 50 i=1,m-j
    y(j)=y(j)+x(i)*x(i+j)
50  continue
  y(j)=y(j)/cov
40  continue
C Make white noise test
  key=0
  n=0
  ajudg=1.96/sqrt(m)
  do 60 i=1,m/2
    if(abs(y(i)).gt.ajudg)then
      key=1
      n=n+1
    endif
60  continue
  cov=cov/m
  return
end
```

APPENDIX B2

SOURCE CODE FOR STEADY STATE MODEL SIMULATION

```
program wall
```

```
C*****
C This program simulate energy consumption of the wall
C under infiltration solar radiation and conduction
C*****
  character fil*10
  data rb0,rw/0.05,2/
C Input data file name
  print*, 'Input output data file name = > '
  read(*,*)fil
  open(12,file=fil,status='unknown')
C Input basic parameters
  h=1/(rb0+rw)
  bt=rw/rb0
  print*, 'Input air flow rate range and march step '
  read(*,*)a1,step
  print*,a1,step
  n=a1/step
  print*,n
  print*, 'Input solar intensity range and march step'
  read(*,*)so1,steps
  print*,so1,steps
  m=so1/steps
  print*,m
C calculation
  do 10 i=1,m+1
  so=(i-1)*steps
  do 20 j=1,n+1
  a=(j-1)*step
  if(abs(a).le.0.0000001)then
  pc=-1
  else
  pc=-a*exp(a)/(exp(a)-1)
  endif
C wall surface temperature
  ct=(-so*rw+pc+a)/(-bt+pc)
C total energy consumption
  q=- (1-ct)*pc/rw
  if(a.lt.0)then
  q=q+abs(a)/rw
  endif
C designed energy consumption
  qd=h + abs(a)/rw - so*rb0/(rb0+rw)
C total energy saving
  sl=(qd-q)
C Air Infiltration Heat Energy Exchange Effetiveness
  if(abs(qd).gt.0.01)then
  eps=(qd-q)/abs(qd)
```

```

else
eps=0
endif
if(eps.gt.1)eps=1
if(eps.lt.-1)eps=-1
if(abs(a).gt.0.00000001)then
s2=(qd-q)/abs(a)*rw
else
s2=0.5
endif
if(s2.gt.1)s2=1
if(s2.lt.-1)s2=-1
write(12,1100)so,a,a*3600/rw/1013,
& ct,q,qd,s1,s2,eps
1100 format(x,9f9.2)
20 continue
10 continue
stop
end

program attic
C*****
C This program investigate the energy performance of the attic
C without cross ventilation. Infiltration/exfiltration only
C*****
character fil*10
data rb0,r1,r2/0.05,0.15,3.5/
C Input data file name
print*,'Input output data file name = > '
read(*,*)fil
open(12,file=fil,status='unknown')
bt=r2/r1
h=1/(r1+r2)
print*,'Input air flow rate range and march step '
read(*,*)a1,step
print*,a1,step
n=a1/step
print*,n
print*,'Input solar intensity range and march step'
read(*,*)so1,steps
print*,so1,steps
m=so1/steps
print*,m
C calculation
do 10 i=1,m+1
so=(i-1)*steps
do 20 j=1,n+1
a=(j-1)*step
if(abs(a).le.0.0001)then
pc=-1
else
pc=-a*exp(a)/(exp(a)-1)
endif
C attic temperature

```

```

    if(a.gt.0)then
      ct=(pc-so*bt*rb0+a)/(pc-bt)
    else
      ct=(pc-bt*so*rb0+a)/(pc-bt+a)
    endif
  C Total energy consumption
  q=- (1-ct)*pc/r2
  if(a.lt.0)then
    q=q+abs(a)/r2
  endif
  C designed load
  qd=(1-so*rb0)*h+abs(a)/r2
  C Total energy saving
  s1=qd-q
  C IHEE
  if(abs(a).lt.0.0001)then
    s2=0.5
  else
    s2=(qd-q)/abs(a)*r2
  endif
  if(abs(qd).gt.0.01)then
    eps=(qd-q)/abs(qd)
  else
    eps=0
  endif
  if(eps.gt.1)then
    eps=1
  endif
  if(eps.lt.-1) eps=-1
  write(12,1100)so,a,a*3600/1013/3.5,ct,q,qd,s1,eps,s2
1100 format(x,9f10.3)
20 continue
10 continue
stop
end

program cross
C*****
C This program compare cross ventilation without infiltration
C*****
character fil*10
data rb0, r1,r2/0.05,0.15,3.5/
C Input data file name
print*, 'Input output data file name = > '
read(*,*)fil
open(12,file=fil,status='unknown')
C Input basic parameters
bt=r2/r1
h=1/(r1+r2)
print*, 'Input air flow rate range and march step '
read(*,*)a1,step
print*,a1,step
n=a1/step

```

```

    print*,n
    print*,'Input solar intensity range and march step'
    read(*,*)so1,steps
    print*,so1,steps
    m=so1/steps
    print*,m
C calculation
    do 10 i=1,m+1
        so=(i-1)*steps
        do 20 j=1,n+1
            a=(j-1)*step
C Cross ventilation model
            ct=(1+so*bt*rb0)/(1+bt+2*a)
C total energy consumption
            q=(1-ct)/r2
C design load
            qd=h-so*rb0*h
C Total energy saving
            s1=qd-q
C IHEE
            if(abs(qd).gt.0.01)then
                eps=(qd-q)/abs(qd)
            else
                eps=0
            endif
            write(12,1100)so,a,a*3600/1013/3.5,ct,q,qd,s1,eps
1100 format(x,8f9.2)
20 continue
10 continue
    stop
    end

    program combin
C*****
C This program simulate combined air infiltration and cross ventilation
C*****
    character fil*10
    data rb0,r1,r2,a1/0.05,0.15,3.5,5/
C Input data file name
    print*,'Input output data file name = > '
    read(*,*)fil
    open(12,file=fil,status='unknown')
    bt=r2/r1
    h=1/(r1+r2)
    print*,'Input air flow rate range and march step '
    read(*,*)a,step
    print*,a,step
    n=a/step
    print*,n
    print*,'Input solar intensity range and march step'
    read(*,*)so1,steps
    print*,so1,steps
    m=so1/steps

```

```
    print*,m
C calculation
  do 10 i=1,m+1
    so=(i-1)*steps
    do 20 j=1,n+1
      a=(j-1)*step
      if(abs(a).le.0.0001)then
        pc=-1
      else
        pc=-a*exp(a)/(exp(a)-1)
      endif
C attic temperature
      ct=(pc-so*bt*rb0+a)/(2*a+pc-bt-a1)
C total energy consumption
      q=-(1-ct)*pc/r2
      if(a.lt.0)then
        q=q+abs(a)/r2
      endif
C designed load
      qd=h+abs(a)/r2-so*h*rb0
C total energy saving
      s1=qd-q
C IHEE
      if(abs(a).gt.0.001)then
        s2=(qd-q)/abs(a)*r2
      else
        s2=0.5
      endif
      if(abs(qd).gt.0.01)then
        eps=(qd-q)/abs(qd)
      else
        eps=0
      endif
      if(eps.gt.1) eps=1
      if(eps.lt.-1)eps=-1
      write(12,1100)so,a,a*3600/1013/3.5,ct,q,qd,s1,eps,s2
1100  format(x,9f10.3)
20  continue
10  continue
    stop
  end
```

APPENDIX B3
SOURCE CODE OF "HOUSE.FOR"

program house

```

C*****
c This program compares idealized house energy consumption and normal
C operation energy consumption based simple assumption
C 1. The wall was seperated in two equal part, leak in
C and leak out, both of them had same air flow rate
C 2. The ceiling was infiltration in summer and exfiltration in
C winter because of the thermal stake influence
C 3. The air flow through attic or ceiling equeled
C to the air flow through the window and door
C*****
character fil*10
data rw/2/
data rb0,r1,r2/0.05,0.15,3.5/
data fw, fc/103.7,180/
ppc(a)=-a*exp(a)/(exp(a)-1)
ctw(so,rw,pc,a,bt)=(-so*rw+pc+a)/(-bt+pc)
ctai(so,rb0,pc,a,bt)=(pc-so*bt*rb0+a)/(pc-bt)
ctae(so,rb0,pc,a,bt)=(pc-bt*so*rb0+a)/(pc-bt+a)
btw=rw/rb0
bta=r2/r1
ha=1/(r1+r2)
hw=1/(rb0+rw)
C Input data file name
print*, 'Input output data file name = > '
read(*,*)fil
open(12,file=fil,status='unknown')
print*, 'Input air flow rate range and march step '
read(*,*)a1,step
print*,a1,step
n=a1/step
print*,n
print*, 'Input solar intensity range and march step'
read(*,*)so1,steps
print*,so1,steps
m=so1/steps
print*,m
C calculation
C solar ratio of the wall and roof 0.67
rr=0.67
do 10 i=1,m+1
so=(i-1)*steps
do 20 j=1,n+1
a=(j-1)*step
C attic air flow rate
if(abs(a).le.0.0001)then

```

```

pcwi=-1
pcwe=-1
pcw=-1
pcaa=-1
pcan=-1
else
C infiltration normal wall
pcwi=ppc(2*a)
C exfiltration normal wall
pcwe=ppc(-a*2)
C idealized house
pcw=ppc(a)
C ceiling normal house
pcan=ppc(-2*a)
C ceiling idealized house
pcaa=ppc(a)
endif
C wall surface/attic temperature
sow=so*rr
ctwi=ctw(sow,rw,pcwi,a*2,btw)
ctwe=ctw(sow,rw,pcwe,-2*a,btw)
ctww=ctw(sow,rw,pcw,a,btw)
if(a.gt.0)then
cta=ctae(so,rb0,pcan,-2*a,bta)
ctaa=ctai(so,rb0,pcaa,a,bta)
else
cta=ctai(so,rb0,pcan,-2*a,bta)
ctaa=ctae(so,rb0,pcaa,a,bta)
endif
C total energy consumption
C idealized house
qw=- (1-ctww)*pcw/rw
qc=- (1-ctaa)*pcaa/r2
if(a.lt.0)then
qw=qw+abs(a)/rw
qc=qc+abs(a)/r2
endif
qi=qw*fw+qc*fc+abs(a)/r2*fc
C normal house
qw1=- (1-ctwi)*pcwi/rw
qw2=- (1-ctwe)*pcwe/rw
qw=(qw1+qw2)/2.
qc=- (1-cta)*pcan/r2
if(a.gt.0)then
qc=qc+abs(a*2)/r2
endif
qn=qw*fw+qc*fc
C designed energy consumption
qw=hw+abs(a)/rw-so*rr*rb0*hw
qc=ha+abs(a*2)/r2-so*rb0*ha
qd=qw*fw+qc*fc
c energy saving of idealized house
s1=(qn-qi)/abs(qn)
if(s1.gt.1)s1=1

```



```
      if(s1.lt.-1)s1=-1
C energy saving compared with design
      s2=(qd-qi)/abs(qd)
      if(s2.gt.1)s2=1
      if(s2.lt.-1)s2=-1
C energy saving compared between normal and design
      s3=(qd-qn)/abs(qd)
      if(s3.gt.1)s3=1
      if(s3.lt.-1)s3=-1
      write(12,1100)so,abs(a),qi,qn,qd,s1,s2,s3
1100  format(x,8f9.3)
20   continue
10   continue
      stop
      end
```

APPENDIX B4

SOURCE CODE OF "DYNA.FOR"

```

program dyna
C*****
C This program investigate the dynamic behave of the wall and attic
C under dynamic condition with solar, air infiltration, and temerature
C as variates.
C*****
  real dat(25,5),twp,dt,troom,dtr,ts,rto,rti,rs
  real cont,ra,ho,hi,acp,up,ref,atair
  real*8 lamd(10),leng(10),lu(10),cp(10)
  real pair(5),psolar(5),ptout(5),pq(5),psq(5),ptroom(5)
  real pqd(5),paair(5)
  integer nn,flag,nw,m(10),flag3
  character cha*80
  common pair,psolar,ptout,ptroom,pq,psq,pqd,paair
1  print*,'This program investigate the dyanmic behave'
  print*,'of the house components'
  print*,'The output of the calculation will be sent to'
  print*,'1)res.prn for thermal performance '
  print*,'2)sim.prn for sample of weather data'
  print*,' Before you run the program, make sure that'
  print*,' You have created following data files;'
  print*,' 1)solar.dat 2)inp.dat'
  pause
C Read solar data file
  open(10,file='solar.dat',status='old')
  I=1
19  READ(10,*,END=199,ERR=199)tim,(dat(I,J),J=1,5)
  I=I+1
  GOTO 19
199  CONTINUE
  close(10)
C Read inp.dat file
  open(20,file='inp.dat',status='old')
  read(20,*)cha
  read(20,*)nn
  read(20,*)cha
  read(20,*)flag
  read(20,*)cha
  read(20,*)twp
  read(20,*)cha
  read(20,*)dt
  read(20,*)cha
  read(20,*)troom
  read(20,*)cha
  read(20,*)dtr
  read(20,*)cha
  read(20,*)ts
  read(20,*)cha

```

```

read(20,*)nd
read(20,*)cha
read(20,*)rto
read(20,*)cha
read(20,*)rti
read(20,*)cha
read(20,*)rs
read(20,*)cha
read(20,*)cont
read(20,*)cha
read(20,*)dta
read(20,*)cha
read(20,*)ra
read(20,*)cha
read(20,*)ho,hi
read(20,*)cha
read(20,*)acp
read(20,*)cha
read(20,*)up
read(20,*)cha
read(20,*)ref
read(20,*)cha
read(20,*)atair
read(20,*)cha
read(20,*)nw
read(20,*)cha
do 12 i=1,nw
read(20,*)lamd(i),leng(i),lu(i),cp(i),m(i)
12  continue
open(40,file='res.prn',status='unknown')
write(40,1000)
1000  format(10x,'Troom, Tout, Solar, Air, Abs(air), Qsp, Pq')
do 20 i=1,nn
if(i.eq.nn)then
flag3=1
else
flag3=0
endif
call gen(i,twp,dt,troom,dtr,ts,dat,nd,rto,rti,rs,cont,ra,dta)
call ener(flag,flag3,ho,hi,acp,up,atair,
& ref,nw,lamd,leng,lu,cp,m)
do 30 lx=1,5
write(40,2000)ptroom(lx),ptout(lx),psolar(lx),
& pair(lx),paair(lx),psq(lx),pq(lx),pqd(lx)
2000  format(x,8f9.2)
30  continue
20  continue
stop
end

```

```

subroutine gen(l1,twp,dt,troom,dtr,ts,dat,
& nd,rto,rti,rs,cont,ra,dta)

```

```

C*****

```

C This program generat input data file for wall and roof

C It suppose a random variat on the kernal function to

C creat weather parameters

C*****

```

character fil*20
REAL DAT(25,5)
integer seed
data pi/3.1415926/
DATA XS1,XT1,XTR1,XA1/4*0./
seed=ll
fil='sam1.prn'
open(31,file=fil,status='unknown')
fil='sam2.prn'
open(32,file=fil,status='unknown')
fil='sam3.prn'
open(33,file=fil,status='unknown')
fil='sam4.prn'
open(34,file=fil,status='unknown')
fil='sam5.prn'
open(35,file=fil,status='unknown')
write(31,*)ts*60
write(32,*)ts*60
write(33,*)ts*60
write(34,*)ts*60
write(35,*)ts*60

```

C*****

C Initialize period was taken as 24 hours

C*****

```

k1=1440/ts
k2=1440*nd/ts
k=1
1 do 101 i=1,2*k1+k2
tim=i*ts/60.
if(tim.gt.24)then
tim=tim-24*int(tim/24)
endif
nx=int(tim)
if(nx.eq.0)then
solar=0.
else
solar=dat(nx,k)+(dat(nx+1,k)-dat(nx,k))*(tim-nx)
endif
tout=twp+0.5*cos(pi*tim/12-3.665)*dt
air=cont*abs(troom-tout)/(abs(troom-twp)+dt/2)
tr=troom
if(i.le.k1.or.i.gt.(k1+k2))then
tr=troom
tout=twp
solar=0
air=0
goto 100
endif
call WALK(SEED,XS1,XS2)
solar=solar*(1+XS2*rs)

```

```

XS2=XS1
call WALK(SEED,XT1,XT2)
tout=tout*(1+xt2*rto)
XT2=XT1
call WALK(SEED,XTR1,XTR2)
tr=troom+XTR2*rti*dtr
XTR2=XTR1
call WALK(SEED,XA1,XA2)
air=air*(dta+XA2*ra)
XA2=XA1
100  continue
      goto(31,32,33,34,35)k
31   write(31,200)i,air,solar,tout,tr
      goto 101
32   write(32,200)i,air,solar,tout,tr
      goto 101
33   write(33,200)i,air,solar,tout,tr
      goto 101
34   write(34,200)i,air,solar,tout,tr
      goto 101
35   write(35,200)i,air,solar,tout,tr
101  continue
200  format(10x,i6,4f15.5)
      if(k.lt.5)then
          k=k+1
          goto 1
      endif
      close(31)
      close(32)
      close(33)
      close(34)
      close(35)
      return
      end

SUBROUTINE WALK(SEED,X,Y)
INTEGER SEED
REAL RANDX
CALL RANDOM(SEED,RANDX)
randx=randx-0.5
Y=X+RANDX
IF(ABS(Y).GT.1)THEN
Y=0
ENDIF
RETURN
END

subroutine random(seed,randx)
integer seed
real randx
seed=2045*seed+1
seed=seed-(seed/1048576)*1048576
randx=real(seed+1)/1048577.0
return

```

end

```

subroutine ener(flag,flag3,ho,hi,acp,up,atair,
& ref,n,lamd,leng,lu,cp,m)

```

```

C*****
C This program simulate dynamic behave of the wall under
C action of the solar, conduction, and air infiltration.
C The ideal difuse wall was assumed.
C Input:
C   lamd(n) Heat conductivity of the materios
C   leng(n) length of the layer
C   lu(n)  density of the material
C   cp(n)  heat ca[acity of the material
C   n      number of solid material layers
C   m(n)   node number of each solid layer
C   ho     convective heat transfer coefficient of outsurface
C   hi     convective heat transfer coefficient of inner surface
C   nd     number of days simulated
C   ts     time step used for simulation
C   tp     time period used for output
C   air    air flow rate kj/k
C   solar  solar radiation W/m^2
C*****
real*8 lamd(10),leng(10),lu(10),cp(10)
real*8 cdx(50),sdx(50),x(50),a(50,50),b(50)
real*8 ccp(50),clu(50),clamd(50)
real*8 slamd(50)
real pair(5),psolar(5),ptout(5),ptroom(5),pq(5),psq(5)
real pqd(5),paair(5)
character fil*20,fil1*20
integer m(10),flag,flag3
common pair,psolar,ptout,ptroom,pq,psq,pqd,paair
data x/50*0./
C*****
C Generate cdx, u, k
C*****
      l=0
      do 20 i=1,n
        dd=leng(i)/m(i)
        do 30 j=1,m(i)
          l=l+1
          cdx(l)=dd
          clamd(l)=lamd(i)
          ccp(l)=cp(i)
          clu(l)=lu(i)
30      continue
20      continue
      print*,'L=', l
C*****
C Generate sdx,k
C*****
      do 40 i=1,l
        if(i.eq.1)then

```

```

    sdx(i)=cdx(i)/2.
    SLAMD(I)=CLAMD(I)
    else
    sdx(i)=(cdx(i-1)+cdx(i))/2.
    fe=cdx(i-1)/sdx(i)/2.
    slamd(i)=1/((1-fe)/clamd(i)+fe/clamd(i-1))
    endif
40  continue
    sdx(l+1)=cdx(l)/2.
    slamd(l+1)=lamd(n)
C*****
C Begin simulation
C*****
C*****
C Caculate heat loss factor
C*****
    r=1/ho+1/hi
    if(flag.eq.2) r=r+1/up
    r01=1/hi
    do 23 i=1,n
    r01=r01+leng(i)/lamd(i)
    r=r+leng(i)/lamd(i)
23  continue
    tair=atair/r01
C*****
C read air flow rate, solar, and temperature
C*****
    do 918 ll=1,5
    pair(ll)=0
    psolar(ll)=0
    pq(ll)=0
    proom(ll)=0
    ptout(ll)=0
    pair(ll)=0
918  continue
    do 919 ll=1,5
    if(ll.eq.1)then
    fil1='res1.prn'
    fil='sam1.prn'
    endif
    if(ll.eq.2)then
    fil='sam2.prn'
    fil1='res2.prn'
    endif
    if(ll.eq.3)then
    fil='sam3.prn'
    fil1='res3.prn'
    endif
    if(ll.eq.4)then
    fil='sam4.prn'
    fil1='res4.prn'
    endif
    if(ll.eq.5)then
    fil='sam5.prn'

```

```

fil1='res5.prm'
endif
open(20,file=fil,status='old')
open(30,file=fil1,status='unknown')
lx=1
read(20,*)ts
k01=1440/ts
i01=0
1  read(20,*,end=199,err=199)no,air,solar,tout,troom
   air=air/r01/acp
   i01=i01+1
C*****
C Create matrices a, b
C*****
2  do 61 i=1,l+3
   b(i)=0
   do 71 j=1,l+3
   a(i,j)=0
71  continue
61  continue
   do 60 i=1,l+2
   if(flag.eq.2)then
   ki=i+1
   else
   ki=i
   endif
   if(i.eq.1)then
   b(ki)=ref*solar+ho*tout
   & +lu(1)*cp(1)*sdx(1)/2./TS*x(ki)
   elseif(i.eq.l+2)then
   b(ki)=hi*troom+lu(n)*cp(n)*sdx(l+1)/2./TS*x(ki)
   else
   b(ki)=CLU(I-1)*CCP(I-1)*cdx(i-1)/ts*x(ki)
   endif
   if(i.eq.1)then
   a(ki,1)=lu(1)*cp(1)*sdx(1)/2./TS+slamd(1)/sdx(1)+ho-ACP*AIR/2.
   a(ki,2)=air*acp/2.-lamd(1)/sdx(1)
   goto 60
   endif
   if(i.eq.l+2)then
   a(ki,ki-1)=-slamd(l+1)/sdx(l+1)-air*acp/2.
   a(ki,ki)=lu(n)*cp(n)*sdx(l+1)/2./TS+hi+
   & slamd(l+1)/sdx(l+1)+AIR*ACP/2.
   goto 60
   endif
   a(ki,ki-1)=-SLAMD(I-1)/sdx(i-1)-ACP/2.*air
   a(ki,ki)=CLU(I-1)*CCP(I-1)*cdx(i-1)/ts
   & +SLAMD(i)/sdx(i)+SLAMD(i-1)/sdx(i-1)
   a(ki,ki+1)=-SLAMD(i)/sdx(i)+ACP/2.*air
60  continue
   if(flag.eq.2)then
   z1=up/(ho+up)
   a(1,1)=z1*ho+2*tair*acp+hi
   a(1,2)=-hi+air*acp

```



```

    b(1)=solar*z1*ref+(z1*ho+2*tair*acp)*tout
    a(2,1)=-hi
    a(2,2)=clu(1)*ccp(1)*sdx(1)/2/ts
    & +hi+slamd(1)/sdx(1)-air*acp/2.
    a(2,3)=air*acp/2.-slamd(1)/sdx(1)
    b(2)=clu(1)*ccp(1)*sdx(1)*x(2)/2./ts
    endif
C*****
C Call GAUSS subroutine
C*****
    if(flag.eq.2)then
    k2=l+3
    k=2
    else
    k=1
    k2=l+2
    endif
    if(lx.eq.1)then
    xp1=0
    do 911 i=1,l
    xp1=xp1+x(i+k)*cdx(i)*CLU(I)*CCP(I)
911  continue
    XCP1=0
    DO 922 I=1,N
    XCP1=XCP1+LENG(I)*LU(I)*CP(I)
922  CONTINUE
    XP1=XP1/XCP1
    endif
    call gauss(k2,a,b,x)
    xp=0
    do 913 i=1,l
    xp=xp+x(i+k)*cdx(i)*CLU(I)*CCP(I)
913  continue
    XCP=0
    DO 923 I=1,N
    XCP=XCP+LENG(I)*LU(I)*CP(I)
923  CONTINUE
    XP=XP/XCP
    if(abs((xp-xp1)/xp).gt.0.00005.and.lx.eq.1)then
    goto 2
    else
    lx=2
    endif
C*****
C Inner surface heat flux
C*****
    q=(troom-x(k2))*hi
    q1=(troom-x(k2))*air*acp
    if(air.lt.0)q1=q1+abs(air)*(troom-tout)*acp
    q2=q1+q
    if(flag3.eq.1)write(30,100)X(k2),XP,q,q1,q2
100  format(3x,5f10.3)
    if(i01.gt.k01)then
    i02=i01-k01

```

```

pair(l1)=pair(l1)*(i02-1)/i02+air/i02
psolar(l1)=psolar(l1)*(i02-1)/i02+solar*ref/i02
ptout(l1)=ptout(l1)*(i02-1)/i02+tout/i02
ptroom(l1)=ptroom(l1)*(i02-1)/i02+troom/i02
pq(l1)=pq(l1)*(i02-1)/i02+q2/i02
paair(l1)=paair(l1)*(i02-1)/i02+abs(air)/i02
endif
goto 1
199  continue
      close(20)
      close(30)
      if(flag.eq.1)then
        bt=(r-1/ho)*ho
        a0=pair(l1)*acp*(r-1/ho)
        if(abs(a0).lt.0.0001)then
          pc=-1
          else
            pc=a0*exp(a0)/(1-exp(a0))
          endif
        ct=(a0+pc-psolar(l1))/(ptroom(l1)-ptout(l1))*(r-1/ho)/(pc-bt)
        psq(l1)=-(1-ct)*pc/(r-1/ho)*(troom-tout)
        if(pair(l1).lt.0)then
          psq(l1)=psq(l1)+abs(pair(l1))*acp*(ptroom(l1)-ptout(l1))
        endif
        else
          r1=1/ho+1/up
          r2=r-1/ho
          bt=r2/r1
          a20=pair(l1)*acp*r2
          a0=tair*acp*r2
          if(abs(a0).lt.0.001)then
            pc=-1
            else
              pc=a20*exp(a20)/(1-exp(a20))
            endif
          fi=psolar(l1)/(ptroom(l1)-ptout(l1))
          if(tair.lt.0.001)then
            ct=(pc-fi*bt/ho+a20)/(pc-bt)
          else
            ct=(pc+a20-fi*bt/ho)/(pc+2*a20-bt-a0)
          endif
          psq(l1)=-(ptroom(l1)-ptout(l1))*(1-ct)*pc/r2
          if(pair(l1).lt.0)then
            psq(l1)=psq(l1)+abs(pair(l1))*acp*(ptroom(l1)-ptout(l1))
          endif
          endif
          pair(l1)=pair(l1)*r01*acp
          paair(l1)=paair(l1)*r01*acp
          pqd(l1)=(1/r+ABS(pair(l1))/r01)*(ptroom(l1)-ptout(l1))
          pqd(l1)=pqd(l1)-psolar(l1)/r/ho
919  continue
      return
      end

```

```
subroutine gauss(n,a,b,x)
real*8 a(50,50),b(50),x(50)
n1=n-1
do 10 i=1,n1
  ip1=i+1
  do 20 j=ip1,n
    if(a(j,i).eq.0)goto 15
    ratio=a(j,i)/a(i,i)
    do 30 k=i,n
      a(j,k)=a(j,k)-ratio*a(i,k)
      if(abs(a(j,k)).le.1e-12) a(j,k)=0
30    continue
    b(j)=b(j)-ratio*b(i)
15  continue
20  continue
10  continue
  x(n)=b(n)/a(n,n)
  do 100 i=1,n1
    k=n-i
    k1=k+1
    va=b(k)
    do 110 j=k1,n
110   va=va-a(k,j)*x(j)
    x(k)=va/a(k,k)
100  continue
  return
end
```

Input Data File "INP.DAT"

Number of simulations nn
4
Flag of wall or attic flag
1
Average outside temperature twp
4
Daily Temperature difference maximum-minimum dt
10
Average room temperature troom
20
Maximum room temperature variation dtr
2
Simulation Step in Minutes ts
5
Number of Days for each simulation nd
5
Outdoor temperature random scale rto
0.5
Indoor temperature random scale rti
0.5
Solar random scale rs
0.5
Air infiltration constant cont
1
Air flow model 0 balance 1 one way
0
Air infiltration random scale ra
1
Convection Coefficient of outside surface and inner surface ho, hi
25 8
Specific heat capacity of air acp
1013
Heat transfer coefficient from outsurface to attic air up
5.6
Absorption ratio of the wall or roof ref
0.6
Cross ventilation rate Kg/m² h atair
5
Number of Solid Wall Layer nw
3
Conductivity, Thickness, Density, Specific Heat, Number of node
1.10 0.12 1900 1050 10
0.064 0.05 150 1218 10
0.33 0.02 1050 1050 2

Input Data File "SOLAR.DAT"

1	0.00	0.00	0.00	0.00	0.00
2	0.00	0.00	0.00	0.00	0.00
3	0.00	0.00	0.00	0.00	0.00
4	0.00	0.00	0.00	0.00	0.00
5	0.00	0.00	0.00	0.00	0.00
6	0.00	0.00	0.00	0.00	0.00
7	0.00	0.00	3.15	0.00	0.00
8	100.91	28.38	504.57	324.82	28.38
9	277.51	47.30	551.88	532.95	47.30
10	428.89	63.07	425.73	668.56	63.07
11	523.49	72.53	214.44	750.55	72.53
12	555.03	75.69	78.84	775.78	78.84
13	523.49	72.53	72.53	750.55	214.44
14	428.89	63.07	63.07	668.56	425.73
15	277.51	47.30	47.30	532.95	551.88
16	100.91	28.38	28.38	324.82	504.57
17	0.00	0.00	0.00	0.00	3.15
18	0.00	0.00	0.00	0.00	0.00
19	0.00	0.00	0.00	0.00	0.00
20	0.00	0.00	0.00	0.00	0.00
21	0.00	0.00	0.00	0.00	0.00
22	0.00	0.00	0.00	0.00	0.00
23	0.00	0.00	0.00	0.00	0.00
24	0.00	0.00	0.00	0.00	0.00

DYNAMIC NUMERICAL SIMULATION RESULTS

T_{room}	T_{out}	Solar	α	$ \alpha $	q_s	q_d	q_{des}
$^{\circ}\text{C}$	$^{\circ}\text{C}$	W/m^2			W/m^2	W/m^2	W/m^2
20.00	4.00	58.26	0.00	0.00	12.25	12.25	12.25
20.00	4.00	8.86	0.00	0.00	14.02	14.02	14.02
20.00	3.99	35.71	0.00	0.00	13.06	13.06	13.06
19.99	3.98	95.13	0.00	0.00	10.93	10.93	10.93
19.99	3.99	36.10	0.00	0.00	13.04	13.04	13.04
20.00	4.01	57.33	0.00	0.00	12.28	12.27	12.27
20.00	3.99	8.92	0.00	0.00	14.02	14.03	14.03
20.00	3.97	35.19	0.00	0.00	13.08	13.10	13.10
20.00	4.01	95.58	0.00	0.00	10.91	10.91	10.91
19.99	3.99	35.53	0.00	0.00	13.06	13.07	13.07
20.00	3.99	57.71	0.00	0.00	12.27	12.28	12.28
20.01	4.00	8.92	0.00	0.00	14.02	14.02	14.02
20.00	4.00	35.11	0.00	0.00	13.08	13.08	13.08
20.00	4.02	96.11	0.00	0.00	10.89	10.88	10.88
19.99	4.00	35.46	0.00	0.00	13.07	13.06	13.06
19.99	3.99	57.60	0.00	0.00	12.27	12.27	12.27
20.01	4.00	8.97	0.00	0.00	14.02	14.02	14.02
20.00	4.01	35.72	0.00	0.00	13.06	13.05	13.05
19.99	4.01	94.56	0.00	0.00	10.94	10.93	10.93
20.01	4.01	35.57	0.00	0.00	13.06	13.06	13.06
20.00	4.00	58.26	0.55	0.55	16.12	16.18	20.40
20.00	4.00	8.86	0.55	0.55	18.37	18.59	22.13
20.00	3.99	35.71	0.55	0.55	17.15	17.31	21.21
19.99	3.98	95.13	0.55	0.55	14.41	14.36	19.05
19.99	3.99	36.10	0.54	0.54	17.10	17.20	21.13
20.00	4.01	57.33	0.54	0.54	16.13	16.18	20.37
20.00	3.99	8.92	0.54	0.54	18.35	18.59	22.13
20.00	3.97	35.19	0.54	0.54	17.16	17.34	21.22
20.00	4.01	95.58	0.55	0.55	14.38	14.33	19.03
19.99	3.99	35.53	0.55	0.55	17.15	17.27	21.20
20.00	3.99	57.71	0.55	0.55	16.13	16.21	20.39
20.01	4.00	8.92	0.55	0.55	18.37	18.61	22.15
20.00	4.00	35.11	0.55	0.55	17.16	17.31	21.19
20.00	4.02	96.11	0.55	0.55	14.37	14.30	19.02
19.99	4.00	35.46	0.55	0.55	17.17	17.27	21.22
19.99	3.99	57.60	0.54	0.54	16.12	16.19	20.38
20.01	4.00	8.97	0.55	0.55	18.38	18.61	22.15
20.00	4.01	35.72	0.55	0.55	17.14	17.28	21.17
19.99	4.01	94.56	0.54	0.54	14.39	14.31	18.97
20.01	4.01	35.57	0.55	0.55	17.15	17.27	21.20
20.00	4.00	58.26	-0.55	0.55	17.21	17.81	20.40
20.00	4.00	8.86	-0.55	0.55	18.53	19.02	22.13
20.00	3.99	35.71	-0.55	0.55	17.82	18.36	21.21
19.99	3.98	95.13	-0.55	0.55	16.19	16.86	19.05
19.99	3.99	36.10	-0.54	0.54	17.77	18.35	21.13
20.00	4.01	57.33	-0.54	0.54	17.19	17.78	20.37

T_{room}	T_{out}	Solar	α	$ \alpha $	q_s	q_d	q_{des}
20.00	3.99	8.92	-0.54	0.54	18.52	19.02	22.13
20.00	3.97	35.19	-0.54	0.54	17.82	18.38	21.22
20.00	4.01	95.58	-0.55	0.55	16.17	16.86	19.03
19.99	3.99	35.53	-0.55	0.55	17.81	18.39	21.20
20.00	3.99	57.71	-0.55	0.55	17.21	17.81	20.39
20.01	4.00	8.92	-0.55	0.55	18.54	19.03	22.15
20.00	4.00	35.11	-0.55	0.55	17.81	18.33	21.19
20.00	4.02	96.11	-0.55	0.55	16.17	16.84	19.02
19.99	4.00	35.46	-0.55	0.55	17.83	18.40	21.22
19.99	3.99	57.60	-0.54	0.54	17.20	17.79	20.38
20.01	4.00	8.97	-0.55	0.55	18.54	19.04	22.15
20.00	4.01	35.72	-0.55	0.55	17.80	18.33	21.17
19.99	4.01	94.56	-0.54	0.54	16.14	16.79	18.97
20.01	4.01	35.57	-0.55	0.55	17.82	18.39	21.20
20.00	4.00	58.26	0.01	0.14	12.29	13.30	12.34
20.00	4.00	8.86	0.00	0.13	14.03	15.06	14.03
20.00	3.99	35.71	0.00	0.14	13.09	14.14	13.13
19.99	3.98	95.13	0.00	0.14	10.94	12.00	10.95
19.99	3.99	36.10	0.00	0.14	13.07	14.11	13.09
20.00	4.01	57.33	0.00	0.14	12.29	13.34	12.30
20.00	3.99	8.92	0.00	0.13	14.04	15.10	14.08
20.00	3.97	35.19	0.00	0.13	13.09	14.15	13.13
20.00	4.01	95.58	0.00	0.13	10.92	11.96	10.93
19.99	3.99	35.53	0.00	0.14	13.08	14.15	13.10
20.00	3.99	57.71	0.00	0.14	12.27	13.35	12.29
20.01	4.00	8.92	0.00	0.14	14.03	15.12	14.05
20.00	4.00	35.11	0.00	0.14	13.08	14.16	13.08
20.00	4.02	96.11	0.01	0.14	10.93	11.97	10.97
19.99	4.00	35.46	0.01	0.14	13.12	14.13	13.17
19.99	3.99	57.60	0.00	0.14	12.28	13.35	12.28
20.01	4.00	8.97	0.00	0.14	14.04	15.09	14.07
20.00	4.01	35.72	0.00	0.13	13.07	14.09	13.09
19.99	4.01	94.56	-0.01	0.13	11.02	11.99	11.05
20.01	4.01	35.57	0.00	0.13	13.09	14.11	13.11

APPENDIX B5

MEASURED RESULTS FOR OUTDOOR TEST CELL

Each test took from a minimum of 2 days to a maximum of 7 days. Each IHEE and energy saving value was calculated from a minimum 20-hour period to maximum 7-day measurement period. The parameter values shown in the table are the average values for each measurement period. Average solar radiation values incident on test cell were calculated from measured horizontal solar radiation using ASHRAE model (described in Appendix A3).

	T _{cell} °C	T _{out} °C	Solar W/m ²	Power W	Air CFM	IHEE	Saving ratio
(Measurement period: July 11 1991 to August 16 1991)							
Normal Leakage	36.8	29.4	85.9	251.0	84.2	0.43	0.26
Infiltration	36.6	29.4	89.5	251.2	84.0	0.39	0.23
	36.4	29.4	92.6	251.6	83.8	0.35	0.21
	36.8	29.4	86.5	250.9	84.2	0.43	0.26
	36.6	29.4	89.5	251.2	84.0	0.39	0.23
	36.4	29.4	92.6	251.6	83.8	0.35	0.21
	37.8	30.3	66.1	249.4	66.7	0.33	0.18
	37.8	30.4	67.4	249.4	66.6	0.32	0.17
	39.7	29.7	82.3	248.8	30.9	0.37	0.13
	40.4	30.1	82.4	248.8	31.0	0.43	0.16
	41.0	30.5	82.9	248.9	31.1	0.49	0.18
	39.6	30.0	83.8	249.8	45.1	0.48	0.22
	39.3	29.6	68.8	249.9	44.9	0.51	0.23
	39.0	29.3	54.4	249.9	44.8	0.53	0.24
	39.6	30.0	83.8	249.8	45.1	0.48	0.22
	39.3	29.7	69.5	249.8	44.9	0.50	0.22
	39.0	29.4	56.2	249.9	44.8	0.51	0.23
	34.6	25.3	60.0	251.6	51.1	0.51	0.25
	34.6	25.3	60.0	251.6	51.1	0.51	0.25
	40.2	29.5	56.9	250.7	28.7	0.52	0.18
	40.2	28.9	53.4	250.8	24.2	0.57	0.17

(Measurement period: June 17 1991 to July 11 1991)							
Normal Leakage	39.0	29.0	80.3	251.8	34.3	0.38	0.14
Exfiltration Flow	39.1	28.9	82.4	251.2	34.5	0.43	0.16
	39.2	28.9	85.7	250.8	34.6	0.46	0.18
	39.0	28.9	78.8	251.8	34.3	0.40	0.15
	39.1	28.9	81.9	251.2	34.5	0.44	0.17
	39.2	28.9	85.7	250.8	34.6	0.46	0.18
	38.6	29.7	77.3	252.2	48.6	0.37	0.17
	39.2	30.5	77.1	252.1	48.6	0.33	0.15
	38.6	29.6	76.0	252.3	48.6	0.38	0.18
	39.2	30.5	76.6	252.2	48.6	0.34	0.16
	37.1	28.8	64.7	245.3	47.2	0.27	0.13
	37.5	29.2	73.8	245.1	47.3	0.26	0.12
	37.1	28.8	64.3	245.3	47.2	0.28	0.13
	37.5	29.2	73.1	245.2	47.3	0.27	0.12
	37.3	29.2	84.0	245.9	61.4	0.37	0.20
	36.1	28.5	94.1	245.9	62.2	0.28	0.15
	37.3	29.2	85.2	245.9	61.4	0.36	0.19
	36.0	28.4	92.0	245.9	62.2	0.30	0.16

(Measurement period: September 11 to 29, 1991)							
Crack Leakage	36.7	26.9	47.6	251.7	31.9	0.33	0.09
Infiltration Flow	36.7	27.0	48.0	251.7	31.9	0.33	0.09
	30.0	23.3	54.5	253.8	74.4	0.23	0.07
	30.0	23.3	54.4	253.8	74.4	0.23	0.07
	35.3	26.9	56.1	249.1	58.6	0.42	0.17
	35.1	26.8	57.2	249.0	58.7	0.40	0.16
	34.8	26.5	53.7	249.2	58.8	0.42	0.17
	35.3	26.9	56.8	249.0	58.6	0.41	0.17
	35.1	26.8	57.6	249.0	58.7	0.40	0.16
	34.8	26.5	54.1	249.2	58.8	0.42	0.17
	33.8	25.3	59.1	249.4	58.9	0.44	0.18
	33.0	26.1	30.2	248.2	79.3	0.35	0.15
	33.0	26.1	30.4	48.2	79.3	0.35	0.15

(Measurement period: October 7 to 27, 1991)							
Crack Leakage	25.8	17.6	79.7	250.7	41.0	0.06	-0.03
Exfiltration Flow	25.8	17.6	79.7	250.7	41.0	0.06	-0.03
	34.3	26.3	87.8	250.2	39.1	-0.04	-0.06
	34.5	26.6	85.3	250.0	39.5	-0.04	-0.06
	34.7	26.7	82.3	249.8	39.9	-0.01	-0.05
	34.4	26.3	86.6	250.2	39.1	-0.02	-0.05
	34.5	26.5	85.0	250.0	39.5	-0.03	-0.05
	34.7	26.8	82.9	249.8	39.9	-0.02	-0.05
	27.6	21.0	76.6	250.2	58.8	-0.02	-0.08

27.4	20.9	80.1	250.4	59.7	-0.06	-10
27.2	20.9	83.4	250.7	60.5	-0.11	-12
27.6	21.1	79.5	250.1	58.7	-0.10	-12
27.4	20.9	80.1	250.4	59.7	-0.06	-10
27.3	20.9	82.8	250.7	60.5	-0.10	-12
28.5	23.1	91.8	249.9	83.6	-0.04	-10
28.0	22.6	79.0	250.3	83.7	-0.06	-11
27.4	21.9	63.2	250.8	83.9	-0.01	-08
28.5	23.2	95.2	249.8	83.6	-0.10	-14
27.9	22.7	80.5	250.2	83.6	-0.09	-13

(Measurement period: September 2 to 15, 1991)

Concent. leakage	33.2	25.7	47.2	253.4	60.7	0.25	0.13
Exfiltration Flow	33.5	26.2	46.7	253.6	60.2	0.21	0.10
	34.0	24.8	43.8	253.1	41.6	0.37	0.15
	33.6	24.8	45.6	253.1	41.7	0.29	0.12
	33.3	28.1	71.6	252.4	80.1	-0.16	-09
	33.8	28.3	73.1	252.2	80.0	-0.10	-06
	33.4	25.9	45.6	253.5	60.5	0.24	0.12
	32.9	27.6	65.4	252.8	80.2	-0.14	-08
	34.5	25.0	44.2	252.6	41.3	0.42	0.17
	33.4	25.9	46.8	253.5	60.5	0.23	0.12
	34.0	24.8	44.6	253.0	41.6	0.35	0.15
	33.6	24.9	47.3	253.1	41.8	0.27	0.11
	33.2	25.7	47.5	253.4	60.7	0.25	0.13
	33.3	28.1	70.9	252.4	80.1	-0.15	-08
	33.8	28.3	73.1	252.2	80.0	-0.10	0.06
	33.5	26.2	46.7	253.6	60.2	0.21	0.10
	32.9	27.6	65.4	252.8	80.2	-0.14	-08

(Measurement period: August 21, 1991 to September 2, 1991)

Concent. Leakage	37.4	29.3	72.0	252.5	59.4	0.33	0.17
Infiltration Flow	36.9	28.7	66.8	252.6	59.4	0.36	0.18
	36.3	28.2	63.7	252.8	59.5	0.36	0.18
	32.7	25.6	53.6	253.3	78.4	0.34	0.19
	32.8	25.5	64.1	253.5	78.2	0.36	0.21
	32.8	25.4	76.8	253.6	78.0	0.37	0.21
	38.1	29.0	67.4	248.6	41.9	0.36	0.15
	38.7	29.3	67.6	248.4	41.8	0.43	0.18
	37.2	28.5	66.5	249.2	42.2	0.25	0.11
	37.7	28.7	63.2	248.8	42.1	0.34	0.14
	38.9	29.8	79.8	248.1	41.6	0.33	0.14
	32.8	25.6	65.7	253.5	78.2	0.34	0.19
	32.7	25.6	53.6	253.3	78.4	0.34	0.19
	38.9	29.8	80.9	248.1	41.6	0.32	0.13

36.3	28.2	64.0	252.8	59.5	0.35	0.18
32.8	25.6	81.5	253.5	78.0	0.31	0.18
37.4	29.3	71.0	252.5	59.4	0.34	0.17
36.9	28.7	67.2	252.6	59.4	0.35	0.18
38.1	29.0	67.2	248.6	41.9	0.36	0.15
38.7	29.3	67.9	248.4	41.8	0.42	0.18
37.7	28.6	60.9	248.9	42.1	0.37	0.15
37.2	28.5	66.9	249.2	42.2	0.24	0.10

APPENDIX B6

SUMMARY OF THE STAM VALIDATION RESULTS

The STAM method was validated by 13 tests carried out from July 21 to September 20, 1990. The following table summarizes the general information of the tests.

The meanings of each column are explained as follows:

1 = test number, the first 6 tests had exfiltration, and the rest of them had infiltration

2 = solar model; (1) ASHRAE; (2) SHACSEJ; (3) Horizontal

4 = start time and date

5 = end time and date

6 = non-dimensional air flow rate

7 = average cell air temperature ($^{\circ}\text{C}$)

8 = average ambient temperature ($^{\circ}\text{C}$)

9 = average equivalent solar radiation (W/m^2)

10 = average heat input (W)

11 = IHEE

12 = standard error of moving average cell-air (STAM) temperature

13 = standard error of moving average ambient temperature

The basic periods were determined by requiring the air temperature difference between the beginning and the end of the period to be less than 0.1°C .

Summary of STAM Validation Results

1	2	4	5	6	7	8	9	10	11	12	13
1	1	05:20/22	00:00/24	0.52	38.4	27.7	67	278	0.28	0	0
1	1	23:00/21	00:40/25	0.52	37.9	27.1	65	278	0.31	0.003	0.013
1	1	02:00/23	00:20/25	0.52	37.4	26.3	59	278	0.40	0.006	0.002
1	1	23:00/23	06:00/25	0.52	37.1	26.2	62	279	0.35	0	0.002
1	2	02:00/23	00:20/25	0.52	37.4	26.3	114	278	0.36	0.006	0.002
1	2	23:00/23	06:00/25	0.52	37.1	26.2	100	279	0.33	0	0.002
1	3	05:20/22	00:00/24	0.52	38.4	27.7	217	278	0.26	0	0
1	3	23:00/21	00:40/25	0.52	37.9	27.1	216	278	0.29	0.003	0.013
1	3	02:00/23	00:20/25	0.52	37.4	26.3	206	278	0.37	0.006	0.002
1	3	23:00/23	06:00/25	0.52	37.1	26.2	213	279	0.32	0	0.002
2	1	01:40/26	04:40/27	0.40	40.6	29.2	88	280	0.22	0.005	0.012
2	1	01:40/26	06:20/28	0.42	41.2	29.9	90	280	0.21	0.003	0.002
2	1	23:40/26	01:20/28	0.43	41.7	30.3	91	280	0.23	0.004	0.019
2	1	23:40/26	02:00/29	0.44	42.3	31.0	85	280	0.26	0.005	0.009
2	1	23:40/26	00:40/30	0.44	42.5	31.2	84	280	0.29	0.002	0.004
2	1	23:40/27	00:40/29	0.44	43.0	31.6	77	281	0.28	0.011	0.011
2	1	00:00/28	00:00/30	0.45	43.0	31.5	79	280	0.33	0.002	0.005
2	1	01:00/29	23:40/29	0.45	43.0	31.5	80	279	0.36	0.001	0.002
2	2	01:40/26	04:40/27	0.40	40.6	29.2	136	280	0.21	0.005	0.012
2	2	01:40/26	06:20/28	0.42	41.2	29.9	140	280	0.19	0.003	0.002
2	2	23:40/26	01:20/28	0.43	41.7	30.3	141	280	0.22	0.004	0.019
2	2	23:40/26	02:00/29	0.44	42.3	31.0	135	280	0.24	0.005	0.009
2	2	23:40/26	00:40/30	0.44	42.5	31.2	135	280	0.27	0.002	0.004
2	2	23:40/27	00:40/29	0.44	43.0	31.6	124	281	0.27	0.011	0.011
2	2	00:00/28	00:00/30	0.45	43.0	31.5	129	280	0.31	0.002	0.005
2	2	01:00/29	23:40/29	0.45	43.0	31.5	134	279	0.34	0.001	0.002
2	3	01:40/26	04:40/27	0.40	40.6	29.2	289	280	0.18	0.005	0.012
2	3	01:40/26	06:20/28	0.42	41.2	29.9	296	280	0.16	0.003	0.002
2	3	23:40/26	01:20/28	0.43	41.7	30.3	299	280	0.19	0.004	0.019
2	3	23:40/26	02:00/29	0.44	42.3	31.0	288	280	0.21	0.005	0.009
2	3	23:40/26	00:40/30	0.44	42.5	31.2	287	280	0.24	0.002	0.004
2	3	23:40/27	00:40/29	0.44	43.0	31.6	268	281	0.24	0.011	0.011
2	3	00:00/28	00:00/30	0.45	43.0	31.5	275	280	0.28	0.002	0.005
2	3	01:00/29	23:40/29	0.45	43.0	31.5	282	279	0.32	0.001	0.002
3	3	00:41/31	04:01/01	0.66	37.3	27.5	62	276	0.29	0.002	0.019
3	3	00:01/01	01:21/02	0.66	38.5	28.4	63	276	0.36	0.001	0.016
3	3	23:41/31	02:01/03	0.67	39.0	28.9	75	276	0.34	0.001	0.012
3	3	23:41/01	00:41/03	0.68	39.5	29.4	86	277	0.33	0.005	0.014
3	3	00:41/31	04:01/01	0.66	37.3	27.5	108	276	0.27	0.002	0.019
3	3	00:01/01	01:21/02	0.66	38.5	28.4	115	276	0.34	0.001	0.016
3	3	23:41/31	02:01/03	0.67	39.0	28.9	131	276	0.32	0.001	0.012
3	3	23:41/01	00:41/03	0.68	39.5	29.4	145	277	0.30	0.005	0.014
3	3	00:41/31	04:01/01	0.66	37.3	27.5	209	276	0.27	0.002	0.019
3	3	00:01/01	01:21/02	0.66	38.5	28.4	206	276	0.34	0.001	0.016
3	3	23:41/31	02:01/03	0.67	39.0	28.9	238	276	0.32	0.001	0.012
3	3	23:41/01	00:41/03	0.68	39.5	29.4	267	277	0.31	0.005	0.014
4	1	04:20/04	02:20/05	0.78	39.2	30.1	83	276	0.21	0.003	0.015
4	2	04:20/04	02:20/05	0.78	39.2	30.1	139	276	0.19	0.003	0.015
4	3	04:20/04	02:20/05	0.78	39.2	30.1	287	276	0.18	0.003	0.015

1	2	4	5	6	7	8	9	10	11	12	13 (cont.)
5	1	23:20/08	01:40/10	0.81	37.1	28.0	64	276	0.28	0.016	0.005
5	2	23:20/08	01:40/10	0.81	37.1	28.0	119	276	0.26	0.016	0.005
5	3	23:20/08	01:40/10	0.81	37.1	28.0	209	276	0.26	0.016	0.005
6	1	03:20/12	02:20/13	0.77	38.7	29.7	95	275	0.19	0.005	0.01
6	1	03:40/12	05:00/14	0.77	38.4	29.1	90	276	0.26	0	0.001
6	1	23:20/12	00:00/14	0.78	38.1	28.8	89	277	0.26	0.003	0.018
6	2	03:20/12	02:20/13	0.77	38.7	29.7	164	275	0.17	0.005	0.01
6	2	03:40/12	05:00/14	0.77	38.4	29.1	157	276	0.23	0	0.001
6	2	23:20/12	00:00/14	0.78	38.1	28.8	160	277	0.23	0.003	0.018
6	3	03:20/12	02:20/13	0.77	38.7	29.7	299	275	0.17	0.005	0.01
6	3	03:40/12	05:00/14	0.77	38.4	29.1	279	276	0.24	0	0.001
6	3	23:20/12	00:00/14	0.78	38.1	28.8	276	277	0.24	0.003	0.018
7	1	03:00/15	04:40/16	1.02	38.2	29.5	92	274	0.33	0.011	0.014
7	1	03:00/15	04:00/17	1.02	38.4	30.0	92	275	0.29	0.001	0.001
7	1	03:00/15	04:00/18	1.02	38.3	29.8	89	275	0.29	0.002	0.001
7	1	03:00/15	04:20/19	1.02	38.3	29.9	89	276	0.29	0.001	0.002
7	1	03:40/15	04:00/20	1.02	38.4	30.1	88	275	0.27	0	0
7	1	23:00/15	23:00/16	1.02	38.6	30.2	90	276	0.28	0.002	0.003
7	1	00:20/16	23:00/17	1.02	38.3	30.0	88	276	0.27	0.002	0.001
7	1	00:00/16	23:00/18	1.02	38.4	30.0	88	276	0.27	0	0
7	1	23:00/15	23:20/19	1.01	38.5	30.1	85	276	0.27	0	0
7	1	23:00/15	23:20/20	1.01	38.5	30.2	86	276	0.26	0	0
7	1	00:20/17	23:00/17	1.02	38.0	29.7	86	276	0.28	0.004	0.004
7	1	00:20/17	23:20/18	1.01	38.3	29.9	87	276	0.27	0	0.001
7	1	23:00/16	23:20/19	1.01	38.5	30.1	84	276	0.27	0	0
7	1	23:00/16	23:20/20	1.01	38.4	30.2	85	275	0.25	0	0
7	1	23:00/17	23:20/18	1.01	38.5	30.1	87	276	0.27	0.004	0.007
7	1	23:20/17	00:20/20	1.01	38.6	30.3	83	276	0.27	0.002	0.004
7	1	23:40/17	01:40/21	1.01	38.6	30.3	84	275	0.25	0	0
7	1	23:40/18	00:40/20	1.01	38.8	30.4	77	275	0.29	0	0.002
7	1	23:00/18	01:00/21	1.01	38.6	30.4	82	275	0.25	0	0.004
7	1	23:20/19	23:20/20	1.01	38.4	30.4	89	275	0.20	0	0.002
7	2	03:00/15	04:40/16	1.02	38.2	29.5	176	274	0.30	0.011	0.014
7	2	03:00/15	04:00/17	1.02	38.4	30.0	189	275	0.25	0.001	0.001
7	2	03:00/15	04:00/18	1.02	38.3	29.8	184	275	0.24	0.002	0.001
7	2	03:00/15	04:20/19	1.02	38.3	29.9	172	276	0.25	0.001	0.002
7	2	03:40/15	04:00/20	1.02	38.4	30.1	165	275	0.24	0	0
7	2	23:00/15	23:00/16	1.02	38.6	30.2	195	276	0.22	0.002	0.003
7	2	00:20/16	23:00/17	1.02	38.3	30.0	189	276	0.22	0.002	0.001
7	2	00:00/16	23:00/18	1.02	38.4	30.0	171	276	0.23	0	0
7	2	23:00/15	23:20/19	1.01	38.5	30.1	158	276	0.24	0	0
7	2	23:00/15	23:20/20	1.01	38.5	30.2	154	276	0.23	0	0
7	2	00:20/17	23:00/17	1.02	38.0	29.7	180	276	0.23	0.004	0.004
7	2	00:20/17	23:20/18	1.01	38.3	29.9	158	276	0.24	0	0.001
7	2	23:00/16	23:20/19	1.01	38.5	30.1	145	276	0.25	0	0
7	2	23:00/16	23:20/20	1.01	38.4	30.2	144	275	0.24	0	0
7	2	23:00/17	23:20/18	1.01	38.5	30.1	135	276	0.27	0.004	0.007
7	2	23:20/17	00:20/20	1.01	38.6	30.3	130	276	0.26	0.002	0.004
7	2	23:40/17	01:40/21	1.01	38.6	30.3	131	275	0.25	0	0
7	2	23:40/18	00:40/20	1.01	38.8	30.4	121	275	0.28	0	0.002
7	2	23:00/18	01:00/21	1.01	38.6	30.4	127	275	0.25	0	0.004
7	2	23:20/19	23:20/20	1.01	38.4	30.4	138	275	0.20	0	0.002

1	2	4	5	6	7	8	9	10	11	12	13 (cont.)
7	3	03:00/15	04:40/16	1.02	38.2	29.5	290	274	0.32	0.011	0.014
7	3	03:00/15	04:00/17	1.02	38.4	30.0	289	275	0.28	0.001	0.001
7	3	03:00/15	04:00/18	1.02	38.3	29.8	284	275	0.27	0.002	0.001
7	3	03:00/15	04:20/19	1.02	38.3	29.9	283	276	0.27	0.001	0.002
7	3	03:40/15	04:00/20	1.02	38.4	30.1	283	275	0.25	0	0
7	3	23:00/15	23:00/16	1.02	38.6	30.2	276	276	0.26	0.002	0.003
7	3	00:20/16	23:00/17	1.02	38.3	30.0	283	276	0.25	0.002	0.001
7	3	00:00/16	23:00/18	1.02	38.4	30.0	282	276	0.25	0	0
7	3	23:00/15	23:20/19	1.01	38.5	30.1	275	276	0.25	0	0
7	3	23:00/15	23:20/20	1.01	38.5	30.2	278	276	0.24	0	0
7	3	00:20/17	23:00/17	1.02	38.0	29.7	287	276	0.25	0.004	0.004
7	3	00:20/17	23:20/18	1.01	38.3	29.9	284	276	0.25	0	0.001
7	3	23:00/16	23:20/19	1.01	38.5	30.1	274	276	0.25	0	0
7	3	23:00/16	23:20/20	1.01	38.4	30.2	278	275	0.23	0	0
7	3	23:00/17	23:20/18	1.01	38.5	30.1	277	276	0.26	0.004	0.007
7	3	23:20/17	00:20/20	1.01	38.6	30.3	270	276	0.25	0.002	0.004
7	3	23:40/17	01:40/21	1.01	38.6	30.3	273	275	0.23	0	0
7	3	23:40/18	00:40/20	1.01	38.8	30.4	256	275	0.26	0	0.002
7	3	23:00/18	01:00/21	1.01	38.6	30.4	267	275	0.23	0	0.004
7	3	23:20/19	23:20/20	1.01	38.4	30.4	286	275	0.18	0	0.002
8	1	05:42/26	02:03/27	0.89	35.4	27.2	100	272	0.15	0.005	0.011
8	1	05:02/26	00:23/28	0.90	35.4	27.5	93	272	0.11	0.013	0.003
8	1	00:03/27	00:23/28	0.91	35.7	27.6	81	273	0.16	0.002	0
8	2	05:42/26	02:03/27	0.89	35.4	27.2	144	272	0.15	0.005	0.011
8	2	05:02/26	00:23/28	0.90	35.4	27.5	135	272	0.11	0.013	0.003
8	2	00:03/27	00:23/28	0.91	35.7	27.6	118	273	0.15	0.002	0
8	3	05:42/26	02:03/27	0.89	35.4	27.2	342	272	0.11	0.005	0.011
8	3	05:02/26	00:23/28	0.90	35.4	27.5	321	272	0.07	0.013	0.003
8	3	00:03/27	00:23/28	0.91	35.7	27.6	282	273	0.12	0.002	0
9	1	02:40/29	04:40/30	0.93	39.4	30.3	72	278	0.36	0	0.001
9	1	00:00/30	01:00/31	0.94	41.0	31.6	83	280	0.38	0.002	0.011
9	2	02:40/29	04:40/30	0.93	39.4	30.3	106	278	0.36	0	0.001
9	2	0:00/30	01:00/31	0.94	41.0	31.6	117	280	0.38	0.002	0.011
9	3	2:40/29	04:40/30	0.93	39.4	30.3	247	278	0.34	0	0.001
9	3	0:00/30	01:00/31	0.94	41.0	31.6	280	280	0.35	0.002	0.011
10	1	0:00/01	02:20/04	0.72	37.6	28.0	68	283	0.24	0.004	0
10	1	05:00/03	04:20/04	0.70	37.6	27.6	75	283	0.31	0.002	0.019
10	2	06:00/01	02:20/04	0.72	37.6	28.0	126	283	0.22	0.004	0
10	2	05:00/03	04:20/04	0.70	37.6	27.6	119	283	0.29	0.002	0.019
10	3	06:00/01	02:20/04	0.72	37.6	28.0	239	283	0.21	0.004	0
10	3	05:00/03	04:20/04	0.70	37.6	27.6	251	283	0.28	0.002	0.019
11	1	06:40/05	04:00/06	0.47	39.2	27.5	75	282	0.41	0.001	0.02
11	1	02:20/05	02:20/07	0.46	39.2	28.0	75	281	0.31	0.002	0.001
11	1	01:40/05	02:20/08	0.46	39.5	28.2	79	280	0.31	0.001	0.002
11	1	02:00/06	05:20/07	0.45	39.2	28.0	72	279	0.27	0.003	0.015
11	1	00:00/06	03:20/08	0.45	39.6	28.4	81	279	0.28	0.001	0.014
11	1	02:40/07	04:00/08	0.45	39.9	28.3	84	279	0.36	0.006	0.016
11	2	06:40/05	04:00/06	0.47	39.2	27.5	163	282	0.34	0.001	0.02
11	2	02:20/05	02:20/07	0.46	39.2	28.0	135	281	0.27	0.002	0.001
11	2	01:40/05	02:20/08	0.46	39.5	28.2	132	280	0.28	0.001	0.002
11	2	02:00/06	05:20/07	0.45	39.2	28.0	108	279	0.27	0.003	0.015
11	2	00:00/06	03:20/08	0.45	39.6	28.4	119	279	0.27	0.001	0.014

1	2	4	5	6	7	8	9	10	11	12	13 (cont.)
11	2	02:40/07	04:00/08	0.45	39.9	28.3	123	279	0.36	0.006	0.016
11	3	06:40/05	04:00/06	0.47	39.2	27.5	246	282	0.38	0.001	0.02
11	3	02:20/05	02:20/07	0.46	39.2	28.0	238	281	0.28	0.002	0.001
11	3	01:40/05	02:20/08	0.46	39.5	28.2	249	280	0.28	0.001	0.002
11	3	02:00/06	05:20/07	0.45	39.2	28.0	224	279	0.25	0.003	0.015
11	3	00:00/06	03:20/08	0.45	39.6	28.4	249	279	0.25	0.001	0.014
11	3	02:40/07	04:00/08	0.45	39.9	28.3	260	279	0.33	0.006	0.016
12	1	01:00/10	03:20/12	0.58	34.3	23.1	43.1	284	0.46	0.001	0.007
12	1	23:20/09	00:20/13	0.59	34.7	23.7	47.7	284	0.42	0.001	0.017
12	1	23:20/09	01:40/14	0.59	35.1	24.2	51.2	284	0.40	0.001	0.006
12	1	23:20/10	05:00/14	0.59	35.5	24.8	58.8	284	0.33	0.004	0.001
12	1	23:40/11	00:00/13	0.60	35.5	24.9	53.4	283	0.35	0.001	0.002
12	1	23:20/11	00:40/14	0.59	35.8	25.2	57.8	284	0.33	0.001	0.002
12	1	23:40/12	01:00/14	0.59	36.0	25.4	60.6	284	0.33	0.004	0.014
12	2	01:00/10	03:20/12	0.58	34.3	23.1	82.5	284	0.43	0.001	0.007
12	2	23:20/09	00:20/13	0.59	34.7	23.7	88.7	284	0.40	0.001	0.017
12	2	23:20/09	01:40/14	0.59	35.1	24.2	91	284	0.38	0.001	0.006
12	2	23:20/10	05:00/14	0.59	35.5	24.8	96.7	284	0.32	0.004	0.001
12	2	23:40/11	00:00/13	0.60	35.5	24.9	94.1	283	0.33	0.001	0.002
12	2	23:20/11	00:40/14	0.59	35.8	25.2	96.6	284	0.32	0.001	0.002
12	2	23:40/12	01:00/14	0.59	36.0	25.4	96.5	284	0.32	0.004	0.014
12	3	01:00/10	03:20/12	0.58	34.3	23.1	128	284	0.45	0.001	0.007
12	3	23:20/09	00:20/13	0.59	34.7	23.7	137	284	0.41	0.001	0.017
12	3	23:20/09	01:40/14	0.59	35.1	24.2	146	284	0.39	0.001	0.006
12	3	23:20/10	05:00/14	0.59	35.5	24.8	168	284	0.33	0.004	0.001
12	3	23:40/11	00:00/13	0.60	35.5	24.9	145	283	0.35	0.001	0.002
12	3	23:20/11	00:40/14	0.59	35.8	25.2	159	284	0.33	0.001	0.002
12	3	23:40/12	01:00/14	0.59	36.0	25.4	168	284	0.33	0.004	0.014
13	1	03:40/15	06:40/16	0.35	40.7	28.5	59	282	0.36	0.002	0
13	1	04:00/15	02:00/18	0.33	39.3	26.8	59	281	0.42	0	0
13	1	03:40/15	02:20/19	0.33	39.4	27.0	64	281	0.36	0.001	0
13	1	05:00/16	23:40/17	0.32	38.4	25.7	59	281	0.46	0.004	0.004
13	1	02:40/16	23:40/18	0.32	38.9	26.4	65	281	0.38	0	0.002
13	1	23:40/16	06:40/18	0.31	37.6	25.1	55	281	0.42	0.007	0.008
13	1	23:40/16	00:20/20	0.31	38.5	26.1	66	281	0.35	0.002	0.001
13	1	01:20/18	02:00/19	0.32	39.6	27.6	79	281	0.19	0.015	0
13	1	06:40/18	00:20/20	0.31	39.2	26.9	74	280	0.30	0.001	0.009
13	2	03:40/15	06:40/16	0.35	40.7	28.5	93	282	0.35	0.002	0
13	2	04:00/15	02:00/18	0.33	39.3	26.8	105	281	0.38	0	0
13	2	03:40/15	02:20/19	0.33	39.4	27.0	109	281	0.33	0.001	0
13	2	05:00/16	23:40/17	0.32	38.4	25.7	112	281	0.41	0.004	0.004
13	2	02:40/16	23:40/18	0.32	38.9	26.4	112	281	0.35	0	0.002
13	2	23:40/16	06:40/18	0.31	37.6	25.1	101	281	0.38	0.007	0.008
13	2	23:40/16	00:20/20	0.31	38.5	26.1	111	281	0.32	0.002	0.001
13	2	01:20/18	02:00/19	0.32	39.6	27.6	119	281	0.19	0.015	0
13	2	06:40/18	00:20/20	0.31	39.2	26.9	117	280	0.28	0.001	0.009
13	3	03:40/15	06:40/16	0.35	40.7	28.5	180	282	0.34	0.002	0
13	3	04:00/15	02:00/18	0.33	39.3	26.8	182	281	0.40	0	0
13	3	03:40/15	02:20/19	0.33	39.4	27.0	192	281	0.34	0.001	0
13	3	05:00/16	23:40/17	0.32	38.4	25.7	183	281	0.44	0.004	0.004
13	3	02:40/16	23:40/18	0.32	38.9	26.4	192	281	0.37	0	0.002
13	3	23:40/16	06:40/18	0.31	37.6	25.1	155	281	0.41	0.007	0.008

1	2	4	5	6	7	8	9	10	11	12	13 (cont.)
13	3	23:40/16	00:20/20	0.31	38.5	26.1	194	281	0.34	0.002	0.001
13	3	01:20/18	02:00/19	0.32	39.6	27.6	217	281	0.19	0.015	0
13	3	06:40/18	00:20/20	0.31	39.2	26.9	220	280	0.28	0.001	0.009

The results summary of DAM are given as follows. The DAM simply used a 24 hours or its multiples as the average period. The period begins at 23:40 and ends at 23:20. The meanings of each column are explained as the following:

1 = test name

2 = solar models; 1- ASHRAE; 2 - SHVACSEJ model; 3 - Horizontal solar

3 = date of start month-day

4 = date of end month-day

5 = non-dimensional air flow rate

6 = average cell air temperature ($^{\circ}\text{C}$)

7 = average cell mass temperature ($^{\circ}\text{C}$)

8 = average ambient air temperature ($^{\circ}\text{C}$)

9 = heat input (W)

10 = equivalent solar radiation (W/m^2)

11 = IHEE

Summary of the DAM Results

1	2	3	4	5	6	7	8	9	10	11
J721-25	1	07-21	07-22	0.53	38.5	33.9	28.7	277	86	0.06
J721-25	1	07-21	07-23	0.52	38.2	33.2	27.3	278	60	0.35
J721-25	1	07-21	07-24	0.53	37.8	32.9	27.1	278	67	0.31
J721-25	1	07-22	07-23	0.50	37.8	32.5	25.8	278	35	0.60
J721-25	1	07-22	07-24	0.52	37.5	32.4	26.3	278	58	0.42
J721-25	1	07-23	07-24	0.54	37.2	32.3	26.8	279	80	0.22
J721-25	2	07-22	07-23	0.50	37.8	32.5	25.8	278	90	0.56
J721-25	2	07-22	07-24	0.52	37.5	32.4	26.3	278	110	0.39
J721-25	2	07-23	07-24	0.54	37.2	32.3	26.8	279	131	0.21
J721-25	3	07-21	07-22	0.53	38.5	33.9	28.7	277	267	0.04
J721-25	3	07-21	07-23	0.52	38.2	33.2	27.3	278	194	0.34
J721-25	3	07-21	07-24	0.53	37.8	32.9	27.1	278	223	0.29
J721-25	3	07-22	07-23	0.50	37.8	32.5	25.8	278	122	0.59
J721-25	3	07-22	07-24	0.52	37.5	32.4	26.3	278	200	0.40
J721-25	3	07-23	07-24	0.54	37.2	32.3	26.8	279	279	0.19
J725-30	1	07-25	07-26	0.40	40.6	35.4	29.7	280	100	0.05
J725-30	1	07-25	07-27	0.42	41.0	35.9	30.1	280	99	0.11
J725-30	1	07-25	07-28	0.43	41.7	36.5	30.7	280	93	0.15
J725-30	1	07-25	07-29	0.43	42.0	36.9	30.8	280	89	0.23
J725-30	1	07-26	07-27	0.44	41.5	36.3	30.5	280	98	0.18
J725-30	1	07-26	07-28	0.44	42.2	37.1	31.1	280	90	0.20
J725-30	1	07-26	07-29	0.44	42.5	37.4	31.2	280	85	0.28
J725-30	1	07-27	07-28	0.44	42.9	37.9	31.8	281	81	0.23
J725-30	1	07-27	07-29	0.45	43.0	37.9	31.6	280	79	0.33
J725-30	1	07-28	07-29	0.45	43.1	37.8	31.3	279	77	0.42
J725-30	2	07-25	07-26	0.40	40.6	35.4	29.7	280	155	0.03
J725-30	2	07-25	07-27	0.42	41.0	35.9	30.1	280	154	0.10
J725-30	2	07-25	07-28	0.43	41.7	36.5	30.7	280	147	0.14
J725-30	2	07-25	07-29	0.43	42.0	36.9	30.8	280	142	0.21
J725-30	2	07-26	07-27	0.44	41.5	36.3	30.5	280	153	0.16
J725-30	2	07-26	07-28	0.44	42.2	37.1	31.1	280	142	0.19
J725-30	2	07-26	07-29	0.44	42.5	37.4	31.2	280	138	0.26
J725-30	2	07-27	07-28	0.44	42.9	37.9	31.8	281	131	0.21
J725-30	2	07-27	07-29	0.45	43.0	37.9	31.6	280	130	0.31
J725-30	2	07-28	07-29	0.45	43.1	37.8	31.3	279	128	0.40
J725-30	3	07-25	07-26	0.40	40.6	35.4	29.7	280	329	0.00
J725-30	3	07-25	07-27	0.42	41.0	35.9	30.1	280	327	0.07
J725-30	3	07-25	07-28	0.43	41.7	36.5	30.7	280	312	0.11
J725-30	3	07-25	07-29	0.43	42.0	36.9	30.8	280	302	0.19
J725-30	3	07-26	07-27	0.44	41.5	36.3	30.5	280	324	0.13
J725-30	3	07-26	07-28	0.44	42.2	37.1	31.1	280	304	0.16
J725-30	3	07-26	07-29	0.44	42.5	37.4	31.2	280	293	0.24
J725-30	3	07-27	07-28	0.44	42.9	37.9	31.8	281	283	0.19
J725-30	3	07-27	07-29	0.45	43.0	37.9	31.6	280	277	0.29
J725-30	3	07-28	07-29	0.45	43.1	37.8	31.3	279	270	0.38
J730-03	1	07-30	07-31	0.67	37.2	33.0	27.9	275	71	0.18
J730-03	1	07-30	08-01	0.67	37.9	33.6	28.2	276	70	0.26
J730-03	1	07-30	08-02	0.67	38.4	34.1	28.7	276	76	0.27
J730-03	1	07-31	08-01	0.67	38.5	34.2	28.5	276	68	0.33

	1	2	3	4	5	6	7	8	9	10	11 (cont.)
J730-03	1	07-31	08-02	0.67	39.0	34.7	29.1	276	79	0.31	
J730-03	1	08-01	08-02	0.68	39.5	35.1	29.6	277	90	0.29	
J730-03	2	07-30	07-31	0.67	37.2	33.0	27.9	275	124	0.16	
J730-03	2	07-30	08-01	0.67	37.9	33.6	28.2	276	124	0.23	
J730-03	2	07-30	08-02	0.67	38.4	34.1	28.7	276	134	0.25	
J730-03	2	07-31	08-01	0.67	38.5	34.2	28.5	276	123	0.31	
J730-03	2	07-31	08-02	0.67	39.0	34.7	29.1	276	138	0.29	
J730-03	2	08-01	08-02	0.68	39.5	35.1	29.6	277	153	0.27	
J730-03	3	07-30	07-31	0.67	37.2	33.0	27.9	275	241	0.16	
J730-03	3	07-30	08-01	0.67	37.9	33.6	28.2	276	230	0.24	
J730-03	3	07-30	08-02	0.67	38.4	34.1	28.7	276	248	0.25	
J730-03	3	07-31	08-01	0.67	38.5	34.2	28.5	276	220	0.31	
J730-03	3	07-31	08-02	0.67	39.0	34.7	29.1	276	251	0.29	
J730-03	3	08-01	08-02	0.68	39.5	35.1	29.6	277	282	0.27	
AU03-05	1	08-03	08-04	0.78	39.2	35.0	29.9	276	78	0.29	
AU03-05	2	08-03	08-04	0.78	39.2	35.0	29.9	276	129	0.27	
AU03-05	3	08-03	08-04	0.78	39.2	35.0	29.9	276	267	0.26	
AU07-10	1	08-07	08-08	0.79	34.7	30.9	26.6	276	94	0.02	
AU07-10	1	08-07	08-09	0.80	35.8	32.0	27.4	276	83	0.11	
AU07-10	1	08-08	08-09	0.82	36.9	33.1	28.3	276	72	0.19	
AU07-10	2	08-07	08-08	0.79	34.7	30.9	26.6	276	156	-0.01	
AU07-10	2	08-07	08-09	0.80	35.8	32.0	27.4	276	145	0.08	
AU07-10	2	08-08	08-09	0.82	36.9	33.1	28.3	276	133	0.16	
AU07-10	3	08-07	08-08	0.79	34.7	30.9	26.6	276	300	-0.01	
AU07-10	3	08-07	08-09	0.80	35.8	32.0	27.4	276	266	0.09	
AU07-10	3	08-08	08-09	0.82	36.9	33.1	28.3	276	232	0.17	
AU11-14	1	08-11	08-12	0.76	38.7	34.6	29.5	275	92	0.22	
AU11-14	1	08-11	08-13	0.77	38.4	34.3	29.2	276	93	0.23	
AU11-14	1	08-12	08-13	0.78	38.1	34.1	28.9	277	93	0.24	
AU11-14	2	08-11	08-12	0.76	38.7	34.6	29.5	275	159	0.20	
AU11-14	2	08-11	08-13	0.77	38.4	34.3	29.2	276	163	0.20	
AU11-14	2	08-12	08-13	0.78	38.1	34.1	28.9	277	167	0.21	
AU11-14	3	08-11	08-12	0.76	38.7	34.6	29.5	275	291	0.20	
AU11-14	3	08-11	08-13	0.77	38.4	34.3	29.2	276	289	0.21	
AU14-21	3	08-12	08-13	0.78	38.1	34.1	28.9	277	288	0.22	
AU14-21	1	08-14	08-15	1.02	38.3	34.8	29.8	274	99	0.30	
AU14-21	1	08-14	08-16	1.02	38.4	34.9	30.1	275	95	0.29	
AU14-21	1	08-14	08-17	1.02	38.3	34.8	29.9	275	91	0.29	
AU14-21	1	08-14	08-18	1.02	38.4	34.8	30.0	276	91	0.29	
AU14-21	1	08-14	08-19	1.02	38.4	34.9	30.1	276	89	0.28	
AU14-21	1	08-14	08-20	1.02	38.4	34.9	30.2	275	89	0.27	
AU14-21	1	08-15	08-16	1.02	38.6	35.0	30.3	276	91	0.28	
AU14-21	1	08-15	08-17	1.02	38.3	34.8	29.9	276	87	0.29	
AU14-21	1	08-15	08-18	1.02	38.4	34.8	30.0	276	88	0.29	
AU14-21	1	08-15	08-19	1.01	38.5	34.9	30.2	276	86	0.28	
AU14-21	1	08-15	08-20	1.01	38.5	34.9	30.2	276	87	0.26	
AU14-21	1	08-16	08-17	1.02	38.1	34.5	29.6	276	82	0.31	
AU14-21	1	08-16	08-18	1.01	38.3	34.7	29.9	276	86	0.29	
AU14-21	1	08-16	08-19	1.01	38.4	34.9	30.1	276	84	0.28	
AU14-21	1	08-16	08-20	1.01	38.4	34.9	30.2	275	86	0.26	
AU14-21	1	08-17	08-18	1.01	38.5	35.0	30.1	276	90	0.27	
AU14-21	1	08-17	08-19	1.01	38.6	35.1	30.4	276	85	0.26	
AU14-21	1	08-17	08-20	1.01	38.6	35.1	30.4	275	87	0.24	

<u>1</u>	<u>2</u>	<u>3</u>	<u>4</u>	<u>5</u>	<u>6</u>	<u>7</u>	<u>8</u>	<u>9</u>	<u>10</u>	<u>11 (cont.)</u>
AU14-21	1	08-18	08-19	1.01	38.8	35.3	30.6	275	81	0.25
AU14-21	1	08-18	08-20	1.01	38.6	35.1	30.5	275	86	0.23
AU14-21	1	08-19	08-20	1.01	38.4	35.0	30.5	275	91	0.20
AU14-21	2	08-14	08-15	1.02	38.3	34.8	29.8	274	191	0.26
AU14-21	2	08-14	08-16	1.02	38.4	34.9	30.1	275	194	0.24
AU14-21	2	08-14	08-17	1.02	38.3	34.8	29.9	275	187	0.25
AU14-21	2	08-14	08-18	1.02	38.4	34.8	30.0	276	175	0.25
AU14-21	2	08-14	08-19	1.02	38.4	34.9	30.1	276	166	0.25
AU14-21	2	08-14	08-20	1.02	38.4	34.9	30.2	275	161	0.24
AU14-21	2	08-15	08-16	1.02	38.6	35.0	30.3	276	197	0.23
AU14-21	2	08-15	08-17	1.02	38.3	34.8	29.9	276	185	0.25
AU14-21	2	08-15	08-18	1.02	38.4	34.8	30.0	276	170	0.25
AU14-21	2	08-15	08-19	1.01	38.5	34.9	30.2	276	159	0.25
AU14-21	2	08-15	08-20	1.01	38.5	34.9	30.2	276	155	0.24
AU14-21	2	08-16	08-17	1.02	38.1	34.5	29.6	276	172	0.27
AU14-21	2	08-16	08-18	1.01	38.3	34.7	29.9	276	156	0.27
AU14-21	2	08-16	08-19	1.01	38.4	34.9	30.1	276	146	0.26
AU14-21	2	08-16	08-20	1.01	38.4	34.9	30.2	275	145	0.24
AU14-21	2	08-17	08-18	1.01	38.5	35.0	30.1	276	139	0.26
AU14-21	2	08-17	08-19	1.01	38.6	35.1	30.4	276	133	0.25
AU14-21	2	08-17	08-20	1.01	38.6	35.1	30.4	275	135	0.23
AU14-21	2	08-18	08-19	1.01	38.8	35.3	30.6	275	127	0.24
AU14-21	2	08-18	08-20	1.01	38.6	35.1	30.5	275	134	0.22
AU14-21	2	08-19	08-20	1.01	38.4	35.0	30.5	275	140	0.19
AU14-21	3	08-14	08-15	1.02	38.3	34.8	29.8	274	314	0.28
AU14-21	3	08-14	08-16	1.02	38.4	34.9	30.1	275	297	0.27
AU14-21	3	08-14	08-17	1.02	38.3	34.8	29.9	275	290	0.28
AU14-21	3	08-14	08-18	1.02	38.4	34.8	30.0	276	288	0.27
AU14-21	3	08-14	08-19	1.02	38.4	34.9	30.1	276	285	0.26
AU14-21	3	08-14	08-20	1.02	38.4	34.9	30.2	275	286	0.25
AU14-21	3	08-15	08-16	1.02	38.6	35.0	30.3	276	280	0.26
AU14-21	3	08-15	08-17	1.02	38.3	34.8	29.9	276	277	0.28
AU14-21	3	08-15	08-18	1.02	38.4	34.8	30.0	276	280	0.27
AU14-21	3	08-15	08-19	1.01	38.5	34.9	30.2	276	277	0.26
AU14-21	3	08-15	08-20	1.01	38.5	34.9	30.2	276	280	0.24
AU14-21	3	08-16	08-17	1.02	38.1	34.5	29.6	276	275	0.29
AU14-21	3	08-16	08-18	1.01	38.3	34.7	29.9	276	280	0.27
AU14-21	3	08-16	08-19	1.01	38.4	34.9	30.1	276	277	0.26
AU14-21	3	08-16	08-20	1.01	38.4	34.9	30.2	275	280	0.24
AU14-21	3	08-17	08-18	1.01	38.5	35.0	30.1	276	284	0.25
AU14-21	3	08-17	08-19	1.01	38.6	35.1	30.4	276	277	0.24
AU14-21	3	08-17	08-20	1.01	38.6	35.1	30.4	275	282	0.22
AU14-21	3	08-18	08-19	1.01	38.8	35.3	30.6	275	270	0.23
AU14-21	3	08-18	08-20	1.01	38.6	35.1	30.5	275	280	0.21
AU14-21	3	08-19	08-20	1.01	38.4	35.0	30.5	275	290	0.18
AU25-28	1	08-25	08-26	0.89	36.0	31.9	27.2	272	86	0.31
AU25-28	1	08-25	08-27	0.90	35.8	31.7	27.4	272	85	0.22
AU25-28	1	08-26	08-27	0.91	35.6	31.6	27.6	273	84	0.13
AU25-28	2	08-25	08-26	0.89	36.0	31.9	27.2	272	124	0.31
AU25-28	2	08-25	08-27	0.90	35.8	31.7	27.4	272	123	0.22
AU25-28	2	08-26	08-27	0.91	35.6	31.6	27.6	273	121	0.13
AU25-28	3	08-25	08-26	0.89	36.0	31.9	27.2	272	294	0.28
AU25-28	3	08-25	08-27	0.90	35.8	31.7	27.4	272	292	0.19

<u>1</u>	<u>2</u>	<u>3</u>	<u>4</u>	<u>5</u>	<u>6</u>	<u>7</u>	<u>8</u>	<u>9</u>	<u>10</u>	<u>11 (cont.)</u>
AU25-28	3	08-26	08-27	0.91	35.6	31.6	27.6	273	290	0.10
AU28-31	1	08-28	08-29	0.93	39.4	35.2	30.6	277	79	0.29
AU28-31	1	08-28	08-30	0.93	40.2	36.0	31.2	279	83	0.32
AU28-31	1	08-29	08-30	0.93	41.0	36.8	31.9	280	87	0.34
AU28-31	2	08-28	08-29	0.93	39.4	35.2	30.6	277	117	0.29
AU28-31	2	08-28	08-30	0.93	40.2	36.0	31.2	279	120	0.32
AU28-31	2	08-29	08-30	0.93	41.0	36.8	31.9	280	124	0.35
AU28-31	3	08-28	08-29	0.93	39.4	35.2	30.6	277	271	0.27
AU28-31	3	08-28	08-30	0.93	40.2	36.0	31.2	279	284	0.30
AU28-31	3	08-29	08-30	0.93	41.0	36.8	31.9	280	296	0.32
AU31-04	1	08-31	09-03	0.73	37.9	32.5	27.2	283	43	0.49
AU31-04	1	08-31	09-04	0.72	37.7	32.6	27.4	283	58	0.41
AU31-04	1	09-03	09-04	0.70	37.6	32.7	27.5	283	74	0.32
AU31-04	2	08-31	09-03	0.73	37.9	32.5	27.2	283	100	0.46
AU31-04	2	08-31	09-04	0.72	37.7	32.6	27.4	283	108	0.39
AU31-04	2	09-03	09-04	0.70	37.6	32.7	27.5	283	117	0.31
AU31-04	3	08-31	09-03	0.73	37.9	32.5	27.2	283	165	0.47
AU31-04	3	08-31	09-04	0.72	37.7	32.6	27.4	283	206	0.39
AU31-04	3	09-03	09-04	0.70	37.6	32.7	27.5	283	248	0.30
SE04-08	1	09-04	09-05	0.47	39.3	33.6	27.3	283	67	0.48
SE04-08	1	09-04	09-06	0.46	39.2	33.7	28.1	281	75	0.29
SE04-08	1	09-04	09-07	0.46	39.5	33.9	28.2	280	80	0.30
SE04-08	1	09-05	09-06	0.46	39.2	33.9	28.8	279	83	0.08
SE04-08	1	09-05	09-07	0.45	39.5	34.1	28.7	279	87	0.20
SE04-08	1	09-06	09-07	0.45	39.9	34.4	28.5	279	90	0.31
SE04-08	2	09-04	09-05	0.47	39.3	33.6	27.3	283	147	0.42
SE04-08	2	09-04	09-06	0.46	39.2	33.7	28.1	281	136	0.26
SE04-08	2	09-04	09-07	0.46	39.5	33.9	28.2	280	134	0.27
SE04-08	2	09-05	09-06	0.46	39.2	33.9	28.8	279	125	0.07
SE04-08	2	09-05	09-07	0.45	39.5	34.1	28.7	279	128	0.19
SE04-08	2	09-06	09-07	0.45	39.9	34.4	28.5	279	132	0.30
SE04-08	3	09-04	09-05	0.47	39.3	33.6	27.3	283	222	0.45
SE04-08	3	09-04	09-06	0.46	39.2	33.7	28.1	281	240	0.27
SE04-08	3	09-04	09-07	0.46	39.5	33.9	28.2	280	253	0.27
SE04-08	3	09-05	09-06	0.46	39.2	33.9	28.8	279	258	0.05
SE04-08	3	09-05	09-07	0.45	39.5	34.1	28.7	279	268	0.17
SE04-08	3	09-06	09-07	0.45	39.9	34.4	28.5	279	278	0.28
SE08-14	1	09-08	09-09	0.63	38.3	31.7	25.4	280	40	0.78
SE08-14	1	09-08	09-10	0.60	35.9	32.3	23.5	282	30	0.71
SE08-14	1	09-08	09-11	0.60	35.6	32.9	23.9	283	44	0.57
SE08-14	1	09-08	09-12	0.60	35.6	33.3	24.2	283	47	0.52
SE08-14	1	09-08	09-13	0.60	35.7	33.6	24.5	283	50	0.48
SE08-14	1	09-09	09-10	0.58	33.6	32.9	21.6	285	20	0.63
SE08-14	1	09-09	09-11	0.58	34.3	33.5	23.1	284	46	0.45
SE08-14	1	09-09	09-12	0.59	34.7	33.9	23.7	284	49	0.42
SE08-14	1	09-09	09-13	0.59	35.1	34.1	24.2	284	53	0.39
SE08-14	1	09-10	09-11	0.58	35.0	34.1	24.6	284	71	0.25
SE08-14	1	09-10	09-12	0.59	35.3	34.3	24.8	284	63	0.30
SE08-14	1	09-10	09-13	0.59	35.5	34.5	25.1	284	64	0.30
SE08-14	1	09-11	09-12	0.60	35.5	34.5	25.0	283	55	0.34
SE08-14	1	09-11	09-13	0.60	35.8	34.7	25.3	284	60	0.32
SE08-14	1	09-12	09-13	0.59	36.1	34.9	25.6	284	65	0.30
SE08-14	2	09-08	09-09	0.63	38.3	31.7	25.4	280	78	0.76

1	2	3	4	5	6	7	8	9	10	11 (cont.)
SE08-14	2	09-08	09-10	0.60	35.9	32.3	23.5	282	69	0.68
SE08-14	2	09-08	09-11	0.60	35.6	32.9	23.9	283	84	0.56
SE08-14	2	09-08	09-12	0.60	35.6	33.3	24.2	283	87	0.50
SE08-14	2	09-08	09-13	0.60	35.7	33.6	24.5	283	90	0.46
SE08-14	2	09-09	09-10	0.58	33.6	32.9	21.6	285	60	0.60
SE08-14	2	09-09	09-11	0.58	34.3	33.5	23.1	284	87	0.43
SE08-14	2	09-09	09-12	0.59	34.7	33.9	23.7	284	90	0.40
SE08-14	2	09-09	09-13	0.59	35.1	34.1	24.2	284	94	0.37
SE08-14	2	09-10	09-11	0.58	35.0	34.1	24.6	284	114	0.24
SE08-14	2	09-10	09-12	0.59	35.3	34.3	24.8	284	106	0.28
SE08-14	2	09-10	09-13	0.59	35.5	34.5	25.1	284	105	0.28
SE08-14	2	09-11	09-12	0.60	35.5	34.5	25.0	283	97	0.33
SE08-14	2	09-11	09-13	0.60	35.8	34.7	25.3	284	100	0.31
SE08-14	2	09-12	09-13	0.59	36.1	34.9	25.6	284	103	0.29
SE08-14	3	09-08	09-09	0.63	38.3	31.7	25.4	280	152	0.76
SE08-14	3	09-08	09-10	0.60	35.9	32.3	23.5	282	104	0.70
SE08-14	3	09-08	09-11	0.60	35.6	32.9	23.9	283	141	0.56
SE08-14	3	09-08	09-12	0.60	35.6	33.3	24.2	283	143	0.51
SE08-14	3	09-08	09-13	0.60	35.7	33.6	24.5	283	150	0.47
SE08-14	3	09-09	09-10	0.58	33.6	32.9	21.6	285	55	0.63
SE08-14	3	09-09	09-11	0.58	34.3	33.5	23.1	284	136	0.45
SE08-14	3	09-09	09-12	0.59	34.7	33.9	23.7	284	140	0.41
SE08-14	3	09-09	09-13	0.59	35.1	34.1	24.2	284	150	0.38
SE08-14	3	09-10	09-11	0.58	35.0	34.1	24.6	284	216	0.24
SE08-14	3	09-10	09-12	0.59	35.3	34.3	24.8	284	182	0.29
SE08-14	3	09-10	09-13	0.59	35.5	34.5	25.1	284	182	0.29
SE08-14	3	09-11	09-12	0.60	35.5	34.5	25.0	283	149	0.34
SE08-14	3	09-11	09-13	0.60	35.8	34.7	25.3	284	164	0.32
SE08-14	3	09-12	09-13	0.59	36.1	34.9	25.6	284	180	0.30
SE14-20	1	09-14	09-15	0.34	40.5	34.8	28.9	281	68	0.20
SE14-20	1	09-14	09-16	0.34	40.1	33.9	27.3	281	51	0.54
SE14-20	1	09-14	09-17	0.33	39.3	33.2	26.8	281	58	0.45
SE14-20	1	09-14	09-18	0.33	39.4	33.3	27.0	281	64	0.38
SE14-20	1	09-14	09-19	0.32	39.2	33.0	26.6	281	60	0.43
SE14-20	1	09-15	09-16	0.33	39.7	33.0	25.8	282	33	0.82
SE14-20	1	09-15	09-17	0.33	38.7	32.4	25.7	281	52	0.56
SE14-20	1	09-15	09-18	0.32	39.0	32.8	26.4	281	62	0.43
SE14-20	1	09-15	09-19	0.32	38.9	32.6	26.1	281	59	0.49
SE14-20	1	09-16	09-17	0.32	37.7	31.7	25.7	281	72	0.26
SE14-20	1	09-16	09-18	0.32	38.6	32.7	26.7	280	77	0.20
SE14-20	1	09-16	09-19	0.31	38.6	32.4	26.2	281	67	0.36
SE14-20	1	09-17	09-18	0.31	39.5	33.6	27.8	280	82	0.14
SE14-20	1	09-17	09-19	0.31	39.0	32.8	26.4	281	65	0.41
SE14-20	1	09-18	09-19	0.30	38.5	31.9	25.1	282	47	0.65
SE14-20	2	09-14	09-15	0.34	40.5	34.8	28.9	281	106	0.19
SE14-20	2	09-14	09-16	0.34	40.1	33.9	27.3	281	87	0.51
SE14-20	2	09-14	09-17	0.33	39.3	33.2	26.8	281	102	0.42
SE14-20	2	09-14	09-18	0.33	39.4	33.3	27.0	281	108	0.35
SE14-20	2	09-14	09-19	0.32	39.2	33.0	26.6	281	102	0.41
SE14-20	2	09-15	09-16	0.33	39.7	33.0	25.8	282	69	0.79
SE14-20	2	09-15	09-17	0.33	38.7	32.4	25.7	281	101	0.53
SE14-20	2	09-15	09-18	0.32	39.0	32.8	26.4	281	108	0.40
SE14-20	2	09-15	09-19	0.32	38.9	32.6	26.1	281	101	0.46

<u>1</u>	<u>2</u>	<u>3</u>	<u>4</u>	<u>5</u>	<u>6</u>	<u>7</u>	<u>8</u>	<u>9</u>	<u>10</u>	<u>11 (cont.)</u>
SE14-20	2	09-16	09-17	0.32	37.7	31.7	25.7	281	132	0.21
SE14-20	2	09-16	09-18	0.32	38.6	32.7	26.7	280	128	0.17
SE14-20	2	09-16	09-19	0.31	38.6	32.4	26.2	281	112	0.33
SE14-20	2	09-17	09-18	0.31	39.5	33.6	27.8	280	124	0.13
SE14-20	2	09-17	09-19	0.31	39.0	32.8	26.4	281	102	0.39
SE14-20	2	09-18	09-19	0.30	38.5	31.9	25.1	282	81	0.63
SE14-20	3	09-14	09-15	0.34	40.5	34.8	28.9	281	205	0.18
SE14-20	3	09-14	09-16	0.34	40.1	33.9	27.3	281	165	0.51
SE14-20	3	09-14	09-17	0.33	39.3	33.2	26.8	281	177	0.43
SE14-20	3	09-14	09-18	0.33	39.4	33.3	27.0	281	190	0.36
SE14-20	3	09-14	09-19	0.32	39.2	33.0	26.6	281	184	0.42
SE14-20	3	09-15	09-16	0.33	39.7	33.0	25.8	282	124	0.80
SE14-20	3	09-15	09-17	0.33	38.7	32.4	25.7	281	164	0.55
SE14-20	3	09-15	09-18	0.32	39.0	32.8	26.4	281	185	0.42
SE14-20	3	09-15	09-19	0.32	38.9	32.6	26.1	281	178	0.47
SE14-20	3	09-16	09-17	0.32	37.7	31.7	25.7	281	203	0.25
SE14-20	3	09-16	09-18	0.32	38.6	32.7	26.7	280	215	0.19
SE14-20	3	09-16	09-19	0.31	38.6	32.4	26.2	281	196	0.34
SE14-20	3	09-17	09-18	0.31	39.5	33.6	27.8	280	226	0.13
SE14-20	3	09-17	09-19	0.31	39.0	32.8	26.4	281	193	0.39
SE14-20	3	09-18	09-19	0.30	38.5	31.9	25.1	282	159	0.62

VITA

Mingsheng Liu was born and brought up in Hebei, China. He attended elementary school in 1965 and finished high school in 1974. Following high school, he spent three years teaching in a village elementary school. Beginning in 1978, he attended Harbin Architectural and Civil Engineering Institute, and finished B. S. and M. S. degrees in 1984 in Heating Ventilation and Air-Conditioning engineering. Following graduation in 1984, he worked in the same school as a lecturer assistant for a year, then was promoted to lecturer in 1985, as a reward for his research and teaching abilities. The building energy conservation research performed by him and others received the National Building Construction and Environment Commission of China team award in 1985. He also received Heilungkiang Province award for his innovative heating network design method in 1987. He organized the Heating Ventilation and Air-conditioning Young Engineer Association of Heilungkiang Province in 1987, and served as Chair during 1987 to 1988. He was invited to Lawrence Berkeley Laboratory to join COMIS (Conjecture Of Multi-zone Infiltration Specialist) in 1988. He came to Texas A&M in 1989, and worked with Professor David E. Claridge as part of the Energy Systems Laboratory.

His permanent mailing address is:

Liu Mingsheng

Second Street, Guo Tai

Ci County, Hebei

P. R. China